Marine Isotope Stage 11 in the Eastern Mediterranean Sea: nearest analogue to the present day?

Dissertation

der Mathematisch-Naturwissenschaftlichen Fakultät

der Eberhard Karls Universität Tübingen

zur Erlangung des Grades eines

Doktors der Naturwissenschaften

(Dr. rer. nat.)

vorgelegt von

Lea Dagmar Numberger-Thuy

aus Flensburg

Tübingen

2010

Tag der mündlichen Qualifikation:	21.02.2011
Dekan:	Prof. Dr. Wolfgang Rosenstiel
1. Berichterstatter:	Prof. Dr. Michal Kučera
2. Berichterstatter:	Prof. Dr. Gerhard Schmiedl

"Chaos is found in greatest abundance wherever order is being sought. It always defeats order, because it is better organized."

— Sir Terry Pratchett

Abstract

Marine Isotope Stage 11 (MIS 11) is known to be the closest analogue to the Holocene (MIS 1) in terms of Earth's orbital configuration during the last 400,000 years. This has often been used as an argument to investigate climate trends of MIS 11, reconstructed from natural geological archives in order to evaluate current and future climate developments. However, the orbital configuration during MIS 11 was not exactly identical to that of MIS 1 and the comparability of climate trends during both interglacials is currently hotly debated.

In this study, the first high resolution palaeoclimatic investigation of MIS 11 is presented here for the Eastern Mediterranean Sea, known to yield an especially sensitive climate archive. High-resolution, continuous multi-proxy palaeoclimatic data have been generated from two sediment cores of this region (ODP Site 964: 36°16'N, 17°45'E, 3658 m; GeoTü-SL96 32°46'N, 19°12'E, 1399 m). The records have been tied to an absolute time scale using an age model based on stable oxygen isotopes, planktonic faunal abundance events and sapropel formations. As a proxy of surface water conditions, assemblage compositions of planktonic foraminifera were determined in 404 samples and supplemented with alkenone unsaturation ratios in one of the cores.

The new MIS 11 data indicate that MIS 11 sapropel formation and onset of interglacial conditions in both cores correlated with the second insolation peak after Termination V. In contrast, the MIS 1 sapropel S1 coincides with the first insolation peak after Termination I. An alignment of these two sapropel formations is here considered to be the best option to evaluate future climate trends of the recent interglacial. The position of the oxygen isotopic peak in GeoTü-SL96 is not associated with a fully developed sapropel and is not clearly identifiable in the sediment record. In contrast, both cores show a significant sapropel layer in MIS 1, indicating a different depth for the oxycline during MIS 11. In addition, the size of the oxygen isotopic peak at ODP Site 964 is larger than in the Holocene at the same site, indicating enhanced monsoonal activity and/or Black Sea discharge during MIS 11, despite a weaker insolation forcing.

The alignment of MIS 11 sapropel to the second insolation maximum of MIS 11 reveals an apparently delayed response of the pelagic system to deglaciation. The pre-sapropel interval of MIS 11 is characterised by glacial planktonic foraminiferal assemblages and apparently glacial alkenone temperatures. Benthic foraminifera concentrations and Ba/Ca ratios in the sediment furthermore suggest high productivity for the pre-sapropel interval. The most likely scenario to explain the apparent delayed response, in stark contrast with global trends and pollen evidence from the Mediterranean region, is high winter productivity during relatively cool and wet interglacial conditions in early MIS 11, fuelled by enhanced influx of terrigenous material, leading to the persistence of glacial planktonic foraminifera assemblages and alkenones representing the cold season signal until the development of the MIS 11 sapropel.

Within the later part of MIS 11, planktonic foraminifera assemblage compositions show three conspicuous phases. The assemblages occurring during these phases resemble faunas known from

later sapropels. As they coincide with insolation maxima and low Ba/Ca and Fe/Al values in the sediment, they appear to be controlled by orbitally driven maxima in seasonality and stratification with low productivity and thus no sapropel formation. In addition, the planktonic foraminifera assemblages throughout late MIS 11 remain dominated by the warm-water indicator *G. ruber*, reaching an absolute maximum in late MIS 11 and the first half of MIS 10 (~ 80 %). This pattern can be explained by unusually warm temperatures during the late phase of MIS 11, which is consistent with alkenone data, combined with extremely low productivity, as indicated by benthic foraminifera concentrations.

During sample preparation, anomalies in shape and size of *G. ruber* were identified, which led to the definition of four different morphotypes within this species, in accordance with literature. Abundances of the morphotypes significantly change between glacials and interglacials, and in three of the morphotypes of *G. ruber*, significant offsets in stable isotope composition were found. Since the isotope shifts among the three *G. ruber* morphotypes are systematic and often exceed 1 ‰, their understanding is essential for the interpretation of all *G. ruber* – based proxy records for palaeoceanographic reconstructions.

The apparent delayed reaction of MIS 11 pelagic ecosystem in the Mediterranean region to global trends, resulting in a sapropel formation coinciding with the second insolation peak of the interglacial period, makes it difficult to align MIS 11 and MIS 1 with respect to the deglaciation. The degree of orbital analogy between MIS 11 and MIS 1 was clearly insufficient to force analogous climatic trends during the two interglacials that could be used to predict the future development of the Holocene without human impact. The alignment of the two interglacial periods based on sapropel formation as proposed here identifies a significant asymmetry between the two interglacials and highlights the anomalous length of MIS 11 as not necessarily representative of the course of the current interglacial.

Zusammenfassung

Das Marine Isotopen Stadium 11 (MIS 11, ca. 400 ka vor Heute), gilt als einer der Zeitabschnitte, der dem heutigen Interglazial im Bezug auf die orbitalen Parameter am nächsten kommt. Dies wurde oft als Anlass genommen, das Klima im MIS 11 zu untersuchen um daraus Rückschlüsse auf aktuelle und zukünftige Klimatrends zu ziehen. Die orbitalen Parameter während MIS 11 und die heutigen sind jedoch nicht exakt identisch, so dass aktuell intensiv diskutiert wird, in wie weit die beiden Stadien überhaupt tatsächlich direkt vergleichbar sind.

Die vorliegende Studie zeigt die erste detaillierte Untersuchung von MIS 11 im östlichen Mittelmeer. Hochauflösende Datensätze wurden für verschiedene paläoklimatologische Proxies an zwei marinen Sedimentkernen, GeoTü-SL96 (32°46'N, 19°12'E, 1399 m, größere Syrte) und ODP Site 964 (36°16'N, 17°45'E, 3658 m, östlich von Sizilien) erstellt. Ein zuverlässiges Altersmodel wurde mithilfe stabiler Isotopen, der Sapropele und signifikanter Änderungen in der Foraminiferenfauna entwickelt. Die Meeresoberflächentemperaturen wurden anhand von Transferfunktionen auf Basis von Faunenzusammensetzungen planktischer Foraminiferen an 404 Proben rekonstruiert und durch Alkenon Messungen an einem der Kerne ergänzt.

Beide Kerne zeigen typische Warmzeitverhältnisse im MIS 11 erst nach der Sapropelbildung, welche mit dem zweiten Insolationsmaximum nach Termination V zusammenfällt. Der Sapropel in MIS 1 fällt im Gegensatz dazu mit dem ersten Insolationsmaximum nach der letzten Eiszeit zusammen. Ein Vergleich der beiden Isotopenstadien ab der Sapropelbildung scheint die beste Möglichkeit zu sein, die beiden Stadien direkt zu vergleichen. Die Position des Peaks in der Sauerstoffisotopie hin zu leichteren Werten im Kern GeoTü-SL96 fällt nicht mit einem deutlich erkennbaren Sapropel in der Sedimentfolge zusammen. Im Gegensatz dazu liegt im MIS 1 Abschnitt beider Kerne jeweils ein deutlich ausgeprägter Sapropel vor. Die verschiedenen Tiefen aus denen die beiden Kerne kommen erklären dieses Phänomen: in MIS 11 muss die Grenzschicht zwischen sauerstoffreichem und sauerstoffarmen Wassern tiefer gelegen haben als zur Zeit der Bildung des Sapropels in MIS 1. Zusätzlich dazu zeigen die sehr leichten Isotopenwerte in ODP Site 964 im entsprechenden Zeitabschnitt einen extrem erhöhten Eintrag von Frischwasser durch vermehrte Monsunaktivität und/oder einer Öffnung zum schwarzen Meer.

Der Abgleich der beiden Sapropele von MIS 11 und MIS 1 lässt eine scheinbar verzögerte Reaktion des pelagischen Systems auf das Ende der Kaltzeit erkennen. Der Zeitraum im MIS 11 vor dem Sapropel ist gekennzeichnet durch glaziale planktonische Foraminiferenvergesellschaftungen und kältere Alkenon Temperaturen. Benthische Foraminiferenhäufigkeiten und Ba/Ca Verhältnisse lassen zudem eine hohe Produktivität für den entsprechenden Zeitraum vermuten. Das wahrscheinlichste Szenario für die verzögerte Reaktion, die in starkem Kontrast zu den globalen Entwicklungen und auf Pollen basierenden Ergebnissen aus der Mittelmeerregion steht, ist hohe Produktivität im Winter mit relativ kühlen und feuchten Bedingungen, angetrieben von erhöhtem Eintrag terrestrischen Materials, wodurch sich eine glaziale Vergesellschaftung planktonischer

Foraminiferen halten konnte und die Alkenone bis zur Bildung des MIS 11 Sapropels das Signal der kalten Jahreshälfte widerspiegeln.

Die Vergesellschaftungen planktonischer Foraminiferen zeigen im weiteren Verlauf von MIS 11 drei auffällige Phasen, die mit Faunen in verschiedenen jüngeren Sapropelen verglichen werden können. Da diese drei Phasen mit Insolationsmaxima und niedrigen Ba/Ca und Fe/Al Verhältnissen im Sediment zusammenfallen, scheinen sie mit orbital gesteuerten Saisonalitätsmaxima und starker Stratifizierung der Wassersäule und niedriger Produktivität, und daher fehlender Sapropele, zusammenzuhängen. Zusätzlich dazu bleiben die Vergesellschaftungen planktonischer Foraminiferen im späteren MIS 11 dominiert von der tropischen/subtropischen Art *G. ruber*, mit Höchstwerten im späten MIS 11/frühen MIS 10. Dieses Muster lässt sich erklären durch außergewöhnlich hohe Temperaturen während dieses Zeitabschnittes, kombiniert mit sehr niedriger Produktivität.

Während der Bearbeitung der Proben fielen Unregelmäßigkeiten in Form und Größe von *G. ruber* auf und führten zu der Definition von vier verschiedenen Morphotypen innerhalb dieser Art. Die Häufigkeiten dieser Morphotypen variieren deutlich zwischen Glazialen und Interglazialen und in drei dieser Morphotypen konnten signifikante Unterschiede in den stabilen Isotopenverhältnissen festgestellt werden. Da diese systematisch sind und oft mehr als 1 ‰ betragen, ist ein besseres Verständnis der Morphotypen von großer Bedeutung für die Interpretation von allen auf *G. ruber* basierenden paläozeanografischen Proxies.

Die scheinbar verzögerte Reaktion des Systems im frühen MIS 11 im Verhältnis zu globalen Entwicklungen erschweren einen Abgleich von MIS 11 und MIS 1 bezüglich des Endes der jeweiligen Kaltzeit. Das Ausmaß der Ähnlichkeit der orbitalen Parameter beider Zeitabschnitte war definitiv zu gering um absolut vergleichbare klimatische Entwicklungen hervorzurufen. Der auf Sapropelen beruhende Abgleich beider Interglaziale legt eine deutliche Asymmetrie zwischen beiden Zeitabschnitten offen und stellt die abnormal lange Dauer von MIS 11 als nicht unbedingt repräsentativ für das heutige Interglazial dar.

1. Introduction

1.1. Marine Isotope Stage 11

The study of past interglacials is potentially useful to understand the natural trends during warm periods of earth's history, such as the current interglacial, the Holocene. However, each of the nearest interglacials was different (Tzedakis, 2009) precluding an insightful comparison with the Holocene. The magnitude and influence on climate development of anthropogenic factors are subject of ongoing, controversial discussion, ranging between suggestions of a long warm future (BERGER & LOUTRE, 2002; LOUTRE & BERGER, 2003) and an already overdue glaciation (RUDDIMAN, 2003, 2007; RUDDIMAN et al., 2005; ROHLING et al., 2010). Of the last four interglacials, the peak interglacial MIS 5e was significantly warmer than the present-day climate due to a different orbital configuration (ROHLING et al., 2004); the peaking interglacial conditions at the onset of MIS 7c did not last long enough to allow for meaningful comparison with the Holocene (LISIECKI & RAYMO, 2005A; 2005B) and the orbital configuration of MIS 9 is not comparable with the Holocene either. In terms of greenhouse gas concentrations, MIS 9 shows some similarities with pre-anthropogenic conditions (RUDDIMAN, 2007; 2008), but the dissimilarity of the orbital configurations and the shorter duration (LISIECKI & RAYMO, 2005A, 2005B) make it an unlikely candidate for comparisons with the Holocene.

The periodic reoccurrence of orbital parameters with long periodicities leave MIS 11 as the most promising candidate for studies of natural interglacial variability and a comparison with the Holocene (e.g. BERGER & LOUTRE, 2003; DROXLER et al., 2003 and references therein). Due to a minimum in the long 400 ka eccentricity cycle (e.g. MILANKOVITCH, 1941; IMBRIE AND IMBRIE, 1980; HOWARD, 1997), the orbital configuration and the associated insolation patterns during MIS 11 appear also to have been most analogous with the Holocene (LOUTRE & BERGER, 2003; fig. 1). This could allow evaluating natural future climate development in the absence of anthropogenic influence. Based on orbital tuning of ice-volume signals in deep-sea sediments, the interglacial MIS 11 is assumed to have occurred between 428 to 362 kyr B.P. (IMBRIE et al., 1984; KARNER & MARRA, 2003; LISIECKI & RAYMO, 2005A, 2005B). Existing records indicate that MIS 11 was unusually warm and exceptionally long, spanning three precession cycles (HOWARD, 1997; DROXLER & FARRELL, 2000; LISIECKI & RAYMO, 2005A, 2005B; JOUZEL et al., 2007; LUETHI et al., 2008; ROHLING et al., 2009). Statistical and modelling approaches show that, in terms

of orbital parameters resulting in glacial-interglacial forcing insolation patterns, MIS 11 is so far the best known analogue to the present day climate in comparison with other related interglacials (BERGER & LOUTRE, 1991; LOUTRE, 2003; LOUTRE & BERGER, 2003).

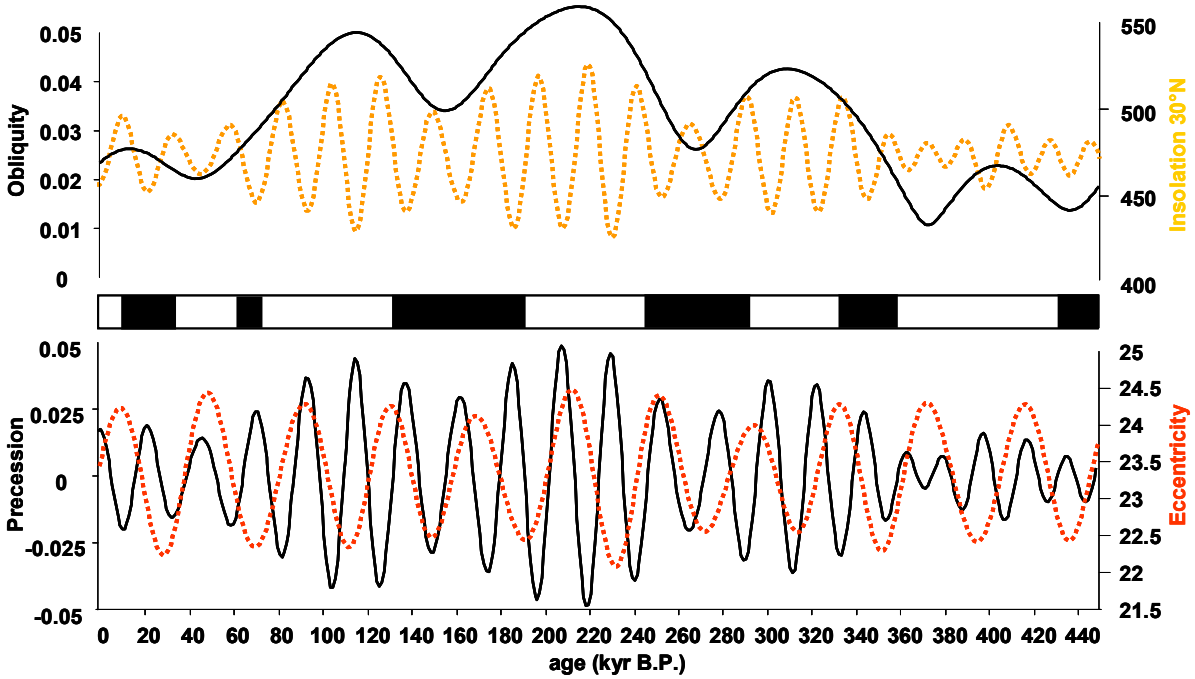

Figure 1: Orbital parameters for the last 450 ka: Obliquity (upper black line), precession (lower black line), summer insolation 30°N (upper dotted line; BERGER & LOUTRE, 1991), eccentricity (lower dotted line), black and white bars indicate MIS boundaries (LISIECKI & RAYMO, 2005).

A special problem of MIS 11 climate trends, called the MIS 11 paradox (BERGER & WEFER, 2003), however, casts doubt on the validity of the orbital analogy: The transition from MIS 12 to MIS 11 is characterised by an unusually high amplitude, perhaps the largest change observed in the glacial records for the last 3 My (e.g. JANSEN et al., 1986; KARNER et al., 2002), but also by the lowest orbital forcing of the five last glacial terminations. For this glacial transition, the link with insolation is so weak that for example the Devil's Hole record (WINOGRAD et al., 1992) has been interpreted as suggesting a decoupling of insolation and climate change, with Termination II preceding orbital forcing by over 10 ka. Along with the long duration of MIS 11, the exceptionally low insolation forcing of Termination V (BERGER & LOUTRE, 1991) and the complex climate evolution during Termination I impede the alignment of the onset of the Holocene and the MIS 11 climate optimum (LOUTRE & BERGER, 2000, 2003; EPICA COMMUNITY MEMBERS, 2004; BROECKER & STOCKER, 2006; CRUCIFIX & BERGER, 2006; RUDDIMAN, 2006A, 2007; DICKSON et al., 2009; ROHLING et al., 2010). BERGER & WEFER (2003) explained the characteristics of MIS 11 with the exceptionally cold MIS 12, which must have been followed by an extremely warm

interglacial due to ice-sheet feedback. Following this reasoning, however, MIS 11 should have been shorter.

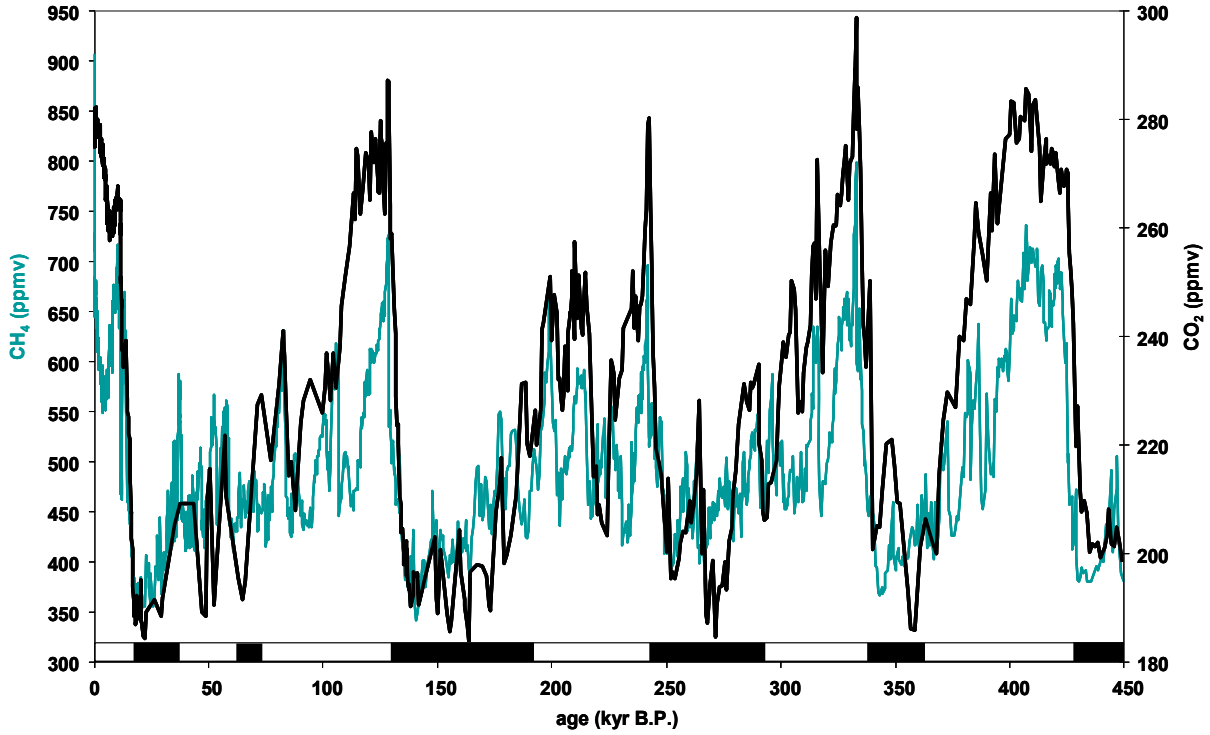

Figure 2: Atmospheric concentrations of the greenhouse gases CO_2 (LUETHI et al., 2008) and methane (LOULERGUE et al., 2008) for the last 450 ka as measured in Antarctic ice cores. White and black bars indicate MIS boundaries (LISIECKI & RAYMO, 2005).

Since insolation alone does not appear sufficient to explain the duration and intensity of MIS 11, CO_2 concentrations during MIS 11 (fig. 2) have been invoked as an explanation for the MIS 11 paradox (e.g. SARMIENTO & LEQUERE, 1996; HOWARD, 1997; DROXLER et al., 1999, 2000, 2003; BERGER & WEFER, 2003). MC MANUS et al. (2003) highlighted that the nearly ice free chapter of MIS 11 lasted longer than those of other interglacials of this time interval, nearly 30.000 years after termination V. This is considered to be controlled by the eccentricity modulation of precession: low eccentricity leads to a dampening of the precessional variations, resulting in the absence of extensive cold sub stages (BERGER & LOUTRE, 1991; MCMANUS, 2003; DE ABREU et al., 2005). CO_2, known as a major climate-driving atmosphere component, turned out to have shown a long period of high concentrations (data Epica Dome Concordia ice core) during peak interglacial MIS 11 (PETIT et al., 1999; EPICA COMMUNITY MEMBERS, 2004; SIEGENTHALER et al., 2005, RUDDIMAN, 2007, 2008), but not the highest among all Quaternary interglacials (RAYNAUD et al., 2005), as well as in the pre-industrialised Holocene (MONNIN et al., 2001, RUDDIMAN, 2007) some 200 years ago. LOUTRE & BERGER (2003) and RUDDIMAN (2007) speculated that the warm oceans of MIS 11 absorbed less CO_2, and reduced productivity in equatorial regions left

large amounts of the greenhouse gas in the atmosphere. Additionally, massive barrier-reef build-up in shelf areas favoured by sea-level high stands released large amounts of CO_2 to the atmosphere (HOWARD & PRELL, 1994; SARMIENTO & LEQUERE, 1996). A modelling approach by KIM & CROWLEY (1994) found that non-anthropogenic CO_2 emissions alone would have reached the critical level in the Holocene to attenuate the influence of the 100 ka Milankovich cycle, producing an exceptionally prolonged and warm interglacial period even without human influence. The settings mentioned above suggest that MIS 11 was sufficiently warm and long-lasting to melt the West Antarctic ice sheet (SCHERER, 2003; SCHERER et al., 1998) and the Greenland ice sheet (LOUTRE, 1995).

The magnitude of ice covering during MIS 11, resulting in changing sea levels, is, however, controversial. On the one hand, sea-level high-stand deposits in Great Britain indicate a sea level about 13 m ± 2 m higher than today (BOWEN, 2003), and other authors suggested sea levels equal or up to 20 m higher than today for low latitudes (e.g. ORTLIEB et al., 2003) and for high latitudes (BRIGHAM-GRETTE, 2009). On the other hand, RAYNAUD et al. (2003) and RUDDIMAN (2006B) suggested ice-volume levels for the comparable time interval similar to present-day ones, which is also supported by stable isotopic data from Red Sea sediments (ROHLING et al., 2009, 2010). Also, in respect to the presumed large sea level differences, global oxygen isotope values are not sufficiently depleted in the heavy isotope ($\delta^{18}O$) during MIS 11, which has often been explained by cooler ocean temperatures than today (E.G. DROXLER et al., 2003). Alternatively, the low oxygen isotopic values might, indeed, rather reflect lower sea-level and larger ice volume than generally assumed (BECQUEY & GERSONDE, 2002; RAYNAUD et al., 2003), a lower salinity (LEA et al., 2003), or a combination of both.

From the subpolar and polar north Atlantic, HELMKE et al. (2003) reported similar boundary conditions for MIS 11, MIS 5.5 and MIS 1, characterized by a strong reduction of ice-rafted debris (IRD) and a high carbonate bioproduction. SST reconstructions in the western equatorial Pacific for MIS 11 show the warmest interglacial temperatures during the last 450 ka, up to one degree warmer than other interglacials during this time interval (LEA et al., 2000, 2003; ORTLIEB et al., 2003; OBA & BANAKAR, 2007). Studies off the Iberian margin found temperatures of MIS 11 not significantly different to those observed in the elapsed portion of the Holocene and came to the conclusion that, in this area, MIS 11 is comparable to the Holocene in terms of orbital parameters and CO_2 concentrations (DEABREU et al., 2005; MARTRAT et al., 2007). BECQUEY & GERSONDE (2002) found temperatures exceeding present-day values only during the MIS 11 climatic optimum in the Southern Ocean. In most

oceanic records (e.g. MCMANUS et al., 2003; BAUCH & ERLENKEUSER, 2003; HODELL et al., 2003), MIS 11 temperature optimum lasted longer than the other interglacials, but sea surface temperatures were only slightly higher or similar to the Holocene.

Continental records of MIS 11 do not fully match the oceanic data. Some studies based on continental records found warmer temperatures for MIS 11 (ROUSSEAU, 2003; KARABANOV et al., 2003), whereas, at other localities, the estimated temperatures were similar or even cooler than the Holocene ones (VIDIC et al., 2003; KUKLA, 2003). In some continental records, MIS 11 ended abruptly due to changes in the climate of continental Asia (KARABANOV et al., 2003). Data on pollen abundances in marine cores (DESPRAT et al., 2005; DE VERNAL & HILLAIRE-MARCEL, 2008) also appear to show considerable differences in the timing of the response of terrestrial vegetation to global forcing, indicating a strong regional modulation.

Further, in the absence of independent stratigraphic markers, marine, terrestrial and ice-core MIS 11 records have normally been correlated by tuning to an orbital time scale, potentially introducing a circular argument in the interpretation of MIS 11 climate trends. In the Eastern Mediterranean, the development of sapropel layers is known to have occurred in pace with insolation forcing (e.g. EMEIS et al., 2000), potentially providing independent means for dating and stratigraphic correlation, as well as for alignment of MIS 11 climate trends with younger, well-studied Mediterranean sapropel events (DELANGE et al., 2008; ROSSIGNOL-STRICK, 1983). Therefore, the Mediterranean is a particularly promising region to study the relationship between regional climate and insolation forcing during MIS 11 and its comparison with MIS 1 trends.

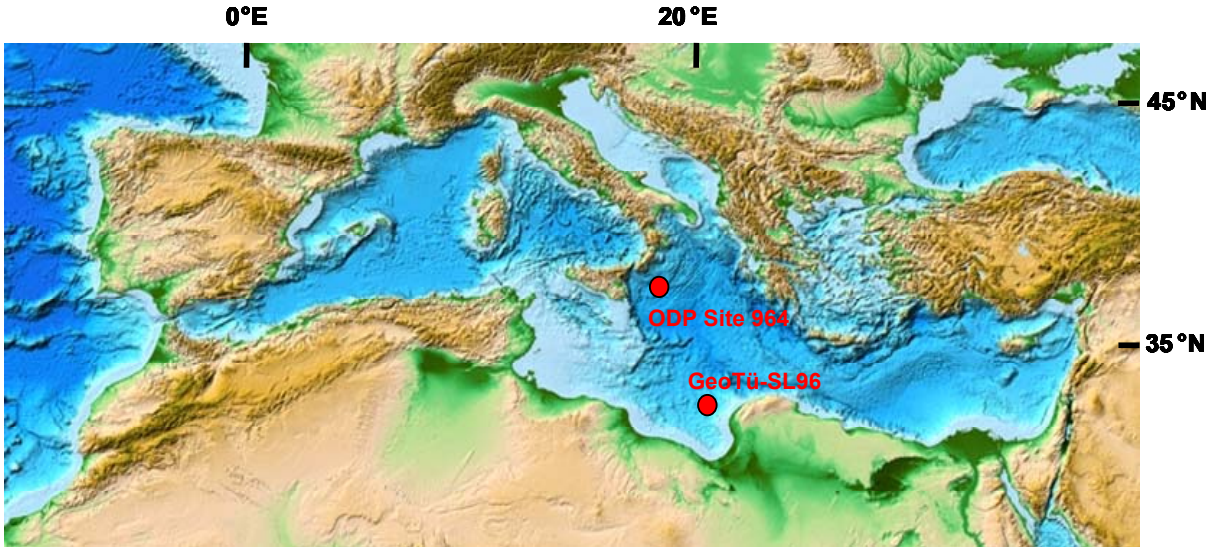

Figure 3: Combined topographic and bathymetric map of the Mediterranean Sea, including the Black Sea and a part of the north Atlantic (ETOPO 1 Global Relief Model; AMANTE & EAKINS, 2008); sediment cores studied in this thesis are indicated by circles.

The high resolution record from the Eastern Mediterranean Sea presented herein derives from two deep sea sediment cores (GeoTü-SL96: 32° 46'N, 19° 12'E, 1399 m; ODP Site 964; 36° 16'N, 17° 45'E′; fig.3) investigating MIS 12 to MIS 9 and MIS 2 to MIS 1. It is the first attempt to assess MIS 11 trends in the Eastern Mediterranean Sea on a sub-millennial scale. The main goal is to find to what degree MIS 11 and MIS 1 are comparable in terms of temperature trends and duration in this area. The Eastern Mediterranean Sea was so far not a preferred area of MIS 11 investigations due to the lack of knowledge of suitable core material. However, the importance of the Mediterranean region at least for southern European climate is evident. Sapropel layers and oxygen isotopes provide an opportunity to develop an independent and reliable age model. Here, it was taken advantage of this potential, determining the position of the sapropel event within MIS 11 and using the resulting insolation alignment to compare regional climate trends with global records on one hand, and with Holocene patterns on the other hand.

1.2. The Mediterranean Sea – a natural climate laboratory

The Mediterranean Sea is an excellent area to evaluate responses of a marine ecosystem to climate change. The semi-enclosed basin has a limited connection to the world ocean and is surrounded by topographically and climatically diverse continental regions, supplying different types of terrigenous sediment (e.g. CALVERT & FONTUGNE, 2001; LARRASOAÑA et al., 2008). Furthermore, the region occupies an interesting position at the boundary between subtropical and mid/high latitude climate systems, making it highly sensitive to even subtle fluctuations (e.g. HAYES et al., 1999; SCHMIEDL et al., 2004; KUHNT et al., 2007, 2008; MILKER et al., 2009; ZIEGLER et al., 2010). Finally, it is very important to estimate and predict ecosystem changes, and to assess the role of anthropogenic influence in this region because of the high population density. Variations in climate in this region have impacts felt throughout Europe, Africa and the Middle East.

Especially the Eastern Mediterranean provides ideal conditions for high resolution investigations of MIS 11 and other interglacials due to the excellent correlation opportunities, low bioturbation (LOEWEMARK et al., 2006) and sedimentation rates in the basin, allowing sub-millennial resolution (sedimentation rate 1.8 to 6.3 cm/kyr sediment in the here presented cores; EMEIS et al., 1996; EMEIS & SAKAMOTO, 1998; KROON et al., 1998; SAKAMOTO et al., 1998). The repeated occurrence of dark organic rich layers (sapropels) in the sediment record, deposited at the beginning of most interglacial periods in the Eastern

Mediterranean region, facilitates excellent correlation among sediment records within the basin (SAKAMOTO et al., 1998; EMEIS et al., 2000, 2003; LOURENS, 2004). The construction of a sapropel-based astronomical timescale for the Mediterranean Sea has started with the pioneering work of ROSSIGNOL-STRICK (1983), who attributed sapropel formation to African monsoon, which, in turn, depends on the orbital configuration and changes in the wind system over NW Africa (e.g. ZIEGLER et al., 2010).

1.2.1. Oceanography and bathymetry

The Mediterranean Sea is divided into two major basins separated by the shallow sill of the Strait of Sicily (fig. 3). The Eastern basin can be divided into two major regions, the western Ionian basin and the eastern Levantine basin. The Mediterranean Sea is a

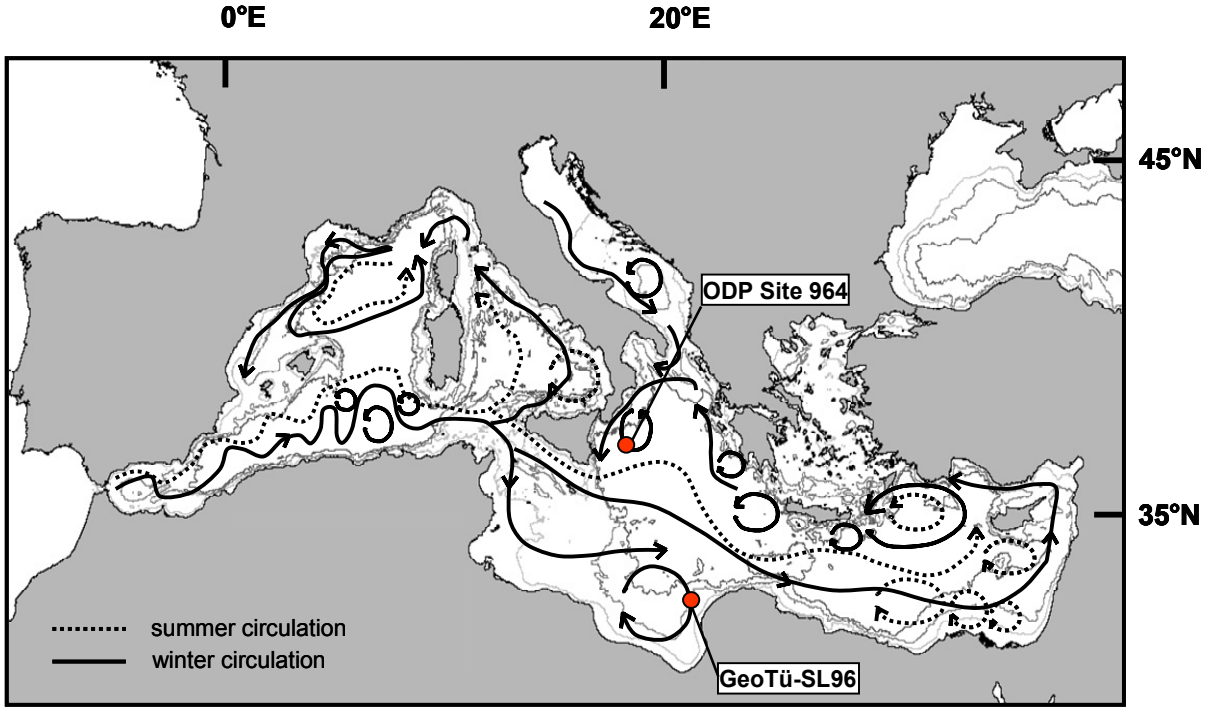

Figure 4: Map of the Mediterranean Sea with schematic illustration of major basin current and gyre systems and their seasonal variability (PINARDI & MASETTI, 2000). Dashed lines denote summer circulation, black lines winter circulation. Red circles denote position of the studied cores.

concentration basin: evaporation exceeds precipitation and runoff (HECHT et al., 1988; PINARDI & MASETTI, 2000; fig. 4). The excess evaporation leads to high salinities at the surface which, after cooling in winter, drive the formation of intermediate water in the Levantine Basin and deep water in the Adriatic and Aegean Sea (e.g. CITA et al., 1977; VERGNAUD-GRAZZINI et al., 1977; THEOCHARIS et al., 1999). As a result, three distinct water mass layers have been identified in the Mediterranean (LACOMBE & TCHERNIA, 1972; HECHT et al., 1988; PINARDI & MASETTI, 2000): the relatively cold (15°C) and low-salinity

(36.5-38.5 ‰) Atlantic Water (AW), entering from the Strait of Gibraltar in the upper approximately top 100 m of the water column; the high-salinity (≥ 38.5 ‰, which also corresponds to maximum surface water salinity) Levantine Intermediate Water (LIW), between 150 and 600 m depth, which is formed in the eastern Levantine basin, and the Eastern Mediterranean Deep Water (EMDW) filling the remaining deep parts of the basin (fig. 5) (BETHOUX, 1980; MALANOTTE-RIZZOLI & HECHT, 1988). The Atlantic surface waters

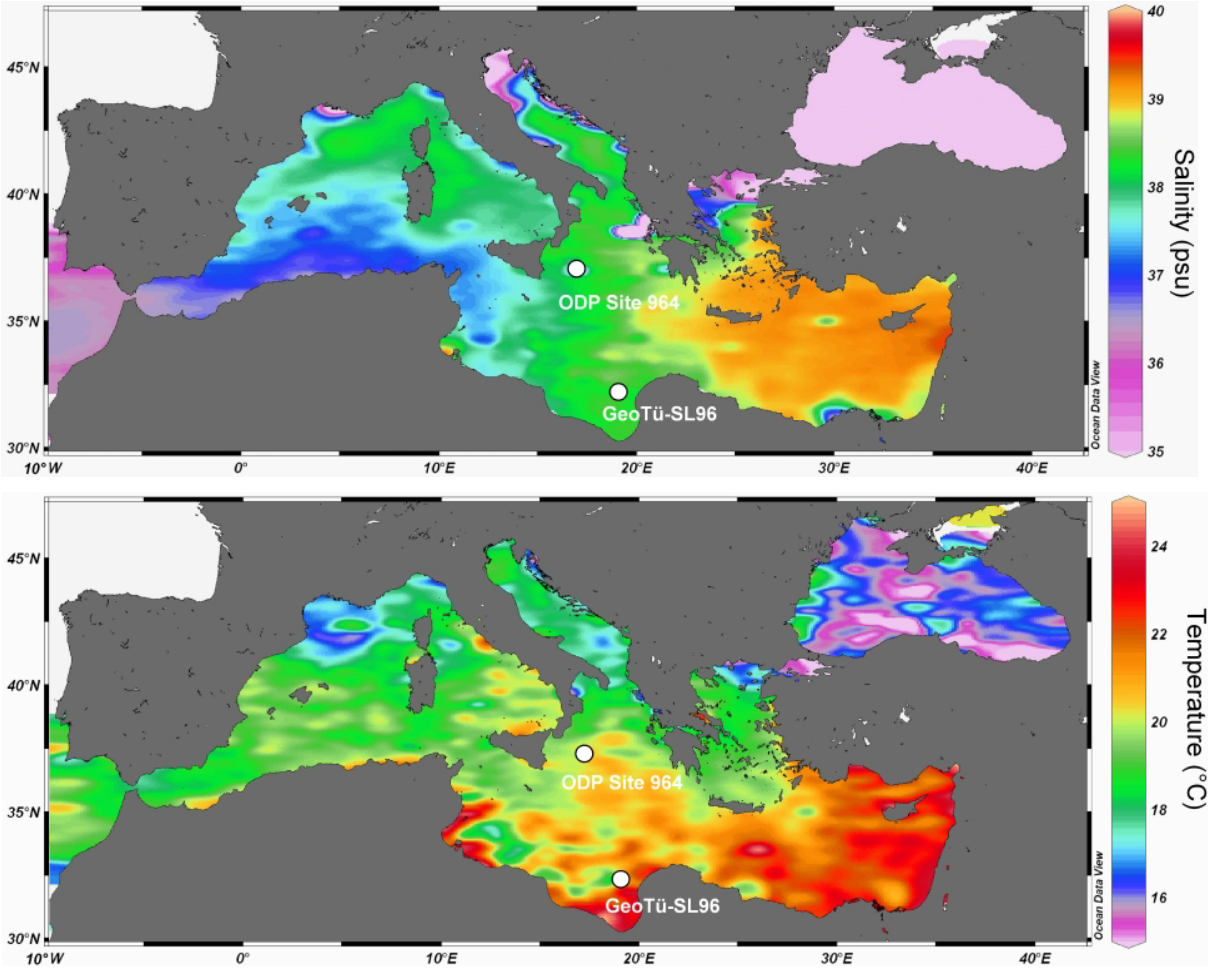

Figure 5: Mediterranean Sea surface (0-1 m depth, average values) salinity (upper panel) and temperature (lower panel; MEDAR Group, 2002).

drastically increase in salinity through evaporation in summer as they move eastwards. In the Adriatic and Aegean basins, Mediterranean deep water formation is driven through sinking of this high-salinity and thus denser water masses after their cooling in winter (fig. 6). In recent times, formation of the water masses in the Mediterranean Sea, especially of EMDW, changes seasonally (WUEST, 1961; LACOMBE & TCHERNIA, 1972; HECHT et al., 1988; PINARDI & MASETTI, 2000).

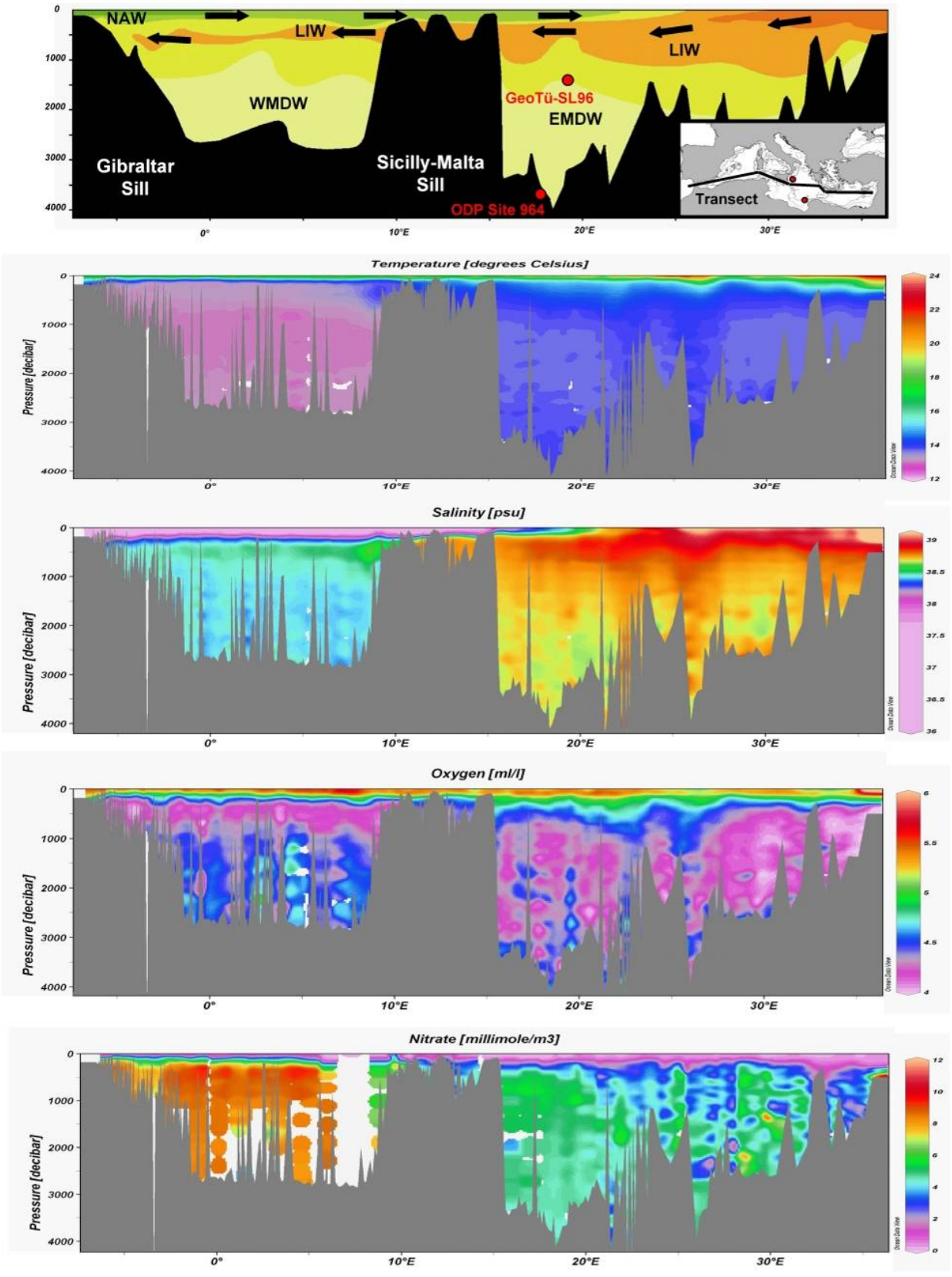

Figure 6: An E-W transect through the Mediterranean (position shown in inset map). The upper panel shows the schematic profile of the Mediterranean Sea, contouring lines denote different water masses as shown by salinity and temperature (NAW: North Atlantic Water; WMDW: Western Mediterranean Deep Water; LIW: Levantine Intermediate Water; EMDW: Eastern Mediterranean Deep Water) and the position of the investigated cores (modified after WUEST, 1961). The lower panels show average values of key oceanographic parameters taken from MEDAR Group, 2002.

Nutrient-depleted modified Atlantic Water enters the Mediterranean Sea through the Strait of Gibraltar, and becomes gradually saltier and warmer through evaporation while it flows eastwards (e.g. PINARDI & MASETTI, 2000). The outflowing intermediate water is more nutrient rich than the inflowing AW (fig. 6), which results in a negative nutrient balance and a widespread oligotrophy in the basin (BETHOUX et al., 1999).

The Eastern Mediterranean surface circulation generates several small-scale cyclonic and anticyclonic gyres and eddies which, due to atmospheric forcing (MALANOTTE-RIZZOLI et al., 1997; PINARDI & MASETTI, 2000) and the irregular topographic structures of the basin (POEM GROUP, 1992) are variable in intensity and location. The Libyan Sea, for instance, presents a local cyclonic gyre, the Cretan gyre (KARAGEORGIS et al., 2008; fig. 7).

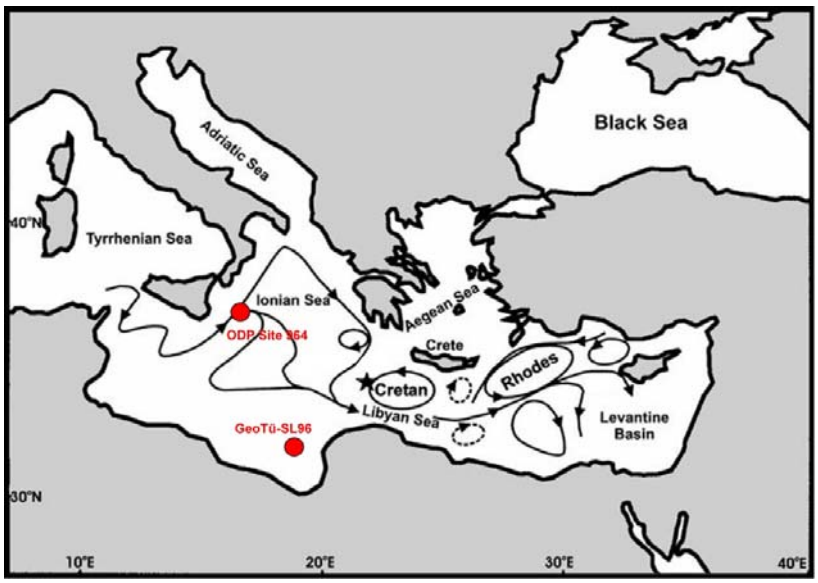

Figure 7: Eastern Mediterranean Sea surface circulation with names of the main gyral structures highlighted (modified after MALANOTTE-RIZZOLI et al., 1997).

This study is carried out between Sicily and the coasts of Libya. It is important to note that, despite their nearby position, the investigated cores of this study reflect different surface ocean conditions. The water masses above the site of core GeoTü-SL96 are dominated by the inflow of the modified Atlantic water (HECHT et al., 1988; PINARDI & MASETTI, 2000), whereas the central Ionian Sea is mainly influenced by the Eastern Mediterranean outflow at intermediate depths and Adriatic and Eastern Mediterranean waters at the surface (PINARDI & MASETTI, 2000).

1.2.2. History of the Eastern Mediterranean Sea

The Eastern Mediterranean basin is a remainder of the Mesozoic Tethys, which originated in the course of the disintegration of Pangaea, with the Eastern Mediterranean mainly influenced by Alpine tectonic evolution (DEWEY et al., 1973). The Eastern Mediterranean Sea forms a curved depression next to the southernmost deformation front of

the Alpine belt. The zone of interaction between the Anatolian, African and Arabian plate faces the easternmost end of the Mediterranean Sea (ROBERTSON, 1998). The Levant continental margin, Eastern Mediterranean, is usually defined as a passive margin that developed between the late Paleozoic and the early to mid-Mesozoic. This margin is thought to be composed of two segments with different structural characteristics. The southern segment (south of the Carmel Structure) was formed by rifting, whereas the origin of the northern segment remains unknown so far (SCHATTNER & BEN AVRAHAM, 2007).

1.2.3. Climatology

The Mediterranean region lies between the climatic system influenced by the North Atlantic Oscillation and the North African monsoon system (THUNELL et al., 1977; MARINO et al., 2009). Present-day climate conditions in the Eastern Mediterranean Sea in particular are mainly controlled by semi-arid climate conditions in Africa, the Arabian Peninsula and

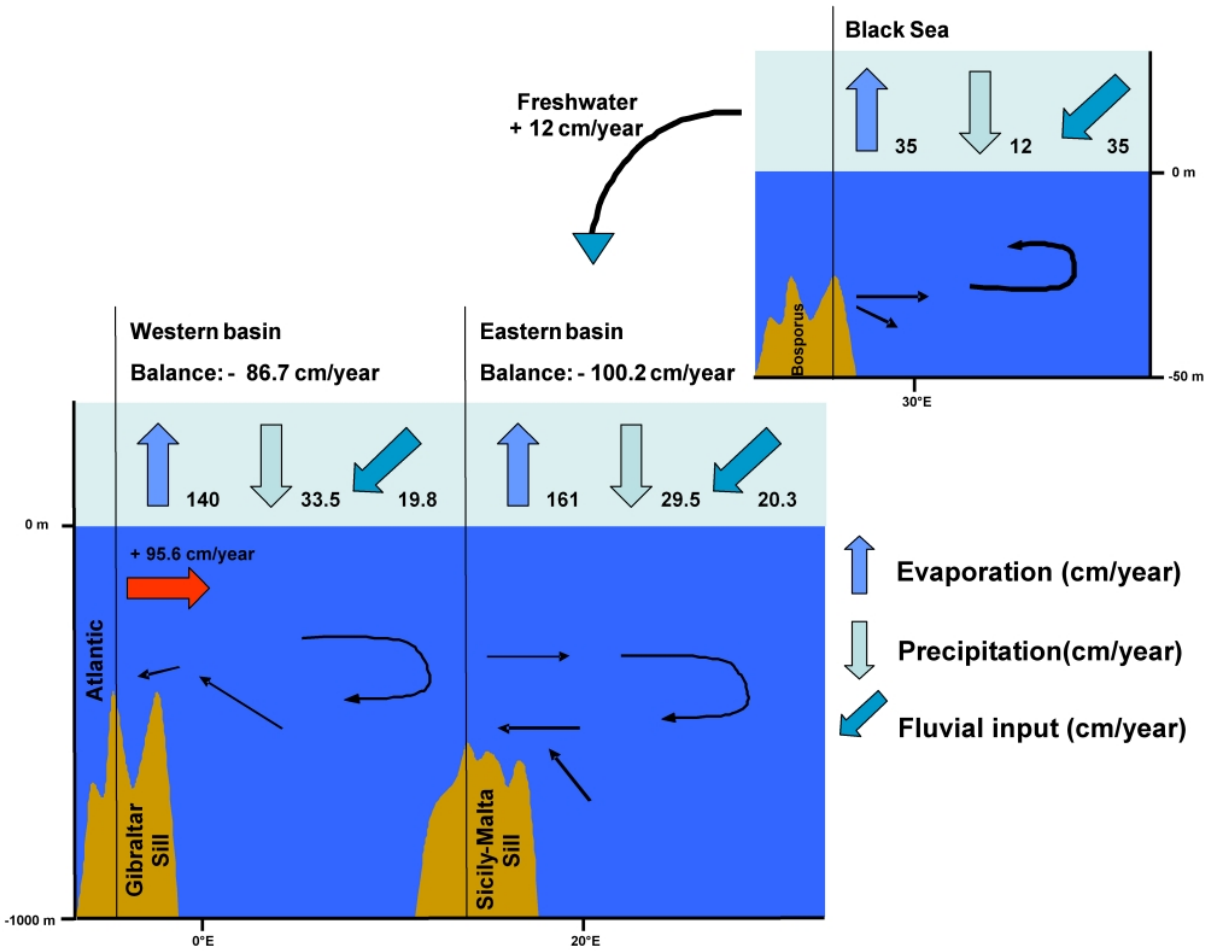

Figure 8: Hydrological budget of the Mediterranean Sea and the Black Sea (modified after BETHOUX AND GENTILI, 1999; HOFRICHTER et al., 2002).

the Near East, resulting in increased evaporation, and by fluctuations of the Intertropical Convergence Zone and the monsoon/ENSO/Indian Ocean dipole system (e.g. SAJI & YAMAGATA, 2003). (fig. 8). Winter air temperatures in the Eastern Mediterranean region range between 12 °C in the Greek archipelago and 16°C in the soutern part of the basin. In summer, air temperatures range between 24 °C in the northern part of the basin and a maximum value of 35 °C in the northeastern part of the basin between Turkey and Cyprus, corresponding to the highest temperatures measured in the entire Mediterranean region (HOFRICHTER et al., 2002).

Precipitation in the Eastern Mediterranean region is very low in general and almost entirely restricted to the winter half of the year. It ranges between annual means of 1071 mm in Antalya and 25 mm in Port Said, following a northward increase in precipitation (HOFRICHTER et al., 2002). The Eastern Mediterranean region is dominated by northwestern to northern winds. Coupled with high evaporation rates, wind stress initiates the anti-estuarine circulation (see section 1.2.1.) throughout the Eastern Mediterranean basin.

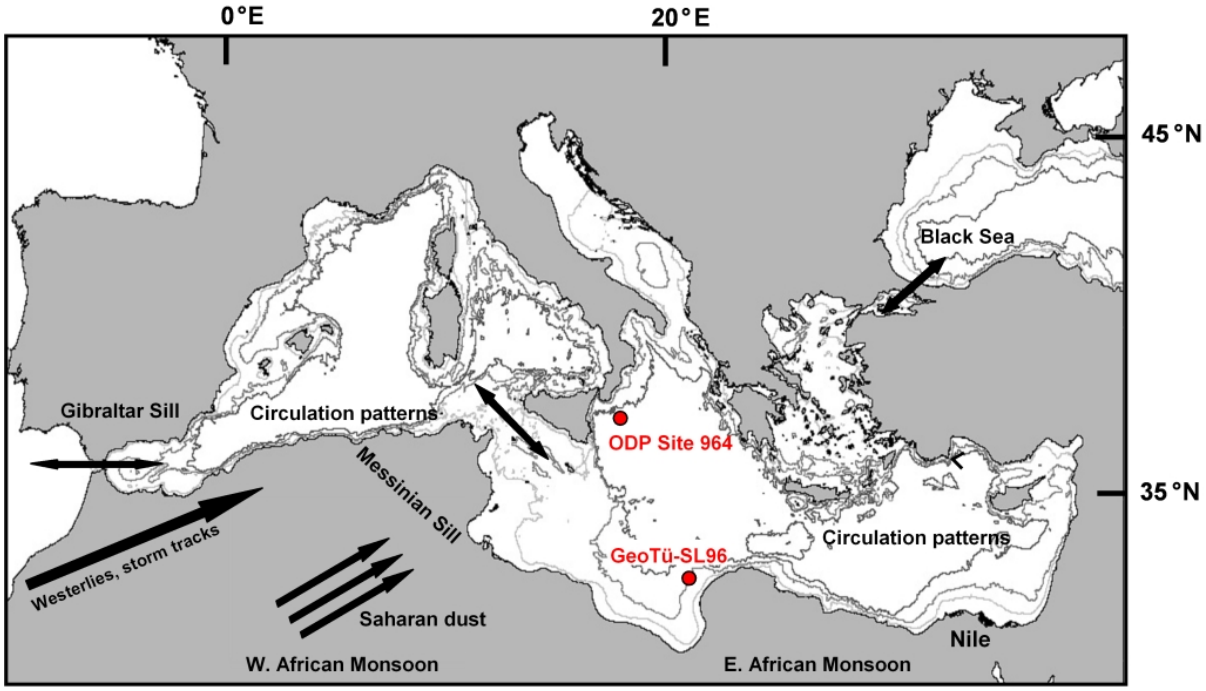

Figure 9: Map schematically illustrating selected influences on Mediterranean oceanography and climate processes; circles denote cores of this study.

River discharge into the Eastern Mediterranean basin mostly occurs through the Nile and the Po Rivers. However, monsoonal maxima over North Africa, driven by astronomical cyclicity, produced fluvial systems of enormous size, which repeatedly manifolded the freshwater inflow to the Mediterranean Sea in Earth history (e.g. ROHLING et al., 2002; fig. 9).

1.2.4. Sapropel development

Eastern Mediterranean sediments are periodically pervaded by dark organic rich layers, known as sapropels (e.g. EMEIS & SAKAMOTO, 1998; EMEIS et al., 2000). The name sapropel is a contraction of ancient Greek words *sapros* and *pelos*, meaning putrefaction and mud, respectively. The word sapropel was created as a synonym for the german word "Faulschlamm" by POTONIÉ & KOERBER (1904).

The first hypothesis of possible existence of these layers was formulated by BRADLEY (1938). The Swedish Deep-Sea Expedition first discovered the expected dark organic rich layers in Eastern Mediterranean sediment cores (KULLENBERG, 1952), later termed as sapropelic layers (OLAUSSON, 1961).

Literature regarding sapropels is very abundant (NEGRI et al., 2009), and various hypotheses were forwarded to explain the formation of sapropels. While initial ideas highlighted stagnation as the driving factor behind sapropel formation (e.g. OLAUSSON, 1961; CAPOZZI & NEGRI, 2009 and references therein), enhanced primary production in the photic zone was soon forwarded as the principle cause of sapropel deposition (e.g. CALVERT, 1983). The current leading explanation draws on two observations: sapropel deposition appears to be associated with strong insolation maxima, and oxygen isotopes in planktonic foraminifera across the sapropels indicate a significant influx of freshwater (CAPOZZI & NEGRI, 2009). The recurrence of sapropels is related to Milankovitch precessional cycles (e.g. ROHLING & GIESKES, 1989; ROHLING & HILGENS, 1991; ROHLING, 1994). Sapropel formation in the Eastern Mediterranean is clearly driven by increased monsoonal precipitation during precessional minima, resulting in enhanced runoff to the Mediterranean (ROSSIGNOL-STRICK, 1983, 1985; ROSSIGNOL-STRICK & PATERNE, 1999; ROSSIGNOL-STRICK et al., 1982). At the

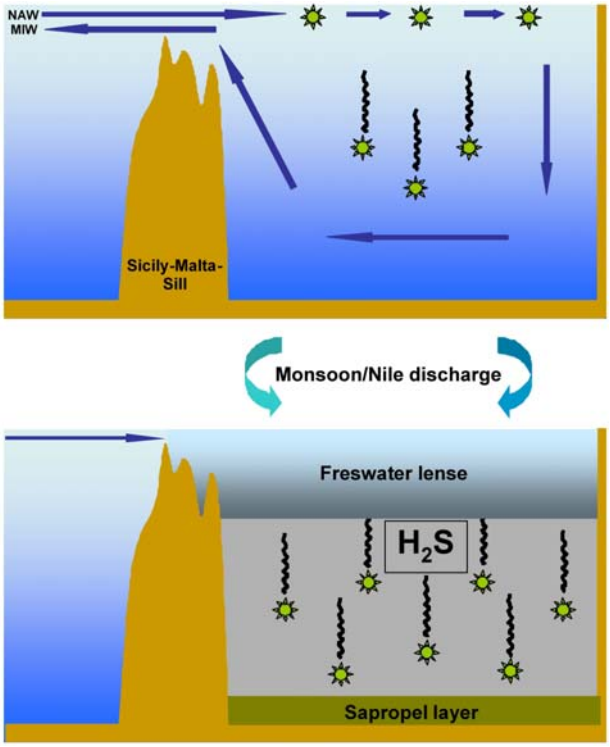

Figure 10: Eastern Mediterranean Sea sapropel development scheme; upper panel shows normal circulation; lower panel shows conditions during sapropel formation phase.

beginning of sapropel formation, enhanced freshwater inflow reduces the excessive evaporation, which inhibits the formation of the LIW and the formation and sinking of more dense water masses (fig. 10). As a result, the Eastern Mediterranean becomes unventilated from mid-depths down to the bottom. Strong and continuous stratification allows organic material to permanently sink to the ground (e.g. ROSSIGNOL-STRICK, 1983; ROHLING, 2001; LOEWEMARK et al., 2006). In the near absence of oxygen, organic matter is preserved, and deposited in the form of dark, organic-rich layers in the sediment.

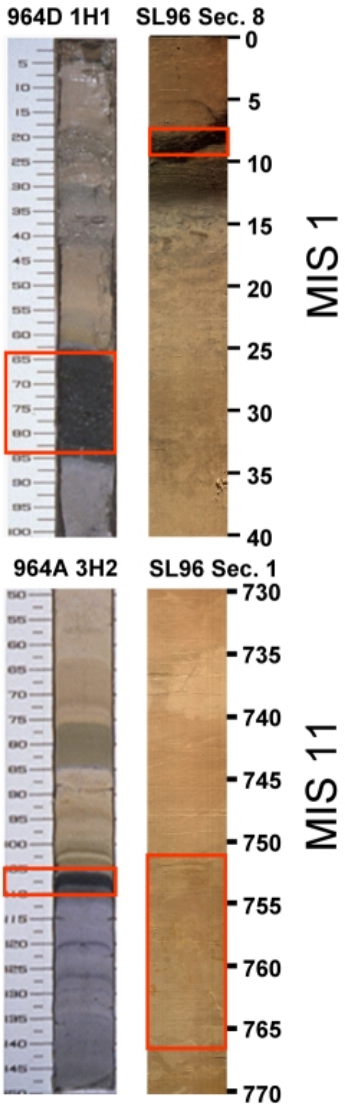

Figure 11: Upper left panel shows Holocene part of ODP Site 964, sapropel indicated by red box; lower left panel shows MIS 11 sapropel (box, EMEIS et al., 1996); right upper panel shows Holocene part of GeoTü-SL96, red box denotes sapropel; lower panel shows MIS 11 area of light oxygen isotope peak, denoted by red box (pictures GeoTü-SL96: U. van Raden).

The last Sapropel (S1, fig. 11; tab. 1), centred at ca. 8 kyr B.P., coincides with a strong freshwater supply to the Mediterranean region (e.g. FONTES & GASSE, 1991; CALLOT & FONTUGNE, 1992; ZANCHETTA et al., 2007) and enhanced monsoon activity (ROHLING et al., 2002). Additionally, an enhanced freshwater flux from the Bosporus may have played a role in the formation of sapropel S1 (LANE-SERFF et al., 1997; SPERLING et al., 2003; VIDAL et al., 2010). The oligotrophic freshwater layer covers deeper water masses with high productivity during sapropel formation. The high productivity in the deeper layer is possible due to specialised diatoms, which are able to exploit nutrients trapped in deeper parts of the water column (KEMP et al., 1998, 1999). Since the late Pleistocene, sapropels occur throughout the whole area of the Eastern Mediterranean.

Table 1: Geochemical and lithological records of MIS 1 and MIS 11 sapropels in investigated sediment cores.

Sapropel	ODP Site 964				GeoTü-SL96			
	Sapropel thickness (geochem, cm total)	Oxidised (cm)	Mn/Al peak	Ba/Al peak	Sapropel thickness (geochem, cm total)	Oxidised (cm)	Mn/Al peak	Ba/Al peak
MIS 1	28	8	y	y	6	3,6	y	y
MIS 11	10	5	n	y	------	------	n	n

1.3. Paleoceanographic methods in the Mediterranean Sea

Reconstruction of past environmental and in particular oceanographic conditions can be achieved through a variety of geochemical and palaeontological methods and proxies. The semi-isolated nature of the Mediterranean water body combined with strong gradients in surface water properties present a challenge to standard palaeoceanographical proxy methods (FERGUSON et al., 2008; CASTANEDA et al., 2010). This is particularly the case in the Eastern Mediterranean, which is characterised by extreme oligotrophy and surface salinities substantially exceeding those in the open ocean (fig. 5, 6). Despite these limitations, geochemical proxies based on analyses of foraminiferal shell calcite, organic biomarkers in sediments, geochemistry of the sediment and micropalaeontological proxies have been nevertheless successfully used to reconstruct surface and deep ocean palaeoceanography of the Mediterranean as well as patterns of sediment delivery and redox-related element cycling (e.g. CACHO et al., 1999, 2000, 2002, 2006; ROSSIGNOL-STRICK & PATERNE, 1999; KUHNT et al., 2007, 2008; ROHLING et al., 2007).

1.3.1. Oxygen and carbon isotopes

Analysis of stable oxygen and carbon isotopes in foraminiferal calcite has been the backbone of palaeoceanography for many decades (e.g. EMILIANI, 1955). Stable isotopic composition of planktonic foraminiferal shells is one of the most important sources of information in Quaternary stratigraphic and palaeoenvironmental reconstructions (e.g. EMILIANI, 1955; SHACKLETON, 1967; RAVELO & HILLAIRE-MARCEL, 2007). Individual species of planktonic foraminifera show distinct depth habitats, seasonal production maxima as well as biological lifestyles (e.g. presence or absence of symbionts), and these differences are all reflected in the isotopic chemistry of their shells (BÉ, 1982; GANSSEN & KROON, 2000; LIN & HSIEH, 2007). Therefore, separate isotopic data from single species are required for meaningful palaeoenvironmental interpretations. Recent work on *G. ruber* (white), the most commonly used palaeoenvironmental indicator in tropical and subtropical regions, indicates a strong link between shell morphology and isotopic chemistry within this species (WANG, 2000; KUROYANAGI & KAWAHATA, 2004; LIN et al., 2004; KAWAHATA, 2005; LOEWEMARK et al., 2005; STEINKE et al., 2005). *Globigerinoides ruber* occurs in two colour variants (white and pink), which show significantly different stable isotopic signals (ROBBINS & HEALY-WILLIAMS, 1991; ROHLING et al., 2004) and distinct geographical

distributions (BÉ & HUTSON, 1977; BÉ, 1982). The white colour variety furthermore shows a remarkable morphological variation, which resulted in the definition of a range of species and subspecies within this form (D'ORBIGNY, 1826, 1839; VAN DEN BROECK, 1876; SAITO et al., 1981). Since morphological variability within this white variety appears rather continuous, it proved difficult to devise consistent criteria for differentiation between the individual types.

The oxygen isotopic ratio reflects the oxygen isotopic composition of the ambient seawater, modified by kinetic fractionation due to temperature, and a range of biochemical and microhabitat-related non-equilibrium processes (RAVELO & HILLAIRE-MARCEL, 2007). To evaluate global ice volume in the context of palaeoclimate reconstruction, stable oxygen isotopes have been measured on different calcite fossil remains. This technique was developed by UREY (1947), who calculated thermodynamic properties and fractionation of isotopes. Techniques of mass spectrometry were educed by NIER (1947). MCCREA (1950), UREY et al. (1951) and EPSTEIN et al. (1953) developed the use of oxygen isotope composition in calcite as a palaeothermometer. Sea surface temperature reconstructions were first used to identify glacial-interglacial cycles by EMILIANI (1955). SHACKLETON AND OPDYKE (1973) finally established the use of marine isotope stages as a stratigraphic tool.

Whereas in the open ocean, the stable oxygen isotope composition of surface waters is relatively uniform across long distances, reflecting large scale hydrological cycles (e.g. DUPLESSY et al., 1992), in marginal basins like the Mediterranean, the isotopic composition of the surface waters is much more sensitive to local processes like freshwater discharge and evaporation (KALLEL et al., 1997). As a consequence, stable oxygen isotopes in the surface water of the Mediterranean Sea mainly reflect the evaporative gradient seen in the surface salinity (fig. 5) with values depleted in the heavy isotope $\delta^{18}O$ documenting the entry of the oceanic surface waters into the basin (ROHLING et al., 2007).

In the past, there were sources of freshwater, in particular monsoon-driven river discharge and the Bosporus opening, periodically reducing surface water salinity, which can be traced across sapropels by distinct light isotopic peaks (e.g. ROSSIGNOL-STRICK & PATERNE, 1999 and references therein).

The $\delta^{13}C$ values of foraminiferal shells reflect the carbon isotopic composition of dissolved inorganic carbon (DIC) in seawater in which calcification took place. As it is further controlled by kinetic fractionation through relatively rapid biogenic calcification and by strong vital effects, the $\delta^{13}C$ is not in isotopic equilibrium with seawater (e.g. RAVELO & HILLAIRE-MARCEL, 2007 and references therein). Foraminiferal shell $\delta^{13}C$ is used to

reconstruct changes in the $\delta^{13}C$ composition of DIC, which, in turn, can be related to the balance of photosynthesis versus respiration and relative mixture of water masses with different $\delta^{13}C$ composition of DIC. In the context of sapropel formation, benthic foraminiferal $\delta^{13}C$ values show a marked decrease during the early and late phase of sapropel formation, indicating a slow-down of deep water circulation and increased riverine input of isotopically light DIC from terrestrial sources into the Eastern Mediterranean (KUHNT et al., 2008). In general, many different factors influence the $\delta^{13}C$ composition of foraminiferal shells, including changes in the global carbon cycle, changes in regional water mass mixing and source, photosynthesis and respiration processes but also ontogenetic and species-specific vital effects and even selective dissolution and thus size fraction of the analysed shells.

1.3.2. Magnesium/calcium ratio

LEA et al. (1999) established Mg/Ca ratio in foraminifera tests as an important proxy to reconstruct oceanic palaeotemperatures. In connection with $\delta^{18}O$ of foraminifera calcite, Mg/Ca ratios allow for a decoupling of temperature and global ice volume, assuming the relationship of $\delta^{18}O$ sea water and salinity is known (KALLEL et al., 1997). This proxy has been accordingly applied in western Mediterranean (CACHO et al., 2006). Recent studies, however, found that enhanced salinity might have a strong influence on Mg/Ca ratios as well. The Eastern Mediterranean Sea, with its present-day high salinity gradient (fig. 5) and relatively uniform temperatures (fig. 5), is an ideal area to test the importance of this influence. FERGUSON et al. (2008) indeed identified a strong apparent relationship between salinity and Mg/Ca ratios: in areas with salinity above the known oceanic range, Mg/Ca ratios in core top planktonic foraminifera were anomalously high. This finding suggests that Mg/Ca is not an ideal proxy for palaeotemperature estimations in the Eastern Mediterranean Sea and so this method has not been used in this study.

Other trace elemental proxies in foraminiferal shells useful for palaeoceanographic reconstructions include the Ba/Ca ratio, which seems to be a strong indicator for river outflow as shown by WELDEAB et al. (2007). In addition, Nd isotopes can be used to identify sources of freshwater and have been used in the Eastern Mediterranean among others by OSBORNE et al. (2010). In the present study, however, emphasis was put on the detection of freshwater, and oxygen isotopes were found to be reliable enough tracers for this purpose, all

the more that Nd isotopes, Ba/Ca ratios and other elements could be influenced by the same potential problems as Mg/Ca in the unusually high evaporative Eastern Mediterranean.

1.3.3. Sediment composition

Marine sediments are a mixture of a number of components derived from different parts of the geosphere. In particular lithogenous components, which originate from continental surfaces, are interesting in palaeoenvironmental reconstructions as their composition can be used to detect changes in the source regions which reflect climate (e.g. HAUG et al., 2001). The Eastern Mediterranean has essentially two sediment sources: clays transported fluvially from the northern borderlands or distally by the Nile, and Aeolian dust mainly derived from North African deserts (WEHAUSEN & BRUMSACK, 1998; fig. 12). The Saharan dust is mainly composed of quartz, kaolinite, palygorskite, illite and Fe- and Al-oxides (e.g. GUERZONI et al., 1997; RUTTEN et al., 2000). The Nile River is one of the largest sources of riverine suspended sediment, with an annual runoff of ~91 km^3 and a sediment load of ~57 kt (FOUCAULT & STANLEY, 1989). The Nile water contains mainly weathering products of basalt (KROM et al., 1999). Smaller rivers in the Aegean Sea are also involved into sediment input to the basin (AKSU et al., 1995). However, apart from fine clay which remains long in suspension (STUUT et al. 2009), all other coarse sediment is trapped in local Aegean basins.

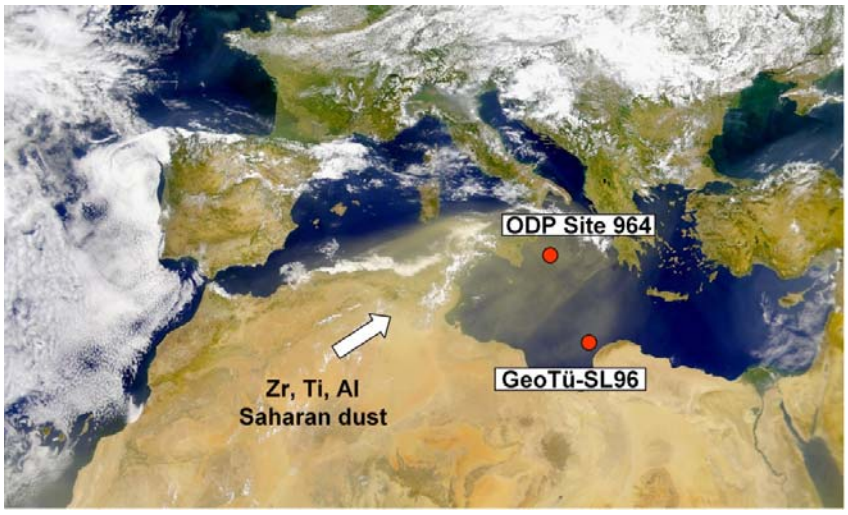

Figure 12: Saharan dust supply and according elements relevant in XRF sediment analysis over the Mediterranean region (GUERZONI et al., 1997; RUTTEN et al., 2000); satellite picture: www-atm.physics.ox.ac.uk).

Sediment information relevant for palaeoenvironmental reconstructions can be extracted in the form of elemental ratios. Variations in aeolian dust supply to the Mediterranean, and thus of aridity in North Africa, on a glacial-interglacial timescale were detected using Si/Al, Zr/Al and Ti/Al ratios (CALVERT & FONTUGNE, 2001; LARRASOAÑA et al., 2008), which are commonly used as grain-size proxies (CALVERT & PEDERSEN, 2007).

Barium is known to concentrate in organic matter during its production and deposition (DYMOND et al., 1992). It has therefore been successfully used as a proxy to track palaeoproductivity (e.g. LANGEREIS et al., 1997; MERCONE et al., 2001; THOMSON et al., 2006). As barium remains largely unaffected by postdepositional oxidation processes, it has been used to identify 'ghost-sapropels', locating phases of high productivity and organic matter deposition in completely oxidised sapropels (THOMSON et al., 1995; VAN SANTVOORT et al., 1997). Iron is an essential nutrient for phytoplankton and is delivered to the Mediterranean mainly through Aeolian dust supply and riverine input (DE BAAR & DE JONG, 2001) and can thus be used to track increased terrigenous input. Volcanic ash is mainly composed of feldspars and pyroxenes predominantly yielding the elements silicon, potassium, iron and titanium, which can therefore be used to identify ash layers in sediment successions (e.g. VINCI, 1985).

1.4. Biomarker proxies

1.4.1. Alkenone measurements

The alkenone method evolved from the observation that certain microalgae of the class Prymnesiophyceae, notably the species *Emiliania huxleyi* and *Gephyrocapsa oceanica* (e.g., MARLOWE et al., 1984), and presumably other living and extinct members of the family Noelaerhabdaceae (e.g., MARLOWE et al., 1990), have or have had the capability to synthesize long-chained alkenones whose extent of unsaturation changes with growth temperature (e.g., MARLOWE et al., 1984; PRAHL & WAKEHAM, 1987). On the basis of this correlation, palaeo-SST can be calculated from the so-called ketone unsaturation index $U^{K}_{37'}$ (e.g., PRAHL & WAKEHAM, 1987).

Alkenone-based SST reconstructions were successfully performed in the Eastern Mediterranean (EMEIS et al. 2000, 2003; CASTANEDA et al., 2010), although alkenone measurements have proven challenging in the Eastern Mediterranean due to the generally low content of organic carbon in non-sapropel layers resulting in low abundances or the complete absence of long-chain alkenones in some sedimentary intervals (SCHILMAN et al., 2003).

1.4.2. TEX_{86} index

An alternative organic geochemical approach for SST reconstructions is the TEX_{86} proxy (SCHOUTEN et al., 2002). It is based on glycerol dialkyl glycerol tetraethers (GDGTs), which are compounds found in the membrane lipids of the Marine Group Crenarchaeota, and uses the correlation between growth temperature and the amount of several types of isoprenoidal GDGTs that are bio-synthesized (SCHOUTEN et al., 2002). Like alkenone-based proxies, the TEX_{86} approach does not seem to be influenced by changes in salinity (WUCHTER et al., 2004). To date, TEX_{86}-based SST reconstructions in the Eastern Mediterranean have been performed on Pliocene sapropels (MENZEL et al., 2006) and more recently on Quaternary sediments (CASTANEDA et al., 2010), where they were shown to generally parallel alkenone-based SST reconstructions.

1.5. Microfossil assemblages

Species abundances of planktonic and benthic microfossils reflect environmental properties during their life, and if the preferences of individual species are known, their abundances in fossil samples can be used as proxies. Microfossils are most useful tools in palaeoenvironmental reconstructions because they are generally very abundant in sediment cores. In the Mediterranean, planktonic foraminifera (e.g. HAYES et al., 2005), calcareous nannoplankton (e.g. INCARBONA et al., 2008) and dinoflagellates (e.g. MUDIE et al., 2001) have been used for surface-water reconstructions while deep-water properties have been inferred from benthic foraminifera (SCHMIEDL et al., 2010 and references therein). Siliceous microfossils, in contrast, are rare in the Mediterranean and thus have found only limited application in palaeoenvironmental reconstructions. Here, emphasis was put on planktonic foraminifera and, to a much lesser extent, benthic foramninifera.

1.5.1. Benthic foraminifera

The tests of benthic foraminifera can be composed of secreted organic tectin, calcite, aragonite, silica or of agglutinated particles. Individual species live on the sediment surface or inside the uppermost centimetres of the sediment. In benthic ecosystems, diversity, species composition and microhabitat preferences (e.g. SCHÖNFELD & NUMBERGER, 2007) of foraminifera basically reflect food and oxygen availability at the sea floor and in the upper

surface sediment (e.g. CORLISS, 1985; JORISSEN et al., 1995; VAN DER ZWAAN et al., 1999; DE RIJK et al., 2000). In the Mediterranean Sea, benthic foraminifera assemblage investigations as well as stable isotopic compositions were used to reconstruct deep water properties (e.g. MACKENSEN et al., 2000; SCHMIEDL et al., 2004; KUHNT et al., 2007; KUHNT et al., 2008; MILKER et al., 2009; SCHMIEDL et al., 2010). In times of sapropel formation, ventilation of the deep water decreases causing oxygen deficiency. Prior to sapropel formation, cool surface waters and high evaporation rates result in high convection and oxic deep waters while strong wind-induced mixing promoted surface-water production, as can be inferred from benthic foraminiferal assemblages (SCHMIEDL et al., 2010 in press). The progressive oxygen depletion at the onset of sapropel events as well as subsequent re-oxygenations and intermittent sapropel interruptions can all be quantitatively characterised by analyses of benthic foraminifera assemblages (e.g. MULLINEAUX & LOHMANN, 1981; NOLET & CORLISS, 1990; JORISSEN, 1999; SCHMIEDL et al. 2010 in press), among others using the oxygenation index developed by SCHMIEDL et al. (2003) combining foraminiferal species diversity and the ratio between indicator taxa for high and low oxygen levels. Another important proxy for the residence time of deep-water masses and thus of deep-water ventilation is the $\delta^{13}C$ signal of the strictly epifaunal *Planulina ariminensis* (KUHNT et al., 2008; SCHMIEDL et al., 2010).

1.5.2. Planktonic foraminifera

Planktonic foraminifera inhabit the pelagic zone of the open ocean. All known species have calcite tests; some species have spines and many species harbour photosynthetic algae symbionts (HEMLEBEN et al., 1989). The diversity of extant planktonic foraminifera is relatively low (~ 50 species worldwide (HEMLEBEN et al., 1989)) in comparison with benthic foraminifera diversity. Some species live in depths of 1000 m or more (BÉ & HUTSON, 1977), but most live within the photic zone of the oceans. The empty shells, which are abandoned after reproduction, account for up to 30 % of the ocean floor sediments (HEMLEBEN et al., 1989) in most areas of the ocean.

The calcareous tests of planktonic foraminifera are widely used for stable isotopic composition measurements (e.g. WEAVER et al., 1997; PEARSON, 1998; NEGRI et al., 1999), e. g. *G. ruber* and *G. bulloides*, which, thanks to their preferred habitat in the uppermost 20-70 m of the water column (HEMLEBEN et al., 1989), are extremely useful to reconstruct conditions at the sea surface.

The present-day Mediterranean is a semi-enclosed basin situated in subtropical climate which, due to the prevailing eastward surface circulation and the high evaporation especially in the eastern part, is characterised by a strong salinity and temperature increase from west to east (WUEST, 1961). Accordingly, the modern planktonic foraminifera fauna of the Eastern Mediterranean is dominated by assemblages with tropical to subtropical elements, in particular *Globigerinoides ruber*, while cool assemblages, comprising groups with cool-subtropical and subpolar (in particular *Globorotalia inflata* and *Globigerina bulloides*) affinities, are more common in the western basin (THUNELL, 1978). Glacial SST reconstructions for the Mediterranean suggest substantially cooler temperatures than present-day ones (e.g. HAYES et al., 2005), inducing a shift in foraminiferal composition towards transitional to subpolar assemblages (e.g. HAYES et al., 1999). Planktonic foraminiferal assemblages have been widely used as palaeoproxies in the Mediterranean for palaeoclimatic reconstructions (among others TODD, 1958; OLAUSSON, 1960, 1961; HERMAN, 1972; CITA et al., 1977; VERGNAUD-GRAZZINI et al., 1977; THUNELL, 1979; ROHLING et al., 1993, 1995; HAYES et al., 1999; BUCCHERI et al., 2002) and past SST in particular (THIEDE, 1978; KALLEL et al., 1997; GONZALEZ-DONOSO et al., 2000; SBAFFI et al., 2001; PEREZ-FOLGADO et al., 2003; HAYES et al., 2005; KUCERA et al., 2005) but also in order to palaeoecologically assess periods of sapropel deposition (e. g. THUNELL et al., 1977; THUNELL et al., 1983; TANG & STOTT, 1993; ROHLING et al., 1997, TRIANTAPHYLLOU et al., 2009).

In addition, the assemblage composition of planktonic foraminifera itself is used to reconstruct palaeotemperatures either qualitatively through interpretation of species composition (e.g. HAYES et al., 1999) or quantitatively through transfer functions (PFLAUMANN et al., 1996; WAELBROECK et al., 1998; HAYES et al, 2005; KUCERA et al., 2005). The basic principle of transfer functions in palaeoenvironmental reconstructions is the translation of a set of known variables (species abundances in a fossil assemblage) into a related unknown variable (palaeoenvironmental parameter to be reconstructed). Transfer functions are typically calibrated on surface sediment data and applied to fossil samples from a period in the past for which a stationarity of the species ecological preferences can be assumed, i.e. typically the late Quaternary (KUCERA et al., 2005). One of the transfer functions used for SST reconstructions in the Mediterranean is known as the "Imbrie-Kipp" transfer function, which uses principal component analysis to reduce species abundances to statistically independent end-member assemblages which are then regressed on the environmental factors (IMBRIE & KIPP, 1971), generating a calibration formula. Another approach applied in the Mediterranean Sea is the modern analogue technique, which

searches a database of modern assemblages in order to identify those that best resemble the fossil assemblage. A more precise and reliable approach for SST estimates is the artificial neural networks (ANN) technique which was established by MALMGREN & NORDLUND (1997) and MALMGREN et al. (2001). The concept of ANN is based on unsupervised learning of a relationship between two sets of variables. The commonly used back propagating ANN is based on a network of interconnected layers, the first consisting of the input variables (e.g. species abundances), followed by a series of hidden layers containing the processing units called neurons, terminated by a single neuron generating the output variable (e.g. SST). ANN-based STT estimates have been already successfully applied to planktonic foraminifera assemblages from the Mediterranean (e.g. HAYES et al., 2005).

2. Material and Methods

2.1. Investigated sites and cores

This study is based on the analysis of sediment sections covering Marine Isotope Stages (MIS) 12 to 10/9 and MIS 2 to 1 in two cores from the Eastern Mediterranean Sea. The gravity core GeoTü-SL96 (32° 46'N, 19° 12'E, 1399 m water depth, total core length 8.02 m) was taken from the greater Syrte during the Meteor cruise M 51/3 in 2001 (HEMLEBEN et al., 2003). The hydraulic piston core ODP Site 964A-3H was taken in the course of ODP Leg 160 in the Ionian Sea (36° 16'N, 17° 45'E´, 3658 m water depth, total core length 25.9 m; (SAKAMOTO et al., 1998).

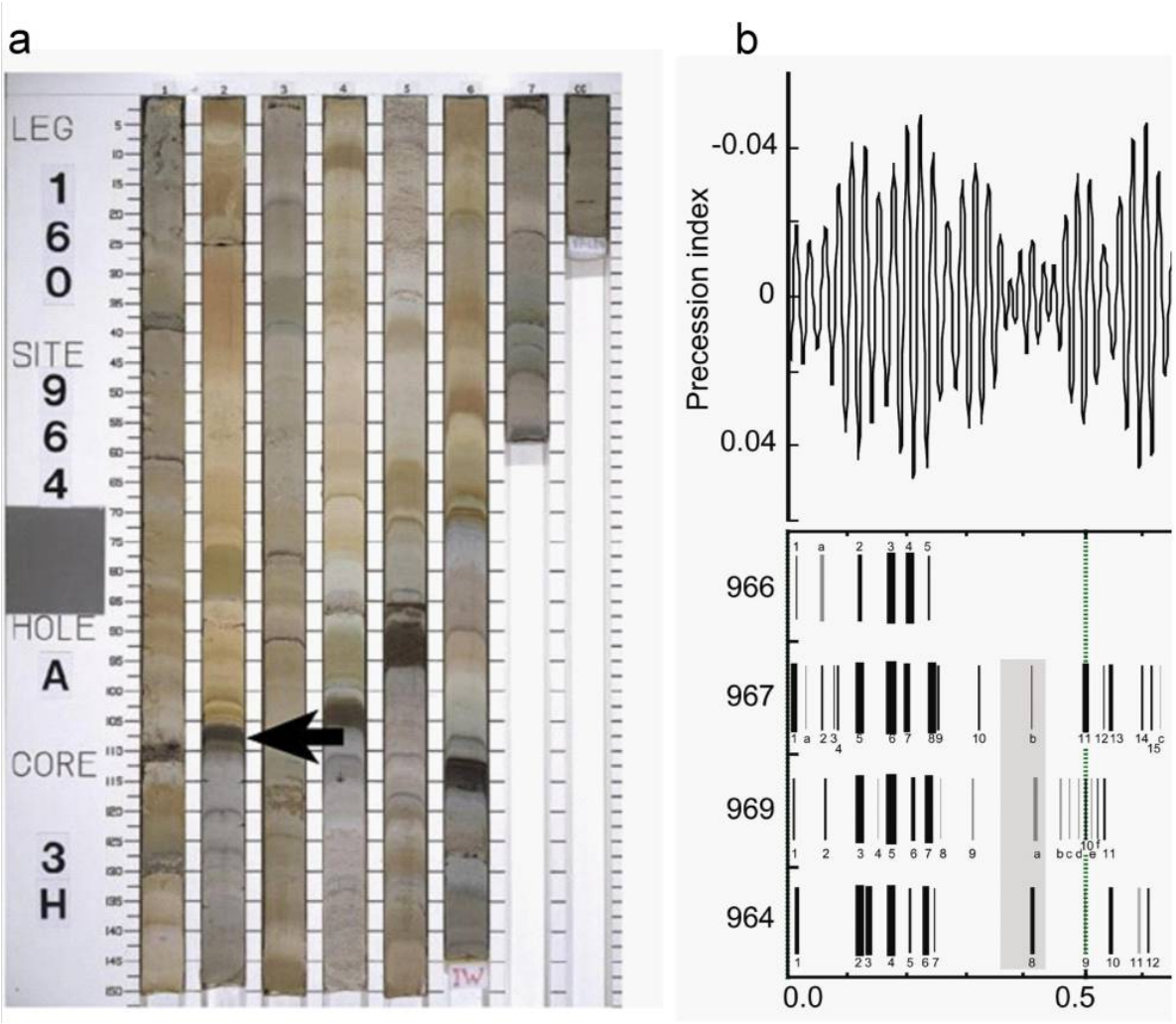

Figure 13: a) MIS 11 sediments from ODP Site 964A; the MIS 11 sapropel is indicated by an arrow (EMEIS et al., 1996); b) Correlation of sapropel horizons from Eastern Mediterranean Leg 160 ODP Sites with the precession index (EMEIS & SAKAMOTO, 1998). The target interval of this project, containing the MIS 11 sapropel, is highlighted

Although MIS 11 has been recovered and identified in sediment cores dating back to Albatross expedition (PETTERSSON, 1946, 1947), there has been until now no detailed study of this interval in the Mediterranean. ROSSIGNOL-STRICK (1983) found that there is a sapropel in MIS 11 and speculated that it must be correlated with the 406 kyr B.P. insolation peak but made no detailed investigation of the core. The selection of the two cores was guided by the following criteria: the central Mediterranean is likely to be most sensitive for planktonic foraminifera fauna as it lies halfway through the Mediterranean SST gradient. Two cores were necessary to replicate the observed patterns and investigate the depth pattern of anoxia development associated with MIS 11 sapropel – this is why the cores have such a large depth difference.

The selection of cores was furthermore guided by the following criteria: continuous sedimentation, lack of sediment disturbance, high sedimentation rate and presence of the 406 kyr B.P. sapropel horizons. Based on these criteria, we have found that ODP Site 964 next to Sicily would deliver about 400 samples for the aimed interval (KROON et al., 1998), and the MIS 11 sapropel was clearly identifiable in section 3H1 at 104 cm in Hole A, which delivers the most undisturbed, continuous sediment record within this interval (MIS 11 and ancient transitions, section 3H1-3H3) and through high sedimentation rates (3.4 – 6.3 cm/kyr) displaying a very high time resolution (150-300 yrs/cm; fig. 13).

In GeoTü-SL 96 piston core, recovered from the north of the greater Syrte, the presence of MIS 11 is displayed through magnetic susceptibility (on board measurements; fig. 14). The sections 7 (600 to 700 cm) and 8 (700 to 800 cm) were chosen from the material to cover MIS 11 and ancient transitions. However, the sedimentation rates of this core are lower (1.8 – 2.2 cm/kyr) delivering a lower time resolution of 450 – 550 yrs/cm).

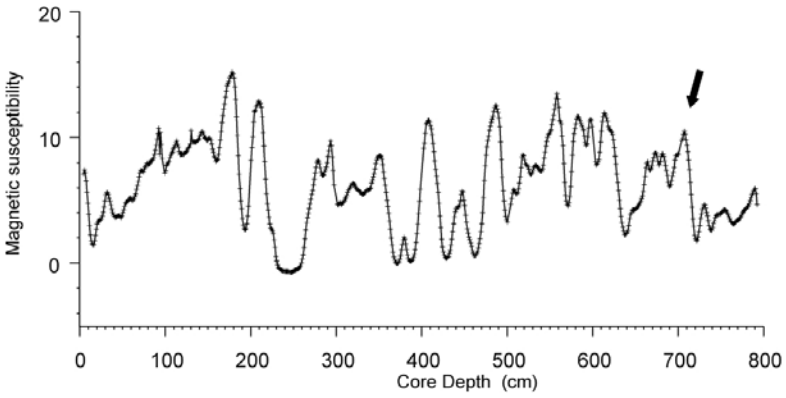

Figure 14: Magnetic susceptibility record from core GeoTü-SL96 (on board measurement). The oldest peak in the core can be interpreted as sapropel of MIS 11, indicated by arrow, suggesting the presence of MIS 11 sediments.

On the other hand, the core contains very well preserved sediment informations and microfossils comparable to those in ODP Site 964. Additionally, core sections to investigate the Holocene part of the cores were sampled. For this purpose, in ODP Site 964 it was necessary to use another

Hole than A due to high disturbances by sampling processes of the core top section in this part. Hole D was alternatively found to have the best preserved material during this interval. In GeoTü-SL96 core top sediments of section 1 are as well preserved as the rest of the core.

2.2. Sample processing

The selected intervals in both cores, assumed to approximately correspond to MIS 1 to 2 and MIS 9 to 12 were sampled by U-channels (2x2 cm). The U-channeled cores have been continuously sampled at 1 cm intervals; altogether 525 single samples were taken (all samples and data are shown in Appendix). The individual 1 cm sediment slices were deep frozen at -30°C and subsequently freeze dried to facilitate disintegration of the sediment particles. The freeze dried samples were soaked in distilled water for half an hour before washing with tap water over a sieve with 63 µm mesh size. In order to remove clay remains from foraminifera shells, the residues were additionally cleaned in an ultrasonic bath for 15 s and washed again. The final residues were transferred onto a filter paper and dried at 40°C for 24 hours. The dried fraction was collected from the filters and dry sieved to obtain size fractions of 63-150 µm and ≥ 150 µm. All fractions and the raw sample were weighed. For XRF measurements, U-chanels were previously covered with a clear film, scanned on intervals of 0.5 to 1 cm by a AVAATECH XRF core scanner in cores of ODP Site 964 A and D and GeoTü-SL96 for MIS 11 and MIS 1, altogether 9 m of sediment in the two cores. Alkenone measurements were carried out every 5 cm of the ODP core working half (4 cm^3 each sample) and analysed (earlier analyses showed too little organic content in GeoTü-SL96 for alkenone data during MIS 11 and ancient stages).

2.3. Analysis of planktonic foraminifera assemblages

The taxonomy of planktonic foraminifera follows HEMLEBEN et al. (1989). A total of 19 species were identified in the studied time intervals. All species of planktonic foraminifera were counted; fragments which represented more than half a specimen and were clearly identifiable were also counted. For faunal analyses, the ≥ 150 µm fraction of each sample was splitted with a microsplitter until a representative aliquot with sufficient numbers of planktonic foraminifera for quantitative census was obtained (N> 300). Morphotypes of *G. ruber* were counted in parallel split. Altogether 425 single samples were counted for these purposes. Representative specimens of all identified species (tab. 2) are

shown on plate I and II). The images were taken by the scanning electron microscope LEO Model 1450 VP at the University of Tübingen. *Globigerinoides trilobus* is considered to be a growth type of *Globigerinoides sacculifer* (see also HEMLEBEN et al., 1989) and is displayed only to document the occurrence of all commonly recognised morphological types of planktonic foraminifera in the analysed samples. As *G. siphonifera* and *G. calida* were not clearly distinguishable in their early adult stages, and since they appear to share similar habitats and physiology, these species were counted together in assemblage counts (HEMLEBEN et al., 1989).

Statistical analyses of planktonic foraminifera abundances were carried out using the PAST version 1.82b software (HAMMER et al., 2001). To characterise trends in the occurrence of planktonic foraminifera species through the glacials and interglacials of this study, a Detrended Correspondence Analysis (DCA) was used (HILL & GAUCH, 1980). This method is an extension of a regular correspondence analysis, which was designed to extract trends in species abundance data and to represent these in a joint species-sample environmental space. Correspondence analysis is therefore widely used by ecologists to identify the main factors or gradients in ecological community data (e.g. WIDMARK & SPEIJER, 1997; EBERWEIN & MACKENSEN, 2006). By detrending the correspondence analysis (DCA), two major problems of correspondence analyses were solved, the "arch effect" and the compression effect of the ends of the gradient (HILL & GAUCH, 1980; GAUCH, 1982). For the DCA, percentages of all counted species were used. However, in some cases, for example to highlight similarities with selected assemblage composition data according to literature (e.g. TRIANTAPHYLLOU et al., 2009), some of the rare species (*Beela digitata, Globigerinoides conglobatus*) were deleted.

Table 2: List of planktonic foraminifera species from the investigated intervals of the two cores and their respective figures on the plates.

Species	Plate	Position
Globigerinoides ruber (d'Orbigny, 1839)	I	A-B
Neogloboquadrina incompta (Cifelli, 1961)	I	C-D
Neogloboquadrina dutertrei (d'Orbigny, 1839)	I	E-F
Globigerina bulloides d'Orbigny, 1826	I	G-H
Globorotalia inflata (d'Orbigny, 1839)	I	I-J
Globigerina falconensis Blow, 1959	I	K-L
Globorotalia truncatulinoides (d'Orbigny, 1839)	I	M-N
Globigerinoides sacculifer (Brady, 1877) with sac.	I	O-P
Globigerinita glutinata (Egger, 1893)	I	Q-R
Turborotalita quinqueloba (Natland, 1938)	I	S-T
Globigerinella siphonifera (d'Orbigny, 1839)	II	A-B
Globigerinella calida (Parker, 1962)	II	C-D
Globoturborotalita rubescens Hofker, 1956	II	E-F
Globorotalia scitula (Brady, 1882)	II	G-H
Globigerinoides conglobatus (Brady, 1879)	II	I-J
Beela digitata (Brady, 1879)	II	K-L
Neogloboquadrina pachyderma (Ehrenberg, 1861)	II	M-N
Globoturborotalita tenella (Parker, 1958)	II	O-P
Globigerinoides sacculifer (Brady, 1877) without sac (= *G. trilobus*)	II	Q-R
Orbulina universa d'Orbigny, 1839	II	S

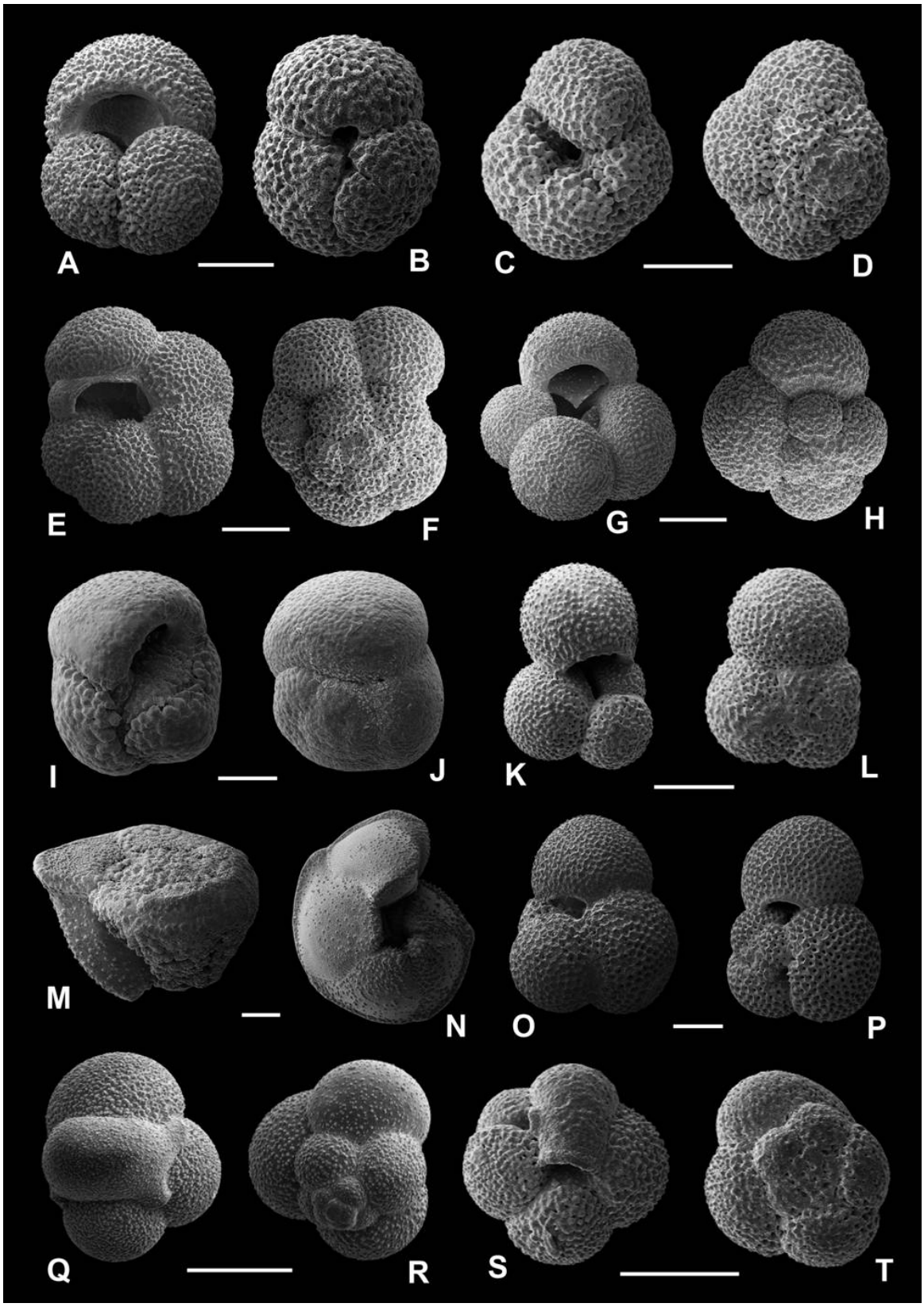

Plate I: SEM images of planktonic foraminifera species from MIS12-MIS1 ODP Site 964. Both cores provide excellent preservation of foraminifera shells. However, due to the higher amount of ODP Site 964 samples these were chosen to deliver specimens for SEM images. The pictures of one species show two specimens from the same sample, front and back view. A-B: *Globigerinoides ruber* (d'Orbigny, 1839), ODP 964, 3H1, 12-13 cm; C-D: *Neogloboquadrina incompta* (Cifelli, 1961), ODP 964, 3H2, 119-120 cm; E-F: *Neogloboquadrina dutertrei* (d'Orbigny, 1839), ODP 964, 3H2, 119-120 cm; G-H: *Globigerina bulloides* d'Orbigny, 1826, ODP 964, 3H1, 12-13 cm; I-J: *Globorotalia inflata* (d'Orbigny, 1839), ODP 964, 3H1, 12-13 cm; K-L: *Globigerina falconensis* Blow, 1959, ODP 964, 3H2, 29-30 cm; M-N: *Globorotalia truncatulinoides* (d'Orbigny, 1839), ODP 964, 3H1, 62-63 cm; O-P: *Globigerinoides sacculifer* (Brady, 1877) with sac chamber, ODP 964, 3H2, 29-30 cm; Q-R: *Globigerinita glutinata* (Egger, 1893), ODP 964, 3H3, 14-15 cm; S-T: *Turborotalita quinqueloba* (Natland, 1938), ODP 964, 3H3, 14-15 cm. All scale bars equal 100 µm.

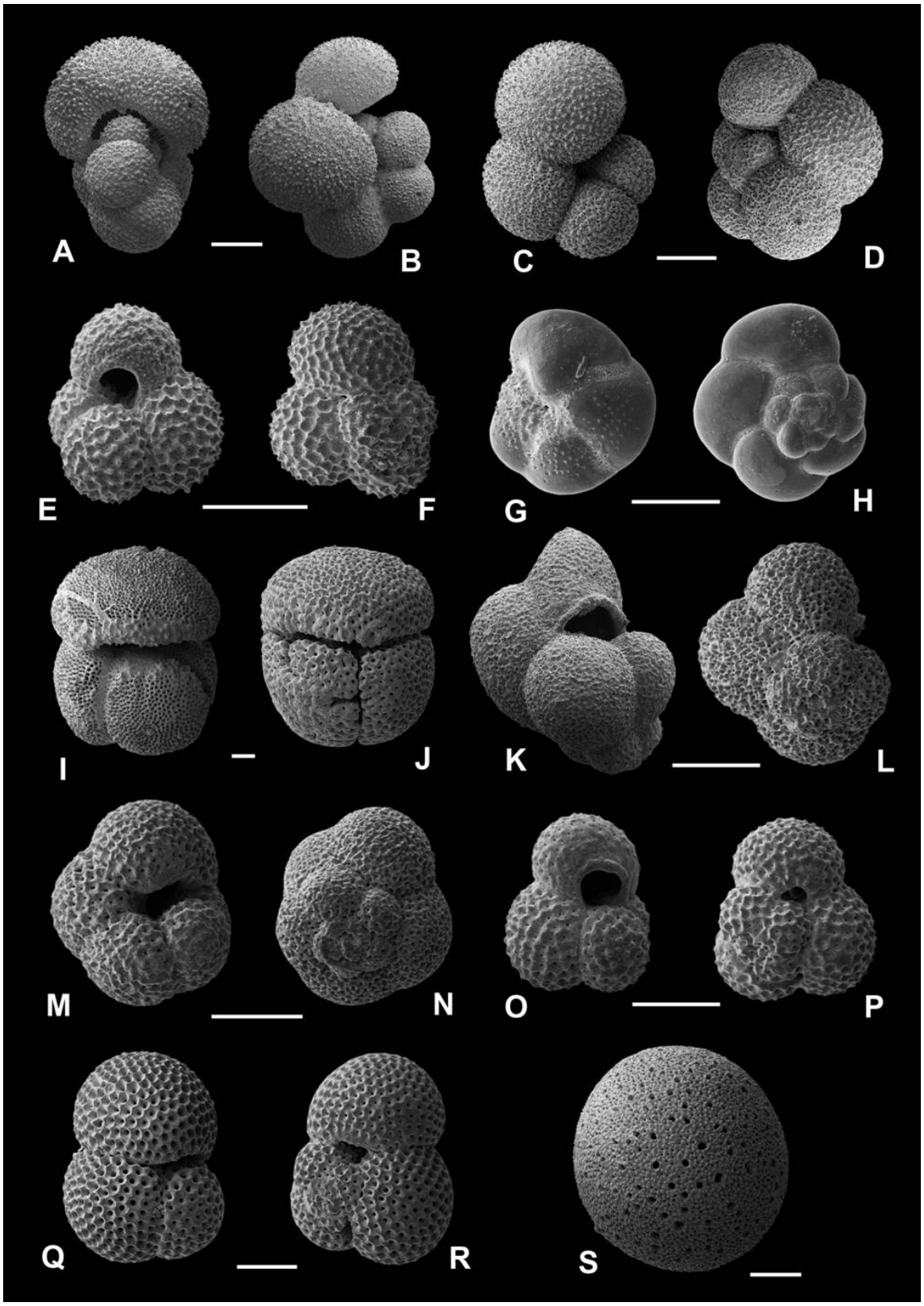

Plate II: A-B: *Globigerinella siphonifera* (d'Orbigny, 1839), ODP 964, 3H2, 29-30 cm; C-D: *Globigerinella calida* (Parker, 1962), ODP 964, 3H2, 9-10 cm; E-F: *Globoturborotalita rubescens* Hofker, 1956, ODP 964, 3H2, 62-63 cm; G-H: *Globorotalia scitula* (Brady, 1882), ODP 964, 3H1, 12-13 cm; I-J: *Globigerinoides conglobatus* (Brady, 1879), ODP 964, 3H2, 11-12 cm; K-L: *Beela digitata* (Brady, 1879), ODP 964, 3H2, 11-12 cm; M-N: *Neogloboquadrina pachyderma* (Ehrenberg, 1861), ODP 964, 3H2, 119-120 cm; O-P: *Globoturborotalita tenella* (Parker, 1958), ODP 964, 3H1, 12-13 cm; Q-R: *Globigerinoides sacculifer* (Brady, 1877) without sac (=*Globigerinoides trilobus*), ODP 964, 3H2, 29-30 cm; S-T: *Orbulina universa* d'Orbigny, 1839, ODP 964, 3H1, 12-13 cm. All scale bars equal 100 µm.

The assemblage counts data were subsequently reduced to the categories used by HAYES et al. (2005) and converted to temperatures using the Artificial Neural Networks developed by HAYES et al. (2005). Average annual and seasonal SST values were reconstructed as the average of the ten artificial neural networks trained by HAYES et al. (2005) specifically for each SST definition. The standard deviation of the ten network outputs was used as a measure of representation of the fossil assemblage in the calibration dataset following the concept of KUCERA et al. (2005).

2.4. Morphotype evaluation of *G. ruber*

Individual species of planktonic foraminifera show distinct depth habitats, seasonal production maxima as well as biological lifestyles (e.g., presence or absence of symbionts) and these differences are all reflected in the isotope chemistry of their shells (BÉ, 1982; GANSSEN & KROON, 2000; LIN & HSIEH, 2007). Therefore, isotope data from single species are required for meaningful palaeoenvironmental interpretations, which imply that species concepts are very important. Planktonic foraminifera species, however, are known to be very variable (e. g. SAITO et al., 1981; HEALY-WILLIAMS et al., 1985; HEMLEBEN et al., 1989; ROBBINS & HEALY-WILLIAMS, 1991; LOEWEMARK et al., 2005). This applies especially to *G. ruber*, which is the most important source of information on surface ocean properties and a dominant species in the Eastern Mediterranean (THUNELL, 1978).

This species has been intensively investigated recently and the morphological variability has been subsumed into a number of distinct forms. In keeping with the broad taxonomical concept of PARKER (1962), individual forms of *G. ruber* analysed in recent geochemical studies have not been characterised taxonomically, but described as "morphotypes" (fig. 15). Up to six morphotypes were defined in the past in different studies (SAITO et al., 1981; ROBBINS & HEALY-WILLIAMS, 1991; LOEWEMARK et al., 2005). These morphotypes show different habitat preferences (KUROYANAGI & KAWAHATA, 2004; LIN & HSIEH, 2007) reflected in their different stable isotope compositions (WANG, 2000; LIN et al., 2004; KAWAHATA, 2005; LOEWEMARK et al., 2005) and Mg/Ca geochemistry (STEINKE et al., 2005). There are at least six genetically distinct types within the white variant of *G. ruber*

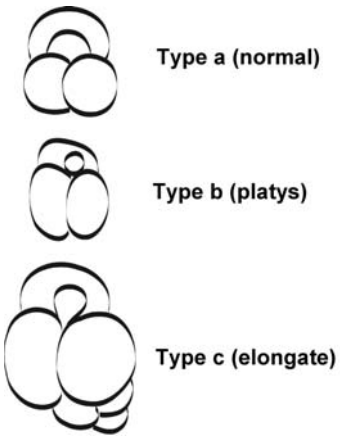

Figure 15: Drafts of typical representatives of *G. ruber* morphotypes showing the extremes of morphological variation.

(DARLING & WADE, 2008, AURAHS et al., 2009) and it is possible that some of these correspond to the distinct morphotypes. The first indication for a possible correlation between shell morphology and genetic differences within the white colour variety of *G. ruber* was recently presented by KUROYANAGI et al. (2008), who found systematic morphological differences (although the sample size was very small) between the genetic Types II and I of *G. ruber* (white), which are consistent with the *G. ruber* s.s. and s.l. concept of WANG (2000).

Whatever the exact nature of the link between genetics and morphology in *G. ruber*, it is clear that a better understanding of the isotopic behaviour and habitat preferences of its morphotypes are essential for meaningful palaeoenvironmental reconstructions (EGGINS et al., 2003; LIN & HSIEH, 2007; SADEKOV et al., 2008). This issue is particularly relevant for applications in the more distant geological past, where hypotheses on the origin of distinct morphotypes must additionally consider the possibility of iterative evolution and extinction of subspecies or species through time and in space.

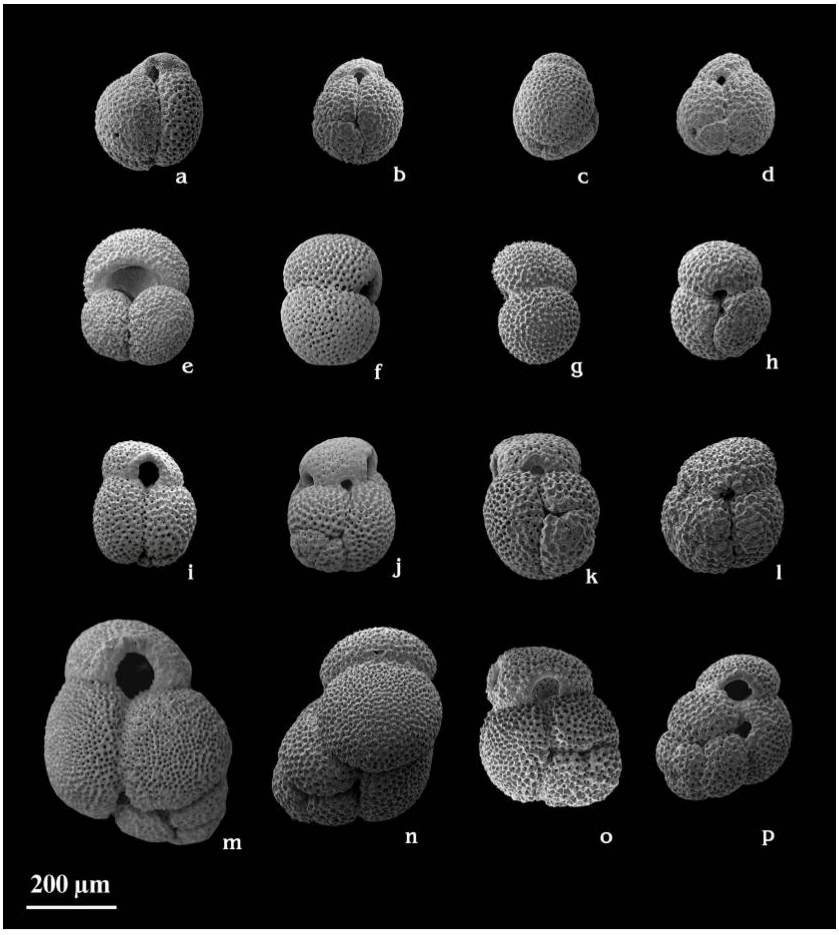

Plate III: SEM images of the different morphotypes of *G. ruber*. a-d: type d, "kummerform"; Fig. 3e-h: type a, "normal"; Fig. 3i-l: type b, "platys"; Fig. 3m-p: type c, "elongate". Specimens a-d taken out of Sample GeoTü-SL96, 665-666 cm; e-f: ODP 964A, 3H2, 32-33 cm; g-l: GeoTü-SL96, 684-685 cm; m-p: ODP 964A, 3H2, 64-65 cm. Column 1: front view; column 2: right side; column 3: left side and column 4: back view of the different morphotypes.

As the *G. ruber*-based proxies are among the most important in palaeoceanography in general, and in the present study in particular, and as individuals of this species displayed considerable variation in shell morphology, it seemed inevitable to systematically assess morphological variability and its possible effect on isotope

geochemistry. In the Mediterranean, AURAHS et al., (2009) documented the presence of multiple genetic types. Morphotypes were not yet investigated in detail. Therefore, in this study emphasis was put on finding possible end members of morphological variability, correspond to the morphotypes, and on assessing the possible variation in stable isotopic composition according to morphological variability.

In order to determine to what degree the individual morphotypes can be objectively separated, the morphological variability in *G. ruber* was first quantitatively assessed in four samples from MIS 11-10 in core GeoTü-SL96 (pl. III).

In each sample, a representative split containing at least 100 specimens of *G. ruber* has been analysed. Each specimen has been assigned to one of the four morphotypes, mounted in standard apertural and lateral views and photographed using a Leica Z16 Apo stereomicroscope fitted with a Q-imaging Micro Publisher 5.0 RTV video camera. A total of 17 morphological parameters representing the shape of the last three chambers and the shape of the entire shell in the two views were manually (length measurements) or automatically (perimeter and area) extracted from the digital images using the Image Pro Plus version 5.0 software (fig. 16).

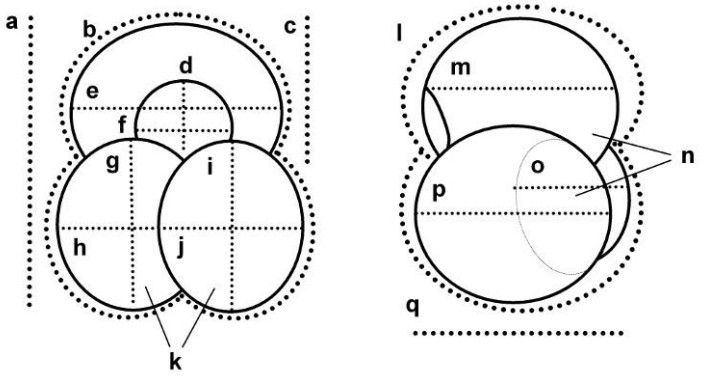

Figure 16: 17 morphological parameters. a: test height (for size normalizing), b: perimeter front, c: chamber n height, d: aperture height, e: chamber n width, f: aperture width, g: chamber n-2 width, h: chamber n-2 height, i: chamber n-1 height, j: chamber n-1 width, k: area front, l: perimeter side, m: chamber n depth, n: area side, o: chamber n-2 depth, p: chamber n-1 depth, q: test depth; representing the shape of the last three chambers and the shape of the entire shell for statistical analysis methods.

All measurements were normalised to shell width following MALMGREN & KENNETT (1976), and the resulting 16 size-independent parameters were statistically analysed. Such normalisation is important since all individual measurements are otherwise highly correlated to each other and the statistical analyses will recover the pattern of size variability as the most important factor in the dataset.

Statistical analyses of morphotype abundances, morphological variability and stable isotope offsets were carried out using the PAST version 1.82b software (HAMMER et al., 2001). Three statistical methods for the size-independent morphometric measurements were used. The Principal Components Analysis (PCA) projects samples (in our case foraminifera) onto linear combinations of variables (in our case shell morphology), so that the resulting

projection captures the largest portion of the variance in the multivariate dataset. This method allows one to visualise the most significant trends in the morphology of the analysed foraminifera. However, there is no guarantee that the most significant morphological trend in the data is identical to the pattern of variation separating the morphotypes. Therefore, an additionally MANOVA CVA (multivariate analysis of variance – canonical variants analysis) were used, which projects the foraminifera onto synthetic variables (axes) so that the differences among pre-defined groups (in our case manually assigned morphotypes) are maximised. This will allow determining whether the manually defined morphotypes can be objectively distinguished by the morphometrical data used and how distinct the individual morphotypes are. In order to determine, whether the differences between the manually defined morphotypes are statistically significant, a pairwise discriminant analyses between all pairs of morphotypes separately for the four samples were applied. The pairwise discriminant analysis determines a linear combination of the morphological variables which maximises the distinction between two pre-defined groups and defines a threshold value separating optimally the two groups. This analysis also allows quantifying how many individuals can be objectively classified to the pre-defined morphotypes.

To characterise trends in the occurrence of *G. ruber* morphotypes through the glacials and interglacials of this study, a Detrended Correspondence Analysis (DCA) has been used (HILL & GAUCH, 1980).

2.5. Analysis of benthic foraminifera assemblages

For ODP Site 964 and GeoTü-SL96 in MIS 11, benthic foraminifera assemblage counts were performed (>0.150 mm, whole sample or > 300 specimens). The picking was carried out by L. Walz and species determinations by Dr. A. Badawi and M. Simon. The data were used to determine the accumulation rates of benthic foraminifera as a measure of sea surface productivity and to get rough, non-quantitative information on deep sea oxygen availability (pl. IV; fig. 17). Taxonomic assessment of benthic foraminifera followed SGARRELLA & MONCHARMONT ZEI, 1993 and JONES, 1994.

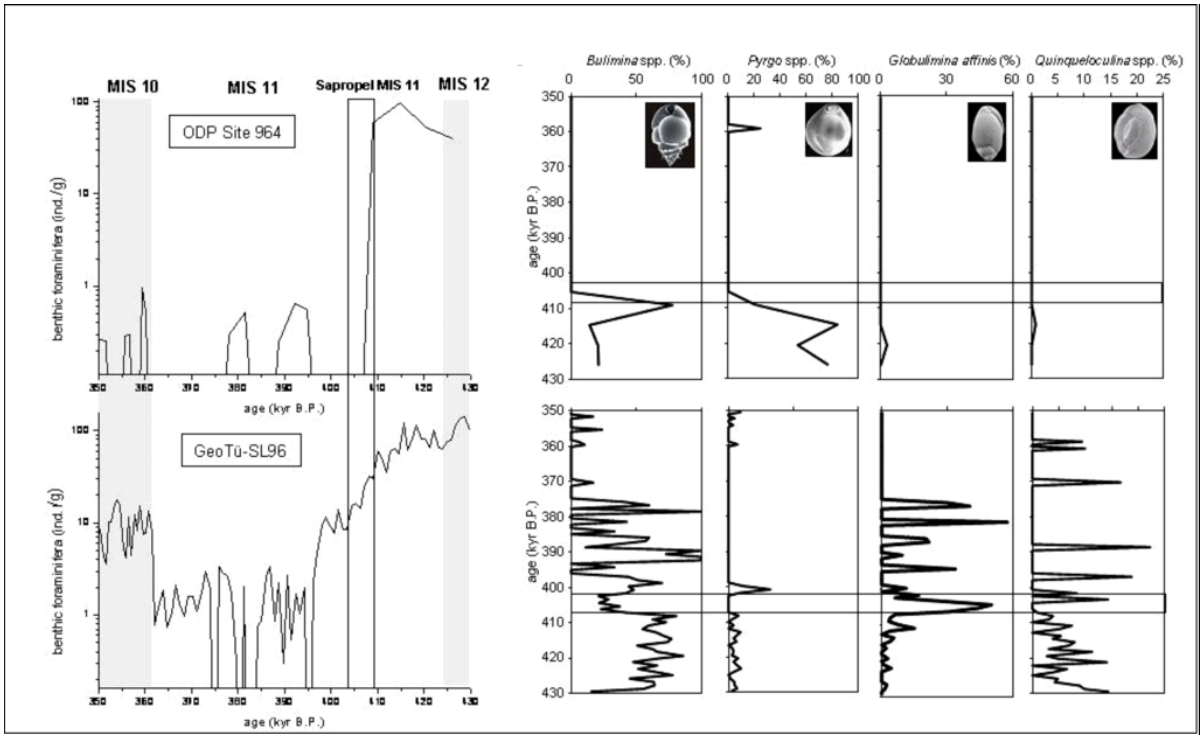

Figure 17: Benthic foraminifera abundances on a logarithmic scale in ODP Site 964 (left side, upper panel) and GeoTü-SL96 (left side, lower panel). Right side shows selected highly abundant species/families in both cores (upper panels show ODP Site 964 counts, lower panels GeoTü-SL96).

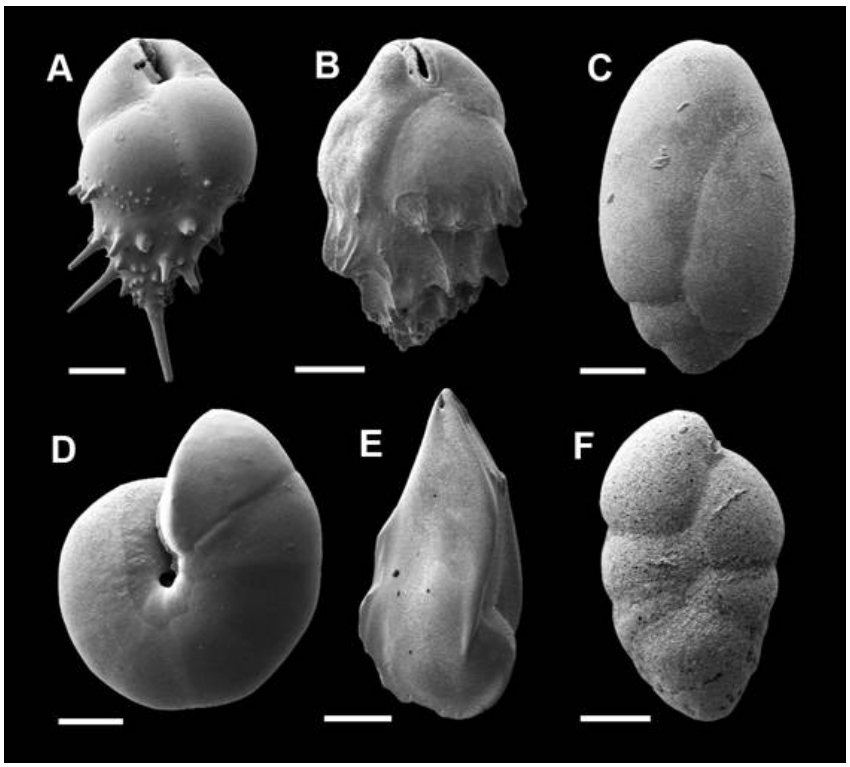

Plate IV: SEM images of selected benthic foraminifera in GeoTü-SL96 and ODP Site 964. A: *Bulimina aculeata* d'Orbigny, 1826; B: *Bulimina mexicana* Cushman, 1922; C: *Globobulimina affinis* (d'Orbigny, 1939); D: *Melonis barleanum* (Williamson, 1858); E: *Lenticulina* sp.; F: *Karreriella bradyi* (Cushman, 1911). All scale bars equal 100 µm, SEM pictures by M. Simon.

2.6. Stable isotope measurements

Stable isotope measurements on *G. ruber* and *G. bulloides*

For stable isotope analyses, 10-12 specimens of either *G. ruber* ("normal" morphotype) or, where this species was too rare, *G. bulloides* were taken from the fraction 315-400 µm to reach the optimal sample weight of 100-150 µg. Following earlier studies (e. g. ROHLING et al., 2004), *G. ruber* is consistently surface dwelling in the Eastern Mediterranean and therefore was the preferred target of this investigation. All measurements on this species in the long records were made on the morphotype "normal". These analyses were made for every sample to achieve a 1 cm resolution record throughout. In addition to the long records, in 115 samples from the intervals MIS 12 to MIS 9 and MIS 2 to MIS 1, 10-12 specimens of each of the various morphotypes of *G. ruber* were taken from the fraction 315-400 µm to reach the optimal sample weight of 100-150 µg. The abundance of the individual morphotypes varied significantly, and some samples thus did not yield enough specimens of each morphotype for isotope analysis. The stable isotope composition of all analysed species and morphotypes were determined at AWI Bremerhaven, Germany with a Finnigan MAT 251 isotope ratio gas mass spectrometer directly coupled to an automated carbonate preparation device (Kiel II) and calibrated via NIST 19 international standard to the PDB scale. All values are given in δ-notation vs. VPDB Vienna Pee Dee Belemnite. The precision of the measurements at 1σ based on repeated analyses of an internal laboratory standard (Solnhofen limestone) over a one-year period was better than 0.08 ‰ and 0.06 ‰ for oxygen and carbon isotopes, respectively.

In order to assess the reproducibility of the individual isotope measurements, 29 samples (see Appendix) from ODP Site 964A-3H2 for the morphotype type a "normal" have been re-picked using the same criteria as above. The stable oxygen and carbon isotope measurements on these samples were carried out at the isotope laboratory at IFM-GEOMAR with a CARBO KIEL automated carbonate preparation device linked on-line to a Finnigan MAT 252 mass spectrometer. External reproducibility was 0.02 ‰ for $\delta^{13}C$ and 0.03 ‰ for $\delta^{18}O$ (1-sigma values), as calculated from 8 replicate analyses of the internal carbonate standard (Solnhofen Limestone) performed before and after the analyses of our specimens. The isotope data are referred to the PDB scale. The difference between the two sets of measurements was 0.11 +/- 0.28 for $\delta^{18}O$ (ranging between -0.65 and 0.65), and -0.23 +/- 0.3

for $\delta^{13}C$ (ranging between -0.8 and 0.45). The reproducibility of the data is excellent and there is no systematic bias (fig. 18).

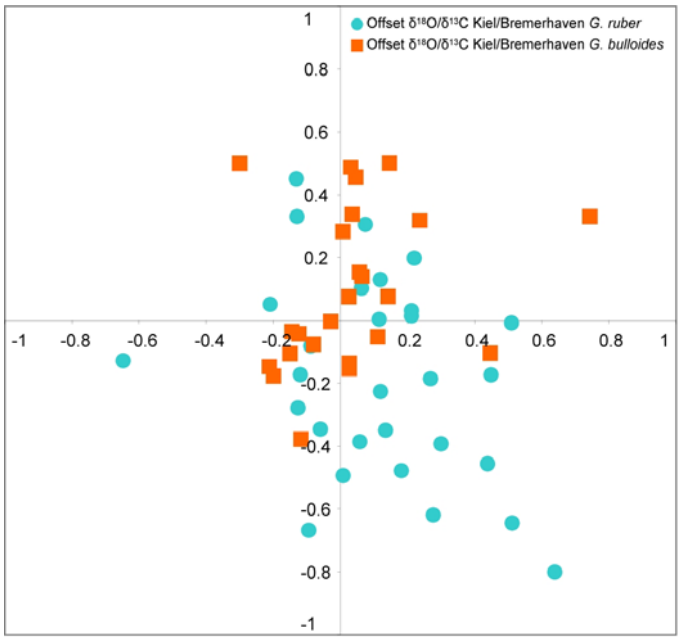

Figure 18: Offset between two different stable isotopic measurement series (Kiel and Bremerhaven) on planktonic foraminifera tests, offset of $\delta^{18}O$ plotted against offset of $\delta^{13}C$ for *G. ruber* (circles) and *G. bulloides* (squares).

2.7. XRF elemental scans

In both cores, intervals spanning MIS 9/MIS 10 to MIS 12 were sampled using U-channels (2x2 cm). X-ray fluorescence (XRF) scans of the GeoTü-SL96 core and the U-channel from ODP Site 964, were carried out by an ITRAX core scanner (CROUDACE et al., 2006) with 1 cm resolution at MARUM, University of Bremen. Selected element ratios in cores ODP Site 964 A and D and GeoTü-SL96 for MIS 11 and MIS 1, normalised to Al, were used to reveal sediment redox changes associated with the sapropels and to assess the origin of terrigenous sediments. Three ash layers had previously been visually identified in the studied section from ODP Site 964 (EMEIS et al., 1996) and confirmed by XRF values (tab. 3). The Santorini volcano was the largest source of volcaniclastic sediment in the Eastern Mediterranean during the late Quaternary. Periodical occurrences of ash layers deposited as turbidites disturbs several parts of the record in ODP Site 964 (e.g. AKSU et al., 2008) and thus were cut out of the record (fig. 19). There were no ash layers in GeoTü-SL96, most probably because it was located too far south of the eruptive centres.

Table 3: Position of ash layers in ODP Site 964, detected by distinct elemental ratio peaks. The ashes, as they do not contain any coarse fraction ≥ 63 µm, were deleted from the record for palaeoceanographic analyses.

Ash layers ODP Site 964	Ash chemistry	Thickness (cm)	cmbsf from	cmbsf to
A	K/Al	3	1738	1741
B	Zr/Al	7	1751	1757
C	Fe/Al	8	1853	1861

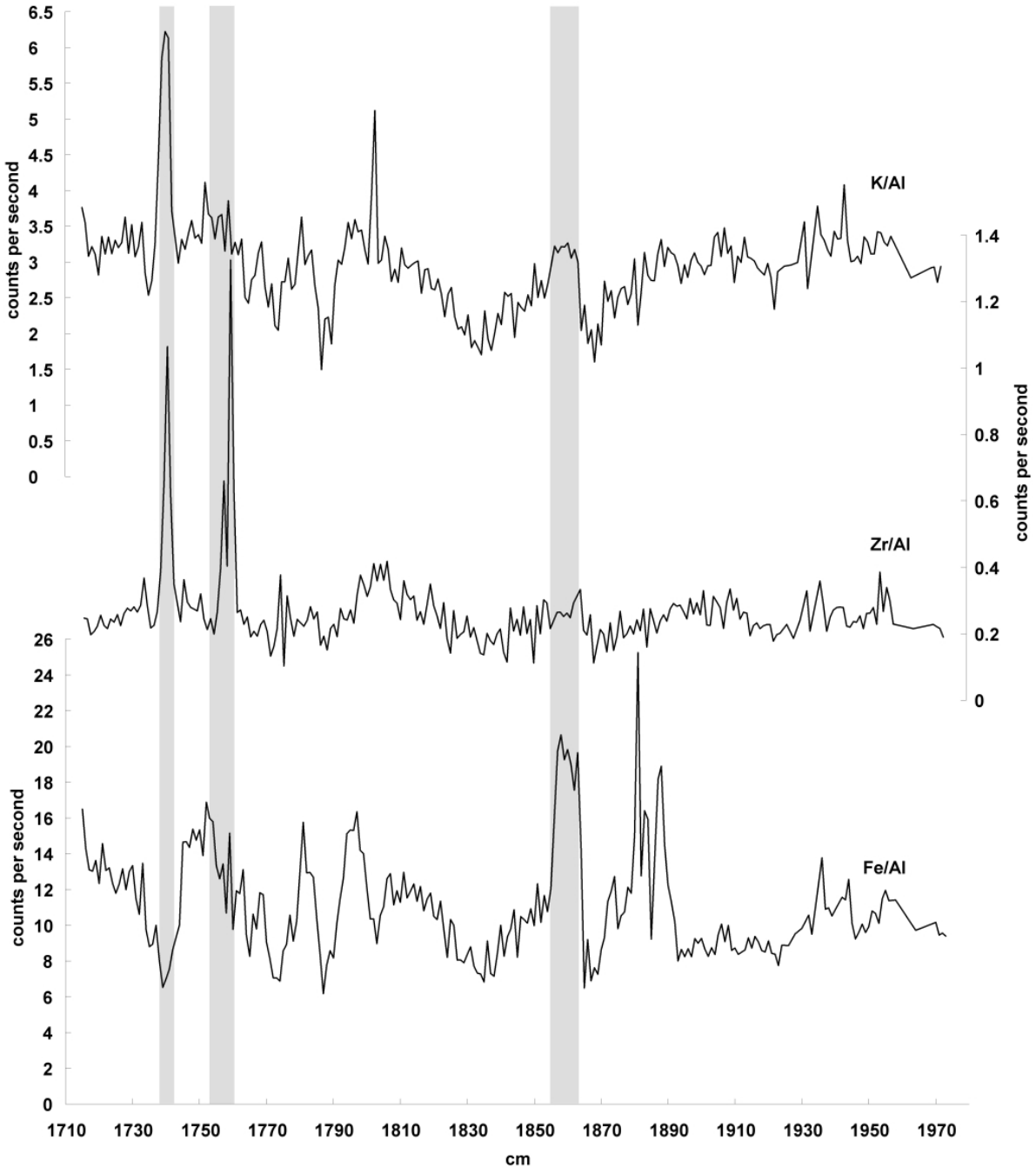

Figure 19: Elemental ratios normalised to aluminium, grey bars denote position of ash layers. Upper panel shows K/Al ratio, middle panel shows Zr/Al ratio and lower panel displays Fe/Al ratio.

2.8. Alkenone measurements

To validate ANN temperature reconstruction by a completely independent palaeothermometer, alkenone measurements were done in the first place at a preliminary low resolution every fifth cm of the core section. At Tübingen University, the 31 samples (4 cm^3) were freeze dried and ground and then sent to the laboratory of the section of marine geology at the "Leibniz Institute for Baltic Sea research, Rostock-Warnemuende, Germany" where

they were processed following the method described in EMEIS et al. (2003). Because of the generally low abundance of $C_{37:4}$ alkenones in the analysed samples and for consistency with existing records of the North Atlantic region (e.g., ROSELL-MELE et al., 1997; VILLANUEVA et al., 1997, 2001; MUELLER et al., 1998), the simplified version of the index U^K_{37}' (PRAHL & WAKEHAM, 1987; MUELLER et al., 1998) was used to calculate palaeotemperatures for the analysed samples: $U^K_{37}' = [C_{37:2}]/ [C_{37:2}+C_{37:3}]$ or $SST = [U^K_{37}'-0.044]0.033$. The standard deviation of the alkenone values were calculated following ALTMAN & BLAND (2005).

3. Results and Discussions

3.1. Chronostratigraphic framework

The prerequisite for palaeoceanographical and palaeoclimatological evaluation of the MIS 11 proxy records was the establishment of a robust chronological framework for

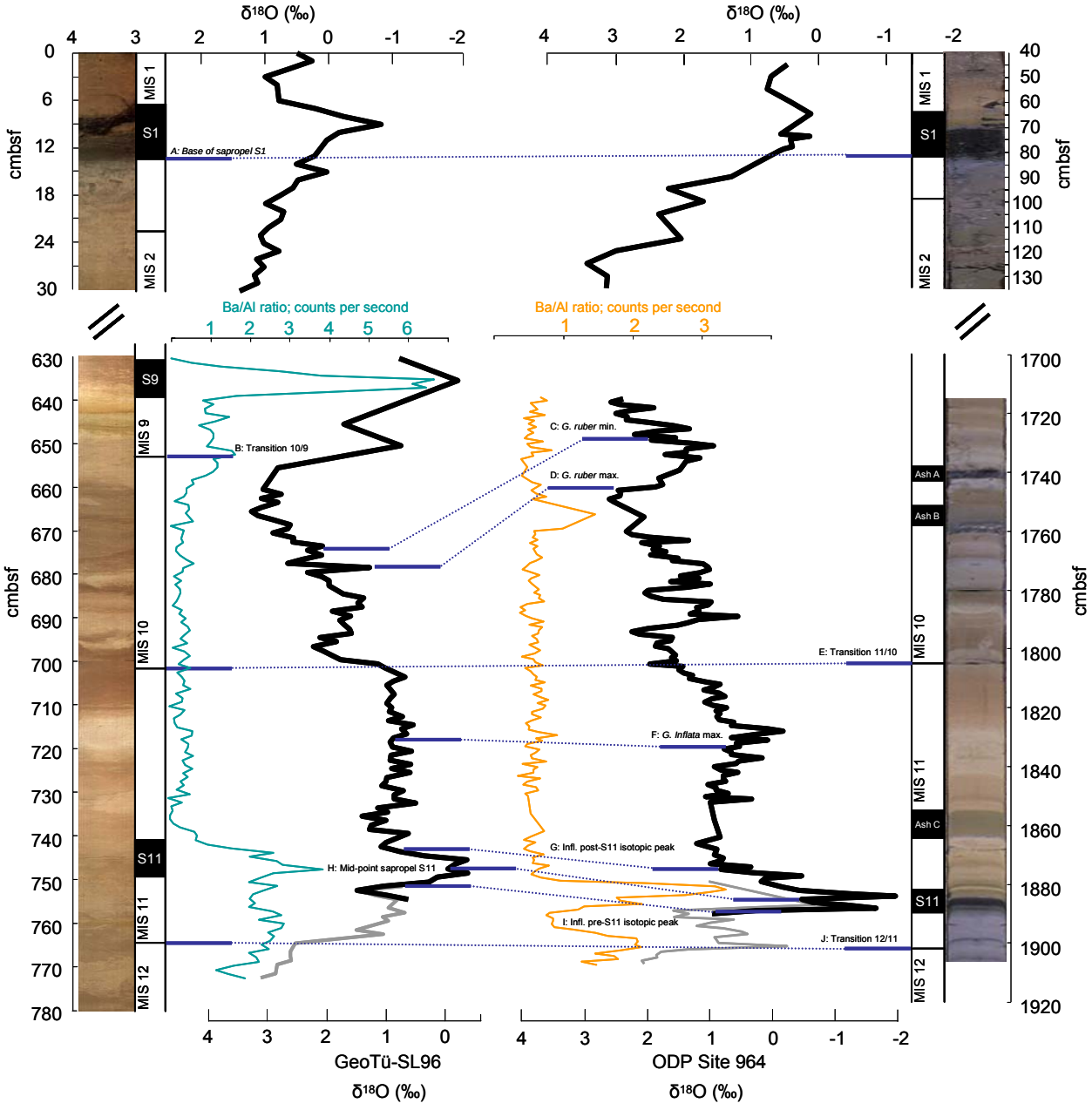

Figure 20: A stratigraphic interpretation of visible sediment structures, Ba/Al profiles and oxygen isotopes by *G. ruber* (thick black line) and *G. bulloides* (thick grey line) and planktonic foraminifera assemblage counts in ODP Site 964 and GeoTü-SL96 for MIS 11 (lower panel). Ba/Al ratios in MIS 11 are denoted by thin lines for both cores. Upper panel shows sediment properties and oxygen isotopes of MIS 1.

the two investigated cores (GeoTü-SL96 and ODP Site 964). This framework was developed in three steps: the first is based on the appearance of sapropel layers, which allow

both the correlation between the cores and an assignment of absolute ages; the second is based on oxygen stable isotope stratigraphy and the third, fine-tuning step is based on the recognition of events recorded as quantitative changes in the planktonic foraminifera assemblages, allowing higher-resolution correlation between the two cores (fig. 20; tab. 4).

Table 4: List of age model tie points and ages for the two investigated cores.

Tie Point	Event	Age (ka)	Reference	ODP Site 964 (cmbsf)	GeoTü-SL96 (cmbsf)
A	Base of S1 sapropel	9.8	de Lange et al. 2008	85	13
B	Transition 10/9	337	Lisiecki and Raymo 2005		655
C	*G. ruber* minimum			1728	673
D	*G. ruber* maximum			1747	679
E	Transition 11/10	362	Lisiecki and Raymo 2005	1811	700
F	*G. inflata* maximum			1836	719
G	Infl. post-Sapropel-isotope-peak			1876	744
H	Mid-point sapropel MIS 11	406	Rossignol-Strick and Paterne 1999; de Lange et al. 2008	1885	747
I	Infl. prae-Sapropel-isotope-peak			1889	751
J	Transition 12/11	424	Lisiecki and Raymo 2005	1902	764

The volcanic ashes found in ODP Site 964 by XRF scans and lithological evaluation were cut out of the sedimentological record of this core before the age model was constructed as there were no coarse fractions (≥ 63 µm) within these intervals (tab. 3; fig. 19).

Sapropel stratigraphy

In order to tune the Holocene part of the cores, the base of sapropel S1 was used (tie point A, tab. 4; DE LANGE et al., 2008) and the sedimentation rate between the base of the sapropel and the top of the core (considered to be recent) was extrapolated to MIS 2 sediment. This approach was considered sufficient, because the MIS 2-1 interval was not the primary focus of this study and the data were used only to obtain a comparative value for the magnitude of proxy changes observed during the MIS 11 target interval.

The first step in the tuning approach of the MIS 12- MIS 9 section was to identify the sapropel layers in both cores. According to the framework developed by ROSSIGOL-STRICK (1983), the analysed sections should have contained the manifestation of sapropels S9 in MIS 9 and S11 in MIS 11. In core ODP Site 964, the sapropel of MIS 11 was clearly

identifiable (tie point H, tab. 4) and the onset of the sapropel was tuned with a lag of 3 ka (ZIEGLER et al., 2010) after the second insolation maximum of MIS 11, dated with 406 kyr B.P. (ROSSIGNOL-STRICK, 1983, 1985; ROSSIGNOL-STRICK & PATERNE, 1999) at the onset of MIS 11 (BERGER & LOUTRE, 1991; DE LANGE et al., 2008), considering that the first insolation peak is unlikely to have produced a sapropel due to relatively low insolation intensity (fig. 21).

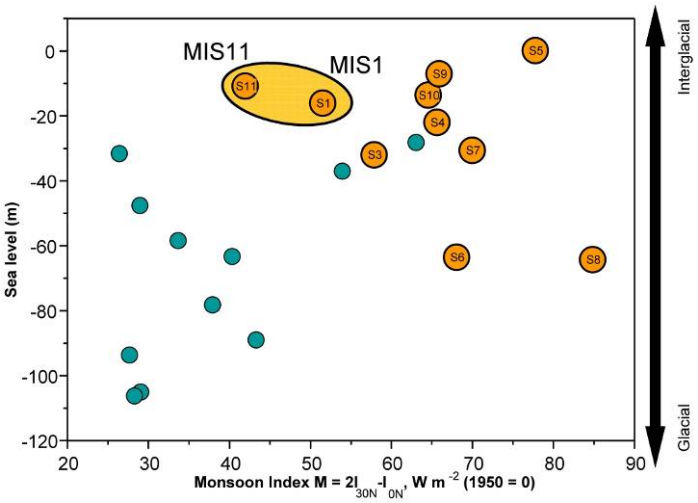

Figure 21: Monsoon index peaks (ROSSIGNOL-STRICK, 1983, 1985) plotted against sea level (ROHLING et al., 2009). Arrow denotes area of glacials and interglacials.

The sapropel of MIS 9 in ODP Site 964 was not recovered in the investigated section. Surprisingly, the two expected Sapropel layers in GeoTü-SL96 could not be identified in the sediment record by identification of a black layer. Therefore, Ba/Al profiles (fig. 20) for this core were inspected to help identify intervals of elevated productivity irrespective of the preservation of organic matter (THOMSON et al., 1995; VAN SANTVOORT et al., 1997). The Ba/Al results show two periods of elevated productivity located in positions consistent with the expected positions of the sapropels. For the ODP core, the scan confirms the position of the visible sapropel and the initial observation that the analysed sections did not contain S9. The freshwater peaks displayed in light stable oxygen isotopes and sapropel formation in MIS 1 and MIS 11 are highly comparable (fig. 20), despite the fact that GeoTü-SL96 sediment record in MIS 11 shows no

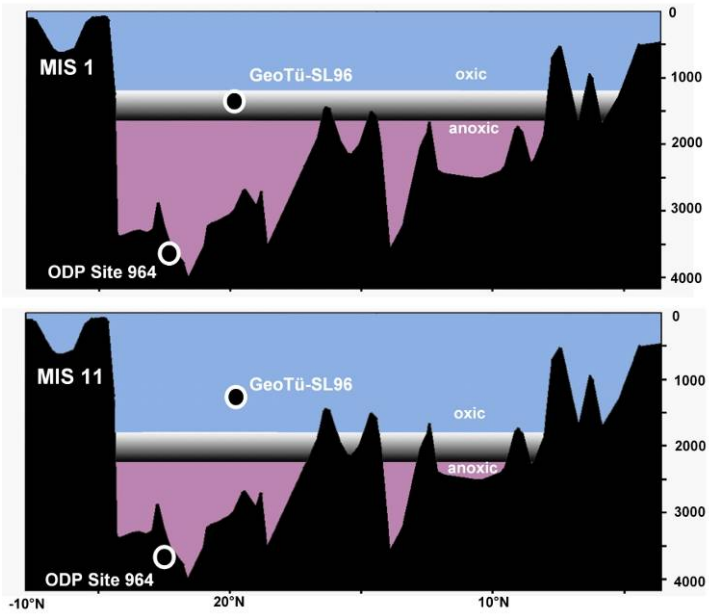

Figure 22: Schematic profile of the Eastern Mediterranean basin, denoting position of cores ODP Site 964 and GeoTü-SL96, showing the inferred depth of oxycline (grey bar) in MIS 11 and MIS 1 (after DE LANGE et al., 2008).

dark layer (fig. 11). The freshwater and Ba/Al peaks coincide with relatively large numbers of benthic foraminifera in this core. The most probable explanation thus seems to be a different depth position of the oxycline for MIS 11 than for MIS 1, rather than an oxidised 'ghost sapropel'. The oxycline might have been about 500 m deeper than for the Holocene sapropel, reaching the depth position of ODP Site 964 but not GeoTü-SL96 (fig. 22).

It is found that sapropel formation/freshwater peak in both investigated cores seem to have been triggered by the second insolation peak after deglaciation in MIS 11, which is in conflict with the situation in MIS 1, where sapropel formation coincided with the first insolation maximum after deglaciation. The alignment of the two freshwater events in MIS 11 and MIS 1 decouples the comparison of these two stages from expected similarity in orbital patters, and allows for an alternative matching of the two records.

Isotope stratigraphy

For this step of the tuning procedure, the $\delta^{18}O$ record in both cores was used to correlate between the cores and with the global MIS stratigraphy. This is possible in the Mediterranean, because the salinity effect due to sea level change accentuates even surface water isotopic signals – in other words, the surface dwelling foraminifera do not only record SST but in fact most of the signal is due to salinity changes (e.g. GONZALEZ-MORA et al., 2008). The $\delta^{18}O$ values from the planktonic foraminifera *G. ruber* and *G. bulloides* tests show very consistent trends in the two cores, allowing the identification of major MIS boundaries, including MIS 11/12 (tie point J, tab. 4); MIS 11/10 (tie point E, tab. 4) and MIS 10/9 (tie point B, tab. 4). The exact positions of the MIS boundaries in both cores were located at points of the steepest gradient in isotopic change. The $\delta^{18}O$ boundaries were given higher priorities than the centres of glacial and interglacial intervals because of higher significance in differences between the stable isotope values at the terminations.
Ages of the terminations were tuned to LISIECKI & RAYMO (2005A, 2005B) benthic stack. Transition 10/9 (tie point B, tab. 4) was only recognised in core GeoTü-SL96 due to the further reach of this section and it was dated with 337 kyr B.P. (LISIECKI & RAYMO, 2005A, 2005B). Transition 11/10 (tie point E, tab. 4) was found in both records and dated with 362 kyr B.P. (LISIECKI & RAYMO, 2005A, 2005B); transition 12/11 (tie point I, tab. 4) was also found in both records and dated with 424 kyr B.P. (LISIECKI & RAYMO, 2005A, 2005B).

In addition to MIS boundaries, the oxygen isotope curves showed strong negative anomalies corresponding in all cases exactly to the position of visible or Ba/Al-determined

sapropels. This allows to define an additional tie point G (tab. 4) "inflectionpoint post-sapropel-isotope-peak", which was found right after the extremely light values (~ -1.6 ‰) accompanying the MIS 11 sapropel in both cores. This tie point was used to correlate both cores but could not be assigned any absolute age, because the duration of the MIS 11 sapropel is not known. The oxygen isotopic peak in ODP Site 964 shows that even in this sapropel most of the organic rich layer is oxidised.

Foraminifera Biostratigraphy

Further improvements of the age model were performed by the planktonic foraminifera assemblage correlations within MIS 11 of the two cores. On the basis of 206 samples from ODP Site 964 and 145 samples of GeoTü-SL96, which were quantitatively analysed, the correlation between the two cores was fine tuned with three biostratigraphic events. Tie Points C and D (tab. 4) correspond to two successive maxima in relative abundances (~ 80 %) of *G. ruber* during early MIS 10, and tie point F (tab. 4) denotes a maximum in *G. inflata* within MIS 11 (~ 20 %).

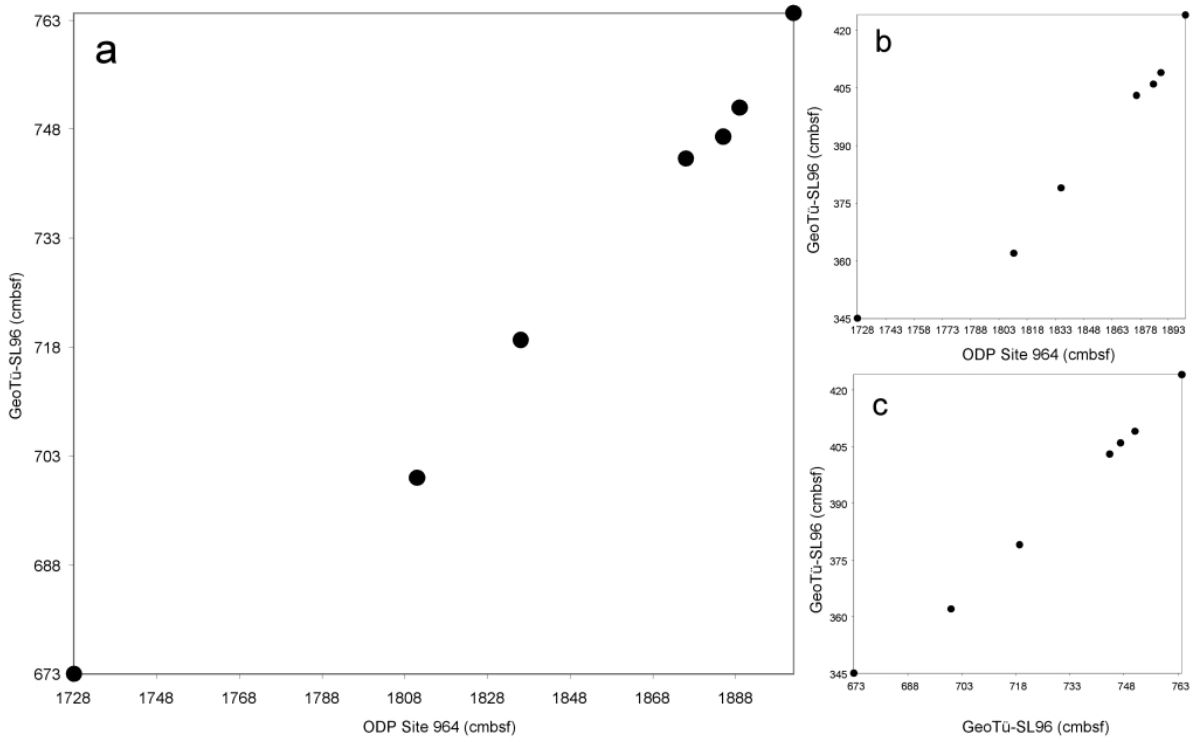

Figure 23: Scatter plot of age model tie points, a: depth (GeoTü-SL96) against depth (ODP Site 964); b: age versus depth (ODP Site 964); c: age against depth (GeoTü-SL96).

These tie points were then used to correlate one core to the other and the common depth scale was then converted to age using the dated age point (fig. 23). The ages of the youngest and oldest samples were extrapolated using the sedimentation rate from the nearest

dated segment of the age model. The sedimentation rates are assumed constant between selected age control points and varied between 3.4 – 6.3 cm/kyr (ODP Site 964) and 1.8 – 2.2 cm/kyr (GeoTü-SL96)

3.2. Comparability of palaeoclimate trends and foraminifera assemblage dynamics in the Eastern Mediterranean between MIS 11 and MIS 1

Stable isotope trends

In order to reconstruct the climate of MIS 11 and to allow for a comparison with the Holocene, the corresponding parts of two Eastern Mediterranean cores were selected for analyses based on the position of the sapropel layer in MIS 11 or, if this layer was not manifested in the sediment record, based on the succession of underlying layers. Both cores present well preserved sapropel layers for MIS 1. ODP Site 964 shows a part of the original sapropel in MIS 11 but GeoTü-SL96 lacks any visible trace of sapropel in MIS 11 (fig. 11). As a first step, a continuous stable isotopic record based on planktonic foraminifera was generated. *G. ruber* was analysed where available, but in MIS 12, this species was too rare and had to be substituted with *G. bulloides* during this time interval. The resulting surface water stable isotopic record across MIS 11 as well as the Holocene reflect distinct events of freshwater inflow to the basin superimposed on a general glacial – interglacial trend (fig. 24). The oldest part of the record is represented by *G. bulloides*-derived values during the transition MIS 12/MIS 11, reflecting a change from colder temperatures as well as the deglacial sea-level rise and associated changes in seawater residence time in the basin into interglacial conditions in both cores. During interglacial conditions of MIS 11 as well as MIS 1, stable oxygen isotope measurements show a distinct peak in both cores with extremely light values corresponding to sapropel deposition, except for MIS 11 in Core GeoTü-SL96, where no sapropel is developed. The freshwater peak is followed by a long period of stable interglacial conditions during MIS 11, terminated by a moderate transition into the glacial MIS 10 (fig. 24); GeoTü-SL96 record displays also transition MIS 10/MIS 9 by a sharp increase of light isotopic values.

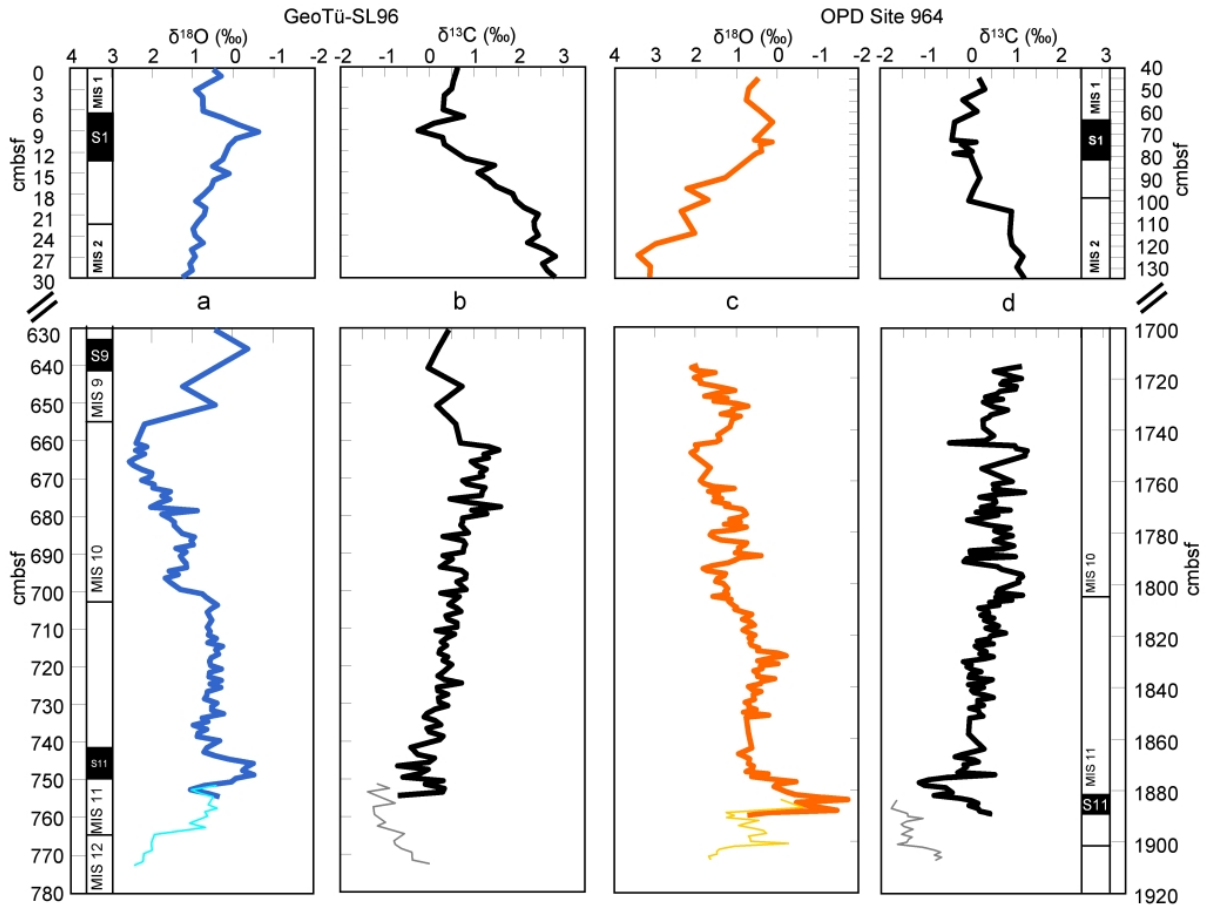

Figure 24: Stable isotopic measurements ($\delta^{18}O$ and $\delta^{13}C$) on the planktonic foraminifera species *G. ruber* (thick line) and *G. bulloides* (thin line) during the Holocene (upper panels) and MIS 9 to MIS 12 (lower panels) in GeoTü-SL96 (panel a and b) and ODP Site 964 (panel c and d).

The interval which contains stable isotope values for both *G. ruber* and *G. bulloides* are available, the offset between oxygen isotope values of the two species are negligible whereas carbon isotopes show a considerable offset, suggesting strong disequilibrium fractionation. In the light of differences in habitat depth between the two species (HEMLEBEN et al., 1989), the nearly identical oxygen isotope values either reflect ambient conditions that were homogeneous irrespective of habitat differences, or a shift in habitat preferences in *G. bulloides*.

The *G. ruber* derived oxygen isotopes display peak values of ~ -1.8 ‰ in ODP Site 964 and peak values of ~ -0.6 ‰ in GeoTü-SL96 coinciding with the sapropel event in MIS 11. Light isotopic signatures stay relatively high around +0.5 ‰ during MIS 11 after sapropel formation. After MIS 10 boundary, light isotopes decrease and show values around + 1.2 ‰. The carbon isotope records measured on shells of *G. ruber* remain stable and show no distinct change of values at the MIS boundaries, except for the transition MIS 12/ MIS 11, where the isotopes were measured on tests of *G. bulloides*. There, a significant difference between values of *G. ruber* and *G. bulloides* can be noticed, which may reflect

vital effects and/or a systematic effect. MIS 11 and MIS 1 values in GeoTü-SL96, regarding an alignment of the two sapropel events, show nearly equal patterns, whereas the pattern in ODP Site 964 shows a distinct offset of ~ 1.8 ‰ between Holocene and MIS 11 during sapropel formation (fig. 24).

Planktonic foraminiferal assemblage dynamics

The planktonic foraminifera assemblage composition for MIS 11 time interval reflects glacial/interglacial changes as well as environmental changes within the investigated glacials and interglacials (fig. 25 a-d). Both cores show highly comparable patterns. A total of 19 species (plate I and II) of planktonic foraminifera were identified in the investigated interval. An extreme glacial fauna with *N. incompta*, *N. dutertrei*, *G. bulloides, G. glutinata* and *T. quinqueloba* inhabited the investigated area during MIS 12. A similar glacial assemblage, although much less extreme in terms of the dominance of the glacial elements, is observed towards the end of MIS 10 in GeoTü-SL96 and also during MIS 2 in both cores. *G. ruber* increases gradually toward the end of MIS 11 into early MIS 10 and is clearly the most dominant species during both interglacials MIS 11 and MIS 1, but also during early MIS 10. The most conspicuous feature of MIS 11 is the strong cyclicity in the abundance of *G. inflata* and *G. truncatulinoides*, which is highly consistent between the two cores.

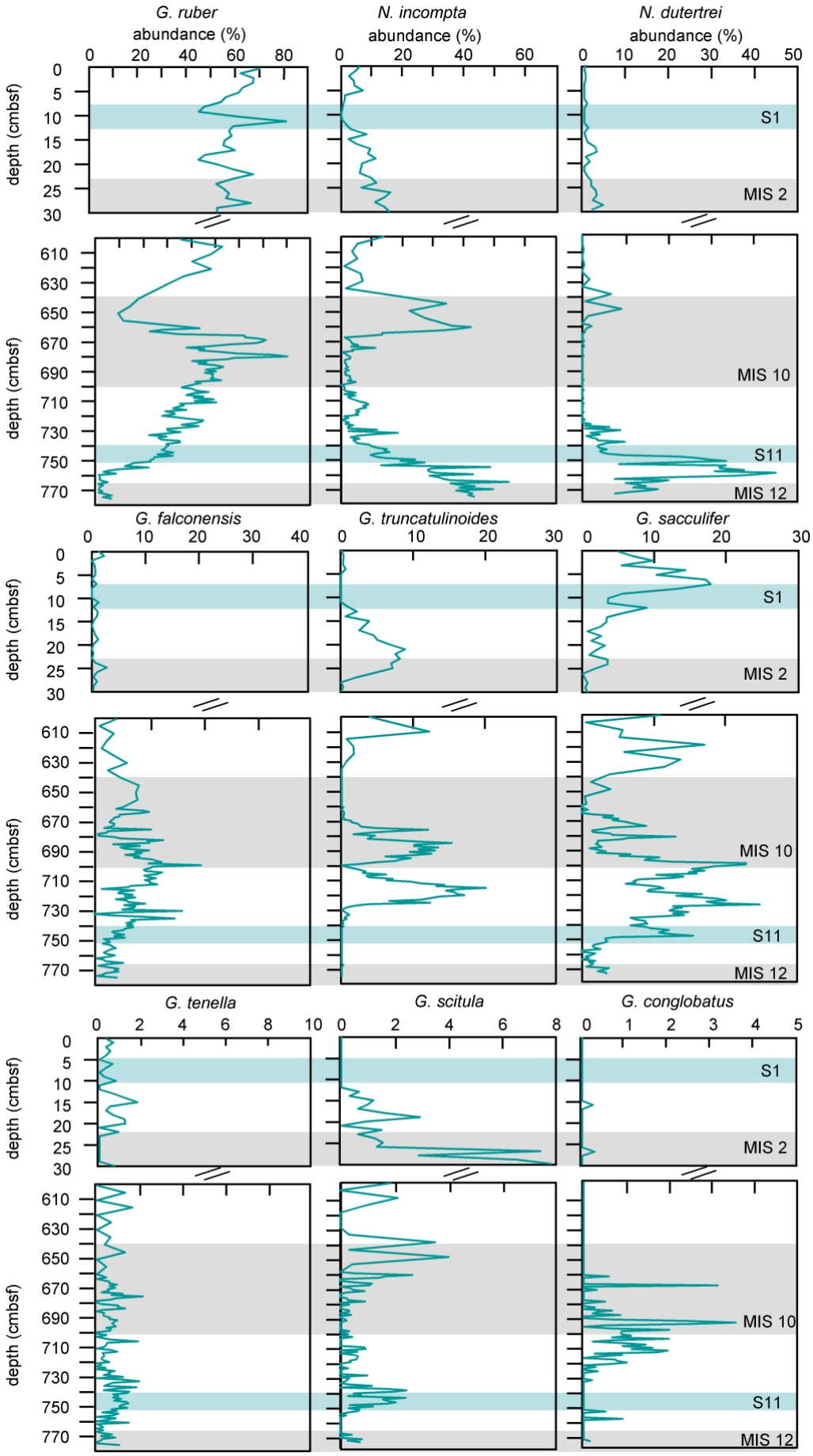

Figure 25: Abundances of planktonic foraminifera species abundances for GeoTü-SL96 (a and b) and ODP Site 964 (c and d) during the investigated interval. Grey bars denote MIS boundaries and sapropel/freshwater peak position.

25b

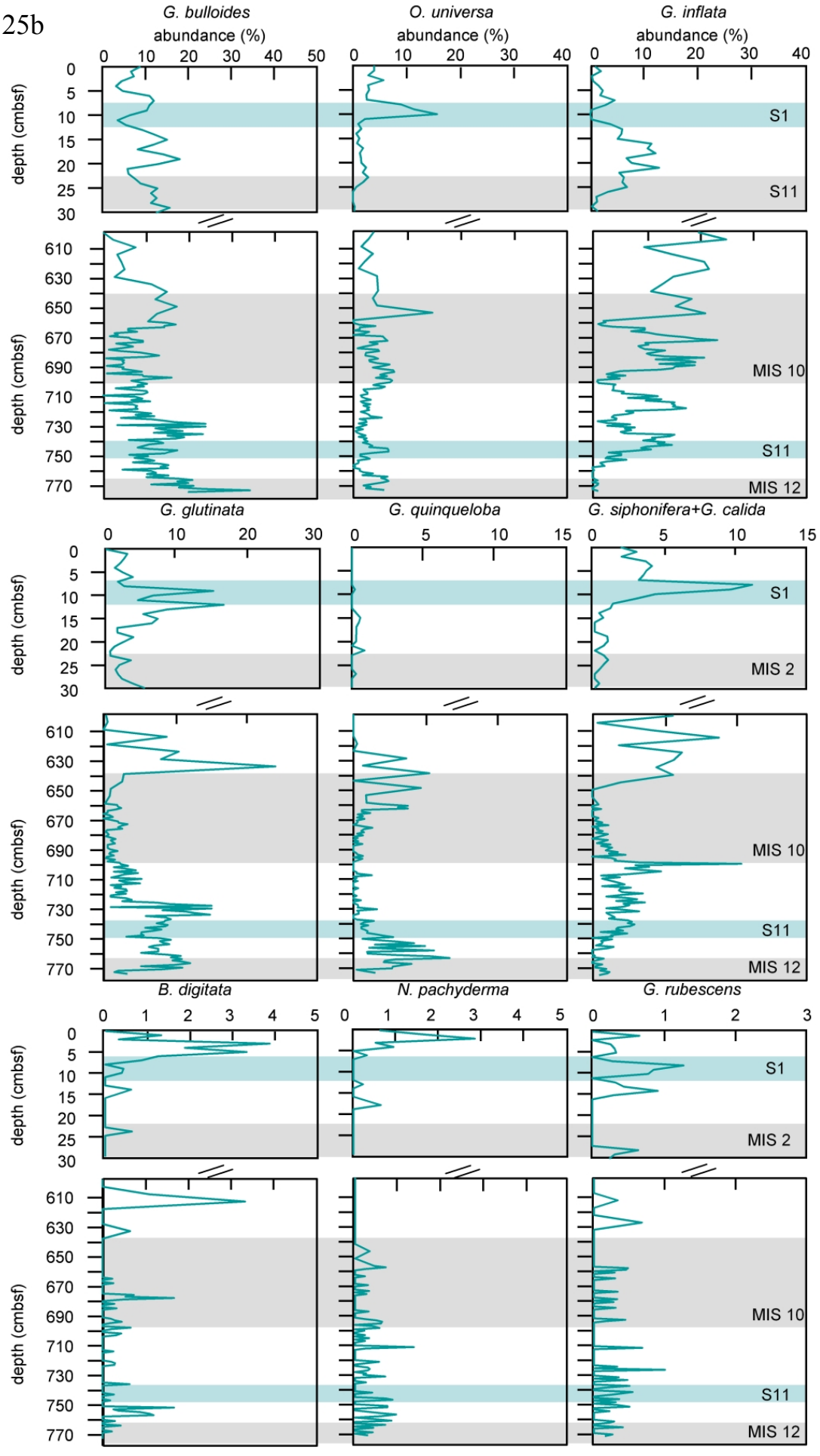
G. bulloides
abundance (%)
O. universa
abundance (%)
G. inflata
abundance (%)
depth (cmbsf)
S1
S11
MIS 10
S11
MIS 12
G. glutinata
G. quinqueloba
G. siphonifera+G. calida
S1
MIS 2
MIS 10
S11
MIS 12
B. digitata
N. pachyderma
G. rubescens
S1
MIS 2
MIS 10
S11
MIS 12

25c

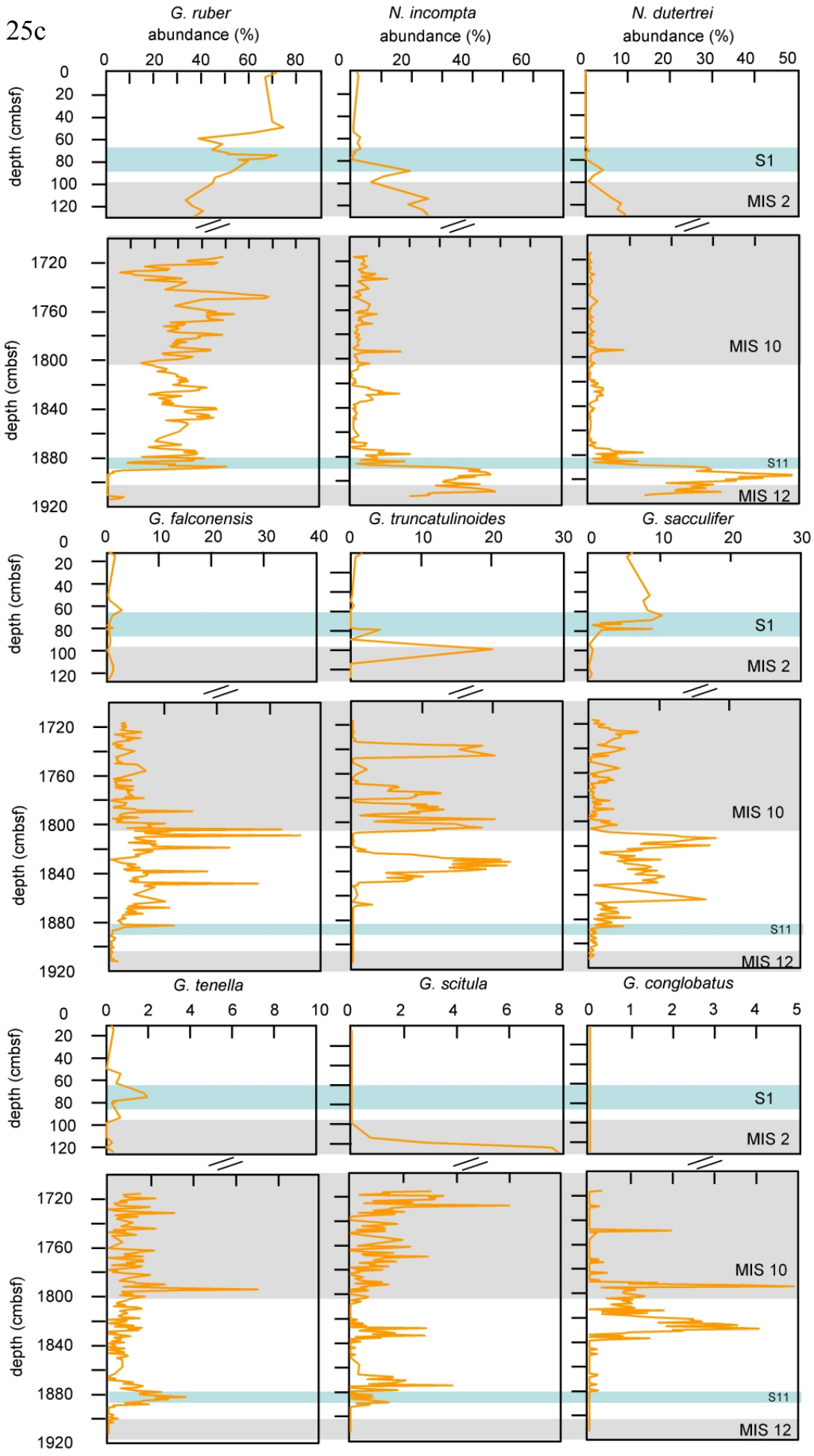
G. ruber
abundance (%)
N. incompta
abundance (%)
N. dutertrei
abundance (%)
depth (cmbsf)
S1
MIS 2
MIS 10
S11
MIS 12
G. falconensis
G. truncatulinoides
G. sacculifer
G. tenella
G. scitula
G. conglobatus

25d

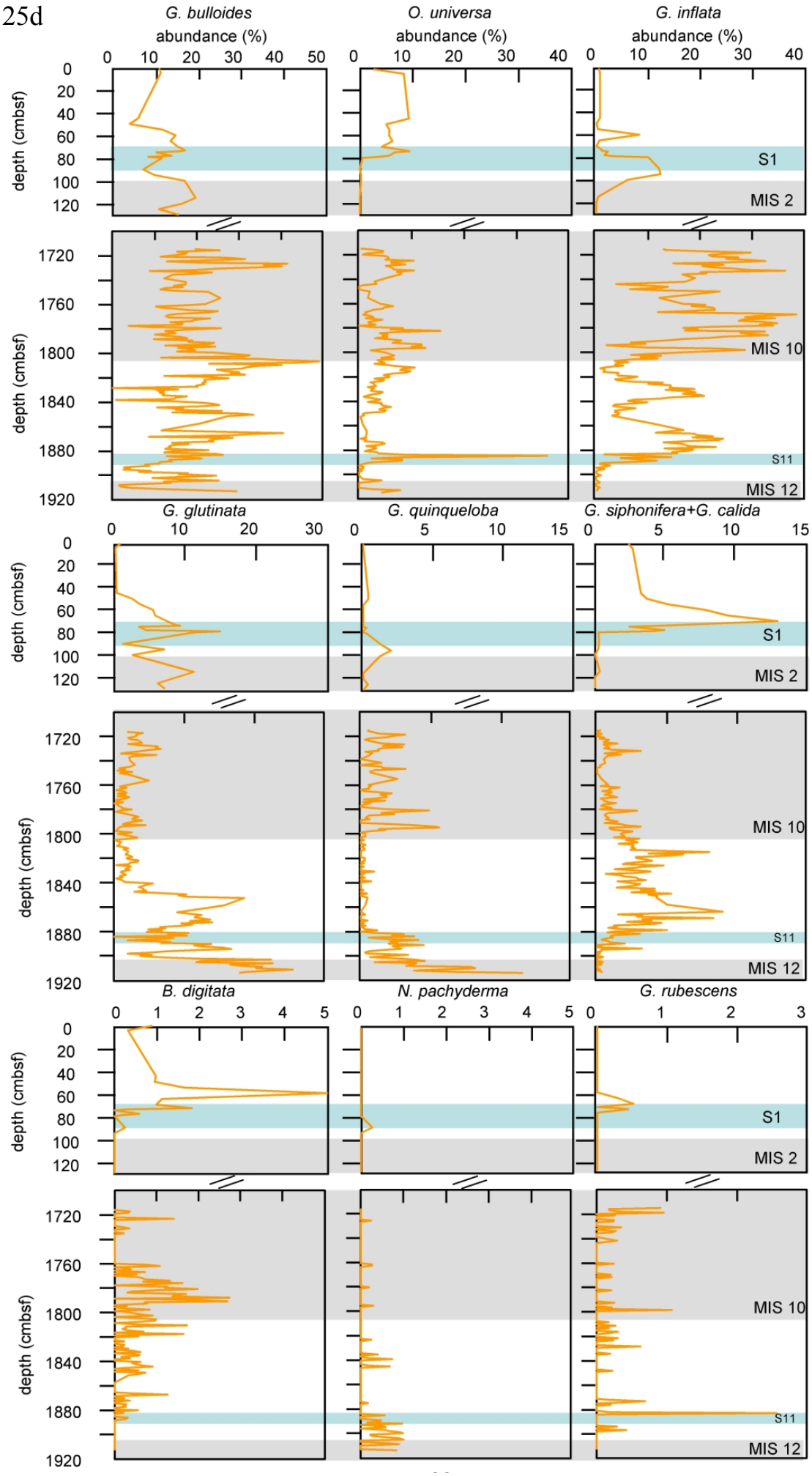
G. bulloides
abundance (%)
O. universa
abundance (%)
G. inflata
abundance (%)
depth (cmbsf)
S1
MIS 2
MIS 10
S11
MIS 12
G. glutinata
G. quinqueloba
G. siphonifera+G. calida
B. digitata
N. pachyderma
G. rubescens

Alignment of sapropel intervals between MIS 11 and MIS 1

The construction of an independent age model (fig. 20; tab. 4) through orbital tuning allows for an independent assessment of the onset and duration of MIS 11 interglacial conditions in the Eastern Mediterranean. There are clearly conspicuous differences between MIS 12/ MIS 11 and MIS 2/ MIS 1 transitions in terms of the timing of sapropel formation: whereas sapropel S1 developed in the course of the first insolation maximum after deglaciation, the sapropel of MIS 11 coincides with the second and more intense insolation peak after termination V (fig. 26). This non-analogue situation suggests that an alignment of the two stages based on the sapropel formation is required when the intention is to extract information about future climate development decoupled from anthropogenic influences. Due to the high comparability of the two sapropel events, an alignment of the two different insolation maxima seems to be the best option, in spite of previous suggestions to align insolation minima (e.g. MASSON-DELMOTTE et al., 2006, RUDDIMAN, 2007). Such system of alignment is consistent with that proposed by ROHLING et al. (2010) on the basis of sea level development between MIS 1 and MIS 11.

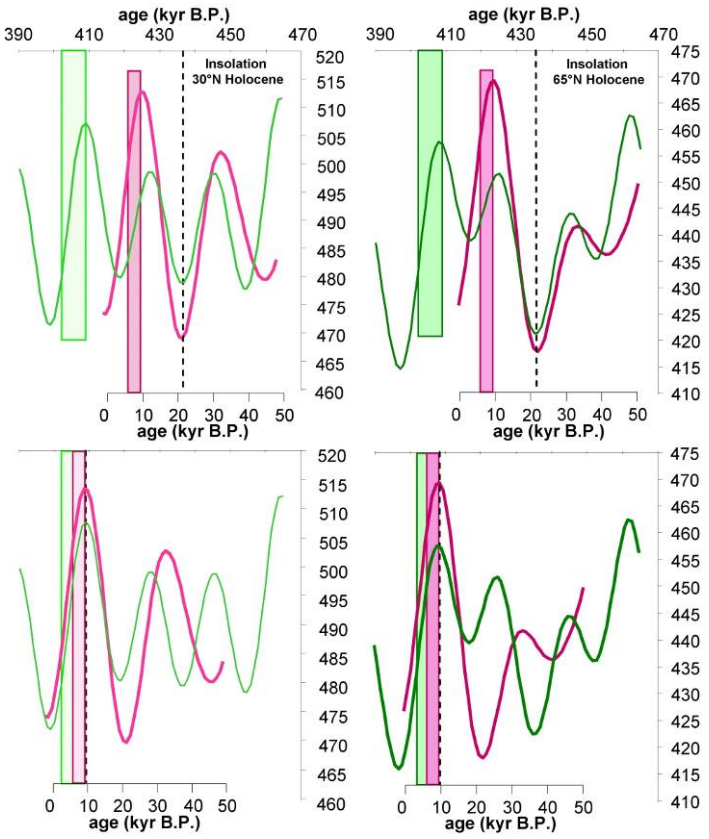

Figure 26: Alignment of Holocene and MIS 11 June insolation at 30°N (left panels) and 65°N (right panels) and climatic pattern in the eastern Mediterranean (BERGER & LOUTRE, 1991). Upper panels show an alignment based on last insolation minimum before deglaciation; lower panels show an alignment based on insolation maxima linked with sapropel development; dotted bars denote position of MIS 11 sapropel, striped bars denote position of MIS 1 sapropel.

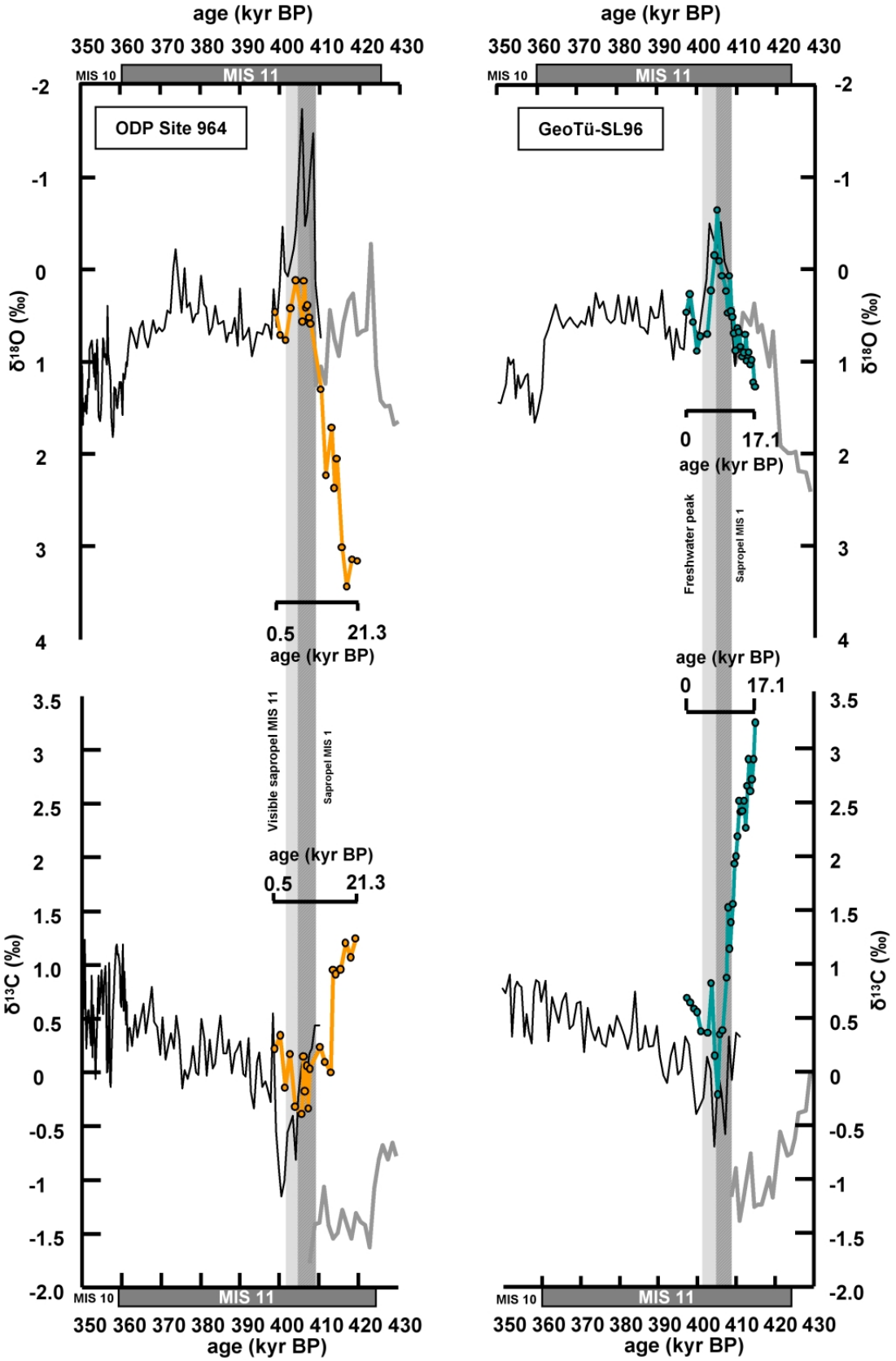

Figure 27: An alignment of stable isotopic data across the two interglacial sapropel intervals in ODP Site 964 (left panels) and GeoTü-SL96 (right panels). Upper panel shows oxygen isotopes, lower panel carbon isotopes. Line with circles denotes measurements on *G. ruber* originated from MIS 1 in both cores. Black line denotes *G. ruber* data of MIS 11, grey line *G. bulloides* data of MIS 12. Grey bar denotes sapropel position/freshwater peak in MIS 11; striped bar sapropel position in MIS 1.

A direct alignment of the sapropel interval of MIS 11 and MIS 1 shows matching oxygen isotopic values in GeoTü-SL96 for both time intervals with peak values of ~ -0.6 ‰ (fig. 27). The comparison of the two stages in ODP Site 964 shows a light oxygen isotope peak in both, but the Holocene peak only reaches values of up to +0.2 ‰ during sapropel interval, whereas the oxygen isotope signal in ODP Site 964 displays a massive freshwater peak, with values ~ -1.8 ‰. In the light of these differences, it is astonishing that the two cores are just ~ 260 sea miles away from each other. Such a large stable oxygen isotopic gradient in the surface waters during MIS 11 would require a strong circulation-controlled pattern of monsoonal freshwater redistribution in the Eastern Mediterranean at that time. The lesser extent of the peak values at Site GeoTü-SL96 implies that this site must have been located directly in the way of the inflowing modified Atlantic surface water, which would carry normal marine isotopic signature during MIS 11, which would be in stark contrast to the present-day situation where ODP Site 964 is apparently more proximal to the inflowing modified Atlantic water (fig. 7). Apart from a monsoonal maximum and thus enhanced Nile runoff, freshwater inflow from the Bosporus opening could have led to the exceptional conditions in MIS 11, as suggested for the Holocene one (LANE-SERFF et al., 1997; SPERLING et al., 2003; VIDAL et al., 2010).

SST trends during MIS 11 and MIS 1

Transfer function SST estimates based on planktonic foraminifera assemblages allow for a direct and methodologically consistent comparison of SST trends for MIS 11 and MIS 1. Additional alkenone measurements from ODP Site 964 were used to verify the transfer function results. This is a result of the fact, that transfer functions are here applied to an interval more than 400 kyrs in the past, where environmental preferences of foraminiferal species could have changed, making the estimates less reliable (KUCERA et al., 2005). The SST estimates in both cores show comparable trends across the MIS 12/MIS 11 boundary, with alkenone SST values in MIS 12 and MIS 11 consistent with annual average SST reconstructed by transfer functions. The records show relatively low temperatures during MIS 12 and during the onset of MIS 11 until sapropel formation (fig. 28). During the MIS 11 sapropel phase, the reconstructed SST reached present-day levels (ODP Site 964: ~ 20 °C; GeoTü-SL96: ~ 21 °C) and stayed within this range throughout MIS 11. Surprisingly, the transfer function SST remained high after the MIS 11/MIS 10 glacial inception and throughout much of MIS 10. These higher glacial SST values during MIS 10

are comparable with values for MIS 2 in the investigated cores and in the results of HAYES et al. (2005) but substantially warmer than the reconstructed values for MIS 12.

A Detrended Correspondence Analysis of the planktonic foraminifera assemblage composition confirms the observed transfer-function derived patterns (fig. 29). The pre-

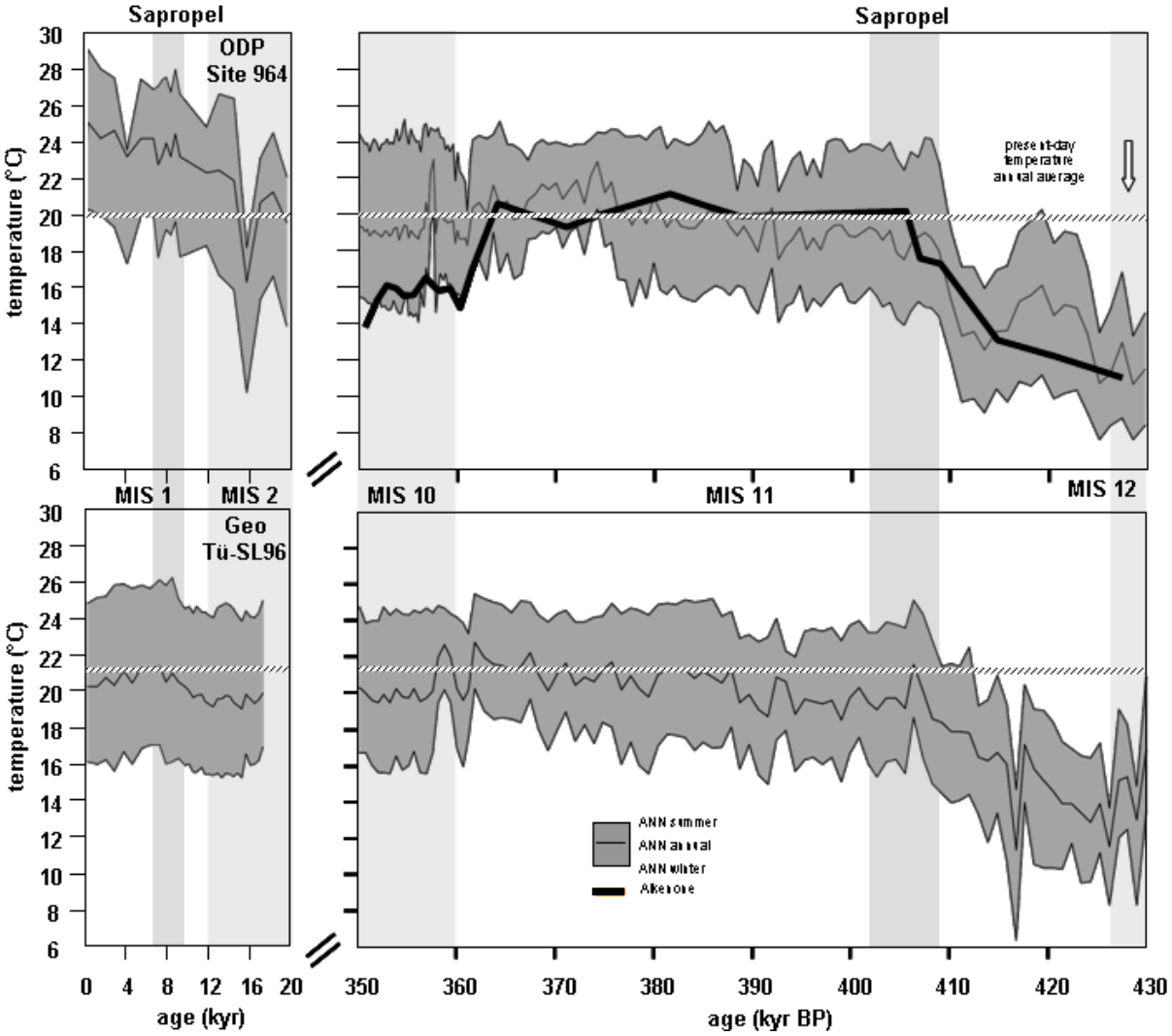

Figure 28: Reconstructed temperatures of MIS 2 to MIS 1 and MIS 12 to MIS 10 in ODP Site 964 (upper panels) and GeoTü-SL96 (lower panels). Transfer function (ANN) based reconstructed temperatures are denoted by the grey filled graphs. The upper boundary of the grey filled graph denotes summer SST, the middle black line denotes annual and the lower boundary winter SST. In the upper right graph, alkenone reconstructed temperatures were denoted by a thick black line (upper right panel). The dashed line in each graph shows present-day temperatures (annual average) at the very place of the two cores taken from world ocean atlas. Glacials are shown by light grey bars, sapropels indicated by black vertical lines.

sapropel fauna of MIS 11 and the sapropel fauna of MIS 11 are strongly related to the fauna of the MIS 12 glacial, whereas sapropel S1, MIS 1 and MIS 2 faunas are consistent with the fauna of the post-sapropel section of MIS 11.

MIS 11 cycles in planktonic foraminifera assemblages

Three distinct periods of significant changes in planktonic foraminifera assemblage counts can be recognised within MIS 11 in both cores (fig. 30). Of the three foraminiferal cycles (phase I-III), the one labelled as phase I is characterised by high *G. inflata* (~ 18 %)

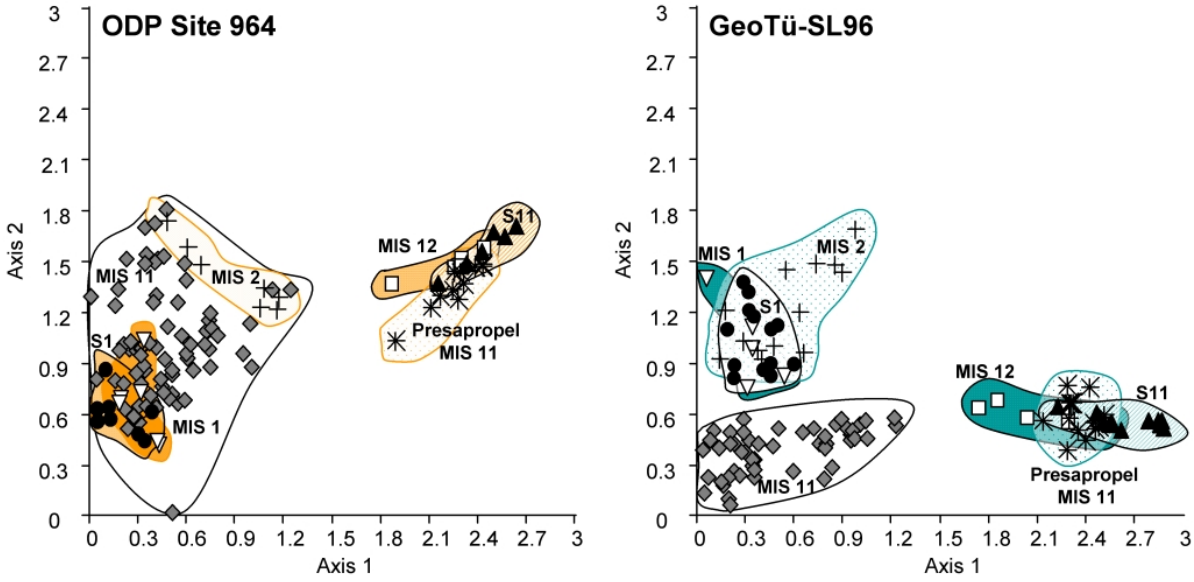

Figure 29: Detrended correspondence analyses of planktonic foraminifera abundances, highlighting the similarities and differences among faunas of individual glacial and interglacial stages in both investigated cores. First axis in ODP Site 964 explains 52.6 %, the second axis 12.2 % of the variability. In GeoTü-SL96, the first axis explains 41.8 % and the second 8.8 %.

abundances together with distinct peaks in *G. glutinata* (~ 15 %) and *G. siphonifera*+*G. calida* (~ 5 %). Phase II presents high *G. inflata* (~ 18 %) and high *G. truncatulinoides* (~ 18 %), but very low *G. glutinata* (~ 2 %) and *G. siphonifera*+*G. calida* (~ 2.5 %) abundances. Phase III is characterised by high abundances of *G. inflata* (~ 30 %) in ODP Site 964 and (~ 20 %) in GeoTü-SL96, high *G. truncatulinoides* (~ 14 %), but also very low *G. glutinata* (~ 1 %) and *G. siphonifera*/*G. calida* (~ 1.5 %). The three foraminiferal phases appear to be centered at 402-394 kyr B.P., 382-373 kyr B.P. and 358-350 kyr B.P. and could thus theoretically be linked to the last three insolation cycles within MIS 11 and early MIS 10, which have a much subdued magnitude compared to the preceding sapropel-triggering insolation maximum at 406 kyr B.P. (fig. 30) and their weakness has been previously

considered important for the long duration of interglacial conditions of MIS 11 (e.g. RAYNAUD et al., 2005). In order to establish a link between the insolation cycles and foraminifera species abundances, it is first necessary to understand which environmental conditions in the upper water column could have been responsible for the observed cyclic pattern in the *G. truncatulinoides* and *G. inflata* abundances. To this end, measurements of elemental ratios in the sediment record provide additional information about environmental settings during these three periods and show that the three planktonic foraminifera abundance peaks correlate with high Ca/Ba ratios, pointing to low productivity in the surface water column during this phase. The peaks are also correlated with low Fe/Al ratios of the bulk sediment, which points to reduced influx of terrestrial material assumably resulting in low productivity. As a potential consequence, benthic foraminifera concentrations remain low to zero throughout MIS 11.

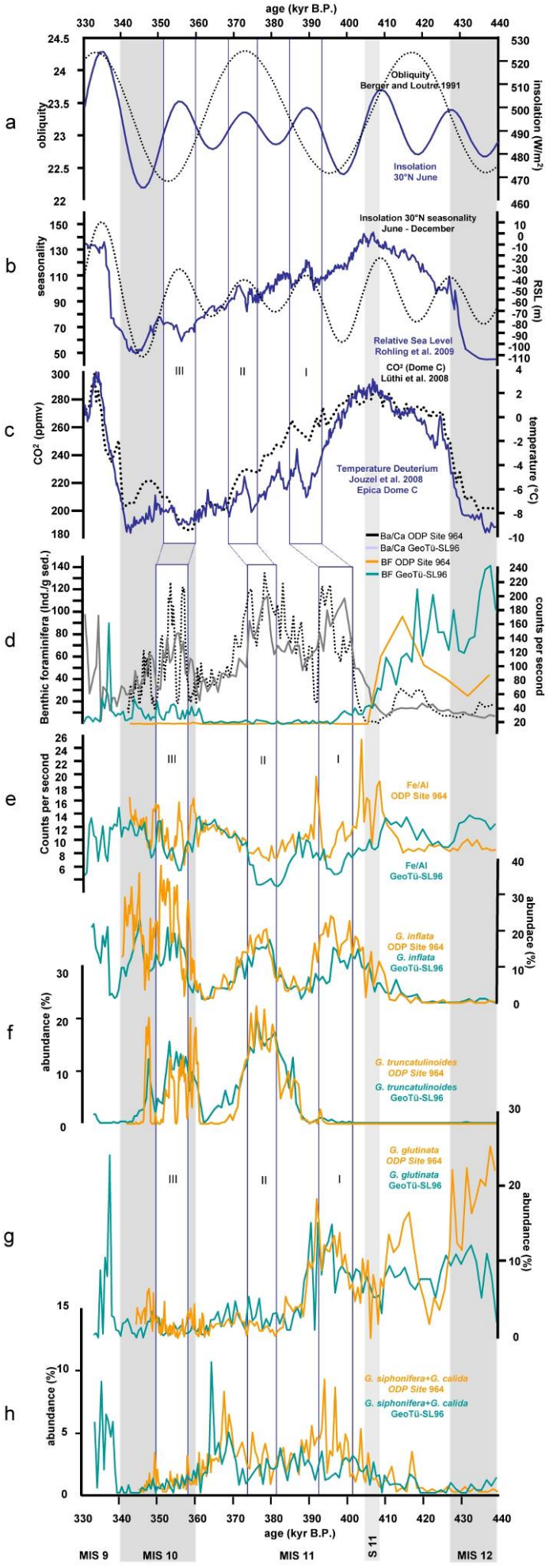

Figure 30: Cycles in planktonic foraminifera abundances and elemental ratios during late MIS 11 compared to global paleoenvironmental trends; a: summer insolation and obliquity (dotted line; BERGER & LOUTRE, 1991); b: panel displays seasonality (June insolation minus December insolation) at 30°N (dotted line) and sea level (ROHLING et al., 2009); c: panel exhibits CO_2 EPICA Dome C data (dotted line; LUETHI et al., 2008) and deuterium derived temperatures of EPICA Dome C (JOUZEL et al., 2007); d: panel presents Ba/Ca elemental ratio in ODP Site 964 (thick black line) and GeoTü-SL96 (thick grey line) and benthic foraminifera abundances in ODP Site 964 (light line) and GeoTü-SL96 (dark line); e: panel denotes Fe/Al elemental ratio in ODP Site 964 in both cores; f: panel reveals *G. inflata* abundances for both cores; g: panel *G. truncatulinoides*; h: panel *G. glutinata* and ninth panel *G. siphonifera* together with *G. calida* for both cores. Vertical grey bars denote MIS boundaries and sapropels, white bars denote phases I to III of foraminifera abundance patterns.

A Detrended Correspondence Analysis of the planktonic foraminifera assemblage counts throughout the three phases highlights the differences in their faunal composition and shows that phase III is most distinct from the MIS 11 Phases I and II (fig. 31).

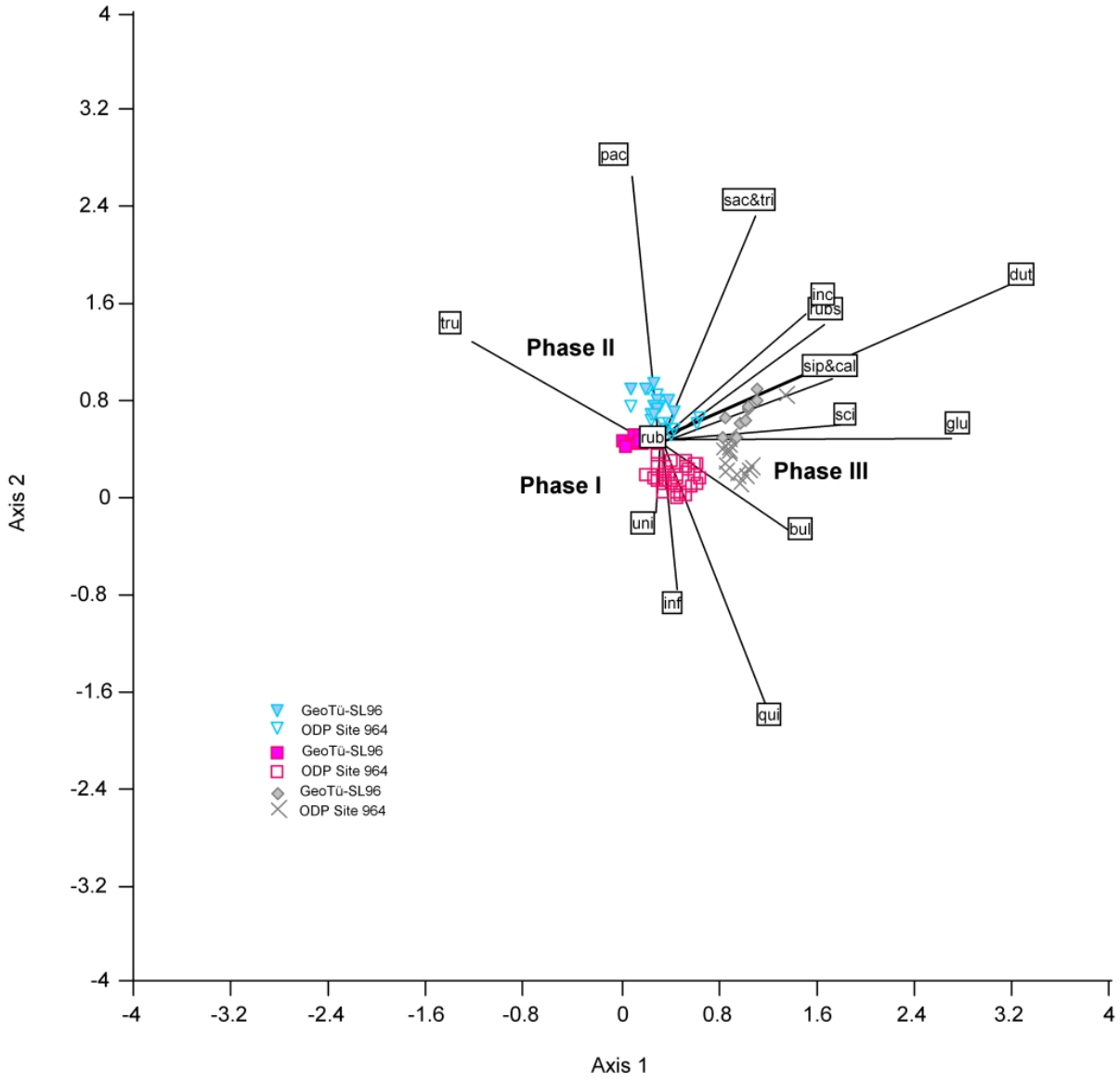

Figure 31: Detrended correspondence analyses of planktonic foraminifera abundances during late MIS 11/early MIS 10 in both first axis explains 11.7 % and second axis 6.3 % of the variability.

Comparability of MIS 11 and MIS 1 in the Eastern Mediterranean region

High resolution stable isotopic and planktonic foraminifera faunal assemblage counts provide new insights into Mediterranean climate history during MIS 11 as well as on possible future climate development without anthropogenic influence. Here, based on

sapropel formation patterns, an alignment of peak interglacial conditions for the second insolation maximum of MIS 11 with the first insolation maximum of MIS 1 is suggested.

In this concept, the sea level high stand of MIS 11 (ROHLING et al., 2009, 2010) coincides with a similar sea level in MIS 1. The similarity between the orbital configurations 400,000 years ago and today has long been pointed out and analyzed (BERGER & LOUTRE, 1991, 2003; DROXLER et al., 2003, and references therein) on the basis of BERGER'S (1978) astronomical calculations. The assumption of similarity of MIS 11 and MIS 1 has been based on the similarity of summer insolation at 65°N (BERGER & LOUTRE, 1991), but a perfect match of all possible orbital parameters is not given for the two time periods. If obliquity is the parameter of choice to align MIS 11 and MIS 1, the similarity would be best at 406 kyr B.P (LEE & POULSEN, 2005; CRUCIFIX & BERGER, 2006).

Origin of MIS 11 climatic cycles

The similarities in CO_2 and CH_4 concentrations of MIS 11 and MIS 1 (without anthropogenic influences; fig. 2) has often been discussed as the main climate-driving factor, in addition to orbitally driven climate development (RUDDIMAN, 2003, 2005, 2006B, 2006C, 2007; HANSEN et al., 2008), and used to speculate that the Holocene should have already been terminated under natural conditions (KUTZBACH et al., 2009; ROHLING et al., 2010), in spite of contrasting opinions (TZEDAKIS, 2009). The sapropel alignment of this study adds an interesting perspective to this discussion. Whereas the alignment to the second insolation maximum of MIS 11 alone would support the assertions by (KUTZBACH et al. 2009; ROHLING et al., 2010), the climatic trends in the Eastern Mediterranean during the rest of MIS 11 would indicate that interglacial conditions in this region could be expected to continue for another 30 ka, irrespective of global climatic trends (fig. 27, 28).

The peak interglacial conditions accompanying sapropel formation during MIS 11 introduce an extremely long period of typically interglacial conditions in the Eastern Mediterranean, possibly stabilized by a sequence of unusually weak insolation maxima. Three distinct cycles in planktonic foraminifera can be linked to these three weaker insolation maxima (fig. 30; phase I to III). A comparison with planktonic foraminifera faunas during various Mediterranean sapropel events (e.g. NEGRI & GIUNTA, 2001; PRINCIPATO et al., 2006; TRIANTAPHYLLOU et al., 2009, 2010) reveals an assemblage composition for the two first phases which is remarkably close to sapropel faunas. All three

phases were dominated by *G. inflata*, and phase II and III also by *G. truncatulinoides*. Phase I can be related to sapropel S1 fauna assemblages with high *G. ruber*, *G. inflata*, *G. glutinata* and *G. bulloides* abundances (PRINCIPATO et al., 2006; TRIANTAPHYLLOU et al., 2009, 2010). Phase II interestingly reflects a fauna as known for the interruption of sapropel S1, strongly dominated by *G. inflata*, *G. truncatulinoides* (PRINCIPATO et al., 2006; TRIANTAPHYLLOU et al., 2009, 2010) and with peaking *G. trilobus* (NEGRI & GIUNTA, 2001). Phase III is more related to sapropel S6, showing more productive and more temperate conditions than the other two phases (GERAGA et al., 2005). This is consistent with the position of this phase in the early glacial MIS 10. The comparability of the MIS 11 faunal events with sapropel-related faunas indicate conditions in the upper water column which must have been in some way similar to the sapropel times. The MIS 11 faunal phases do not appear to be linked to changes in SST (fig. 28), freshwater influx (no isotopic peaks) or increased productivity, as evidenced by low barium and iron concentrations and low abundances of benthic foraminifera (fig. 30).

If they are to be linked to insolation maxima, then this could only be through changes in upper water column structure in terms of increased stratification and/or enhanced seasonality and stocking circulation. This factor is common to all sapropel intervals (ROSSIGNOL-STRICK & PATERNE, 1999) thus corroborating the sapropel-like character of the planktonic foraminifera assemblages.

This hypothesis, however, mostly relies on semi-quantitative comparison of trends in foraminifera abundances and geochemical evidence with previous studies on some sapropels of the last 400.000 years (e.g. TRIANTAPHYLLOU et al., 2009). In order to unravel factors controlling abundance patterns of *G. inflata* and *G. truncatulinoides* and their relationship with sapropel formation, more high resolution microfossil and geochemical investigations on sapropel events are necessary, including those not considered here, as well as near sapropel events or phases of enhanced stratification and/or seasonality.

3.3. Glacial-like winter conditions during early MIS 11 in the Eastern Mediterranean

High-resolution stable isotope measurements on the planktonic foraminifera *Globigerinoides ruber* and *Globigerina bulloides* were carried out for both cores and revealed a highly coherent and reproducible pattern dominated by the global glacial/interglacial signal, with distinct excursions towards light oxygen isotope values (fig. 20). The prominent isotope excursion in both cores in the first half of MIS 11 coincides with a visible sapropel layer in ODP Site 964, and with distinct peaks in Ba/Al in both cores (fig. 20). This isotope event can thus be best explained as a manifestation of enhanced freshwater discharge into the Eastern Mediterranean, occurring in response to insolation-driven African monsoon maximum, analogous to the younger, well-studied Mediterranean sapropel events (DeLange et al., 2008; Rossignol-Strick, 1983).

An age model for both cores was obtained by tuning the inflection points of the $\delta^{18}O$ curves to the benthic stack from Lisiecki & Raymo (2005a, 2005b). In this age model, the onset of the MIS 11 sapropel strikes 15-20 ka after the Termination V (fig. 20, tab. 4). This would indicate that the sapropel deposition in MIS 11 in the Eastern Mediterranean region was linked to the second insolation maximum of MIS 11 at 409 kyr B.P. The African monsoon variability responsible for freshwater forcing of sapropels in the Mediterranean responds to summer insolation at mid latitudes (Rossignol-Strick, 1983). Average summer insolation at 30°N for MIS 11 (Berger & Loutre, 1991) reveals that the insolation peak during Termination V at 427 kyr B.P. was exceptionally weak (fig. 26). Observations on the occurrence of Mediterranean sapropels in response to orbital forcing indicate that sapropel events are linked only to large insolation peaks (Rossignol-Strick, 1985; Sakamoto et al., 1998; Emeis et al., 2000, 2003). The observed magnitude of the $\delta^{18}O$ excursion associated with the MIS 11 sapropel (fig. 27) is similar to or even larger than that observed during the Holocene S1 sapropel (DeLange et al., 2008). For these reasons, the possibility of aligning the MIS 11 sapropel with the 427 kyr B.P. insolation maximum is excluded. An alignment of the MIS 11 sapropel with the 409 kyr B.P. insolation peak provides an additional constrain on the age model (tab. 4): midpoints of sapropel deposition are known to occur approximately 3 kyr after insolation maxima (DeLange et al., 2008; Emeis et al., 2003). The sedimentation rates (cm/kyr) for the resulting age model vary between 0.6 and 0.8 for ODP Site 964 and 0.5 and 0.9 for GeoTü-SL96. An alternative alignment of the MIS 11 sapropel to the 427 kyr B.P. insolation peak would result in anomalously high sedimentation rates of

5.7 cm/kyr during early MIS 11 in both cores, further indicating that the MIS 11 sapropel should be linked to the 409 kyr B.P. insolation maximum.

Next, in order to characterise the climatic response of the Eastern Mediterranean region to global forcing during the investigated period, high-resolution counts of planktonic foraminifera assemblages were generated throughout MIS 11 in both cores. These data were used to define three distinct events (*G. inflata* peak, *G. ruber* peak, *G. ruber* minimum) in MIS 11 that were used to further refine the correlation between the two cores (fig. 20). The position of the *G. ruber* peak and *G. ruber* minimum in MIS 10 in GeoTü-SL96 has been confirmed by the identification of the MIS 9/MIS 10 boundary in the $\delta^{18}O$ record, followed by a distinct Ba/Al peak at 635 cm, marking the position of the MIS 9 sapropel (fig. 20). The faunal counts were then converted to SST using the Artificial Neural Networks transfer function method by HAYES et al. (2005). The foraminiferal transfer function results were supplemented by low-resolution alkenone data from core ODP Site 964 as an independent proxy for SST (fig. 28).

The results indicate a coherent SST development, both in terms of the pattern and of the absolute values throughout MIS 12 and MIS 11, with alkenone SST being most comparable to the transfer function reconstruction of annual average SST (fig. 28). Unlike open ocean SST records in the North Atlantic (MCMANUS et al., 1999; BAUCH et al., 2000; MARTRAT et al., 2007; HELMKE et al., 2008; DE VERNAL & HILLAIRE-MARCEL, 2008; STEIN et al., 2009), which show a warming trend in pace with global climate forcing (JOUZEL et al., 2007; LUETHI et al., 2008; ROHLING et al., 2009), the Eastern Mediterranean SST remained close to the MIS 12 glacial level throughout the entire pre-sapropel portion of MIS 11 (fig. 32). It is first during the sapropel event that the planktonic foraminifera fauna shifts to a typical interglacial composition, dominated by *G. ruber* (HAYES et al., 1999), indicating annual SST close to the present-day level of ~21°C (LOCARNINI et al., 2005). This shift occurs in phase in both cores and is mirrored by the alkenone record from ODP Site 964 (fig. 32). Following the sapropel deposition associated with the 409 kyr B.P. insolation peak, the planktonic foraminifera fauna continues to be dominated by warm-water indicators throughout the remaining part of MIS 11, leading to high ANN SST estimates, again mirrored by alkenone data. In contrast, alkenone-based North Atlantic SST records (MARTRAT et al., 2007; STEIN et al., 2009) indicate a gradual cooling after the MIS 11 climate optimum, which ends shortly after the Mediterranean sapropel event. Those records

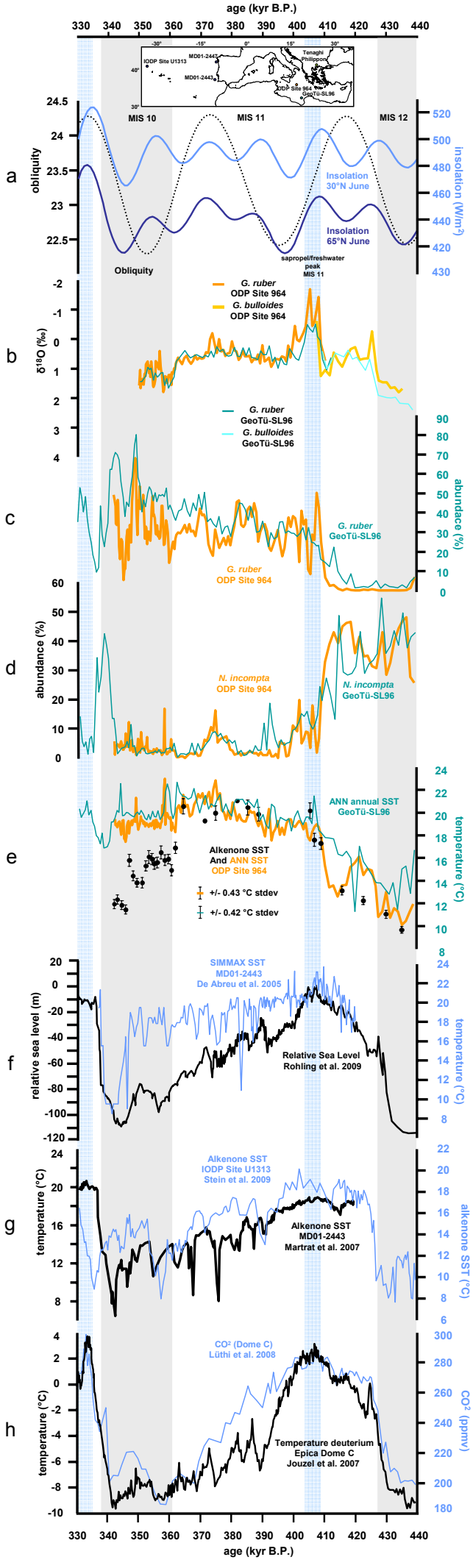

Figure 32: Paleoclimatic records across MIS 11 in the Eastern Mediterranean compared with oceanic records and global climate trends and location map of the different datasets. All alkenone and SIMMAX datasets were tuned to the same age scale using their respective stable isotopic records; a: dotted black line denotes obliquity; upper line represents summer (June) insolation at 30°N; lower line insolation at 65°N summer perihelion (BERGER & LOUTRE, 1991); b: stable isotopic measurements ($\delta^{18}O$) of core ODP Site 964 (thick line) and GeoTüSL96 (thin line) in MIS 11; dark line denotes *G. ruber* derived values for ODP Site 964; light line *G. bulloides*; thick line denotes *G. ruber* derived values; d: thin line denotes *G. ruber* abundance (%) for GeoTü-SL96; thick line denotes *G. ruber* abundance (%) for ODP Site 964; d: thin line denotes *N. incompta* abundance (%) for GeoTü-SL96; thick line denotes *N. incompta* abundance (%) for ODP Site 964; e: thin line denotes ANN derived annual SST of GeoTü-SL96, thick line denotes ANN derived annual SST of ODP Site 964, black dots with error bars of standard deviation (ALTMAN & BLAND, 2005) denotes alkenone derived SST temperatures of ODP Site 964; f: thin line represent SIMMAX generated SST of core MD01-2443 off the Iberian Margin (DE ABREU et al., 2005); thick line denotes sea level reconstruction (ROHLING et al., 2009); g: thin line denotes alkenone SST from core U1313 from north Atlantic (STEIN et al., 2009); thick line represents alkenone SST of core MD01-2443 off Iberian Margin (MARTRAT et al., 2007); h: thin line denotes EPICA Dome Concordia CO_2 data (LUETHI et al., 2008); thick line represents deuterium temperature data (JOUZEL et al., 2007). Grey bars denote glacial periods and sapropel formation.

are in line with global climate trends, which indicate a decrease in Antarctic temperatures, CO_2 levels and growth of continental ice sheets beginning between 425 and 427 kyr B.P. (JOUZEL et al., 2007; LUETHI et al., 2008; ROHLING et al., 2009; fig. 32).

Because our records have been independently tuned to an orbital age model, the apparent delayed response of Eastern Mediterranean foraminiferal faunas to global forcing during early MIS 11 must be a real phenomenon. This is in stark contrast to global trends, meaning that the Eastern Mediterranean would have been decoupled from the oceanic system for more than 10 ka which seems unlikely. Terrestrial pollen records from Southern France (REILLE et al., 2000) and Greece (TZEDAKIS et al., 2003, 2006) furthermore suggest that the early phase of MIS 11 was cooler than one would expect for an interglacial, but certainly not glacial. Palynological data in the Mediterranean region show a significant change in vegetation after termination V, with a development of MIS 11 vegetation in two cycles. As *Pinus* and *Quercus* appear, signalling the deglaciation, climatic settings seem to be more related to interglacial conditions, but significantly cooler and wetter for the first insolation/vegetation cycle (indicated, among others, by *Carpinus, Abies* and *Picea*) than for the second cycle (as suggested by *Pistacia* and *Olea/Fraxinus* for example) (TZEDAKIS et al., 2003). Thus, an alternative explanation for the occurrence of glacial-like foraminiferal assemblage composition and relatively low alkenone derived SST must be found.

The first insolation cycle in pre-sapropel MIS 11 was accompanied by a low sea level (ROHLING et al., 2009) which could have prevented recolonisation of the Mediterranean, or at least the eastern basin, by typical interglacial assemblage either physically because of the shallow Gibraltar and/or Sicily sills, or indirectly because of its effect in the circulation regime and thus in productivity. If the Eastern Mediterranean remained highly productive during the first cycle, species that are normally associated with colder waters (e.g. LALLI & PARSONS, 1997) could become to dominate the assemblage as they are also known to be linked to high productivity (e.g. HEMLEBEN et al., 1989), potentially independent of temperature. Indeed, relatively high Ba/Al ratios coupled with high concentrations of benthic foraminifera (fig. 33), indicating a massive flux of organic matter to the seafloor throughout the early MIS 11, higher even than during MIS 10, are consistent with high productivity. Relatively high Ti/Al ratios (fig. 33) suggest that higher terrestrial material influx to the Eastern Mediterranean was a potential driving force behind the higher productivity during early MIS 11.

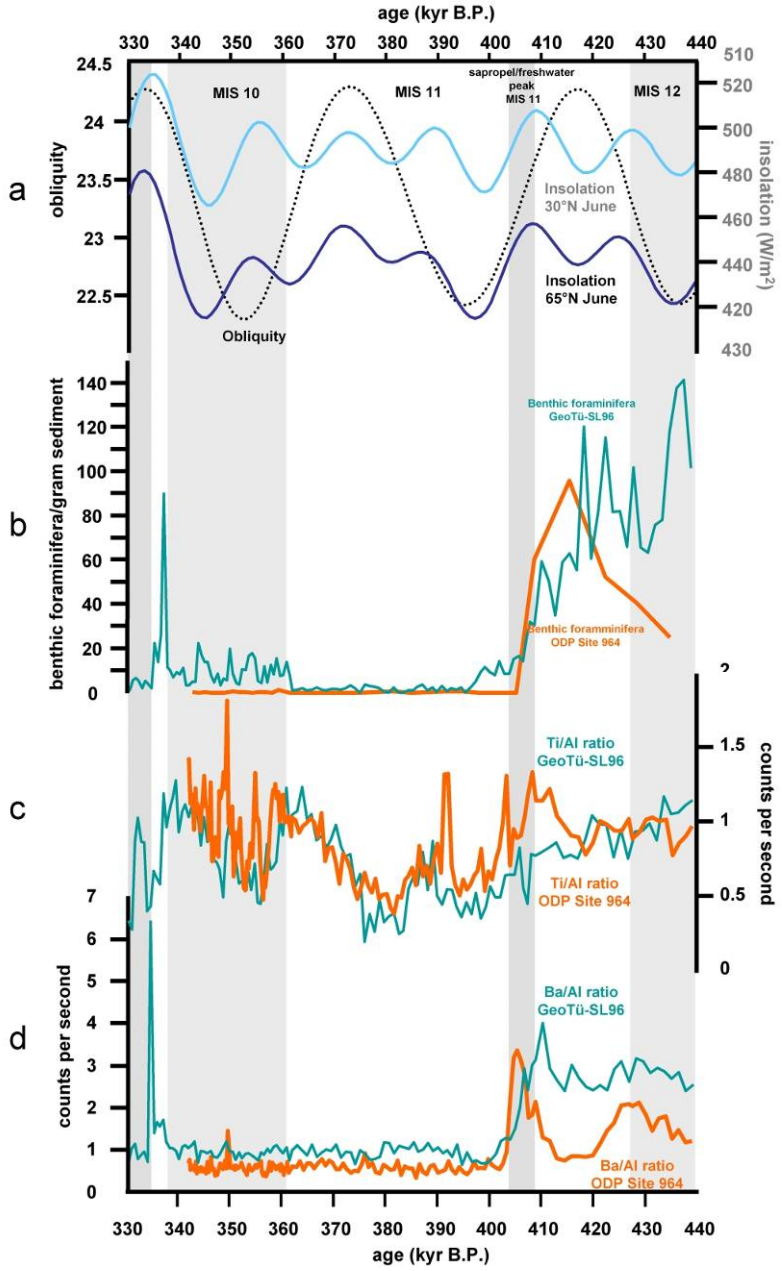

Figure 33: Orbital data, XRF elemental scans and benthic foraminifera count data versus age axis showing productivity and nutrient origin; a: dotted line denotes orbital obliquity; upper line represents insolation at 30°N; lower line insolation at 65°N summer perihelion (BERGER & LOUTRE, 1991); b: benthic foraminifera counts per gram sediment; thin line denotes record of GeoTü-SL96; thick line denotes ODP Site 964; c: thin line denotes Ti/Al ratio in GeoTü-SL96 and thick line denotes Ti/Al ratio in ODP Site 964; d: thin line denotes Ba/Al ratio in GeoTü-SL96 and thick line denotes Ba/Al ratio in ODP Site 964.

In order to reconcile the alkenone-based SST reconstructions with non-glacial conditions, the alkenone values in early MIS 11 would have to represent the cold season signal and then at about the sapropel time they would have to switch to represent yearly average. Thus, high productivity during early MIS 11 would have to occur during winter, biasing the alkenone signal towards the cold season.

Supporting evidence comes from pollen records suggesting a long period of increased moisture availability through reduced summer evaporation and more equally distributed precipitation for the first cycle of early MIS 11 for the Mediterranean region (TZEDAKIS et al., 2003), leading to higher aboreal to non-aboreal ratios and thus higher biomass. Similarly muted seasonality coupled with high annual precipitation for early MIS 11 is suggested by pollen and illite records for continental interior Asia (PROKOPENKO et al., 2010). As there is no evidence for the appearance of a summer precipitation regime in the northern and Eastern Mediterranean region for early MIS 11 (TZEDAKIS et al., 2003), the most plausible scenario

is that of a high winter productivity fuelled by higher influx of terrestrial material through higher and/or more equally distributed precipitation during the winter half.

The first sign of glacial inception in the Mediterranean records presented herein is observed during the MIS 11/MIS 10 transition at 362 kyr B.P., indicated by 3°C colder alkenone temperatures. The planktonic foraminifera fauna, however, remained dominated by *G. ruber*, which achieved exceptionally high abundances in the early MIS 10, exceeding 80%. A typical glacial fauna only appeared in GeoTü-SL96 in the second half of MIS 10, following the strong 65°N summer insolation minimum at 345 kyr B.P. (fig. 32). This event is clearly indicated in the alkenone record from ODP Site 964, which shows a further 3°C cooling at that time.

Planktonic foraminifera assemblage based SIMMAX transfer function SST record off Portugal (DE ABREU et al., 2005) remains close to the peak interglacial level throughout the late part of MIS 11, even though alkenone (MARTRAT et al., 2007) and pollen (DESPRAT et al., 2005) data from the same location indicate an end of the thermal optimum at 395 kyr B.P. (fig. 32). Next, a pollen record from ODP Site 646 (DE VERNAL & HILLAIRE-MARCEL, 2008) places the onset of the thermal maximum of MIS 11, indicated by anomalously high *Picea* pollen abundances, to 405 kyr B.P., consistent with insolation forcing. This thermal maximum ends at 385 kyr B.P., although most global and ocean records show a much earlier onset of cooling after the MIS 11 optimum, around 395-405 kyr B.P. Finally, pollen records from Greece, when tuned to March and June perihelion orbital configurations seem to indicate a prolonged period of interglacial conditions throughout the late part of MIS 11 (TZEDAKIS et al., 2003, 2006).

3.4. Habitats, abundance patterns and isotope signals of morphotypes of the planktonic foraminifer *Globigerinoides ruber* (d'Orbigny) in the Eastern Mediterranean Sea since the Marine Isotope Stage 12.[1]

Considering the differences of individual species in biological lifestyle reflected in the stable isotopic chemistry of the species' shell (BÉ, 1982; GANSSEN & KROON, 2000; LIN & HSIEH, 2007), isotope data from single species are required for meaningful palaeoenvironmental interpretations, implying that robust species concepts are at the very base of many palaeoceanographical proxies. In the course of this study, anomalies in shape and size of *G. ruber* were identified, which led to the definition of four different morphotypes within this species, in accordance with literature. As paleoceanographic techniques employed in the Eastern Mediterranean Sea are predominantly based on *G. ruber* (e.g. GONZALES–MORA et al., 2008), it seemed inevitable to clearly define the relevant morphotypes and systematically assess the stable isotopic geochemistry of their shell and explore risks of lumping the morphotypes and benefits of considering them separately in geochemical analysis.

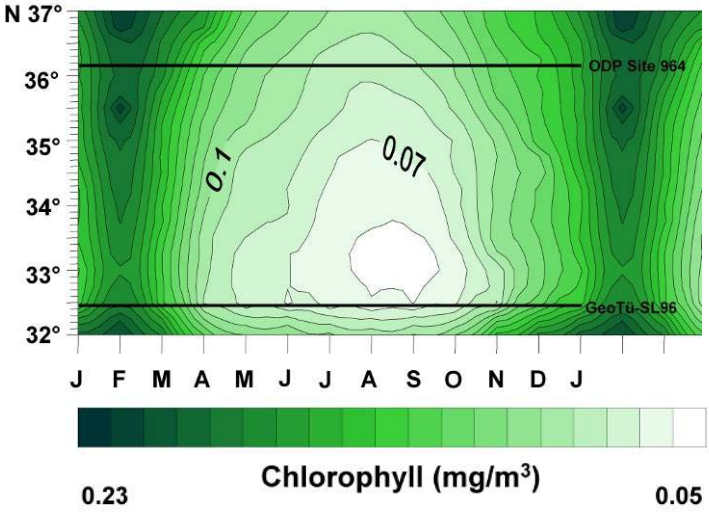

Figure 34: Stacked profiles of chlorophyll concentrations of one year along a transect between the locations (horizontal lines) of ODP Site 964 and GeoTü-SL96 (SeaWIFS chlorophyll data set; GREGG & CASEY, 2004).

The records from the two cores analysed in this study allow a comparison of the behaviour of *G. ruber* morphotypes since the late Quaternary MIS 12. Their position in the central Mediterranean implies that they can monitor both the western and the Eastern Mediterranean *G. ruber* populations and their expansions or retractions during the glacial cycles. Importantly, despite their nearby position, the cores reflect different surface ocean conditions (fig. 4, 5, and 34).

In order to quantitatively assess the degree of separation among the three analysed morphotypes (Plate IV), principal components analyses of the morphological variables measured on *G. ruber* (white) (fig. 16) specimens were carried out separately on four samples (two glacial samples from MIS 10 and two interglacial samples from MIS 11).

[1] This chapter has been published as Numberger et al. 2009

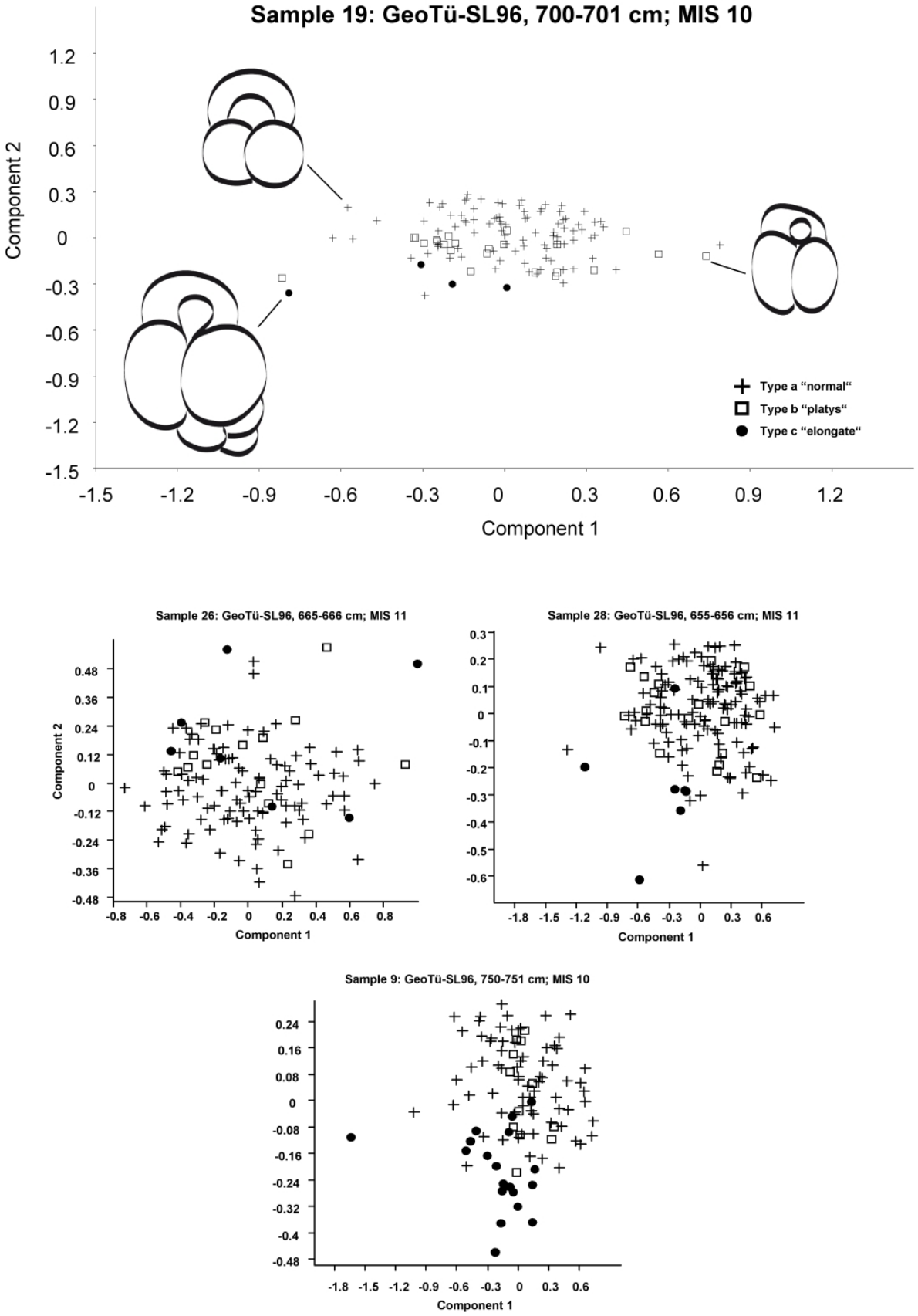

Figure 35: Principal components analysis (PCA) of size-normalised morphological characters measured on shells of *G. ruber* (white) in two glacial and two interglacial samples. Small drawings show outlines of the actual specimens in umbilical view (all drawings are to the same scale).

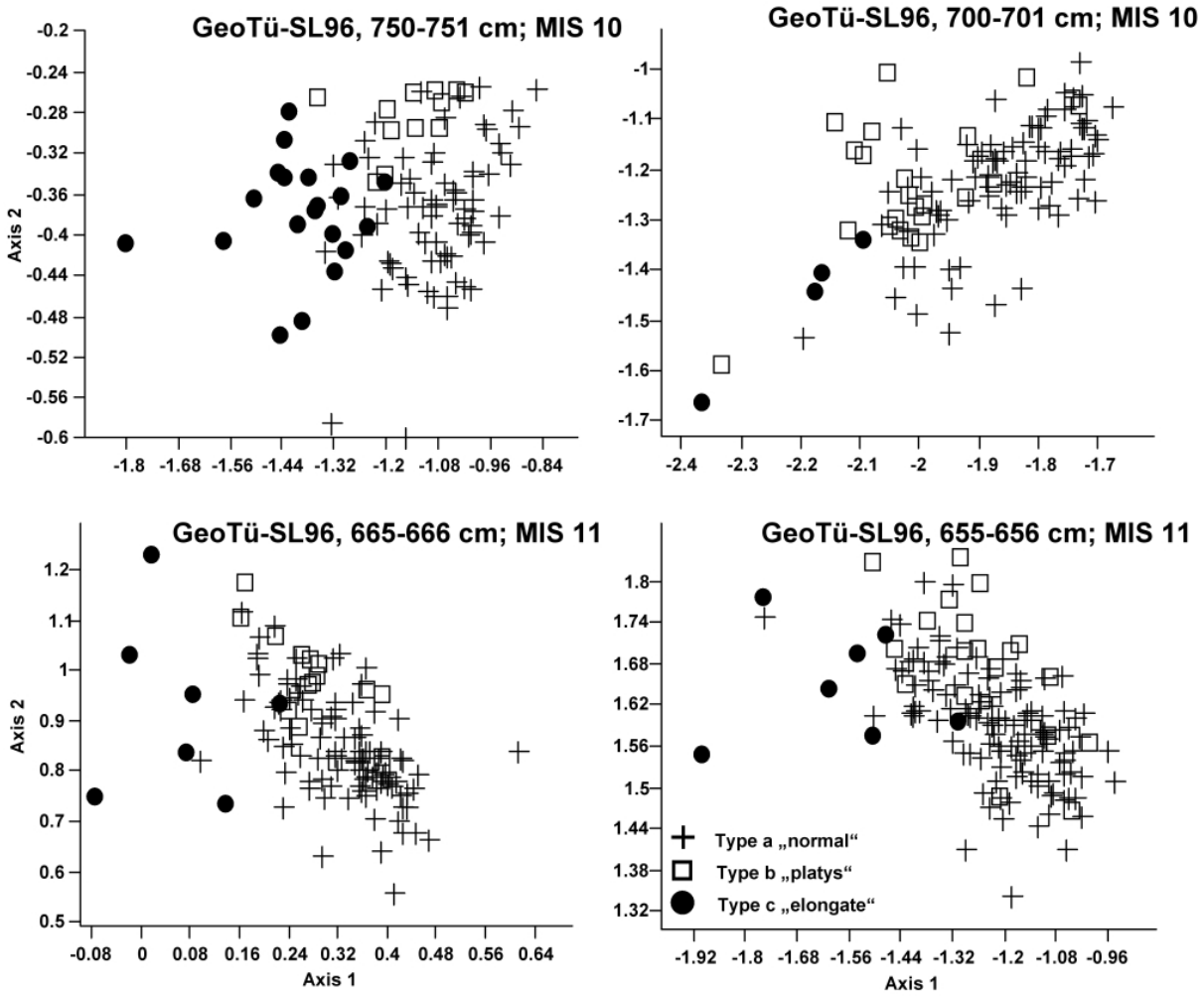

Figure 36: MANOVA CVA analysis of size-normalised morphological characters measured on shells of *G. ruber* (white) in two glacial and two interglacial samples.

The kummerform morphotypes were excluded from the analyses in order to avoid the bias caused by the abnormal shape of the last chamber. The analyses were carried out separately on each sample to minimise the effect of ecophenotypic differences between the samples, which is superimposed on the within-sample variability due to the morphotypes. The four samples were selected because they contained all morphotypes in sufficient abundance, cover the glacial-interglacial gradient and give one replicate for each MIS from the same core. For each analysis, the plane of the first and second principal components accounts for 70- 82 % of the total variance in the data; the first axis seems to be associated with size-normalised shell perimeter, which is a measure of shell lobateness, while the second axis tends to reflect the shape of the last chamber. The distribution of specimen scores in the plane of the two principal components reveals a continuous and homogenous morphospace in *G. ruber* (white) with a large degree of overlap in the morphology of the three analysed types. The samples from the glacial MIS 10 appear to indicate a slightly

higher degree of separation among the morphotypes, especially of type c "elongate" (fig. 35).

The continuous distribution of specimens and large overlaps between morphotypes in the morphospace defined by the first two principal components axes clearly indicate that the largest component of morphological variability in *G. ruber* (white) captured by the selected 16 variables is not associated with the distinction among the morphotypes. Therefore, in order to determine to what degree our subjective definition and identification of these morphotypes can be supported by quantitative data, a MANOVA/CVA on the three subjectively defined morphotypes was performed in each of the four samples (fig. 36).

The analyses (fig. 36) indicate that even when the projection of the multivariate morphological data is set to maximise the between-group variance, the morphospace remains continuous. However, in this case, specimens of the three morphotypes occupy less overlapping segments of the morphospace and the variable loadings on the MANOVA/CVA are different (more complex) than in the PCA analysis. In general, in all four analyses, the first axis seems to be associated with the general form of the shell (high loadings of multiple variables), separating the type c "elongate" and second axis reflects the form of the penultimate and n-2 chamber, separating the type b "platys". Pairwise discriminant analyses between morphotypes carried out separately in each sample reveal that on the basis of the 16 morphological variables 96-100% of the specimens could be correctly assigned to type c "elongate" and 80-90 % could be correctly assigned to type b "platys". In all samples and morphotype pairs, Hotteling's T^2 tests indicate highly significant ($p<0.05$-0.001) differences in morphology.

Morphotype abundances

To evaluate the ecological behaviour of the individual morphotypes during glacials and interglacials, their mutual proportions as well as the relative abundances of all *G. ruber* types and *G. ruber* (pink) among all planktonic foraminifera were determined in both cores (fig. 37).

The abundance of *G. ruber* total shows a comparable pattern in both cores. The transition from MIS 12 to MIS 11 marks the onset of a gradual increase continuing throughout MIS 11 and culminating in late MIS 11 and early MIS 10. An increase in the total abundance of *G. ruber* is seen also during the transition between MIS 2 and MIS 1, although the glacial background levels during MIS 2 were much higher than during MIS 12.

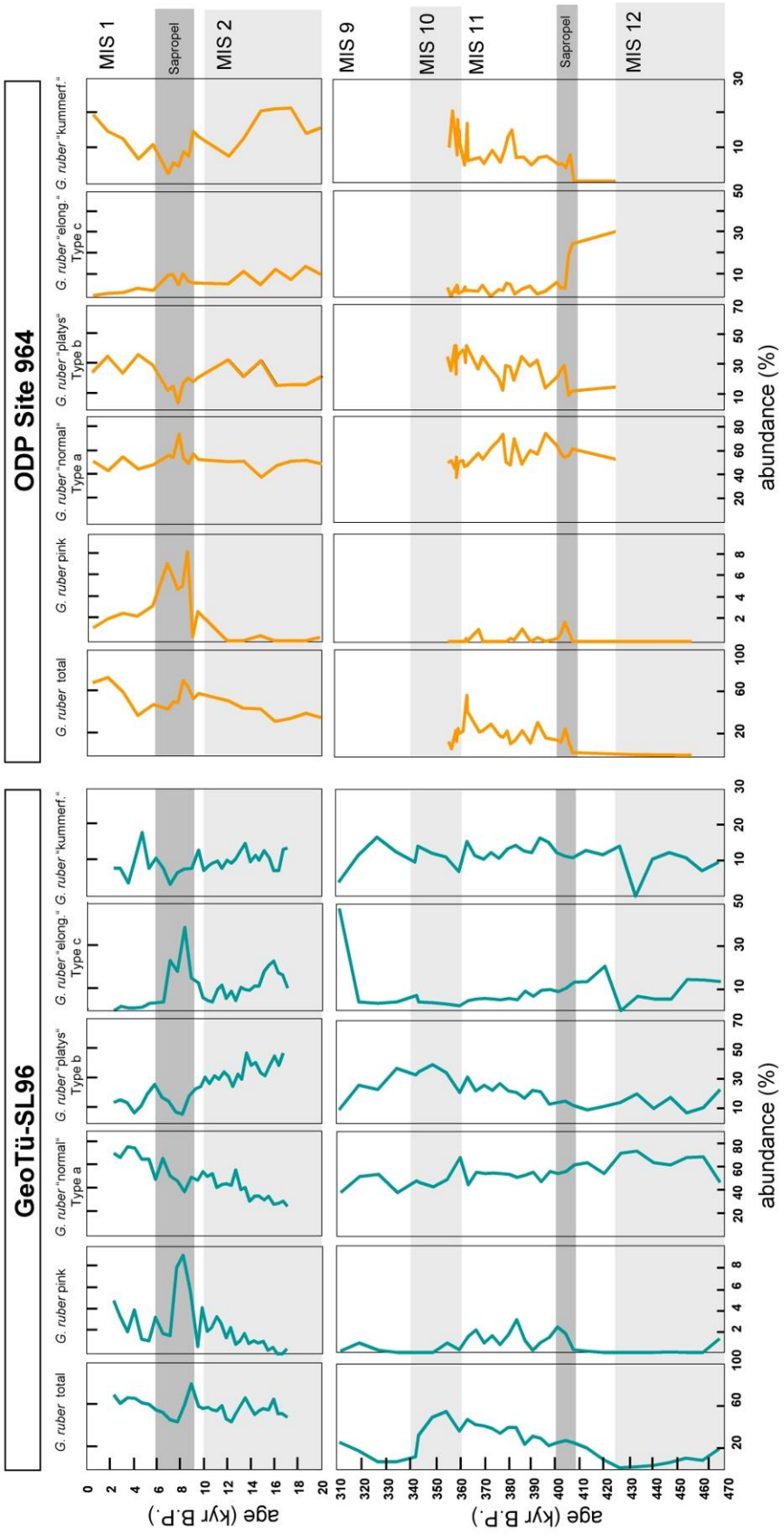

Figure 37: Census counts of *G. ruber* (white) morphotypes and of the abundance of all *G. ruber* types and *G. ruber* (pink) among all planktonic foraminifera in samples from Core GeoTü-SL96 and ODP Site 964. Morphotype abundance data are not shown for MIS 12 in Core ODP Site 964; due to the extremely low abundance of *G. ruber*, the total number of specimens available was less than 15.

The abundance of *G. ruber* (pink) shows a pattern which is consistent not only between the cores, but also for both investigated glacial terminations. This variety was virtually absent

during the glacials, its abundances peaked at the onset of the sapropel S1 in both cores as well as in the sapropel of MIS 11 and remained low but detectable throughout MIS 11.

Throughout the analysed interval, the abundance of kummerform specimens remained relatively stable, fluctuating in both cores around 10 % (fig. 37). The abundance of type c "elongate" increased in core GeoTü-SL96 during the transition from MIS 12 to MIS 11, and the highest values in both cores are seen early in MIS 11, declining towards MIS 10. A peak abundance of this type during the early Holocene sapropel S1 is seen in both cores as well, but the type was more common during MIS 2 than in the Holocene (fig. 37). The two most abundant types a "normal" and b "platys" show mutually opposite patterns, caused by the closure in the data, which have to sum to 100 %. The relative proportions of these two types show a complex pattern, with the highest proportion of "platys" during MIS 10 at both sites and during MIS 2 in the GeoTü-SL96 record (fig. 37).

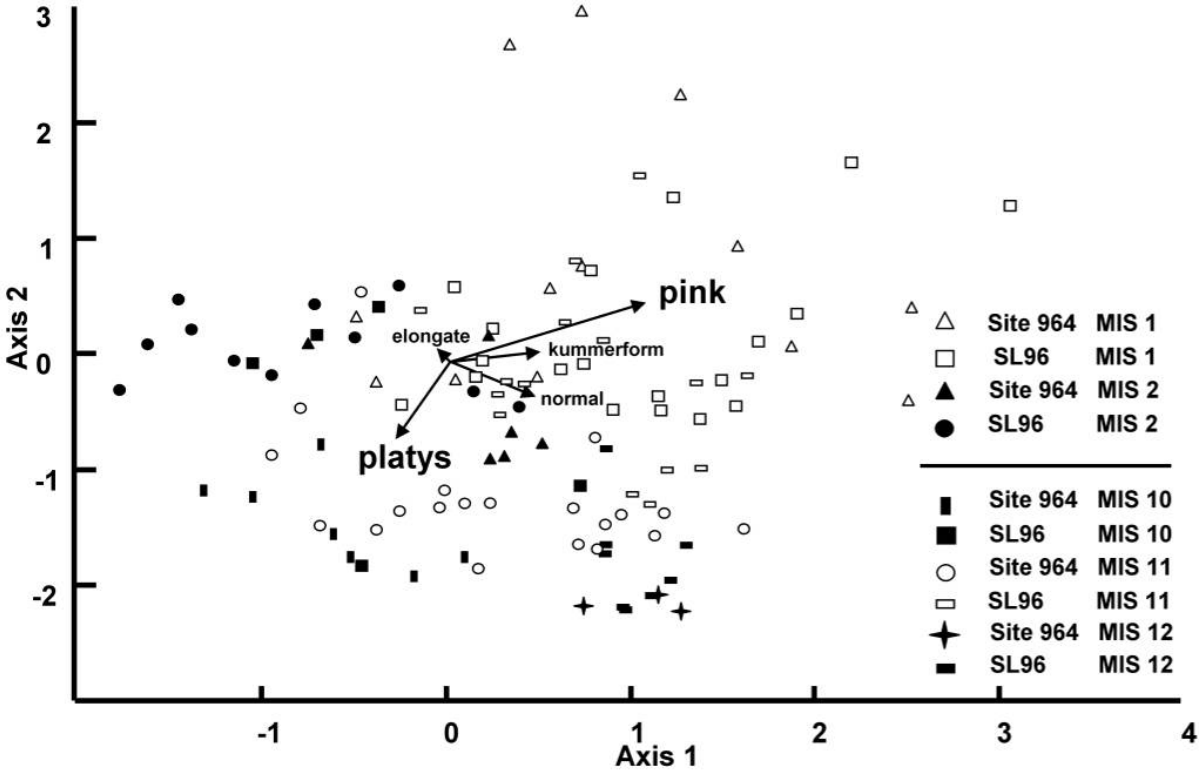

Figure 38: Detrended correspondence analysis of census counts of different morphotypes in ODP Site 964 (right panels) and GeoTü-SL96 (left panels) showing the differences between the glacials (black signs) and interglacials (white signs).

In order to highlight the association patterns between morphotypes and glacial/interglacial stages, a correspondence analysis of the relative abundances of these types as well as of *G. ruber* (pink) has been carried out (fig. 38).

The two first axes of the correspondence analysis explained 95.1 % of the total variance in the 5-variable dataset. They show a weak but interpretable pattern where the warm/interglacial stages are associated with *G. ruber* (pink) whereas the cold/glacial stages are characterised by higher proportions of *G. ruber* type b (platys). Interestingly, assemblages from MIS 11 in ODP Site 964 appear "colder" than those from core GeoTü-SL96 and the Holocene. In addition, the assemblages from MIS 12 in both cores deviate from both MIS 10 and MIS 2. This abundance of *G. ruber* during MIS 12 is generally the lowest of all glacials in both cores (fig. 38).

Stable isotope signals of *G. ruber* morphotypes

The stable isotope profiles from the three analysed morphotypes of *G. ruber* (white) in both cores (fig. 39) show a typical Mediterranean glacial/interglacial pattern (SPROVIERI et al., 1998; ROHLING et al., 2004; LOEWEMARK et al., 2006).

Glacial terminations are characterised by 1-2 ‰ decrease in $\delta^{18}O$, with distinct peaks towards extremely light values during the sapropels. The $\delta^{13}C$ values show a similar trend with higher values during the glacials and lighter values during the interglacials, although the sapropel peaks are less distinct than in the oxygen isotopes and in core GeoTü-SL96 the $\delta^{13}C$ values are comparatively lower during MIS 12 and extremely high during MIS 2 (fig. 39). These general trends in the oxygen isotope data are robust and consistent with global stratigraphies and were thus used to help constrain the age model for both cores (tab. 4).

Throughout the records at both sites, there are substantial and systematic offsets in $\delta^{18}O$ and $\delta^{13}C$ values between the morphotypes. These offsets differ between the two sites and between glacials and interglacials. An analysis of pooled data from individual MIS intervals in both cores reveals that in all cases the offsets are statistically (highly) significant, with average offsets reaching almost 1 ‰ and individual offsets reaching almost 1.5 ‰ (tab. 5, fig. 40).

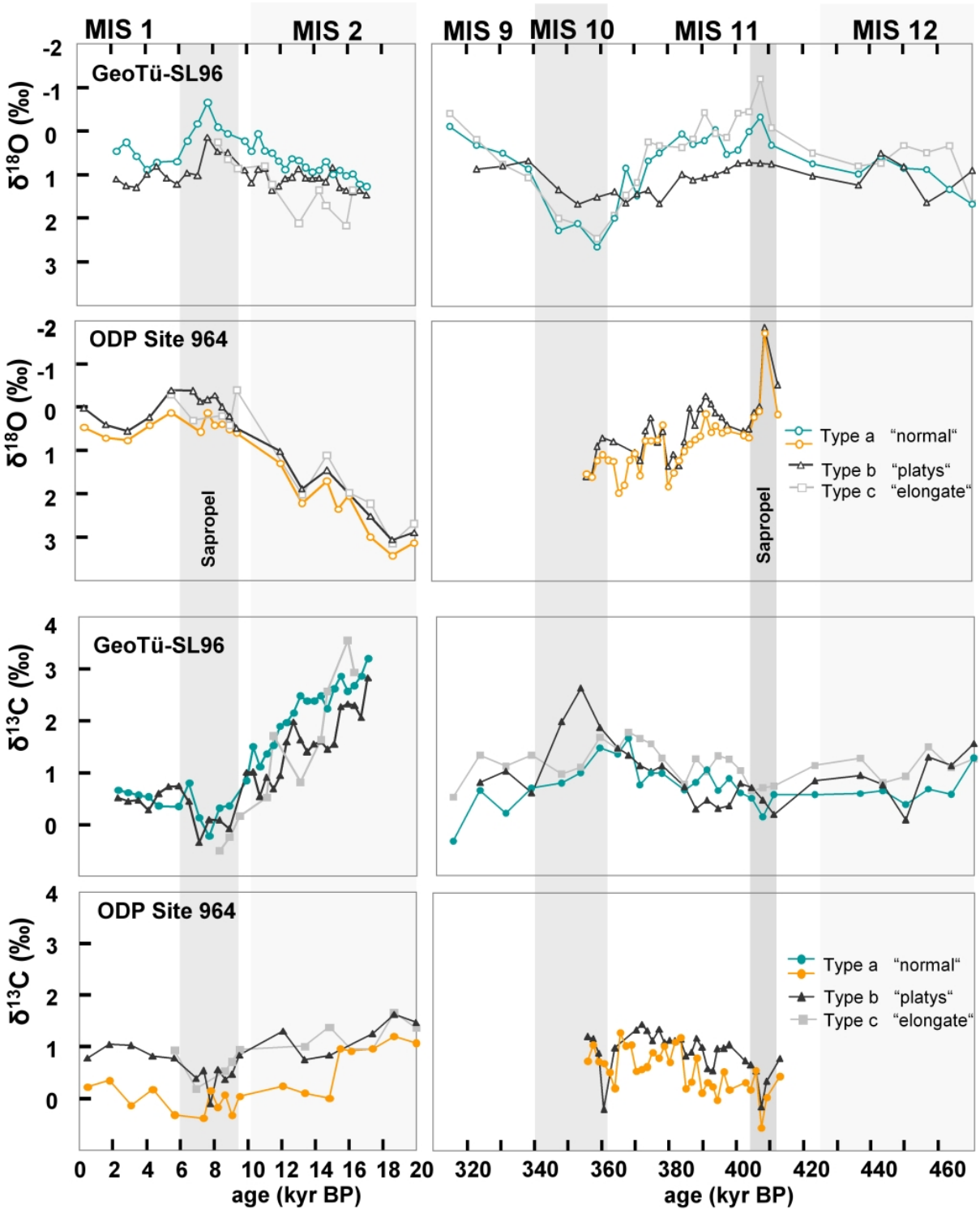

Figure 39: Stable isotopic records from individual morphotypes of *G. ruber* (white).

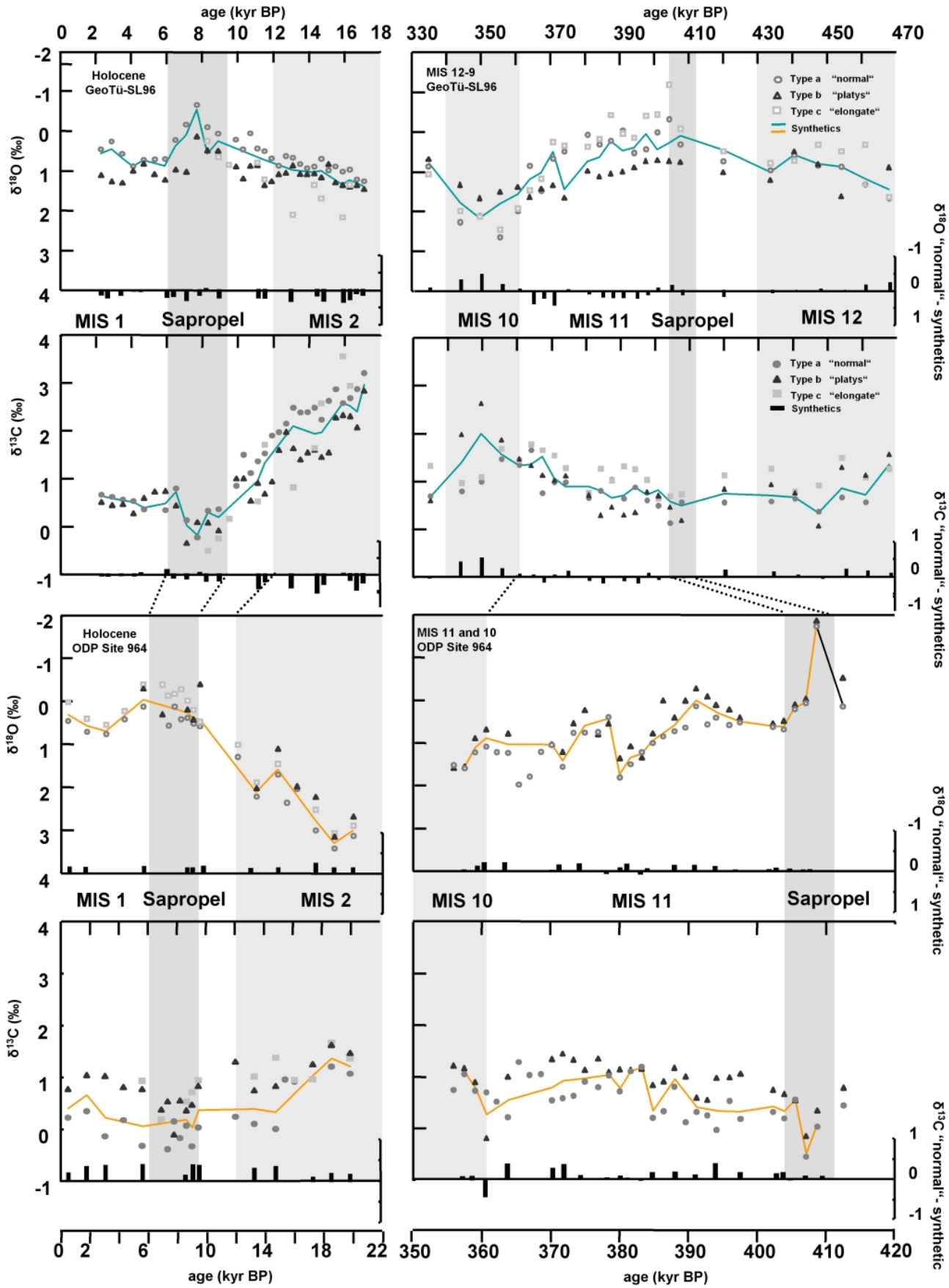

Figure 40: Synthetic stable isotopic records calculated as averages of values for individual morphotypes weighted by their proportions. Histograms show offsets between these synthetic values to *G. ruber* (white) type a "normal" values.

Table 4: Average offsets in stable isotope measurements for different morphotypes of *G. ruber* during MIS 2 - MIS 1 and MIS 12 - MIS 9. Three stars denote $p < 0.001$, two stars $p < 0.01$ and one star $p < 0.05$.

			MIS 1			MIS 2		
	Core	Type	Average offset	No. o. samp.	Sig.	Average offset	No. o. samp.	Sig.
$\delta^{18}O$	964	normal-platys	0.37	12	***	0.30	6	***
$\delta^{18}O$	SL96	normal-platys	-0.64	17	***	-0.25	13	***
$\delta^{18}O$	964	normal-elongate	0.43	4	**	0.39	4	**
$\delta^{18}O$	SL96	normal-elongate	-0.50	4	**	-0.88	5	**
$\delta^{13}C$	964	normal-platys	-0.71	12	**	-0.46	6	**
$\delta^{13}C$	SL96	normal-platys	0.26	17	**	0.64	13	**
$\delta^{13}C$	964	normal-elongate	-0.92	6	*	-0.51	6	*
$\delta^{13}C$	SL96	normal-elongate	0.53	4	*	0.19	5	*
			MIS 9			MIS 10		
	Core	Type	Average offset	No. o. samp.	Sig.	Average offset	No. o. samp.	Sig.
$\delta^{18}O$	964	normal-platys				0.18	4	***
$\delta^{18}O$	SL96	normal-platys	-0.05	11	***	0.87	4	***
$\delta^{18}O$	964	normal-elongate						
$\delta^{18}O$	SL96	normal-elongate	0.22	11	***	0.13	4	***
$\delta^{13}C$	964	normal-platys				0.03	4	*
$\delta^{13}C$	SL96	normal-platys	-0.11	11	***	-0.99	4	***
$\delta^{13}C$	964	normal-elongate						
$\delta^{13}C$	SL96	normal-elongate	-0.44	11	*	-0.14	4	*
			MIS 11			MIS 12		
	Core	Type	Average offset	No. o. samp.	Sig.	Average offset	No. o. samp.	Sig.
$\delta^{18}O$	964	normal-platys	0.29	25	***			
$\delta^{18}O$	SL96	normal-platys	-0.61	16	***	-0.12	7	***
$\delta^{18}O$	964	normal-elongate						
$\delta^{18}O$	SL96	normal-elongate	0.17	14	***	0.33	8	***
$\delta^{13}C$	964	normal-platys	-0.47	25	*			
$\delta^{13}C$	SL96	normal-platys	0.17	16	***	-0.27	7	***
$\delta^{13}C$	964	normal-elongate						
$\delta^{13}C$	SL96	normal-elongate	-0.37	14	*	-0.43	8	*

In core GeoTü-SL96, type b "platys" shows consistently heavier $\delta^{18}O$ and lighter $\delta^{13}C$ values than type a "normal", whereas at ODP Site 964 the opposite pattern is observed. Exceptions are the offsets observed during MIS 10, which in core GeoTü-SL96 resemble the offset seen at ODP Site 964 and vice versa. The fewer isotope data that were available for the rarer type c "elongate" indicate that during MIS 1 and 2, this type exhibited the lightest $\delta^{18}O$ signal at ODP Site 964 and the heaviest signal in core GeoTü-SL96.

Morphological variability

The multivariate analyses (fig. 35, 36) indicate that the morphological variability within the morphospecies *G. ruber* (white) in the central Mediterranean was rather continuous during MIS 10 and 11, as far as the analysed variables are concerned. The MANOVA/CVA analyses in figure 36, however, confirm that the subjectively distinguished morphotypes represent separate segments of the morphospace and thus morphologically meaningful units. This is further underscored by the different occurrence patterns of the types during glacial and interglacial cycles and the significantly different isotope signals among them. The morphotypes correspond at least in part to previously described species (D'ORBIGNY, 1826, 1839; VAN DEN BROECK, 1876), and the merit of merging these species (and the morphotypes) into a broad species concept of *G. ruber* (white) for the sake of taxonomic consistency as introduced by PARKER (1962) is thus strongly challenged by our results. In addition, it is noteworthy that the separation of the morphotypes was stronger during MIS 10 than in MIS 11 (based on the pairwise discriminant analyses), suggesting that the morphology of the three types was not stationary through time and that the types responded to this climatic transition and diverged.

Although our observations alone cannot provide a conclusive evidence for the nature of the morphotypes, they are consistent with the study by KUROYANAGI et al. (2008), who observed a link between shell morphology and genetic distinction in *G. ruber* (white) from the Pacific Ocean. In addition, the presence of a strong ecological separation among morphologically similar (or even identical) "cryptic genetic types" seems to be common in planktonic foraminifera (e.g., DARLING et al., 2006, 2007; DE VARGAS et al., 2001). Given these observations, preference is given to the hypothesis that the late Quaternary Mediterranean morphotypes as defined in this study also represent genetically and ecologically distinct populations. If a direct correlation between morphology and mode of life is assumed, it remains unclear why the types have not diverged morphologically more than currently observed. Either the divergence among the types is relatively recent or the morphology of their shells is not under a strong selective pressure. In any case, our preferred hypothesis would imply that the taxonomical status of *G. ruber* (white) has to be revised away from the broad concept of PARKER (1962).

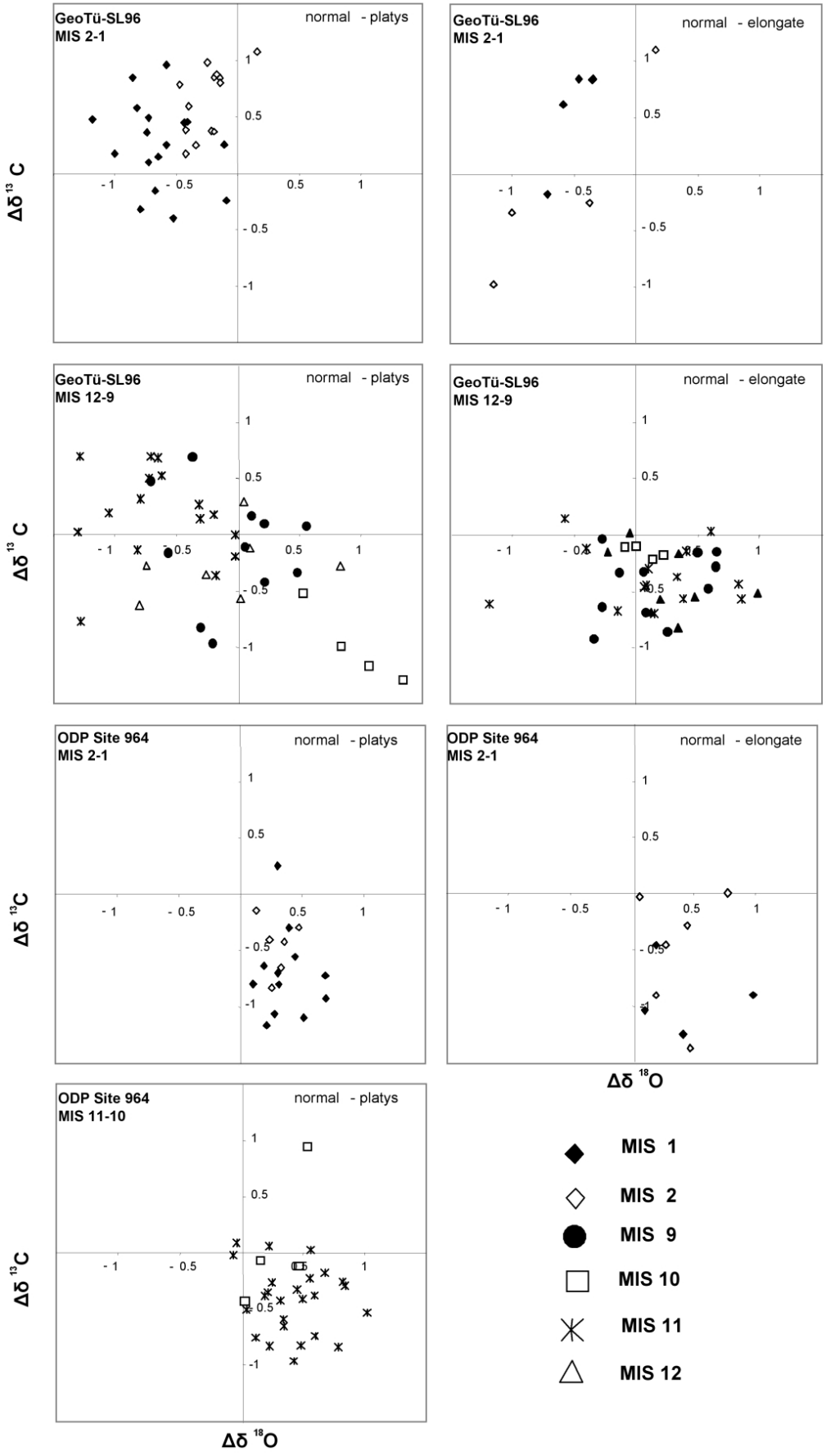

Figure 41: Stable isotopic differences between *G. ruber* (white) morphotypes during MIS 1-2 and MIS 9-12.

In contrast to *G. ruber* (white), the *G. ruber* (pink) variety is linked to warmer surface waters and previous studies indicate that its range extended to the Mediterranean only during warm periods. For example in the western Mediterranean Sea, PÉREZ-FOGALDO et al. (2004) recorded *G. ruber* (pink) in the Holocene and MIS 5e. LINARES et al. (1999) investigated planktonic foraminiferal faunas from the Algerian coast of the western Mediterranean (ODP Sites 975 and 976) throughout the entire Quaternary and dated the first occurrence of *G. ruber* (pink) to MIS 9. In this study, the pink variety was found to be rare but continuously present in the central Mediterranean throughout MIS 11, which thus constitutes the oldest (~ 470 kyr B.P.) report of *G. ruber* (pink) in the Mediterranean Sea.

Depth habitats and seasonal preferences of *G. ruber* morphotypes

In order to understand the isotope offsets (fig. 41) between the morphotypes, $\delta^{18}O$ values from the Holocene sections (post-sapropel values only) of both cores were converted to calcification temperatures. This exercise could not be carried out for type c "elongate", which did not yield enough specimens for isotope analyses in the late Holocene.

Figure 42 shows the temperature pattern for four defined depths (0 m, 30 m, 50 m and 100 m) during one year for the position of the two investigated sites together with calculated mean calcification temperatures of the morphotypes "normal" and "platys". The plots reveal a clearly lower mean calcification temperature for type b "platys" for GeoTü-SL96 than for ODP Site 964, while specimens of type a "normal" appear to have calcified at the same temperature at both localities.

Given the average yearly temperature cycle at both sites (fig. 42), it is clear that the main growth and calcification of *G. ruber* (white) type a "normal" could have only occurred in the top 50 m of the water column during the summer/early autumn (June-October). At ODP Site 964, type b "platys" shows a growth maximum slightly higher in the water column (top 30 m) or somewhat later in the summer season (August-October). In core GeoTü-SL96, the calculated average calcification temperature of type b "platys" is more than 2°C colder than that of type a "normal" and implies a deeper habitat during the summer (around 50 m water depth) or an even production throughout the year, leading to a seasonally averaged signal in the isotope data. The latter explanation is here considered less likely as it would be epected to lead to a large scatter in the stable isotope data which are based on a relatively few specimens (10-12).

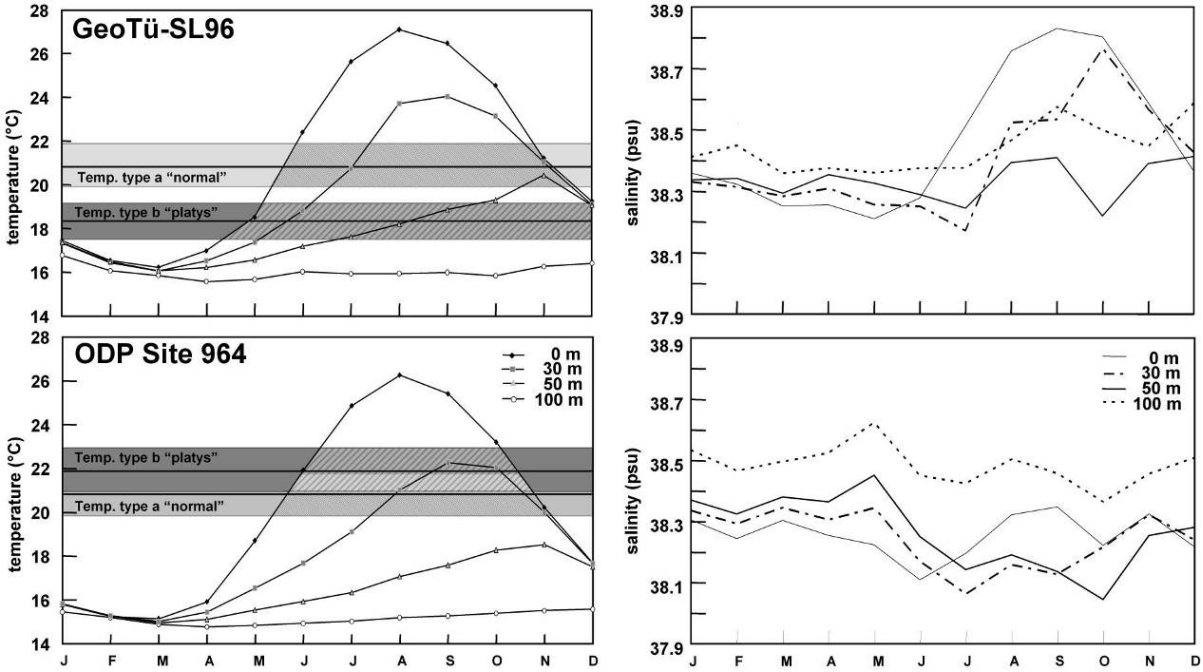

Figure 42: Temperature and salinity of the two cores in four depths within the upper 100 m of the water column (ANTONOV et al., 2006, LOCARNINI et al., 2006). Mean calcification temperatures calculated from $\delta^{18}O$ values (BEMIS et al., 1998; THUNELL et al., 1999) for type a "normal", light grey box denotes calculated mean temperature of $\delta^{18}O$ values, diagonal right striped box period of possible calcification; for type b platys dark grey bar denotes calculated mean temperature of $\delta^{18}O$ values, diagonal left striped box period of possible calcification. The cross striped section denotes the overlapping area. The boxes are +/- 1 standard deviation wide, the line denotes average temperature.

The seasonal salinity cycles at the location of core GeoTü-SL96 show the development of a strong summer halocline, which appears to be associated with low primary productivity (fig. 34). It would thus appear that at this site, individuals of type b "platys" shifted their habitat underneath the halocline to avoid the highly stratified and oligotrophic surface water (fig. 42). In such a scenario, type a "normal" may be bound to the surface to benefit from symbiont activity whereas type b "platys" could be more dependant on algal or zooplankton prey (HEMLEBEN et al., 1989), which would have its maximum beneath the halocline. This speculation would suggest differences in symbiont activity between the two types, which can be tested by examining their carbon isotope offsets. Indeed, the type a "normal" carbon isotope values are heavier in the Holocene section of core GeoTü-SL96 than those of type b "platys" (tab. 5), which assumedly lived deeper in the water column in this area. The heavier carbon isotopes in type a "normal" are consistent with a stronger photosynthetic activity of the algal symbionts in the shallower habitat of this type. In core ODP Site 964, the carbon isotope offset between the two types is reversed, confirming the observation from oxygen isotope data that at this location, type a "normal" and type b "platys" occupied essentially the same portion of the water column. This observed negative

offset could thus represent a difference in the vital effect between the two types, lending further support to their classification as separate species.

Habitat differences among morphotypes of *G. ruber* (white) have been noted in previous studies. HECHT & SAVIN (1972) examined "kummerform" and "normal" *G. ruber* for morphotype occurrence and stable isotope composition. They reported differing depths for the two *G. ruber* forms: 0-85 m (20 m in average) for "normal" and 0-120 m (66 m in average) for "kummerform". However, this depth discrepancy is not directly comparable to our results as the "kummerform" type is interpreted as stress-induced ecophenotypic variation by HECHT & SAVIN (1972). However, the depth range for type a "normal" found in the present study, hardly exceeding 50 m, is significantly shallower than the range for kummerform specimens found by HECHT & SAVIN (1972).

In the Pacific Ocean, WANG (2000) and LOEWEMARK et al. (2005) compared stable isotope signals of two *G. ruber* morphotypes and found that *G. ruber* s.l. appears to calcify in a deeper water layer than *G. ruber* s.s. LIN et al. (2004) showed that $\delta^{13}C$ values in different morphotypes (*G. ruber* s.s. and *G. ruber* s.l.) reflect different nutrient availability due to stratification of the water column. These results were confirmed by Mg/Ca data of STEINKE et al. (2005), SADEKOV et al. (2008), KUROYANAGI & KAWAHATA (2004) and by KAWAHATA (2005) from evaluation of plankton tow samples in the seas around Japan.

The differences in stable isotope compositions of the three morphotypes (type a "normal", type b "platys" and type c "elongate") of *G. ruber* highlighted in the present study confirm the observations of previous works concerning different depth preferences of the morphotypes (KUROYANAGI & KAWAHATA, 2004; LIN & HSIEH, 2007). However, the reversed patterns of the offset in stable isotope values in the two most abundant morphotypes (type a "normal" and type b "platys") for the two cores of this study (tab. 5, fig. 41, 42) implies that habitat preferences of individual types may be regionally variable, depending on the oceanographic situation (productivity, stratification).

Behaviour of *G. ruber* during glacial and interglacial cycles

The present study is the first attempt to highlight significant changes in *G. ruber* (white) morphotype abundance and stable isotope composition for MIS 12 to 9 in comparison to MIS 2 and 1. The types show consistent differences between glacials and interglacials (fig. 37, 41) and between the two cores (fig. 39, fig. 41). The reversed sign of the offset in stable isotope composition between the two studied cores is systematically

observed both in MIS 2 and 1 and MIS 12 to 9. This strongly suggests stratigraphically consistent oceanographic differences between the two sites.

The two sites in the Eastern Mediterranean basin are characterised by different hydrographical settings. GeoTü-SL96 off Libyan margin is influenced by the inflow of Atlantic waters from the western basin; ODP Site 964 comes from an area, were the Levantine intermediate waters leave the region in direction of the western basin (MILLOT & TAUPIER-LETANGE, 2005). The difference in the setting between the two Sites is reflected in the seasonal development of a higher salinity and temperature surface layer in the second half of the year at the position of core GeoTü-SL96, which is not observed at ODP Site 964 (fig. 42). The consistent isotope offsets between the *G. ruber* types indicate that this oceanographic contrast between the two sites persisted on glacial-interglacial time scales and remained strong enough to influence the ecology and geochemistry of the studied *G. ruber* (white) morphotypes.

An exception to the offset sign reversal pattern of the stages is MIS 10. The sign and magnitude of the offset in isotope composition was approximately similar for both cores at that time, which indicates more homogenous regional conditions, attenuating the oceanographic variations between the two studied sites. The exceptional state of MIS 10 is additionally illustrated by the continuous increase in the abundance of *G. ruber* (white), from late MIS 11 well into the MIS 10 glacial.

Anomalously high sea surface temperatures in the MIS 10 glacial interval, close to interglacial temperatures, are found in a range of oceanic records (BASSINOT et al., 1994, MD90-963, equatorial Indian Ocean; MCMANUS et al., 1999, ODP Site 980, North Atlantic Ocean, and CORTESE et al., 2004, ODP Site 1089, subantarctic Atlantic Ocean). This study documents for the first time similarly exceptional conditions during MIS 10 in the Eastern Mediterranean Sea.

The ecological divergence of the morphotypes strongly supports a differential interpretation of *G. ruber* (white)-based paleoceanographic proxy records for the Mediterranean during the late Quaternary. Separate consideration of the types avoids bias in palaeoclimatological signals caused by the effects of differing habitat preferences, and provides at the same time a new potentially powerful method to extract information of surface-water stratification and productivity regimes in the Eastern Mediterranean. As illustrated by the present study, high relative abundances of type b “platys” are indicative of high productivity, which in our case is normally associated with glacial conditions. In

addition, there is evidence for a correlation and nutrient availability and thus the degree of stratification.

In order to estimate the possible magnitude of bias in isotope records due to morphotype lumping, a synthetic isotope record was calculated as an average of stable isotope composition of the morphotypes weighted by their abundance (fig. 40). The offsets between synthetic and "normal" morphotype $\delta^{18}O$ values (histogram at the bottom of the plots in figure 40) range between -0.23 and 0.33 ‰, showing opposite signs at the two sites. For GeoTü-SL96 both $\delta^{18}O$ and $\delta^{13}C$ are predominantly lighter than the synthetic record whereas at ODP Site 964 the synthetic values tend to be heavier, especially during glacial periods (fig. 40). The magnitude of the $\delta^{18}O$ offsets correspond to differences in temperature of up to 1°C (BEMIS et al., 1998; THUNELL et al., 1999). Fluctuations of such magnitude could potentially be extracted from bulk *G. ruber* (white) isotope records where abundances of morphotypes vary through time even in the absence of any primary environmental forcing. Our results indicate that isotope offsets between morphotypes and their mutual proportions could vary in space and through time calling for caution when interpreting isotope records in the Mediterranean throughout the late Quaternary.

4. Conclusions

In order to compare the climatic trends between MIS 11 and the present interglacial in the Eastern Mediterranean, high resolution faunal, isotopic and sediment-property records have been generated for two Eastern Mediterranean sediment cores covering the entire MIS 11 interval. An age model has been established on the basis of stable oxygen isotopes, planktonic faunal abundance events and sapropel formations

The alignment of the two sapropel events in both MIS 11 and MIS 1 allows for a correlation of these two stages with respect to similar sea levels and preindustrial greenhouse gas concentrations. The first insolation peak in MIS 11 seems to have been too weak to trigger full interglacial conditions related to sapropel formation in this region; therefore alignment is based on the second insolation maximum. Thus, despite the rough similarity due to repeating 400 ka and 100 ka Milankovitch cycles, the assumed comparability of orbital settings of MIS 11 and MIS 1 is discarded for the Eastern Mediterranean region.

Sapropels of MIS 11 and MIS 1 were found in ODP Site 964 as clearly identifiable dark layers and distinct peaks in Ba/Al ratios and/or in $\delta^{18}O$ values (fig. 20). Sapropel formation in GeoTü-SL96 (1399 m), in contrast, occurred in MIS 1, but not during MIS 11 peak interglacial conditions. Even though a freshwater peak could be detected, and enhanced Ba/Al ratios were observed, no dark layer in the sediment record could be found and most importantly there were still benthic foraminifera in relatively large numbers present. MIS 11 and MIS 1 sapropels are differentiated by the depth of the oxycline during sapropel formation phases. In MIS 1 the oxycline must have been 500 m higher in the water column than in MIS 11. ODP Site 964 shows an extremely strong peak in light oxygen isotopes during MIS 11, which is difficult to reconcile with the weak insolation forcing of the MIS 11 monsoonal maximum. It is speculated that this freshwater peak could reflect enhanced freshwater inflow to the Eastern Mediterranean basin due to Bosporus opening in combination with African monsoonal and riverine output.

Foraminiferal assemblage composition analysis of MIS 11 revealed the presence of glacial-like assemblages, resulting in ANN-based SST estimates compatible with glacial conditions. Although corroborated by relatively low alkenone temperatures, these apparent glacial conditions in early MIS 11 are in stark contrast with global trends and pollen evidence from the Mediterranean region. The most probable scenario to explain this anomaly

is high winter productivity during relatively cool and wet interglacial conditions in early MIS 11, fuelled by enhanced influx of terrigenous material through high moisture availability and higher terrestrial biomass, leading to the persistence of glacial planktonic foraminifera assemblages, and alkenones representing the cold season signal until the development of the MIS 11 sapropel at 409 kyr B.P. Peak interglacial conditions started with the second, stronger, insolation maximum of MIS 11, triggering the MIS 11 sapropel event, and were subsequently sustained over the three following precession cycles. The later part of MIS 11 is characterised by muted magnitude of insolation forcing, linked to exceptionally low eccentricity, which could explain the stability of the regional climate. Such situation has also been observed during MIS 15 to MIS 13 in Lake Baikal record (PROKOPENKO et al., 2002). The existence of glacial-like winter conditions until the development of the MIS 11 sapropel at 409 kyr B.P. clearly discredits MIS 11 as an analogue to Holocene climate development, no matter how the interglacials are aligned (BROECKER & STOCKER, 2006; RUDDIMAN, 2005, 2006A, 2007; CRUCIFIX & BERGER, 2006). In combination with the observed stability of interglacial conditions throughout MIS 11, the records highlight a non-linear response of the regional Mediterranean climate to orbital forcing, with a threshold-like sensitivity to the amplitude of the insolation forcing.

As planktonic foraminifera are sources of paleoceanographic information, their ecological preferences and biology in the context of climate history are important factors to understand. High resolution planktonic foraminifera assemblage counts reflect environmental changes throughout the basin. Three distinct phases of benthic foraminiferal changes can be identified throughout the basin, coinciding with insolation maxima. The composition of these peaks can be related to planktonic foraminifera assemblages during some later sapropel formation phases. As neither productivity, nor freshwater input nor SST show any major trends reconcilable with the three sapropel-like foraminiferal phases in any meaningful way, the only possibility of relating them to the three insolation maxima is by invoking stratification and seasonality maxima. Such surface-water conditions are common to phases of sapropel deposition (ROSSIGNOL-STRICK, 1983, 1985), thus explaining the similarity with later sapropel assemblages.

The surface environment of the Eastern Mediterranean Sea during these faunal peaks could thus represent sapropel-like conditions with respect to the structure of the surface water column (stratification, seasonality), although the insolation forcing did not reach threshold conditions for true sapropel formation during these phases.

Throughout the last decades, *G. ruber*-based proxies have been crucial for palaeoclimate research. Abundances and stable isotope measurements on this species are important methods to reconstruct past climate. Three morphotypes of *G. ruber* (white) from late Quaternary sediments of two Mediterranean cores (ODP Site 964 and GeoTü-SL96) from the Eastern Mediterranean are found to show significantly different stable isotope compositions, reflecting different habitat preferences. The isotope offset between type a ("normal") and type b ("platys") shows opposite patterns at the two sites. An analysis of Holocene records suggests that type a "normal" has a constant depth habitat at both locations and is characterised by maximum growth in summer months in the top 50 m of the water column. Type b "platys" appears to share a similar habitat with type a "normal" at ODP Site 964, only slightly shifted towards shallower waters or warmer months, but in GeoTü-SL96, it shows a clearly deeper signal (around 50 m in the water column), as if avoiding the oligotrophic surface waters that develop during the summer in the Greater Syrte. Glacials and interglacials from MIS 2 to 1 and MIS 12 to 9 are consistently characterised by changes in abundance and stable isotope composition of the morphotypes. Type b "platys" tends to be more abundant during glacials; type c "elongate" is more abundant during deglaciation and early interglacials. Separate consideration of the three studied morphotypes of *G. ruber* (white) in terms of relative abundance and stable isotope composition yields potentially meaningful factors for palaeoceanographic proxy records in the late Quaternary. In view of the strong link between morphological variability and habitat distinction in *G. ruber*, confirmed by our results, it would seem worth investigating whether such phenomena also occur in other species of planktonic foraminifera which show a similarly high degree of intraspecific morphological variability.

To sum up, it can be generally concluded that the here established alignment of MIS 11 and MIS 1 climatic trends in the Eastern Mediterranean, based on the sapropel events in both intervals, provides a promising opportunity to understand the phase relationships of changes in climatic parameters on global and regional scales under orbital conditions similar to those of the present interglacial and thus to assess potential future climate developments. The influence of human impact on the world climate, with exorbitant greenhouse gas emissions, is hardly predictable. Inferrences from past analogues to predict future climatic developments without human impact are likely to be severely hampered by even small discrepancies between the investigated isotopic stages.

Acknowledgements

In the first place I would like to thank my family for their incredible support and the love they gave me all the time.

I want to express my special thanks to Michal Kučera for all he taught me, for the reviews, discussions, advice, generosity and the freedom in ideas and working.

I would like to thank Christoph Hemleben for supporting the project with advice, sample material, data and reviews. I also warmly thank Gerhard Schmiedl for being my second reviser.

I am grateful for all the help of the working group to solve smaller and bigger problems, especially to Hartmut Schulz, Michael Siccha, Margret Bayer and Wilfried Rönnfeld.

I also would like to give a warm-hearted thank to Margita Lachenmaier and Brigitte Blankenhorn who always assisted with administrative duties.

Ralf Aurahs, Annekatrin Enge, Peter Fittkau, Petra Heinz, Tobias Moller, Ulrike van Raden, Franziska Simmank, Margit Simon, Gabriele Trommer and Anne Ulmer are thanked for having been such good colleagues during PhD times.

Another thank you goes to Libuse Rammersdorfer who always kindly helped find rare literature.

I also owe Nadia Al-Sabouni and Paola Kučera a special thank for improving my English.

My student helpers and laboratory workers, especially Ramona Hoffmann, Sophie Jehle and Lisa Walz, are thanked for their help in the project.

I want to thank my collaborators Amani Badawi, Lucia DeAbreu, Angela Hayes, Andreas Mackensen, Belen Martrat, Jerry McManus, Eelco Rohling, Ursula Röhl, Joachim Schönfeld, Ralf Schiebel, Solveig Seidenkrantz, Heinrich Taubald, Maria Triantaphyllou, Chronis Tzedakis and Antje Völker for providing practical help, advice, samples, discussions and data.

I would like to address another thank-you to Mike Reich and the new working group in Göttingen, for their support during the last months.

Ben, thank you for all you did for me during PhD times, for discussions, practical help, sharing night shifts, beeing always there, cooking, coffee and much more. You are amazing, thank you.

A. References

Aksu, A. E., Jenner, G., Hiscott, R. N. & Isler, E. B., (2008): Occurrence, stratigraphy and geochemistry of Late Quaternary tephra layers in the Aegean Sea and the Marmara Sea. Marine Geology, 252(3-4): 174-192.

Altman, D. G. & Bland, J. M., (2005): Standard deviations and standard errors. British Medical Journal, 331: 903.

Aksu, A. E., Yasar, D. & Mudie, P. J., (1995): Origin of the late glacial-Holocene hemipelagic sediments in the Aegean Sea: clay mineralogy and carbonate cementation. Marine Geology, 123: 33-59.

Amante, C. & Eakins, B. W., (2008): ETOPO1 1 Arc-Minute Global Relief Model: Procedures, Data Sources and Analysis. National Geophysical Data Center, National Environmental Satellite, Data and Information Service, National Oceanic and Atmospheric Administration, U. S. Department of Commerce, Boulder, Colorado, USA. http://www.ngdc.noaa.gov/mgg/global/global.html

Antonov, J. I., Locarnini, R. A., Boyer, T. P., Mishonov, A. V. & Garcia, H. E., (2006): World Ocean Atlas 2005, Volume 2: Salinity. S. Levitus, Ed. NOAA Atlas NESDIS 62, U.S. Government Printing Office, Washington, D.C., 182 pp.

Aurahs, R., Grimm, G. W., Hemleben, V., Hemleben, C. & Kucera, M., (2009): Geographical distribution of cryptic genetic types in the planktonic foraminifer *Globigerinoides ruber*. Molecular Ecology, 18: 1692-1706.

Bassinot, F. C., Labeyrie, L. D., Vincent, E., Quidelleur, X., Shackleton, N. J. & Lancelot, Y., (1994): The astronomical theory of climate and the age of the Brunhes-Matuyama magnetic reversal. Earth and Planetary Science Letters, 126: 91-108.

Bauch, H. A. & Erlenkeuser, H., (2003): Interpreting glacial-interglacial changes in ice volume and climate from subarctic deep water foraminiferal $\delta^{18}O$. In: Droxler, A. W., Poore, R. Z. & Burckle, L. H. (Eds.), Earth's climate and orbital eccentricity: the marine isotope stage 11 question. Geophysical Monograph 137, Washington, DC, 87-102.

Bauch, H. A., Erlenkeuser, H., Helmke, J. P. & Struck, U., (2000): A paleoclimatic evaluation of marine oxygen isotope stage 11 in the high-northern Atlantic (Nordic seas). Global and Planetary Change, 24(1): 27-39.

Bé, A. W. H., (1982): Biology of planktonic Foraminifera. University of Tennessee Department of Geological Sciences Studies in Geology, 1982: 51-89.

Bé, A. W. H. & Hutson, W. H., (1977): Ecology of planktonic foraminifera and biogeographic patterns of life and fossil assemblages in the Indian Ocean. Micropaleontology, 23(4): 369-414.

Becquey, S. & Gersonde, R., (2002): Past hydrographic and climatic changes in the Subantarctic Zone of the South Atlantic - The Pleistocene record from ODP Site 1090. Palaeogeography, Palaeoclimatology, Palaeoecology, 182: 221-239.

Bemis, B. E., Spero, H. J., Bijma, J. & Lea, D. W., (1998): Reevaluation of the oxygen isotopic composition of planktonic foraminifera: experimental results and revised paleotemperature equations. Paleoceanography, 13/2: 150-160.

Berger, A., (1978): Long-term variations of daily insolation and Quaternary climatic changes. Journal of Atmospheric Sciences, 35(12): 2362-2367.

Berger, A. & Loutre, M. F., (1991): Insolation values for the climate of the last 10 million years. Quaternary Science Reviews, 10: 297–317.

Berger, A. & Loutre, M. F., (2002): An exceptionally long Interglacial ahead? Science, 297: 1287-1288.

Berger, A. & Loutre, M. F., (2003): Climate 400,000 years ago, a key to the future? In: Droxler, A. W., Poore, R. Z. & Burckle, L. H. (Eds), Earth's climate and orbital eccentricity: the marine isotope stage 11 question. Geophysical Monograph 137, Washington, DC, 41-59.

Berger, W. H. & Wefer, G., (2003): On the dynamics of the ice ages: Stage-11 paradox, mid-brunhes climate shift, and 100-ky cycle. In: Droxler, A. W., Poore, R. Z. & Burckle, L. H. (Eds), Earth's climate and orbital eccentricity: the marine isotope stage 11 question. Geophysical Monograph 137, Washington, DC, 41-59.

Bethoux, J. P., (1980): Mean water fluxes across sections in the Mediterranean Sea, evaluated on the basis of water and salt budgets and of observed salinities. Oceanologica Acta, 3: 79-88.

Bethoux, J. P., Gentili, B., Morin, P., Nicolas, E., Pierre, C. & Ruiz-Pino, D., (1999): The Mediterranean Sea: a miniature ocean for climatic and environmental studies and a key for the climatic functioning of the North Atlantic. Progress in Oceanography, 44: 131–146.

Bowen, D. Q., (2003): Uncertainty in oxygen isotope stage 11 sea-level: an estimate of ~13 ± 2 m from Great Britain. In: Droxler, A. W., Poore, R. Z. & Burckle, L. H. (Eds), Earth's climate and orbital eccentricity: the marine isotope stage 11 question. Geophysical Monograph 137, Washington, DC, 131-144.

Bradley, W.H., (1938): Mediterranean sediments and Pleistocene sea levels. Science, 88: 376-379.

Brigham-Grette, J., (2009): Contemporary Arctic change: A paleoclimate deja vu? Proceedings of the National Academy of Sciences of the United States of America, 106(44): 18431-18432.

Broecker, W. S., & Stocker, T. F., (2006): The Holocene CO2 rise: Anthropogenic or natural? Eos Transactions of the American Geophysical Union, 87(3), 27-29.

Buccheri, G., Capretto, G., Donato, V., Esposito, P., Ferruzza, G., Pescatore, T., Ermolli, E., Senatore, M., Sprovieri, M., Bertoldo, M., Carella, D. & Madoina, G., (2002): A high resolution record of the last deglaciation in the southern Tyrrhenian Sea: environmental and climatic evolution. Marine Geology, 186: 447-470.

Cacho, I., Grimalt, J. O. & Canals, M., (2002): Response of the Western Mediterranean Sea to rapid climatic variability during the last 50,000 years: a molecular biomarker approach. Journal of Marine Systems, 33-34: 253-272.

Cacho, I., Grimalt, J. O., Sierro, F. J., Shackleton, N. J. & Canals, M., (2000): Evidence of enhanced Mediterranean thermohaline circulation during rapid climatic coolings. Earth and Planetary Science Letters, 183: 417-429.

Cacho, I., Pelejero, C., Grimalt, J. O., Calafat, A. M. & Canals, M., (1999): C37 alkenone measurements of sea surface temperature in the Gulf of Lions (NW Mediterranean). Organic Geochemistry, 33: 557-566.

Cacho, I., Shackleton, N., Elderfield, H., Sierro, F. J. & Grimalt, J. O., (2006): Glacial rapid variability in deep-water temperature and delta O-18 from the Western Mediterranean Sea. Quaternary Science Reviews, 25: 3294-3311.

Callot, Y. & Fontugne, M., (1992): Water tables levels in Holocene paleolakes from the Northeastern Grand Erg Occidental (Algeria). Comptes rendus de l'Académie des Sciences Série II, 315(4): 471-477.

Calvert, S. E., (1983): Geochemistry of Pleistocene sapropel and associated sediments from the Eastern Mediterranean. Oceanologica Acta, 6: 255-267.

Calvert, S. E. & Fontugne, M. R., (2001): On the late Pleistocene-Holocene sapropel record of climatic and oceanographic variability in the eastern Mediterranean. Paleoceanography, 16: 78-94.

Calvert, S. E. & Pedersen, T. F., (2007): Elemental proxies for palaeoclimatic and palaeoceanographic variability in marine sediments: interpretation and application. Developments in Marine Geology, 1: 567-644.

Capozzi, R. & Negri, A., (2009): Role of sea-level forced sedimentary processes on the distribution of organic carbon-rich marine sediments: A review of the Late Quaternary sapropels in the Mediterranean Sea. Palaeogeography, Palaeoclimatology, Palaeoecology, 273: 249-257.

Castañeda, I. S., Schefuß, E., Pätzold, J., Sinnighe Damsté, J. S., Weldeab, S. & Schouten, S., (2010): Millennial-scale sea surface temperature changes in the eastern Mediterranean (Nile River Delta region) over the last 27,000 years. Paleoceanography, 25: PA1208.

Cita, M. B., Vergnaud Grazzini, C., Robert, C., Chamley, H., Ciaranfi, N. & d'Onofrio, S., (1977): Paleoclimatic record of a long deep sea core from the Eastern Mediterranean. Quaternary Research, 8: 205–235.

Corliss, B. H., (1985): Microhabitats of benthic foraminifera within deep-sea sediments. Nature, 314(6010): 435-438.

Cortese, G., Abelmann, A. & Gersonde, R., (2004): A glacial warm water anomaly in the subantarctic Atlantic Ocean, near the Agulhas Retroflection. Earth and Planetary Science Letters, 222(3-4): 767-778.

Croudace, I. W., Rindby, A. & Rothwell, R. G., (2006): ITRAX: Description and evaluation of a new multifunction X-ray core scanner. In: Rothwell, R.G. (ed.), New Techniques

in Sediment Core Analysis. Geological Society, London, Special Publications, 267: 51–63.

Crucifix, M. & Berger, A., (2006): How long will our interglacial be? EOS Transactions of the American Geophysical Union, 87(35): 352-353.

D'Orbigny, A. D., (1826): Tableau méthodique de la classe des céphalopodes. Annales Des Sciences Naturelles, 14: 277 pp.

D'Orbigny, A. D., (1839): Voyage à l'Amérique méridionale. Strasbourg, France.

Darling, K. F., Kucera, M., Kroon, D. & Wade, C. M., (2006): A resolution for the coiling direction paradox in *Neogloboquadrina pachyderma*. Paleoceanography, 21(2): PA2011.

Darling, K. F., Kucera, M. & Wade, C. M., (2007): Global molecular phylogeography reveals persistent arctic circumpolar isolation in a marine planktonic protist. Proceedings of the National Academy of Sciences of the United States of America, 104(12): 5002-5007.

Darling, K. F. & Wade, C. M., (2008): The genetic diversity of planktic foraminifera and the global distribution of ribosomal RNA genotypes. Marine Micropaleontology, 67: 216-238.

De Abreu, L., Abrantes, F. F., Shackleton, N. J., Tzedakis, P. C., McManus, J. F., Oppo, D. W. & Hall, M. A., (2005): Ocean climate variability in the eastern North Atlantic during interglacial marine isotope stage 11: A partial analogue to the Holocene? Paleoceanography, 20: PA3009.

De Baar, H. J. W. & De Jong, J. T. M., (2001): Distributions, Sources and Sinks of iron in Seawater. In: Turner, D. R. & Hunter, K. A. (Eds): The Biogeochemistry of Iron in Seawater. IUPAC Series on Analytical and Physical Chemistry of Environmental Systems, 7: 123-254.

DeLange, G. J., Thomson, J., Reitz, A., Slomp, C. P., Principato, M. S., Erba, E. & Corselli, C., (2008): Synchronous basin-wide formation and redox-controlled preservation of a Mediterranean sapropel. Nature Geoscience, 1: 606–610.

De Rijk, S., Hayes, A. & Rohling, E. J., (1999): Eastern Mediterranean sapropel S1 interruption: an expression of the onset of climatic deterioration around 7 ka BP. Marine Geology, 153: 337-343.

Desprat, S., Sanchez Goni, M.-F., Turon, J.-L., McManus, J. F., Loutre, M. F., Duprat, J., Malaize, B., Peyron, O. & Peypouquet, J.-P., (2005): Is vegetation responsible for glacial insolation inception during periods of muted changes? Quaternary Science Reviews, 24(12-13): 1361-1374.

De Vargas, C., Renaud, S., Hilbrecht, H. & Pawlowski, J., (2001): Pleistocene adaptive radiation in *Globorotalia truncatulinoides*: Genetic, morphologic, and environmental evidence. Paleobiology, 27(1): 104-125.

De Vernal, A. & Hillaire-Marcel, C., (2008): Natural variability of Greenland climate, vegetation, and ice volume during the past million years. Science, 320(5883): 622-625.

Dewey, J. F., Pitman, W. C., Ryan, W. B. F. & Bonnin, J., (1973): Plate Tectonics and evolution of the Alpine System. Geological Society of America Bulletin, 84: 3137-3180.

Dickson, A.J., Beer, C. J., Dempsey, C., Maslin, M. A., Bendle, J. A., McClymont, E. L. & Pancost, R. D., (2009): Oceanic forcing of the Marine Isotope Stage 11 interglacial. Nature Geoscience, 2(6): 427-432.

Droxler, A. W. & Farrell, J. W., (2000): Marine Isotope Stage 11 (MIS 11): new insights for a warm future. Global and Planetary Change, 24: 1-5.

Droxler, A. W., Poor, R. & Burckle, L., (1999): Data on past climate warmth may lead to better model of warm future. Eos Transactions, American Geophysical Union, 80(26): 289.

Droxler, A. W., Alley, R. B., Howard, W. R., Poore, R. Z. & Burckle, L. H., (2003): Unique and exceptionally long Interglacial Marine Isotope Stage 11: Window into Earth warm future climate. In: Droxler, A. W., Poore, R. Z. & Burckle, L. H. (Eds.), Earth's climate and orbital eccentricity: the marine isotope stage 11 question. Geophysical Monograph 137, Washington, DC, 1-14.

Duplessy, J.-C., Labeyrie, L., Arnold, M., Paterne, M., Duprat, J. & van Weering, T. C. E. (1992). Changes in surface salinity of the North Atlantic Ocean during the last deglaciation. Nature, 358: 485-488.

Dymond, J., Suess, E. & Lyle, M., (1992): Barium in deep-sea sediments: A geochemical proxy for paleoproductivity. Paleoceanography, 7: 163-181.

Eberwein, A. & Mackensen, A., (2006): Regional primary productivity differences off Morocco (NW-Africa) records by modern benthic foraminifera and their stable carbon isotopic composition- Deep-Sea Research, part I-oceanographic research papers. 53, 1397-1400.

Eggins, S., De Deckker, P. & Marshall, J., (2003): Mg/Ca variation in planktonic foraminifera tests: Implications for reconstructing palaeo-seawater temperature and habitat migration. Earth and Planetary Science Letters, 212: 291-306.

Emeis, K.-C., Brumsack, H.-J., Kopf, A. & Rullkötter, J., (1996): Kontinentkollisionen und Klimawechsel im Mittelmeer: Ergebnisse von Leg 160 des Internationalen Tiefseebohrprogramms (ODP). Geowissenschaften, 14: 18-22.

Emeis, K.-C., Robertson, A. H. F., Richter, C., et al., (1996): Proceedings of the Ocean Drilling Program, Initial Reports, 160. College Station, TX.

Emeis, K.-C. & Sakamoto, T, (1998): The sapropel theme of leg 160. Proceedings of the ODP: Scientific results, 160: 29-36.

Emeis, K.-C., Sakamoto, T., Wehausen, R. & Brumsack, H.-J., (2000): The sapropel record of the eastern Mediterranean Sea - Results of Ocean Drilling Program Leg 160. Palaeoceanography, Palaeoclimatology, Palaeoecology, 158(3-4): 371-395.

Emeis, K.-C., Schulz, H., Struck, U., Rossignol-Strick, M., Erlenkeuser, H., Howell, M. W., Kroon, D., Mackensen, A., Ishizuka, S., Oba, T., Sakamoto, T. & Koizumi, I., (2003):

Eastern Mediterranean surface water temperatures and δ18O composition during deposition of sapropels in the late Quaternary. Paleoceanography, 18: 5.1-5.18.

Emiliani, C., (1955): Pleistocene temperatures. Journal of Geology, 63: 538-578.

EPICA community members, (2004): Eight glacial cycles from an Antarctic ice core. Nature, 429: 623–628.

Epstein, S. & Mayeda, T., (1953): Variation of O-18 content of water from natural sources. Geochimica et Cosmochimica Acta, 4: 213-224.

Ferguson, J. E., Henderson, G. M., Kucera, M. & Rickaby, R. E. M., (2008): Systematic change of foraminiferal Mg/Ca ratios across a strong salinity gradient. Earth and Planetary Science Letters, 265: 153-166.

Fontes, J. C. & Gasse, F., (1991): Chronology of the major paleohydrological events in NW Africa durring the late Quaternary. PALHYDAF results. Hydrobiologia, 214: 367-372.

Foucault, V. A. & Stanley, D.J., (1989): Late Quaternary palaeoclimatic oscillation in East Africa recorded by heavy minerals in the Nile delta. Nature, 339: 44-46.

Ganssen, G. M. & Kroon, D., (2000). The isotopic signature of planktonic foraminifera from NE Atlantic surface sediments: Implications for the reconstruction of past oceanic conditions. Journal of the Geological Society, 157: 693-699.

Gauch, H. G., Jr., (1982): Multivariate Analysis in Community Structure. Cambridge University Press, Cambridge, 1-298.

Geraga, M., Tsaila-Monopolis, S., Ioakim, C., Papatheodorou, G., Ferentinos, G., (2005): Short-term climate changes in the southern Aegean Sea over the last 48.000 years. Palaeogeography, Palaeoclimatology, Palaeoecology, 220: 311-332.

Gonzalez-Donoso, J., Serrano, F. & Linares, D., (2000): Sea surface temperature during the Quaternary at ODP sites 976 and 975 (western Mediterranean). Palaeogeography, Palaeoclimatology, Palaeoecology, 162: 17-44.

Gonzalez-Mora, B., Sierro, F. J. & Schönfeld, J., (2008): Temperature and stable isotope variations in different water masses from the Alboran Sea (Western Mediterranean) between 250 and 150 ka. Geochemistry, Geophysics, Geosystems, 9: 1-14.

Gregg, W.W. & Casey, N.W., (2004): Global and regional evaluation of the SeaWiFS chlorophyll data set. Abstract Remote Sensing of Environment, 93: 463–479.

Guerzoni, S., Molinaroli, E. & Chester, R., (1997): Saharan dust input to the western Mediterranean Sea: depositional patterns, geochemistry and sedimentology implications. Deep-Sea Research, 44: 631-654.

Hammer, Ø., Harper, D. A. T. & Ryan, P. D., (2001): Past: Paleontological statistics software package for education and data analysis. Palaeontologia Electronica, 1-9. http://palaeoelectronica.org/2001_1/past/issue1_01.htm

Hansen, J., Saito, M., Kharecha, P., Beerling, D., Berner, R., Masson-Delmotte, V., Pagani, M., Raymo, M., Royer, D. L. & Zachos, J. C., (2008): Target atmospheric CO2: where should humanity aim? Open Atmospheric Sciences Journal, 2: 217-231.

Haug, G. H., K. A. Hughen, D. M. Sigman, L. C. Peterson, U. Röhl, (2001): Southward migration of the intertropical convergence zone through the Holocene. Science, 293: 1304-1308.

Hayes, A., Rohling, E. J., De Rijk, S., Kroon, D. & Zachariasse, W. J., (1999): Mediterranean planktonic foraminiferal faunas during the last glacial cycle. Marine Geology, 153(1-4): 239–252.

Hayes, A., Kucera, M., Kallel, N., Sbaffi, L. & Rohling, E. J., (2005): Glacial Mediterranean sea surface temperatures based on planktonic foraminiferal assemblages. Quaternary Science Reviews, 24: 999–1016.

Healy-Williams, N., Ehrlich, R. & Williams, D. F., (1985): Morphometric and stable isotopic evidence for subpopulations of *Globorotalia truncatulinoides*. Journal of Foraminiferal Research, 15: 242-253.

Hecht, A. D. & Savin, S. M., (1972): Phenotypic variation and oxygen isotope ratios in recent planktonic foraminifera. Journal of Foraminiferal Research, 2/2: 55-67.

Hecht, A. D., Pinardi, N. & Robinson, A. R., (1988): Currents, water masses, Eddies and Jets in the eastern Mediterranean Levantine basin. Journal of Physical Oceanography, 18: 1320-1353.

Helmke, J. P., Bauch, H. A. & Erlenkeuser, H., (2003): Development of glacial and interglacial conditions in the Nordic seas between 1.5 and 0.35 Ma. Quaternary Science Reviews, 22(15-17): 1717-1728.

Helmke J.P., Bauch, H. A., Roehl, U. & Kandiano, E. S., (2008): Uniform climate development between the subtropical and subpolar northeast Atlantic across Marine Isotope Stage 11. Climate of the Past, 4: 181-190.

Hemleben, C., Spindler, M. & Erson, O. R., (1989): Modern planktonic foraminifera. Springer, Berlin, 363 pp.

Hemleben, Ch., Hörnle, K., Jørgensen, B. B. & Roether, W., (2003): Ostatlantik-Mittelmeer-Schwarzes Meer, Cruise No. 51, 12. September - 28. December 2001.- Meteor-Berichte, Universität Hamburg, 3-1: 1-225.

Herman, Y., (1972): Quaternary eastern Mediterranean sediments: micropalaeontological climatic record. In: Stanley, D. J. (Ed.): The Mediterranean Sea. Dowden, Hutchinson & Ross, Stroudsburg, PA, 129-147.

Hill, M. O. & Gauch, H. G., (1980): Detrended correspondence analysis: An improved ordination technique. Plant ecology, 42(1-3): 47-58.

Hodell, D. A., Kanfoush, S. L., Venz, K. A., Charles, C. D. & Sierro. F. J., (2003): The mid-Brunhes transition in ODP sites 1089 and 1090 (Subantarctic south Atlantic). In: Droxler, A. W., Poore, R. Z. & Burckle, L. H. (Eds.), Earth's climate and orbital eccentricity: the marine isotope stage 11 question. Geophysical Monograph 137, Washington, DC, 113-129.

Hofrichter, R., Kern, W., Beckel, L., Domnig, I., Zankl, A. & Hein, A., (2002): 3. Geographie und Klima. In: Hofrichter, R. (Ed.): Das Mittelmeer. Spektrum Akademische Verlag, Heidelberg, Berlin, 102-195.

Howard, W. R. & Prell, W. L., (1994): Late Quaternary $CaCO_3$ Production and Preservation in the Southern Ocean: Implications for Oceanic and Atmospheric Carbon Cycling. Paleoceanography, 9(3): 453-482.

Howard, W. R., (1997): A warm future in the past. Nature, 388: 418-419.

Imbrie, J. & Imbrie, J. Z., (1980): Modeling the climatic response to orbital variations. Science, 207: 943-953.

Imbrie, J., Hays, J. D., Martinson, D. G., McIntyre, A., Mix, A. C., Morley, J. J., Pisias, N. G., Prell, W. L. & Shackleton, N. J., (1984): The orbital theory of Pleistocene climate: support from a revised chronology of the marine δ18O record. In: Berger, A., Imbrie, J., Hays, H., Kukla, G. & Saltzman, B. (Eds.), Milankovitch and Climate: Understanding the Response to Astronomical Forcing, Proceedings of the NATO Advanced Research Workshop held 30 November - 4 December, 1982 in Palisades, NY., 69 pp.

Imbrie, J. & Kipp, N. G., (1971): A new micropaleontological method for paleoclimatology: Application to a Late Pleistocene Caribbean core. In: Turekian, K. K. (Ed.): The Late Cenozoic Glacial Ages. Yale University Press, New Haven, 71-181.

Incarbona, A., Di Stefano, E., Sprovieri, R., Bonomo, S., Censi, P., Dinarès-Turell & Spoto, S., (2008): Variability in the vertical structure of the water column and paleoproductivity reconstruction in the central-western Mediterranean during the Late Pleistocene. Marine Micropaleontology, 69: 26-41.

Jansen, J. H. F., Kuijpers, A. & Troelstra, S. R., (1986): A mid-Brunhes climatic event: Long-term changes in global atmosphere and ocean circulation. Science, 232: 619-622.

Jones, R. W., (1994): The Challenger Foraminifera. Oxford University Press, Oxford, New York, Tokyo, 1-149.

Jorissen, F. J., (1999): Benthic foraminiferal microhabitats below the sediment-water interface. Modern foraminifera: 161-179.

Jorissen, F. J., deStigter, H. C. & Widmark, J. G. V., (1995): A conceptual model explaining benthic foraminiferal microhabitats. Marine Micropaleontology, 26(1-4): 3-15.

Jouzel, J., Masson-Delmotte, V., Cattani, O., Dreyfus, G., Falourd, S., Hoffmann, G., Minster, B., Nouet, J., Barnola, J. M., Chappellaz, J., Fischer, H., Gallet, J. C., Johnsen, S., Leuenberger, M., Loulergue, L., Luethi, D., Oerter, H., Parrenin, F., Raisbeck, G., Raynaud, D., Schilt, A., Schwander, J., Selmo, E., Souchez, R., Spahni, R., Satuffer, B., Steffensen, J. P., Stenni, B., Stocker, T. F., Tison, J. L., Werner, M. & Wolff, E. W., (2007): Orbital and millennial Antarctic climate variability over the past 800,000 years. Science, 317: 793–796.

Kallel, N., Paterne, M., Duplessy, J., Vergnaud-Grazzini, C., Pujol, C., Labeyrie, L., Arnold, M., Fontugne, M. & Pierre, C., (1997): Enhanced rainfall in the Mediterranean region during the last sapropel event. Oceanologica Acta, 20: 697-712.

Karabanov, E., Prokopenko, A., Williams, D., Khursevich, G., Kuzmin, M., Bezrukova, E. & Gvozdkov, A., (2003): High-resolution MIS 11 record from the continental sedimentary archive of Lake Baikal, Siberia. In: Droxler, A. W., Poore, R. Z. &

Burckle, L. H. (Eds.), Earth's climate and orbital eccentricity: the marine isotope stage 11 question. Geophysical Monograph 137, Washington, DC, 223-230.

Karageorgis, A. P., Gardner, W. D., Georgopoulos, D., Mishonov, A. V., Krasakopoulou, E. & Anagnostou, C., (2008): Particle dynamics in the Eastern Mediterranean Sea: a synthesis based on light transmission, PMC, and POC archives (1991–2001). Deep-Sea Research, 55: 177–202.

Karner, D. B. & Marra, F., (2003): 40Ar/39Ar dating of Glacial Termination V and the duration of Marine Isotopic Stage 11. In: Droxler, A. W., Poore, R. Z. & Burckle, L. H. (Eds.), Earth's climate and orbital eccentricity: the marine isotope stage 11 question. Geophysical Monograph 137, Washington, DC, 61-66.

Karner, D. B., Levine, J., Medeiros, B. P. & Muller, R. A., (2002): Constructing a stacked benthic $\delta^{18}O$ record. Paleoceanography, 17: 1030.

Kawahata, H., (2005): Stable isotopic composition of two morphotypes of *Globigerinoides ruber* (white) in the subtropical gyre in the north pacific. Paleontological Research, 9(1): 27-35.

Kemp, A. E. S., Pearce, R. B., Koizumi, I., Pike, J., & Rance, S. J., (1999): The role of mat-forming diatoms in the formation of Mediterranean sapropels. Nature, 398: 57-61.

Kemp, A. E. S., Pearce, R. B., Pike, J. & Marshall, J. E. A., (1998): Microfabric and microcompositional studies of Pliocene and Quaternary sapropels from the eastern Mediterranean. Proceedings of the ODP, Scientific Results, 160: 349–364.

Kim, K.-Y. & Crowley, T. J., (1994): Modelling the climate effect of unrestricted greenhouse emissions over the next 10,000 years. Geophysical Research Letters, 21: 681-684.

Krom, M. D., Cliff, R. A., Eijsink, L. M., Herut, B. & Chester, R., (1999): The characterisation of Saharan dusts and Nile particulate matter in surface sediments from Levantine basin using Sr isotopes. Marine Geology, 155: 319-330.

Kroon, D., Alexander, I., Little, M., Lourens, L.J., Matthewson, A., Robertson, A. H. F. & Sakamoto, T., (1998): Oxygen isotope and sapropel stratigraphy in the Eastern Mediterranean during the last 3.2 million years. In: Robertson, A. H. F., Emeis, K.-C., Richter, C. & Camerlenghi, A. (Eds.), Proceedings of the Ocean Drilling Program, Scientific Results, 160: 181-189.

Kucera, M., Weinelt, M., Kiefer, T., Pflaumann, U., Hayes, A., Weinelt, M., Chen, M. T., Mix, A. C., Barrows, T. T., Cortijo, E., Duprat, J., Juggins, S. & Waelbroeck, C., (2005): Reconstruction of sea-surface temperatures from assemblages of planktonic foraminifera: multi-technique approach based on geographically constrained calibration data sets and its application to glacial Atlantic and Pacific Oceans. Quaternary Science Reviews, 24(7-9): 951-998.

Kuhnt, T., Schmiedl, G., Ehrmann, W., Hamann, Y. & Andersen, N., (2008): Stable isotopic composition of Holocene benthic foraminifers from the Eastern Mediterranean Sea: Past changes in productivity and deep water oxygenation. Palaeogeography, Palaeoclimatology, Palaeoecology, 268(1-2): 106-115.

Kuhnt, T., Schmiedl, G., Ehrmann, W., Hamann, Y. & Hemleben, C., (2007): Deep-sea ecosystem variability of the Aegean Sea during the past 22 kyr as revealed by Benthic Foraminifera. Marine Micropaleontology, 64(3-4): 141-162.

Kukla, G., (2003): Continental records of MIS 11. In: Droxler, A. W., Poore, R. Z. & Burckle, L. H. (Eds.), Earth's climate and orbital eccentricity: the marine isotope stage 11 question. Geophysical Monograph 137, Washington, DC, 207-211.

Kullenberg, B., (1952): On the salinity of water contained in marine sediments. Meddelanden fran Oceanografiska Institutet Göteberg, 21: 1-38.

Kuroyanagi, A. & Kawahata, H., (2004): Vertical distribution of living planktonic foraminifera in the seas around Japan. Marine Micropaleontology, 53(1-2): 173-196.

Kuroyanagi, A., Tsuchiya, M., Kawahata, H. & Kitazato, H., (2008): The occurrence of two genotypes of the planktonic foraminifer *Globigerinoides ruber* (white) and paleo-environmental implications. Marine Micropaleontology, 68: 236-243.

Kutzbach, J. E., Ruddiman, W. F., Vavrus, S. J. & Philippon, G., (2009): Climate model simulation of anthropogenic influence on greenhouse-induced climate change (early agriculture to modern): the role of ocean feedbacks. Climatic Change, doi:10.1007/s10584-009-9684-1, 31 pp.

Lacombe, H. & Tchernia, P., (1972): Caractères hydrologiques et circulation des eaux en Mediterranée. In: Stanley, J. D. (ed.), The Mediterranean Sea. Stanley Dowden, Hutchinson and Ross, Stroutsberg, 26-36.

Lalli, C. M. & Parsons, T. R., (1997): Biological Oceanography: An Introduction. Butterworth Heinemann, Oxford, 1-314.

Lane-Serff, G. F., Rohling, E. J., Bryden, H. L. & Charnock, H., (1997): Postglacial connection of the Black Sea to the Mediterranean and its relation to the timing of sapropel formation. Paleoceanography, 12(2): 169–174.

Langereis, C.G., Dekkers, M.J., Lange, G.J.d., Paterne, M., and vanSantvoort, P.J.M., (1997): Magnetostratigraphy and astronomical calibration of the last 1.1 Myr from an eastern Mediterranean piston core and dating of short events in the Brunhes: Geophysical Journal international.

Larrasoaña, J.C., Roberts, A.P., and Rohling, E.J., (2008): Magnetic susceptibility of eastern Mediterranean marine sediments as a proxy for Saharan dust supply?: Marine Geology, 254: 224-229.

Lea, D. W., Mashiotta, T. A. & Spero, H. J., (1999): Controls on magnesium and strontium uptake in planktonic foraminifera determined by live culturing. Geochimica et Cosmochimica Acta, 63: 2369-2379.

Lea, D. W., Pak, D. K. & Spero, H. J., (2000): Climate Impact of Late Quaternary Equatorial Pacific Sea Surface Temperature Variations. Science, 289: 1719-1724.

Lea, D. W., Pak, D. K. & Spero, H. J., (2003): Sea surface temperatures in the Western Equatorial Pacific during Marine Isotope Stage 11. In: Droxler, A. W., Poore, R. Z. & Burckle, L. H. (Eds.), Earth's climate and orbital eccentricity: the marine isotope stage 11 question. Geophysical Monograph 137, Washington, DC, 147-156.

Lee, S. Y. & Poulsen, C. J., (2005): Tropical Pacific climate response to obliquity forcing in the Pleistocene. Paleoceanography, 20(4): PA4010.

Lin, H. L. & Hsieh, H. Y., (2007): Seasonal variations of modern planktonic foraminifera in the South China Sea. Deep Sea Research Part II: Tropical Studies in Oceanography, 54: 1634-1644.

Lin, H. L., Wang, W. C. & Hung, G. W., (2004): Seasonal variation of planktonic foraminiferal isotopic composition from sediment traps in the South China Sea. Marine Micropaleontology, 53(3-4): 447-460.

Linares, D., González-Donoso, J. M., & Serrano, F., (1999): Paleoceanographic conditions during the Quaternary at Site 976 (Alboran Sea) and 975 (Menorca Rise) inferred from the planktonic foraminiferal assemblages: basis for a biostratigraphy. Proceedings of the Ocean Drilling Program Scientific Results, 161. College Station, Texas (Ocean Drilling Program), 44-59.

Lisiecki, L. E. & Raymo, M. E., (2005a): A Pliocene–Pleistocene stack of 57 globally distributed benthic 18O records. Paleoceanography, 20: PA1003.

Lisiecki, L. E. & Raymo, M. E., (2005b): Correction to "A Pliocene-Pleistocene stack of 57 globally distributed benthic $\delta^{18}O$ records". Paleoceanography, 20: PA2007.

Locarnini, R. A., Mishonov, A. V., Antonov, J. I., Boyer, T. P., Garcia, H. E., (2006): World Ocean Atlas 2005, Volume 1: Temperature. S. Levitus, Ed. NOAA Atlas NESDIS 61, U.S. Government Printing Office, Washington, D.C., 182 pp.

Loewemark, L., Hong, W. L., Yui, T. F. & Hung, G. W., (2005): A test of different factors influencing the isotopic signal of planktonic foraminifera in surface sediments from the northern South China Sea. Marine Micropaleontology, 55/1-2: 49-62.

Loewemark, L., Lin, Y., Chen, H.-F., Yang, T.-N., Beier, C., Werner, F., Lee, C.-Y., Song, S.-R. & Kao, S.-J., (2006): Sapropel burn-down and ichnological response to late Quaternary sapropel formation in two ~400 ky records from the eastern Mediterranean Sea. Palaeogeography, Palaeoclimatology, Palaeoecology, 239: 406-425.

Loulergue, L., Schilt, A., Spanhi, R., Masson-Delmotte, V., Blunier, T., Lemieux, B., Barnola, J.-M., Raynaud, D., Stocker, T. F. & Chappel, J., (2008): Orbital and millennial-scale features of atmospheric CH_4 over the past 800,000 years. Nature, 453: 383-386.

Lourens, L. J., (2004): Revised tuning of Ocean Drilling Program Site 964 and KC01B (Mediterranean) and implications for the D18O, tephra, calcareous nannofossil, and geomagnetic reversal chronologies of the past 1.1 Myr. Paleoceanography, 19: PA310.

Loutre, M. F., (1995): Greenland Ice Sheet over the next 5000 years. Geophysical Research Letters, 22(7): 783-786.

Loutre, M. F., (2003): Clues from MIS 11 to predict the future climate – a modelling point of view. Earth and Planetary Science Letters, 212: 213-224.

Loutre, M. F. & Berger, A., (2000): Future Climatic Changes: Are We Entering an Exceptionally Long Interglacial? Climatic Change, 46: 61-90.

Luethi, D., Le Floch, M., Bereiter, B., Blunier, T., Barnola, J.-M., Siegenthaler, U., Raynaud, D., Jouzel, J., Fischer, H., Kawamura, K. & Stocker, T. F., (2008): High-resolution carbon dioxide concentration record 650,000–800,000 years before present. Nature, 453: 379-382.

Mackensen, A., Schumacher, S., Radke, J., & Schmidt, D. N., (2000): Microhabitat preferences and stable carbon isotopes of endobenthic foraminifera: clue to quantitative reconstruction of oceanic new production? Marine Micropaleontology, 40(3): 233-258.

Malanotte-Rizzoli, P. & Hecht, A., (1988): Large-scale properties of the Eastern Mediterranean : A review. Oceanologica Acta, 11(4): 323-335.

Malanotte-Rizzoli, P., Manca, B. B., Ribera d'Alcalà, M., Theocharis, A., Bergamasco, A., Bregant, D., Budillon, G., Civitarese, G., Georgopoulos, D., Michelato, A., Sansone, E., Scarazzato, P. & Souvermezoglou, E., (1997): A synthesis of the Ionian Sea hydrography, circulation and water mass pathways during POEM-Phase I. Progress in Oceanography, 39: 153–204.

Malmgren, A. E. & Kennett, J. P., (1976): Biometric analysis of phenotypic variation in recent *Globigerina bulloides* d'Orbigny in the Southern Indian Ocean. Marine Micropaleontology, 1: 3-25.

Malmgren, B. A., Kucera, M., Nyberg, J. & Waelbroeck, C., (2001): Comparison of statistical and artificial neural networks for estimating past sea surface temperatures from planktonic foraminifer census data. Paleoceanography, 16(5): 520-530.

Malmgren, B. A. & Nordlund, U., (1997): Application of artigficial neural networks to paleoceanographic data. Palaeogeography Palaeoclimatology Palaeoecology, 136: 359-373.

Marino, G., Rohling, E.J., Sangiorgi, F., Hayes, A., Casford, J.L., Lotter, A.F., Kucera, M., and Brinkhuis, H., (2009): Early and middle Holocene in the Aegean Sea: interplay between high and low latitude climate variability: Quaternary Science Reviews, 28: 3246-3262.

Marlowe, I. T., Brassell, S. C., Eglinton, G. & Green, J. C., (1990): Long-chain alkenones and alkyl alkenoates and the fossil coccolith record of marine sediments. Chemical Geology, 88(3-4): 349-375.

Marlowe, I. T., Green, J. C., Neal, A. C., Brassell, S. C., Eglinton, G. & Course, P. A., (1984): Long-chain (N-C37-C39) alkenones in the prymnesiophyceae - Distribution of alkenones and other lipids and their taxonomic significance. British phycological journal, 19(3): 203-216.

Martrat B., Grimalt, J. O., Shackleton, N. J., de Abreu, L., Hutterli, M. A. & Stocker, T. F., (2007): Four climate cycles of recurring deep and surface water destabilizations on the Iberian Margin. Science, 317: 502–507.

Masson-Delmotte, V., Dreyfus, G., Braconnot, P., Johnsen, S., Jouzel, J., Kageyamal, M., Landais, A., Loutre, M. F., Nouet, J., Parrenin, F., Raynaud, B., Stenni, B. & Tuenter, E., (2006): Past temperature reconstructions from deep ice cores: relevance for future climate change. Climate of the Past, 2(2): 145-165.

McCrea, J. M., (1950): On the isotopic chemistry of carbonates and a paleotemperature scale. The Journal of Chemical Physics, 18: 849-857.

McManus, J. F., Oppo, D. W. & Cullen, J. L., (1999): A 0.5-million-year record of millennial-scale climate variability in the North Atlantic. Science, 283: 971-975.

McManus, J., Oppo, D., Cullen, J. & Healey, S., (2003): Marine Isotope Stage 11 (MIS 11): Analog for Holocene and Future Climate? In: Droxler, A. W., Poore, R. Z. & Burckle, L. H. (Eds.), Earth's climate and orbital eccentricity: the marine isotope stage 11 question. Geophysical Monograph 137, Washington, DC, 147-156.

MEDAR Group, 2002 - MEDATLAS/2002 database. Mediterranean and Black Sea database of temperature salinity and bio-chemical parameters. Climatological Atlas. IFREMER Edition (4 CDroms).

Menzel, D., Hopmans, E. C., Schouten, S. & Sinnighe Damsté, J. S., (2006): Membrane tetraether lipids of planktonic Crenarchaeota in Pliocene sapropels of the eastern Mediterranean Sea. Palaeogeography, Palaeoclimatology, Palaeoecology, 239: 1-15.

Mercone, D., Thomson, J., Abu-Zied, R.H., Croudace, I.W., and Rohling, E.J., (2001): High-resolution geochemical and micropalaeontological profiling of the most recent eastern Mediterranean sapropel: Marine Geology, 177: 25-44.

Milankovitch, M., (1941): Kanon der Erdbestrahlung und seine Anwendung auf das Eiszeitenproblem. Académie royale serbe. Éditions speziales, 133(XX): 633.

Milker, Y., Schmiedl, G., Betzler, C., Romer, M., Jaramillo-Vogel, D. & Siccha, M., (2009): Distribution of recent benthic foraminifera in shelf carbonate environments of the Western Mediterranean Sea. Marine Micropaleontology, 73(3-4): 207-225.

Millot, C. & Taupier-Letage, I., (2005): Circulation in the Mediterranean Sea. The Handbook of Environmental Chemistry, Volume K (The Natural Environment and the Biological Cycles) Springer-Verlag, 29-66.

Monnin, E., Indermuehle, A., Daellenbach, A., Flueckiger, J., Stauffer, B., Stocker, T. F., Raynaud, D. & Barnola, J.-M., (2001): Atmospheric CO2 Concentrations over the Last Glacial Termination. Science, 291: 112-114.

Mudie, P. J., Harland, R., Matthiessen, J. & De Vernal, A., (2001): Marine dinoflagellate cycsts and high latitude Quaternary paleoenvironmental reconstructions: an introduction. Journal of Quaternary Science, 16: 595-602.

Mueller, P. J., Kirst, G., Ruhland, G., von Storch, I., & Rossell-Mele, A., (1998): Calibration of the alkenone paleotemperature index Uk´37 based on core-tops from the eastern South Atlantic and the global ocean (60°N-60°S). Geochimica et Cosmochimica Acta, 62: 1757-1772.

Mullineaux, L. S. & Lohmann, G. P., (1981): Late Quaternary stagnations and recirculation of the Eastern Mediterranean changes in the deep water recorded by fossil benthic foraminifera. Journal of Foraminiferal Research, 11(1): 20-39.

Negri, A., Capotondi, L. & Keller, J., (1999): Calcareous nannofossils, planktonic foraminifera and oxygen isotopes in the late Quaternary sapropels of the Ionian Sea. Marine Geology, 157(1-2): 89-103.

Negri, A., Ferretti, A., Wagner, T. & Meyers, P. A., (2009): Organic-carbon-rich sediments through the Phanerozoic: Processes, progress and perspectives. Palaeogeography, Palaeoclimatology, Palaeoecology, 273: 213-217.

Negri, A. & Giunta, S., (2001): Calcareous nannofossil paleoecology in the sapropel S1 of the Eastern Ionian sea: paleoceanographic implications. Palaeogeography, Palaeoclimatology, Palaeoecology, 169: 101-112.

Nier, A. O., (1947): A mass spectrometer for isotope and gas analysis. Review of Scientific Instruments, 18: 398-411.

Nolet, G. J. & Corliss, B. H., (1990): Marine benthic foraminiferal evidence for reduced deep-water circulation during sapropel deposition in the Eastern Mediterranean. Geology, 94(1-2): 109-130.

Oba, T. & Banakar, V. K., (2007): Comparison of interglacial warm events since the Marine Isotope Stage 11. The Quaternary Research, 46(3): 223-234.

Olausson, E., (1960): Descriptions of sediment from the Mediterranean and Red Sea. Reports of the Swedish Deep Sea Expedition 1946-47, 8(5): 287-334.

Olausson, E., (1961): Studies in deep sea cores. Deep Sea Expedition 1947-48, 8: 337-391.

Ortlieb, L., Guzmán, N. & Marquardt, C., (2003): A longer-lasting Interglacial episode during Isotopic Stage 11: marine terrace evidence in tropical Western Americas. In: Droxler, A. W., Poore, R. Z. & Burckle, L. H. (Eds.), Earth's climate and orbital eccentricity: the marine isotope stage 11 question. Geophysical Monograph 137, Washington, DC, 147-156.

Osborne, A. H., Marino, G., Vance, D. & Rohling, E. J., (2010): Eastern Mediterranean surface water Nd during Eemian sapropel S5: monitoring northerly (mid-latitude) versus southerly (sub-tropical) freshwater contributions. Quaternary Science Reviews, 29: 2473-2483.

Parker, F. L., (1962): Planktonic foraminiferal species in Pacific sediments. Micropaleontology, 8/2: 219-254.

Pearson, P. N., (1998): Stable isotopes and the study of evolution in planktonic foraminifera. Paleontological Society Papers, 4: 138-178.

Perez-Folgado, M., Sierro, F. J., Flores, J. A., Cacho, I., Grimalt, J. O., Zahn, R. & Shackleton, N., (2003): Western Mediterranean planktonic foraminifera events and millennial climatic variability during the last 70 kyr. Marine Micropaleontology, 48: 49-70.

Petit, J. R., Jouzel, J., Raynaud, D., Barkov, N. I., Barnola, J.-M., Basile, I., Bender, M., Chappellaz, J., Davis, M., Delaygue, G., Delmotte, M., Kotlyakov, V. M., Legrand, M., Lipenkov, V. Y., Lorius, C., Pépin, L., Ritz, C., Saltzman, E. & Stievenard, M., (1999): Climate and atmospheric history of the past 420,000 years from the Vostok ice core, Antarctica. Nature, 399: 429-436.

Pettersson, H., (1946): Oceanographic work in the Mediterranean. The Geographical Journal, 107: 163-166.

Pettersson, H., (1947): The Swedish deep-sea expedition. The Geographical Journal, 110: 145-148.

Pflaumann, U., Duprat, J., Pujolö, C. & Labeyrie, L., (1996): SIMMAX: a modern analog technique to deduce Atlantic sea surface temperatures from planktonic foraminifera in deep-sea sediments. Paleoceanography, 11(1): 15-35.

Pinardi, N. & Masetti, E., (2000): Variability of the large scale general circulation of the Mediterranean Sea from observations and modelling: a review. Palaeogeography Palaeoclimatology Palaeoecology, 158(3-4): 153-174.

POEM Group, (1992): General circulation of the Eastern Mediterranean. Earth-Science Reviews, 32: 285–309.

Poore, R. Z., Osterman, L., Curry, W. B. & Phillips, R. L., (1999): Late Pleistocene and Holocene meltwater events in the western Arctic Ocean. Geology, 27(8): 759-762.

Potonié, H. & Koerber, F., (1904): Naturwissenschaftliche Wochenschrift. Volume III Jena, Gustav Fischer 1904, 1040 pp.

Prahl, F. G. & Wakeham S. G., (1987): Calibration of unsaturation patterns in long-chain ketone compositions for paleotemperature assessment. Nature, 330: 367–369.

Principato, M., Crudeli, D., Ziveri, P., Slomp, C. P., Coselli, C., Erba, E. & de Lange, G. J., (2006): Phyto- and Zooplankton paleofluxes during the deposition of sapropel S1 (Eastern Mediterranean): biogenic carbonate preservation and paleoecological implications. Palaeogeoraphy, Palaeoclimatology, Palaeoecology, 235: 8-27.

Prokopenko, A.A., Williams, D.F., Kuzmin, M.I., Karabanov, E.B., Khursevich, G.K. & Peck, J.A., (2002): Muted climate variations in the continental Siberia during the mid-Pleistocene epoch. Nature, 418, 65-68.

Prokopenko, A.A., Bezrukova, E. V., Khursevich, G. K., Solotchina, E. P., Kuzmin, M. I. & Tarasov, P. E., (2010): Climate in continental interior Asia during the longest interglacial of the past 500 000 years: the new MIS 11 records from Lake Baikal, SE Siberia. Climate of the Past, 6: 31-48.

Ravelo, A. C. & Hillaire-Marcel, C., (2007): The use of oxygen and carbon isotopes of foraminifera in paleoceanography. In: Hillaire-Marcel and de Vernal, (Eds.), Developments in Marine Geology, Volume 1, Proxies in late Cenozoic Paleoceanography. Elsevier, 735–764.

Raynaud, D., Loutre, M. F., Ritz, C., Chappellaz, J., Barnola, J.-M., Jouzel, J., Lipenkov, V. Y., Petit, J.-R. & Vimeux, F., (2003): Marine Isotope Stage (MIS) 11 in the Vostok Ice Core: CO2 forcing and stability of East Antarctica. In: Droxler, A. W., Poore, R. Z. & Burckle, L. H. (Eds.), Earth's climate and orbital eccentricity: the marine isotope stage 11 question. Geophysical Monograph 137, Washington, DC, 27-40.

Raynaud, D., Barnola, J.-M., Souchez, R., Lorrain, R., Petit, J.-R., Duval, P. & Lipenkov, V. Y., (2005): Palaeoclimatology: The record for marine isotopic stage 11. Nature, 436: 39-40.

Reille, M., de Beaulieu, J.-L., Svobodova, H., Andrieu-Ponel, V. & Goeury, C., (2000): Pollen analytical biostratigraphy of the last five climatic cycles from a long continental

sequence from the Velay region (Massif Central, France). Journal of Quaternary Science, 15(7): 665-685.

Robertson, A. H. F., (1998): Mesozoic-Tertiary tectonic evolution of the easternmost Mediterranean area: integration of marine and land evidence. In: Robertson, A. H. F., Emeis, K.-C., Richter, C. & Camerlenghi, A. (Eds.), Proc. ODP Scientific Results, 160: 723-782.

Robbins, L. L. & Healy-Williams, N., (1991): Toward a classification of planktonic-foraminifera based on biochemical, geochemical, and morphological criteria. Journal of Foraminiferal Research, 21(2): 159-167.

Rohling, E. J., (1994): Review and new aspects concerning the formation of eastern Mediterranean sapropels. Marine Geology, 122: 1-28.

Rohling, E. J., (2001): The dark secret of the Mediterranean - a case history in past environmental reconstruction. http://www.soes.soton.ac.uk/staff/ejr/DarkMed/dark-title.html

Rohling, E. J., Braun, K., Grant, K., Kucera, M., Roberts, A. P., Siddall, M., & Trommer, G., (2010): Comparison between Holocene and Marine Isotope Stage-11 sea-level histories. Earth and Planetary Science Letters, 291: 97-105.

Rohling, E. J., den Dulk, M., Pujol, C. & Vergnaud-Grazzini, C., (1995): Abrupt hydrographic changes in the Alboran Sea (Western Mediterranean) around 8000 yrs BP. Deep-Sea Research, 42: 1609-1619.

Rohling, E. J. & Gieskes, W. W. C., (1989): Late Quaternary changes in Mediterranean intermediate water density and formation rate. Paleoceanography, 4: 531-545.

Rohling, E. J., Grant, K., Bolshaw, M., Roberts, A. P., Siddall, M., Hemleben, Ch., & Kucera, M., (2009): Antarctic temperature and global sea level closely coupled over the past five glacial cycles. Nature Geoscience, 2: 500-504.

Rohling, E. J., Grant, K., Hemleben, C., Siddall, M., Hoogakker, B. A. A., Bolshaw, M. & Kucera, M., (2007): High rates of sea-level rise during the last interglacial period. Nature, 1: 38-42.

Rohling, E. J., & Hilgen, F. J., (1991): The eastern Mediterranean climate at times of sapropel formation: a review. Geologie en Mijnbouw, 70: 253-264.

Rohling, E. J., Jorissen, F. J., Vergnaud-Grazzini, C. & Zachariasse, W. J., (1993): Northern Levantine and Adriatic Quaternary planktic foraminifera; reconstruction of paleoenvironmental gradients. Marine Micropaleontology, 21: 191-218.

Rohling, E. J., Mayewski, P. A., Abu-Zied, R. H., Casford, J. S. L. & Hayes, A., (2002): Holocene atmosphere-ocean interactions: records from Greenland and the Aegean Sea. Climate Dynamics, 18: 587–593.

Rohling, E. J., Sprovieri, M., Cane, T., Casford, J. S. L., Cooke, S., Bouloubassi, I., Emeis, K.-C., Schiebel, R., Rogerson, M., Hayes, A., Jorissen, F. J. & Kroon, D., (2004): Reconstructing past planktic foraminiferal habitats using stable isotope data: a case history for Mediterranean sapropel S5. Marine Micropaleontology, 50: 89–123.

Rosell-Melé, A., Maslin, M. A., Maxwell, J. R. & Schaeffer, P., (1997): Biomarker evidence for ‘‘Heinrich’’ events. Geochimica et Cosmochimica Acta, 61: 1671–1678.

Rossignol-Strick, M., (1983): African monsoons, an immediate climate response to orbital insolation. Nature, 30: 446-449.

Rossignol-Strick, M., (1985): Mediterranean Quaternary sapropels, an immediate response of the African monsoon to variation of insolation. Palaeogeography, Palaeoclimatology, Palaeoecology, 49: 237-263.

Rossignol-Strick, M., Nesteroj, W., Olive, P., Vergnaud-Grazzini, C., (1982): After the deluge: Mediterranean stagnation and sapropel formation. Nature, 295: 105-110.

Rossignol-Strick, M. & Paterne, M., (1999): A synthetic pollen record of the eastern Mediterranean sapropels of the last 1 Ma: implications for time-scale and formation of sapropels. Marine Geology, 153(1999): 221-237.

Rousseau, D.-D., (2003): The continental record of Stage 11: a review. In: Droxler, A. W., Poore, R. Z., Burckle, L. H. (Eds.), Earth’s climate and orbital eccentricity: the marine isotope stage 11 question. Geophysical Monograph 137, Washington, DC, 213-222.

Ruddiman, W. F., (2003): The anthropocene greenhouse era began thousands of years ago. Climatic Change, 61: 261-293.

Ruddiman, W. F., (2005): Cold climate during the closest Stage 11 analog to recent millennia. Quaternary Science Reviews, 24: 1111–1121.

Ruddiman, W. F., (2006a): Cold climate during the closest Stage 11 analog to recent millennia. Quaternary Science Reviews, 24(10-11): 1111-1121.

Ruddiman, W. F., (2006b): Ice-driven CO2 feedback on ice volume. Climate of the Past, 2(1): 43-55.

Ruddiman, W. F., (2006c): On “The Holocene CO2 rise: anthropogenicor natural”. Eos Transactions of the American Geophysical Union, 87(35): 352-353.

Ruddiman, W. F., (2007): The early anthropogenic hypothesis: Challenges and responses. Reviews of Geophysics, 45(3): RG4001.

Ruddiman, W. F., (2008): The challenge of modelling interglacial CO2 and CH4 trends. Quaternary Science Reviews, 27(5-6): 445-448.

Ruddiman, W. F., Vavrus, S. J. & Kutzbach, J. E., (2005a): A test of the overdue-glaciation hypothesis. Quaternary Science Reviews, 24(1-2): 1-10.

Rutten, A., de Lange, G. D., Ziveri, P., Thomson, J., van Santvoort, P. J. M. & Corselli, C., (2000): Recent terrestrial and carbonate fluxes in the pelagic eastern Mediterranean; a comparison between sediment trap and surface sediment. Palaeogeoraphy, Palaeoclimatology, Palaeoecology, 158: 197-213.

Sadekov, A., Eggins, S. M., De Deckker, P. & Kroon, D., (2008): Uncertainties in seawater thermometry deriving from intratest and intertest Mg/Ca variability in *Globigerinoides ruber*. Paleoceanography, 23: PA1215.

Saito, T., Thompson, P. R. & Breger, D., (1981): Systematic index of recent and Pleistocene planktonic foraminifera. University of Tokio Press, 190 pp.

Saji, N. H. & Yamagata, T., (2003): Indian ocean dipole mode events and African rainfall variability. CLIVAR Exchanges, 27: 1–4.

Sakamoto, T., Janecek, T. & Emeis, K.-C., (1998): Continuous sedimentary sequences from the eastern Mediterranean Sea: composite depth sections. In: Robertson, A.H.F., Emeis, K.-C., Richter, C., Camerlenghi, A. (Eds.), Proceedings of the Ocean Drilling Program, Scientific Results, 160. College Station, TX (Ocean Drilling Program), 37-51.

Sarmiento, J. L. & Le Quéré, C., (1996): Oceanic carbon dioxide uptake in a model of century-scale global warming. Science, 274: 1346-1350.

Sbaffi, L., Wezel, F. C., Kallel, N., Paterne, M., Cacho, I., Ziveri, P. & Shackleton, N., (2001): Response of the pelagic environment to Palaeoclimatic changes in the central Mediterranean Sea during the Late Quaternary. Marine Geology, 178: 39-62.

Schattner, U., & Ben-Avraham, Z., (2007): Transform margin of the northern Levant, eastern Mediterranean: From formation to reactivation. Tectonics, 26: TC5020.

Scherer, R. P., (2003): Quaternary Interglacials and the West Antarctic ice sheet. In: Droxler, A. W., Poore, R. Z. & Burckle, L. H. (Eds.), Earth's climate and orbital eccentricity: the marine isotope stage 11 question. Geophysical Monograph 137, Washington, DC, 103-112.

Scherer, R. P., Aldahan, A., Tulaczyk, S., Possnert, G., Engelhardt, H. & Kamb, B., (1998): Pleistocene collapse of the West Antarctic ice sheet. Science, 281: 82-85.

Schilman, B., Almogi-Labin, A. & Bar-Matthews, M., (2003): Late Holocene productivity and hydrographic variability in the eastern Mediterranean inferred from benthic foraminiferal stable isotopes. Paleoceanography, 18(3): 1064.

Schmiedl, G., Kuhnt, T., Ehrmann, W., Emeis, K.-C., Hamann, Y., Kotthoff, U., Dulski, P & Pross, J., (2010, in press): Climatic forcing of eastern Mediterranean deep-water formation and benthic ecosystems during the past 20000 years. Quaternary Science Reviews, (2010).

Schmiedl, G., Mitschele, A., Beck, S., Emeis, K.-C., Hemleben, C., Schulz, H., Sperling, M. & Weldeab, S., (2003): Benthic foraminiferal record of ecosystem variability in the eastern Mediterranean Sea during times of sapropel S5 and S6 formation. Palaeogeography, Palaeoclimatology, Palaeoecology, 190: 139-164.

Schmiedl, G., Pfeilsticker, M., Hemleben, C. & Mackensen, A., (2004): Environmental and biological effects on the stable isotope composition of recent deep-sea benthic foraminifera, from the western Mediterranean Sea. Marine Micropaleontology, 51(1-2): 129-152.

Schoenfeld, J, & Numberger, L., (2007): The benthic foraminiferal response to the 2004 spring bloom in the western Baltic Sea. Marine Micropaleontology, 65(1-2): 78-95.

Schouten, S., Hopmans, E. C., Schefuß, E. & Sinnighe Damsté, J. S., (2002): Distributional variations in marine crenarchaeotal membrane lipids: A new tool for reconstructing ancient sea water temperatures? Earth and Planetary Science Letters, 204: 265-274.

Sgarrella, F. & Moncharmont Zei, M., (1993): Benthic foraminifera of the Gulf of Naples, Italy: Systematics and autoecology. Bolletino della Società Paleontologica Italiana, 32: 145-264.

Shackleton, N. J., (1967): Oxygen isotope analyses and Pleistocene temperatures re-assessed. Nature, 215(5096): 15-17.

Shackleton, N. J., & Opdyke, N. D., (1973): Oxygen isotope and palaeomagnetic stratigraphy of equatorial Pacific core V28-238: Oxygen isotope temperatures and ice volumes on a 105 and 10 year scale. Quaternary Research, 3: 39-55.

Siegenthaler, U., Stocker, T. F., Monnin, E., Luethi, D., Schwander, J.; Stauffer, B., Raynaud, D., Barnola, J.-M., Fischer, H., Masson-Delmotte, V. & Jouzel, J., (2005): Stable Carbon Cycle–Climate Relationship during the Late Pleistocene. Science, 310: 1313-1317.

Sperling, M., Schmiedl, G., Hemleben, C, Emeis, K.-C., Erlenkeuser, H. & Grootes, P. M., (2003): Black Sea impact on the formation of eastern Mediterranean sapropel S1? Evidence from the Marmara Sea. Palaeogeography, Palaeoclimatology, Palaeoecology, 190(SI): 9-21.

Sprovieri, R., Di Stefano, E., Howell, M., Sakamoto, T., Di Stefano, A. & Marino, M., (1998): Integrated calcareous plankton biostratigraphy and cyclostratigraphy at Site 964. In: Robertson, A. H. F., Emeis, K.-C., Richter, C., Camerlenghi, A. (Eds.), Proceedings of the Ocean Drilling Program, Scientific Results, 160. College Station, TX (Ocean Drilling Program), 155-165.

Stein, R., Hefter, J., Gruetzner, J., Voelker, A. Naafs, B. D. A., (2009): Variability of surface water characteristics and Heinrich-like events in the Pleistocene midlatitude North Atlantic Ocean: Biomarker and XRD records from IODP Site U1313 (MIS 16-9). Paleoceanography, 24: PA2203.

Steinke, S., Chiu, H. Y., Yu, P. S., Shen, C. C., Loewemark, L., Mii, H. S. & Chen, M. T., (2005): Mg/Ca ratios of two *Globigerinoides ruber* (white) morphotypes: Implications for reconstructing past tropical/subtropical surface water conditions. Geochemistry, Geophysics, Geosystems, 6: Q11005.

Stuut, J. B., Smalley, I. & O'Hara-Dhand, K., (2009): Aeolian dust in Europe: African sources and Europena deposits. Quaternary International, 198: 234-245.

Tang, C. M. & Stott, L. D., (1993): Seasonal salinity changes during Mediterranean sapropel deposition 9,000 years B.P. Evidence from isotopic analyses of individual planktonic foraminifera. Paleoceanography, 8: 473-494.

Theocharis, A., Balopoulos, E., Kioroglou, S., Kontoyiannis, H. & Iona, A., (1999): A synthesis of the circulation and hydrography of the South Aegean Sea and the Straits of the Cretan Arc. Progress in Oceanography, 44(4): 469-509.

Thiede, J., (1978): A glacial Mediterranean. Nature, 276: 680-683.

Thomson, J., Croudace, I.W., and Rothwell, R., (2006): A geochemical application of the ITRAX scanner to a sediment core containing eastern Mediterranean sapropel units: New Techniques in Sediment Core Analysis. Geological Society, London.

Thomson, J., Higgs, N.C., Wilson, T.R.S., Croudace, I.W., Lange, G.J.D., and Santvoort, P.J.M.V., (1995): Redistribution and geochemical behaviour of redox-sensitive elements around S1, the most recent eastern Mediterranean sapropel: Geochimica et Cosmochimica Acta, v. 59, p. 3487-3501.

Thunell, R. C., (1978): Distribution of recent planktonic foraminifera in surface sediments of the Mediterranean Sea. Marine Micropaleontology, 3: 147-173.

Thunell, R. C., (1979): Eastern Mediterranean Sea during the last glacial maximum; an 18,000-years B.P. reconstruction. Quaternary Research, 11: 353-372.

Thunell, R., Tappa, E., Pride, C. & Kincaid, E., (1999): Sea-surface temperature anomalies associated with the 1997-1998 El Nino recorded in the oxygen isotope composition of planktonic foraminifera. Geology, 27 (9): 843-846.

Thunell, R. C., Williams, D. F. & Cita, M. B., (1983): Glacial anoxia in the eastern Mediterranean. Journal of Foraminiferal Research, 13: 283-290.

Thunell, R.C., Williams, D.F., and Kennett, J.P., (1977): Late Quaternary paleoclimatology, stratigraphy and sapropel history in eastern Mediterranean deep-sea sediments: Marine Micropaleontology, v. 2, p. 371-388.

Todd, R., (1958): Foraminifera from western deep-sea cores. Report of the Swedish Deep Sea Expedition, 1946-47, 8: 167-215.

Triantaphyllou, M. V., Antonarakou, A., Dimiza, M. & Anagnostou, C., (2010): Calcareous nannofossil and planktonic foraminiferal distributional patterns during deposition of sapropels S6, S5 and S1 in the Libyan Sea (Eastern Mediterranean). Geo-marine letters, 30(1): 1-13.

Triantaphyllou, M. V., Koukousioura, O. & Dimiza, M. D., (2009): The presence of the Indo-Pacific symbiont-bearing foraminifer Amphistegina lobifera in Greek coastal ecosystems (Aegean Sea, Eastern Mediterranean). Mediterranean marine science, 10(2): 73-85.

Tzedakis, P. C., (2009): The MIS 11–MIS 1 analogy, southern European vegetation, atmospheric methane and the "early anthropogenic hypothesis". Climate of the Past Discussion, 5: 1337–1365.

Tzedakis, P. C., McManus, P. C., Hooghiemstra, H., Oppo, D. W. & Wijmstra, T. A., (2003): Comparison of changes in vegetation in northeast Greece with records of climate variability on orbital and suborbital frequencies over the last 450,000 years. Earth and Planetary Science Letters, 212: 197–212.

Tzedakis, P. C., Hooghiemstra, H. & Pälike, H., (2006): The last 1.35 million years at Tenaghi Philippon: revised chronostratigraphy and long-term vegetation trends. Quaternary Science Reviews, 25: 3416–3430.

Tzedakis, P. C., Pälike, H., Roucoux, K. H. & de Abreu, L., (2009): Atmospheric methane, southern European vegetation and low-mid latitude links on orbital and millennial timescales. Earth and Planetary Science Letters, 277: 307-317.

Urey, H. C., (1947): The thermodynamics of isotopic substances. Journal of the Geochemical Society, 1947: 562-581.

Urey, H. C., Lowenstam, H. A., Epstein, S. & McKinney, C. R., (1951): Measurements of paleotemperatures and temperatures of the Upper Cretaceous of England, Denmark, and the southeastern United States. Geological Society of America Bulletin, 62: 399-416.

Van den Broeck, E., (1876): Etude sur les foraminiferes de la Barbade (Antilles). Annales de la Société Belge de Microscopie, 1: 55-152.

Van der Zwaan, G. J., Duijnstee, I. A. P., den Dulk, M., Ernst, S. R., Jannink, N. T. & Kouwenhoven, T. J., (1999): Benthic foraminifers: proxies or problems? A review of paleocological concepts. Earth-Science reviews, 46(1-4): 213-236.

VanSantvoort, P.J.M., deLange, G.J., Langereis, C.G., Dekkers, M.J., and Paterne, M., (1997): Geochemical and paleomagnetic evidence for the occurrence of "missing" sapropels in eastern Mediterranean sediments: Paleoceanography, 12, p. 773-786.

Vergnaud-Grazzini, C., Ryan, W. B. F. & Cita, M. B., (1977): Stable isotopic fractionation, climate change and episodic stagnation in the Eastern Mediterranean during the Late Quaternary. Marine Micropaleontology, 2: 353–370.

Vidal, L., Ménot, G., Joly, C., Bruneton, H., Rostek, F., Cagatay, M. N., Major, C. & Bard, E., (2010): Hydrology in the Sea of Marmara during the last 23 ka: Implications for timing of Black Sea connections and sapropel deposition. Paleoceanography, 25: PA1205.

Vidic, N. J., Verosub, K. L., Singer, M. J., (2003): The Chinese loess perspective on Marine Isotope Stage 11 as an extreme Interglacial. In: Droxler, A. W., Poore, R. Z. & Burckle, L. H. (Eds.), Earth's climate and orbital eccentricity: the marine isotope stage 11 question. Geophysical Monograph 137, Washington, DC, 231-240.

Villanueva, J., Calvo, E., Pelejero, C., Grimalt, J. O., Boelaert, A., Labeyrie, L., (2001): A latitudinal productivity band in the central North Atlantic over the last 270 kyr: An alkenone perspective. Paleoceanography, 16(6): 617-626.

Villanueva, J., Grimalt, J. O., Cortijo, E., Vidal, L. & Labeyrie, L., (1997): A biomarker approach to the organic matter deposited in the North Atlantic during the last climatic cycle. Geochimica et Cosmochimica Acta, 61(21): 4633-4646.

Vinci, A., (1985): Distribution and chemical composition of tephra layers from eastern Mediterranean abyssal sediments. Marine Geology, 64: 143-155.

Waelbroeck, C., Labeyrie, L., Duplessy, J., Guiot, J., Labracherie, M., Leclaire, H. & Duprat, J., (1998): Improving past sea surface temperatures estimates based on planktonic fossil faunas. Paleoceanography, 13(3), 272-283.

Wang, L. J., (2000): Isotopic signals in two morphotypes of *Globigerinoides ruber* (white) from the South China Sea: Implications for monsoon climate change during the last glacial cycle. Palaeogeography, Palaeoclimatology, Palaeoecology, 161(3-4): 381-394.

Weaver, P. P. E., Neil, H. & Carter, L., (1997): Sea surface temperature estimates from the Southwest Pacific based on planktonic foraminifera and oxygen isotopes. Palaeogeography Palaeoclimatology Palaeoecology, 131(3-4): 241-256.

Wehausen, R., and H.-J. Brumsack, (1998): The formation of Pliocene Mediterranean sapropels: constraints from high-resolution major and minor element studies. Proc. ODP Sci. Res., 160: 207-218.

Weldeab, S., Lea, D. W., Schneider, R. R. & Andersen, N., (2007): 155,000 years of West African monsoon and ocean thermal evolution. Science, 316: 1303-1307.

Widmark, J. G. V. & Speijer, R. P., (1997): Benthic foraminiferal faunas and trophic regimes at the terminal Cretaceous Tethyan seafloor. Palaios, 12: 354-371.

Winograd, I. J., Coplen, T. B., Landwehr, J. M., Riggs, A. C., Ludwig, K. R., Szabo, B. J., Kolesar, P. T., & Revesz, K. M., (1992): Continuous 500,000-Year Climate Record from Vein Calcite in Devils Hole, Nevada. Science, 258: 255-260.

Wuchter, C., Schouten, S., Coolen, M. J. L. & Sinnighe Damsté, J. S., (2004): Temperature-dependent variation in the distribution of tetraether membrane lipids of marine Crenarchaeota: Implications for TEX_{86} paleothermometry. Paleoceanography, 19: PA4028.

Wuest, G., (1961): On the vertical circulation of the Mediterranean Sea. Journal of Geophysical Research, 66: 3261–3271.

Zanchetta, G., Borghini, A., Fallick, A. E., Bonadonna, F. P. & Leone, G., (2007): Late Quaternary palaeohydrology of Lake Pergusa (Sicily, southern Italy) as inferred by stable isotopes of lacustrine carbonates. Journal of Paleolimnology, 38(2): 227-239.

Ziegler, M., Tuenter, E. & Lourens, L. J., (2010): The precession phase of the boreal summer monsoon as viewed from the eastern Mediterranean (ODP Site 968). Quaternary Science Reviews, 29: 1481-1490.

B. Appendix

GeoTü-SL96, Holocene, planktonic foraminifera counts, ANN results

Core	cm	age	Sample weight (g)	PF/g	Split	sum split (PF)	entire sum (PF)	ANN annual	ANN summer	ANN winter
GeoTüSL96Holo	0.5	0.00	0.44	5509	8	303	2424	20.25	24.80	16.06
GeoTüSL96Holo	1.5	0.88	0.458	5520	8	316	2528	20.19	25.11	15.96
GeoTüSL96Holo	2.5	1.75	0.249	24867	16	387	6192	20.73	25.20	16.15
GeoTüSL96Holo	3.5	2.63	0.201	12736	8	320	2560	20.29	25.84	15.60
GeoTüSL96Holo	4.5	3.50	0.216	11111	8	300	2400	21.07	25.90	16.60
GeoTüSL96Holo	5.5	4.38	0.322	7950	8	320	2560	20.42	25.64	15.95
GeoTüSL96Holo	6.5	5.25	0.253	11130	8	352	2816	21.25	25.79	16.80
GeoTüSL96Holo	7.5	6.13	0.103	48621	16	313	5008	21.20	25.62	16.98
GeoTüSL96Holo	8.5	7.00	0.131	56916	16	466	7456	21.32	26.15	16.99
GeoTüSL96Holo	9.5	7.70	0.405	20188	16	511	8176	20.44	25.80	15.91
GeoTüSL96Holo	10.5	8.30	0.308	16364	16	315	5040	20.95	26.24	16.06
GeoTüSL96Holo	11.5	8.90	0.306	16314	16	312	4992	20.48	25.05	16.27
GeoTüSL96Holo	12.5	9.50	0.474	7646	8	453	3624	20.20	24.48	15.87
GeoTüSL96Holo	13.5	9.90	0.192	13625	8	327	2616	19.99	24.67	15.91
GeoTüSL96Holo	14.5	10.30	0.176	30273	16	333	5328	19.61	24.28	15.52
GeoTüSL96Holo	15.5	10.70	0.209	30852	16	403	6448	19.72	24.63	15.50
GeoTüSL96Holo	16.5	11.10	0.249	20434	16	318	5088	19.77	24.34	15.78
GeoTüSL96Holo	17.5	11.50	0.205	24351	16	312	4992	19.41	24.29	15.37
GeoTüSL96Holo	18.5	11.90	0.278	19511	16	339	5424	19.25	24.17	15.39
GeoTüSL96Holo	19.5	12.30	0.226	45876	32	324	10368	19.08	24.02	15.29
GeoTüSL96Holo	20.5	12.70	0.616	8494	16	327	5232	19.56	24.60	15.43
GeoTüSL96Holo	21.5	13.10	0.448	11857	16	332	5312	19.56	24.69	15.16
GeoTüSL96Holo	22.5	13.50	0.332	15373	16	319	5104	19.75	24.84	15.45
GeoTüSL96Holo	23.5	13.90	0.344	14744	16	317	5072	19.66	24.72	15.35
GeoTüSL96Holo	24.5	14.30	0.368	13957	16	321	5136	19.36	24.52	15.26
GeoTüSL96Holo	25.5	14.70	0.372	12989	16	302	4832	19.16	24.13	15.42
GeoTüSL96Holo	26.5	15.10	0.324	8617	8	349	2792	19.00	23.83	15.18
GeoTüSL96Holo	27.5	15.50	0.308	16156	16	311	4976	19.79	24.36	16.52
GeoTüSL96Holo	28.5	15.90	0.297	17239	16	320	5120	19.54	24.08	15.84
GeoTüSL96Holo	29.5	16.30	0.43	7795	8	419	3352	19.27	24.01	15.96
GeoTüSL96Holo	30.5	16.70	0.348	10046	8	437	3496	19.47	24.25	16.14
GeoTüSL96Holo	31.5	17.10	0.472	7102	8	419	3352	19.85	24.91	16.87

GeoTü-SL96, Holocene, planktonic foraminifera counts

Core	cm	age	Orbulina universa	Globigerinoides conglobatus	Globigerinoides ruber total	Globoturborotalita tenella	Globigerinoides sacc total	Sphaeroidinella dehiscens	siphonifera & calida	Globigerina bulloides	Globigerina falconensis	Beela digitata	Globoturborotalita rubescens	Turborotalita quinqueloba	Neogloboquadrina pachyderma L	Neogloboquadrina dutertrei	P/D integrade & N. pachyderma R	Pulleniatina obliquiloculata	Globorotalia inflata	Globorotalia truncatulinoides total	Globorotalia crassaformis	Globorotalia hirsuta	Globorotalia scitula	Globorotalia menardii & tumida	Globigerinita glutinata
GeoTüSL96Holo	0.5	0.00	13	0	232	1	16	0	6	29	4	0	0	0	2	1	21	0	3	0	0	0	0	0	1
GeoTüSL96Holo	1.5	0.88	12	0	189	2	21	0	9	20	7	4	2	0	5	0	15	0	6	1	0	0	0	0	10
GeoTüSL96Holo	2.5	1.75	9	0	214	1	31	0	6	23	0	1	0	0	9	1	9	0	1	1	0	0	0	0	9
GeoTüSL96Holo	3.5	2.63	22	0	261	2	21	0	14	17	2	15	1	0	2	1	17	0	2	1	0	0	0	0	9
GeoTüSL96Holo	4.5	3.50	9	0	202	1	46	0	13	10	2	6	1	0	3	0	15	0	5	2	0	0	0	0	5
GeoTüSL96Holo	5.5	4.38	9	0	185	0	31	0	11	14	2	10	1	0	0	0	22	0	7	0	0	0	0	0	8
GeoTüSL96Holo	6.5	5.25	8	0	180	2	55	0	11	35	0	4	0	0	1	0	5	0	6	0	0	0	0	0	13
GeoTüSL96Holo	7.5	6.13	9	0	191	1	63	0	11	42	3	3	1	0	0	0	5	0	16	0	0	0	0	0	7
GeoTüSL96Holo	8.5	7.00	28	0	148	0	41	0	35	34	0	0	4	0	0	2	3	0	9	0	0	0	0	0	9
GeoTüSL96Holo	9.5	7.70	53	0	211	1	26	0	45	48	0	2	4	1	0	0	3	0	1	0	0	0	0	0	71
GeoTüSL96Holo	10.5	8.30	80	0	312	4	18	0	22	32	0	2	4	0	0	0	2	0	0	0	0	0	0	0	35
GeoTüSL96Holo	11.5	8.90	7	0	255	0	11	0	9	11	4	0	0	0	0	0	2	0	1	0	0	0	0	0	15
GeoTüSL96Holo	12.5	9.50	3	0	185	0	28	0	4	17	1	0	1	0	0	0	6	0	12	3	0	0	0	0	52
GeoTüSL96Holo	13.5	9.90	7	0	261	3	27	0	5	42	5	0	2	0	1	4	16	0	27	10	0	0	3	0	40
GeoTüSL96Holo	14.5	10.30	2	0	192	4	11	0	1	40	3	2	3	1	0	0	28	0	19	2	0	0	1	0	18
GeoTüSL96Holo	15.5	10.70	4	0	186	6	11	0	2	50	1	1	1	2	0	1	9	0	17	13	0	0	4	0	25
GeoTüSL96Holo	16.5	11.10	3	1	223	2	10	0	0	48	0	0	0	2	0	3	21	0	46	13	0	0	4	0	27
GeoTüSL96Holo	17.5	11.50	6	0	191	1	2	0	0	26	1	0	0	1	1	8	31	0	34	8	0	0	2	0	6
GeoTüSL96Holo	18.5	11.90	4	0	149	2	8	0	0	44	2	0	0	1	2	9	28	0	38	14	0	0	5	0	6
GeoTüSL96Holo	19.5	12.30	5	0	153	4	4	0	3	61	4	0	0	1	0	1	39	0	23	17	0	0	10	0	14
GeoTüSL96Holo	20.5	12.70	5	0	172	4	10	0	3	42	1	0	0	1	0	4	23	0	25	22	0	0	3	0	9
GeoTüSL96Holo	21.5	13.10	8	0	194	0	6	0	2	19	0	0	0	0	0	0	22	0	42	29	0	0	0	0	5
GeoTüSL96Holo	22.5	13.50	6	0	224	3	3	0	0	20	1	0	0	3	0	0	21	0	18	25	0	0	5	0	3
GeoTüSL96Holo	23.5	13.90	9	0	188	0	11	0	2	24	0	0	0	0	0	2	32	0	20	26	0	0	2	0	3
GeoTüSL96Holo	24.5	14.30	6	0	166	0	11	0	3	28	2	2	0	0	0	5	37	0	19	22	0	0	4	0	12
GeoTüSL96Holo	25.5	14.70	2	0	178	0	5	0	2	41	9	0	0	0	0	5	22	0	22	23	0	0	5	0	7
GeoTüSL96Holo	26.5	15.10	0	0	174	0	0	0	1	34	3	0	0	0	0	8	49	0	10	14	0	0	4	0	5
GeoTüSL96Holo	27.5	15.50	0	1	197	0	1	0	0	44	1	0	0	1	0	10	50	0	4	7	0	0	26	0	7
GeoTüSL96Holo	28.5	15.90	0	0	207	0	2	0	0	35	3	0	2	0	0	6	35	0	4	0	0	0	9	0	8
GeoTüSL96Holo	29.5	16.30	1	0	169	0	1	0	1	50	1	0	1	0	0	14	46	0	1	1	0	0	21	0	13
GeoTüSL96Holo	30.5	16.70	1	0	221	3	3	0	0	52	1	0	1	0	0	7	67	0	6	0	0	0	33	0	24
GeoTüSL96Holo	31.5	17.10	1	0	215	4	6	0	3	29	1	1	0	1	0	11	91	0	0	0	0	0	57	0	17

GeoTü-SL96, MIS 11, stable isotopes, ANN 1/4

core	cmbsf	age	δ18O *G. ruber*	δ13C *G. ruber*	δ18O *G. bulloides*	δ13C *G. bulloides*	ANN annual	ANN summer	ANN winter
Geo-TüSL96	600.5	330.29	0.83	0.42			20.37	24.81	16.47
Geo-TüSL96	605.5	330.90	1.45	0.56			19.62	24.78	15.31
Geo-TüSL96	610.5	331.51	1.13	0.87			19.99	24.88	15.61
Geo-TüSL96	615.5	332.12	0.57	0.59			20.27	25.62	15.76
Geo-TüSL96	620.5	332.73	0.92	0.73			21.07	25.44	17.05
Geo-TüSL96	625.5	333.34	0.14	-0.20			19.82	24.33	15.95
Geo-TüSL96	630.5	333.95	0.45	0.43			20.23	24.30	16.33
Geo-TüSL96	635.5	334.56	-0.38	0.19			19.22	22.83	15.45
Geo-TüSL96	640.5	335.17	0.42	-0.03			18.80	23.14	15.40
Geo-TüSL96	645.5	335.78	1.24	0.74			18.00	21.85	14.69
Geo-TüSL96	650.5	336.39	0.43	0.16			17.80	21.09	14.75
Geo-TüSL96	655.5	337.00	2.18	0.59			17.27	20.84	14.05
Geo-TüSL96	660.5	337.61	2.39	0.70			18.24	22.12	14.47
Geo-TüSL96	661.5	338.22	2.13	1.32			16.90	21.31	13.75
Geo-TüSL96	662.5	338.83	2.41	1.56			16.92	21.24	13.87
Geo-TüSL96	663.5	339.44	2.18	1.22			17.01	21.33	13.92
Geo-TüSL96	664.5	340.05	2.41	1.33			17.52	21.72	14.29
Geo-TüSL96	665.5	340.66	2.55	0.95			19.23	23.65	15.50
Geo-TüSL96	666.5	341.27	2.47	1.07			19.23	23.65	15.50
Geo-TüSL96	667.5	341.88	2.25	1.28			19.55	23.94	15.73
Geo-TüSL96	668.5	342.49	2.00	1.15			20.23	24.94	16.45
Geo-TüSL96	669.5	343.10	2.04	1.19			20.05	24.76	16.25
Geo-TüSL96	670.5	343.71	2.25	0.75			22.65	24.90	20.40
Geo-TüSL96	671.5	344.32	1.95	0.84			19.78	24.64	15.92
Geo-TüSL96	672.5	344.93	1.97	1.24			19.82	24.62	15.97
Geo-TüSL96	673.5	345.54	1.55	1.18			20.04	24.61	16.42
Geo-TüSL96	674.5	346.15	1.75	1.18			20.01	24.93	15.96
Geo-TüSL96	675.5	346.76	1.56	0.46			19.88	24.05	16.28
Geo-TüSL96	676.5	347.37	1.82	0.89			19.76	24.86	15.29
Geo-TüSL96	677.5	347.98	2.03	1.59			19.65	24.62	15.33
Geo-TüSL96	678.5	348.59	0.87	0.96			19.95	24.99	15.57
Geo-TüSL96	679.5	349.20	1.76	1.28			20.08	24.92	15.84
Geo-TüSL96	680.5	349.80	1.56	0.74			19.88	25.04	15.57
Geo-TüSL96	681.5	350.41	1.45	0.75			20.24	24.70	16.62
Geo-TüSL96	682.5	351.02	1.45	0.70			19.91	23.76	16.63
Geo-TüSL96	683.5	351.63					19.53	23.91	15.91
Geo-TüSL96	684.5	352.24	1.25	0.87			19.40	23.90	15.53
Geo-TüSL96	685.5	352.85	0.96	0.31			19.88	24.69	15.54
Geo-TüSL96	686.5	353.46	1.04	0.76			19.42	24.24	15.48
Geo-TüSL96	687.5	354.07	0.98	0.81			20.17	24.56	16.45
Geo-TüSL96	688.5	354.68	1.40	0.78			19.70	24.31	15.67
Geo-TüSL96	689.5	355.29	1.15	0.77			19.66	24.24	15.95
Geo-TüSL96	690.5	355.90	1.29	0.31			20.20	24.49	16.69
Geo-TüSL96	691.5	356.51	1.24	0.51			19.45	24.33	15.54

GeoTü-SL96, MIS 11, stable isotopes, ANN 2/4

core	cmbsf	age	δ18O *G. ruber*	δ13C *G. ruber*	δ18O *G. bulloides*	δ13C *G. bulloides*	ANN annual	ANN summer	ANN winter
Geo-TüSL96	692.5	357.12	1.16	0.36			19.68	24.60	15.47
Geo-TüSL96	693.5	357.73	1.14	0.24			20.06	24.33	16.65
Geo-TüSL96	694.5	358.34	1.58	0.72			21.91	24.76	19.39
Geo-TüSL96	695.5	358.95	1.34	0.83			22.59	24.62	20.13
Geo-TüSL96	696.5	359.56	1.67	0.81			21.90	24.26	19.38
Geo-TüSL96	697.5	360.17	1.55	0.62			20.17	24.09	16.89
Geo-TüSL96	698.5	360.78					19.50	23.81	15.86
Geo-TüSL96	699.5	361.39	1.29	0.82			20.08	23.21	17.44
Geo-TüSL96	700.5	362.00	0.76	0.26			22.72	25.36	20.14
Geo-TüSL96	701.5	362.94	0.66	0.67			21.87	25.11	18.95
Geo-TüSL96	702.5	363.87					21.52	24.93	18.49
Geo-TüSL96	703.5	364.81	0.38	0.44			21.46	24.83	18.53
Geo-TüSL96	704.5	365.74	0.53	0.62			21.23	24.33	18.50
Geo-TüSL96	705.5	366.68	0.63	0.70			21.40	25.00	18.29
Geo-TüSL96	706.5	367.62	0.57	0.38			22.18	24.90	19.59
Geo-TüSL96	707.5	368.55	0.52	0.41			20.95	24.20	17.90
Geo-TüSL96	708.5	369.49	0.58	0.61			20.02	23.82	16.72
Geo-TüSL96	709.5	370.43	0.62	0.62			21.02	24.32	17.89
Geo-TüSL96	710.5	371.36	0.55	0.16			21.58	24.49	18.89
Geo-TüSL96	711.5	372.30	0.60	0.57			20.34	23.86	17.26
Geo-TüSL96	712.5	373.23	0.40	0.37			20.82	23.81	18.17
Geo-TüSL96	713.5	374.17	0.61	0.27			20.58	24.13	17.16
Geo-TüSL96	714.5	375.11	0.26	0.39			21.18	24.15	18.33
Geo-TüSL96	715.5	376.04	0.42	0.24			21.65	24.86	18.02
Geo-TüSL96	716.5	376.98	0.35	0.21			20.09	24.29	15.96
Geo-TüSL96	717.5	377.91	0.54	0.41			20.85	24.62	17.18
Geo-TüSL96	718.5	378.85	0.58	0.31			20.15	24.46	15.95
Geo-TüSL96	719.5	379.79	0.54	0.50			19.71	24.25	15.48
Geo-TüSL96	720.5	380.72	0.28	0.41			20.94	24.77	16.99
Geo-TüSL96	721.5	381.66	0.57	0.32			21.25	24.87	17.66
Geo-TüSL96	722.5	382.60	0.59	0.19			21.18	24.77	17.61
Geo-TüSL96	723.5	383.53	0.29	0.34			21.23	25.05	17.49
Geo-TüSL96	724.5	384.47	0.56	0.72			20.77	24.94	16.79
Geo-TüSL96	725.5	385.40	0.30	0.18			21.10	24.98	17.22
Geo-TüSL96	726.5	386.34	0.62	0.20			20.79	25.13	16.87
Geo-TüSL96	727.5	387.28	0.64	0.40			20.49	24.14	16.92
Geo-TüSL96	728.5	388.21	0.70	0.21			21.25	24.41	18.02
Geo-TüSL96	729.5	389.15	0.40	0.22			19.38	22.97	15.75
Geo-TüSL96	730.5	390.09	0.53	0.41			19.87	23.14	17.06
Geo-TüSL96	731.5	391.02	0.52	0.12			19.01	22.77	15.38
Geo-TüSL96	732.5	391.96	0.23	-0.06			18.62	23.03	14.85
Geo-TüSL96	733.5	392.89	0.76	-0.12			20.80	24.03	17.34
Geo-TüSL96	734.5	393.83	0.62	0.13			20.53	22.20	17.86
Geo-TüSL96	735.5	394.77	0.98	0.25			18.74	21.90	15.62

GeoTü-SL96, MIS 11, stable isotopes, ANN 3/4

core	cmbsf	age	δ18O *G. ruber*	δ13C *G. ruber*	δ18O *G. bulloides*	δ13C *G. bulloides*	ANN annual	ANN summer	ANN winter
Geo-TüSL96	736.5	395.70	0.64	-0.05			19.60	23.34	16.26
Geo-TüSL96	737.5	396.64	0.85	0.01			19.46	23.48	16.34
Geo-TüSL96	738.5	397.57	0.87	0.30			19.33	23.35	15.99
Geo-TüSL96	739.5	398.51	0.32	0.23			19.52	23.54	16.34
Geo-TüSL96	740.5	399.45					18.40	22.80	15.02
Geo-TüSL96	741.5	400.38	0.65	-0.41			19.65	23.64	16.52
Geo-TüSL96	742.5	401.32	0.71	-0.34			20.22	23.87	17.43
Geo-TüSL96	743.5	402.26	0.45	-0.26			19.42	23.24	15.99
Geo-TüSL96	744.5	403.19	0.10	0.12			18.97	23.29	15.27
Geo-TüSL96	745.5	404.13	-0.50	-0.01			19.65	23.85	16.13
Geo-TüSL96	746.5	405.06	-0.34	-0.71			19.65	23.72	16.21
Geo-TüSL96	747.5	406.00	-0.24	-0.02			19.06	23.52	15.47
Geo-TüSL96	748.5	406.75	-0.52	-0.22			21.52	25.08	18.58
Geo-TüSL96	749.5	407.50	-0.08	-0.60			20.00	24.28	16.29
Geo-TüSL96	750.5	408.25	0.03	0.31			18.47	22.81	14.91
Geo-TüSL96	751.5	409.00	0.68	-0.09	-1.16	0.41	18.27	21.41	14.40
Geo-TüSL96	752.5	410.38	1.05	0.34	-0.89	1.02	17.80	21.55	13.82
Geo-TüSL96	753.5	411.77	0.63	0.30	-1.38	0.79	17.78	21.36	13.95
Geo-TüSL96	754.5	413.15	0.33	-0.71	-1.19	0.48	17.69	22.40	14.29
Geo-TüSL96	755.5	414.54	0.25	-0.07			16.35	19.23	13.19
Geo-TüSL96	756.5	415.92	1.20	0.65	-0.76	0.61	16.19	19.51	11.65
Geo-TüSL96	757.5	417.31			-1.25	0.37	16.62	20.88	13.27
Geo-TüSL96	758.5	418.69	1.04	0.57	-1.24	0.68	15.97	19.29	10.62
Geo-TüSL96	759.5	420.08			-1.23	0.61	11.22	14.56	6.27
Geo-TüSL96	760.5	421.46					17.04	20.33	13.87
Geo-TüSL96	761.5	422.85	0.90	0.51	-0.98	1.06	15.69	18.98	10.47
Geo-TüSL96	762.5	424.23			-1.17	0.68	15.09	18.96	10.23
Geo-TüSL96	763.5	425.62	1.13	0.62			14.50	18.29	10.28
Geo-TüSL96	764.5	427.00	0.93	0.62	-0.56	1.93	13.81	17.18	10.19
Geo-TüSL96	765.5	428.38	0.29	0.99			13.76	16.81	11.59
Geo-TüSL96	766.5	429.77	1.17	-0.05	-0.79	2.00	13.28	16.46	9.39
Geo-TüSL96	767.5	431.15	0.91	0.96	-0.76	2.01	12.77	16.31	9.47
Geo-TüSL96	768.5	432.54	0.87	0.27	-0.62	1.99	13.81	17.12	11.05
Geo-TüSL96	769.5	433.92	1.29	0.40	-0.39	2.19	11.40	13.54	8.22
Geo-TüSL96	770.5	435.31	0.78	1.04			15.04	18.99	11.89
Geo-TüSL96	771.5	436.69	1.32	0.63	-0.37	2.21	15.28	18.15	12.39
Geo-TüSL96	772.5	438.08	1.34	0.83	-0.01	2.42	12.86	14.78	8.18
Geo-TüSL96	773.5	439.46	0.72	0.45			16.72	20.78	13.36
Geo-TüSL96	774.5	440.85	0.50	0.57			16.29	20.07	12.80
Geo-TüSL96	775.5	442.23	0.34	-0.05			14.15	14.51	9.95
Geo-TüSL96	776.5	443.62	1.31	1.05			14.72	18.48	9.72
Geo-TüSL96	777.5	445.00	1.22	0.89			17.29	21.24	13.66
Geo-TüSL96	778.5	446.38	1.34	0.69			16.78	20.65	13.38
Geo-TüSL96	779.5	447.77	1.26	0.50			17.17	21.31	13.76

GeoTü-SL96, MIS 11, stable isotopes, ANN 4/4

core	cmbsf	age	δ18O *G. ruber*	δ13C *G. ruber*	δ18O *G. bulloides*	δ13C *G. bulloides*	ANN annual	ANN summer	ANN winter
Geo-TüSL96	780.5	449.15	1.12	0.57			16.95	21.42	13.55
Geo-TüSL96	781.5	450.54	1.15	0.55			18.14	21.55	14.26
Geo-TüSL96	782.5	451.92	0.95	0.55			17.17	21.22	13.53
Geo-TüSL96	783.5	453.31	1.05	0.37			17.50	21.58	14.01
Geo-TüSL96	784.5	454.69	0.57	0.24			15.77	19.01	10.75
Geo-TüSL96	785.5	456.08	1.30	0.44			17.97	22.16	14.77
Geo-TüSL96	786.5	457.46	2.16	0.53			18.50	22.97	15.48
Geo-TüSL96	787.5	458.85	2.16	1.01			20.10	24.24	17.24
Geo-TüSL96	788.5	460.23	1.83	0.52			18.34	23.03	14.85
Geo-TüSL96	789.5	461.62	2.02	0.58			18.52	23.03	15.24
Geo-TüSL96	790.5	463.00	1.99	1.47			18.30	22.97	14.88
Geo-TüSL96	791.5	464.38	2.05	0.69			18.89	23.71	15.16
Geo-TüSL96	792.5	465.77					19.03	23.82	15.16

GeoTü-SL96, MIS 11 planktonic foraminifera counts, benthic foraminifera counts 1/4

core	cmbsf	age	dry weight sed. (g)	split	summe split	no. planktonic forams	sum planktonic forams/g	sum benthic foraminifera	benthics in g/sediment	magnetic susceptibility
Geo-TüSL96	600.5	330.29	3.025	8	263	2104	695.54	1	0.33	29.5
Geo-TüSL96	605.5	330.90	4.079	32	528	16896	4142.19	22	5.39	13
Geo-TüSL96	610.5	331.51	4.466	32	279	8928	1999.10	28	6.27	28.5
Geo-TüSL96	615.5	332.12	4.146	32	303	9696	2338.64	21	5.07	38
Geo-TüSL96	620.5	332.73	4.195	8	378	3024	720.86	7	1.67	32.5
Geo-TüSL96	625.5	333.34	3.375	128	302	38656	11453.63	17	5.04	26
Geo-TüSL96	630.5	333.95	2.982	32	297	9504	3187.12	11	3.69	16.5
Geo-TüSL96	635.5	334.56	2.71	128	311	39808	14689.30	5	1.85	9
Geo-TüSL96	640.5	335.17	3.523	64	282	18048	5122.91	78	22.14	7
Geo-TüSL96	645.5	335.78	3.993	32	301	9632	2412.22	55	13.77	16
Geo-TüSL96	650.5	336.39	4.043	64	296	18944	4685.63	106	26.22	14.5
Geo-TüSL96	655.5	337.00	4.098	16	460	7360	1796.00	368	89.80	13.5
Geo-TüSL96	660.5	337.61	4.218	8	445	3560	844.00	48	11.38	19
Geo-TüSL96	661.5	338.22	3.67	8	418	3344	911.17	36	9.81	22.5
Geo-TüSL96	662.5	338.83	5.03	16	446	7136	1418.69	34	6.76	48
Geo-TüSL96	663.5	339.44	4.25	8	481	3848	905.41	38	8.94	31
Geo-TüSL96	664.5	340.05	4.69	16	342	5472	1166.74	38	8.10	21.5
Geo-TüSL96	665.5	340.66	4.649	16	339	5424	1166.70	51	10.97	17
Geo-TüSL96	666.5	341.27	3.93	8	339	2712	690.08	12	3.05	18
Geo-TüSL96	667.5	341.88	3.88	16	428	6848	1764.95	12	3.09	19.5
Geo-TüSL96	668.5	342.49	4.71	16	338	5408	1148.20	22	4.67	20
Geo-TüSL96	669.5	343.10	4.46	16	465	7440	1668.16	22	4.93	23
Geo-TüSL96	670.5	343.71	3.745	16	388	6208	1657.68	83	22.16	25
Geo-TüSL96	671.5	344.32	4.03	16	534	8544	2120.10	65	16.13	26
Geo-TüSL96	672.5	344.93	4.06	16	436	6976	1718.23	55	13.55	27
Geo-TüSL96	673.5	345.54	4.97	32	333	10656	2144.06	68	13.68	33
Geo-TüSL96	674.5	346.15	4.24	16	441	7056	1664.15	31	7.31	28
Geo-TüSL96	675.5	346.76	3.554	4	465	1860	523.35	16	4.50	26.5
Geo-TüSL96	676.5	347.37	3.24	4	441	1764	544.44	27	8.33	24
Geo-TüSL96	677.5	347.98	4.13	16	303	4848	1173.85	13	3.15	20
Geo-TüSL96	678.5	348.59	4.17	16	411	6576	1576.98	26	6.24	12
Geo-TüSL96	679.5	349.20	4.18	32	377	12064	2886.12	23	5.50	15.5
Geo-TüSL96	680.5	349.80	3.973	32	543	17376	4373.52	78	19.63	19
Geo-TüSL96	681.5	350.41	3.58	8	400	3200	893.85	30	8.38	33.5
Geo-TüSL96	682.5	351.02	3.76	8	304	2432	646.81	16	4.26	24.5
Geo-TüSL96	683.5	351.63	3.4	4	305	1220	358.82	12	3.53	23
Geo-TüSL96	684.5	352.24	4.07	8	362	2896	711.55	42	10.32	21.5
Geo-TüSL96	685.5	352.85	3.774	32	397	12704	3366.19	38	10.07	23
Geo-TüSL96	686.5	353.46	3.25	64	305	19520	6006.15	53	16.31	25
Geo-TüSL96	687.5	354.07	3.25	64	308	19712	6065.23	57	17.54	20
Geo-TüSL96	688.5	354.68	3.62	64	327	20928	5781.22	56	15.47	14.5
Geo-TüSL96	689.5	355.29	3.32	16	503	8048	2424.10	17	5.12	13.5
Geo-TüSL96	690.5	355.90	3.851	32	354	11328	2941.57	16	4.15	15.5
Geo-TüSL96	691.5	356.51	3.93	64	318	20352	5178.63	46	11.70	17.5

GeoTü-SL96, MIS 11 planktonic foraminifera counts, benthic foraminifera counts
2/4

core	cmbsf	age	dry weight sed. (g)	split	summe split	no. planktonic forams	sum planktonic forams/g	sum benthic foraminifera	benthics in g/sediment	magnetic susceptibility
Geo-TüSL96	692.5	357.12	3.88	32	504	16128	4156.70	17	4.38	15
Geo-TüSL96	693.5	357.73	3.53	16	427	6832	1935.41	44	12.46	26.5
Geo-TüSL96	694.5	358.34	4.14	8	511	4088	987.44	34	8.21	32.5
Geo-TüSL96	695.5	358.95	4.16	16	343	5488	1319.23	64	15.38	21
Geo-TüSL96	696.5	359.56	3.89	4	450	1800	462.72	29	7.46	17.5
Geo-TüSL96	697.5	360.17	4.6	8	605	4840	1052.17	35	7.61	32.5
Geo-TüSL96	698.5	360.78	1.78	4	318	1272	714.61	24	13.61	33
Geo-TüSL96	699.5	361.39	2.94	16	332	5312	1806.80	24	8.02	32
Geo-TüSL96	700.5	362.00	3.992	16	305	4880	1222.44	3	0.78	30
Geo-TüSL96	701.5	362.94	2.56	8	458	3664	1431.25	3	1.20	32
Geo-TüSL96	702.5	363.87	3.32	8	349	2792	840.96	6	1.85	32
Geo-TüSL96	703.5	364.81	3.25	8	346	2768	851.69	2	0.73	33.5
Geo-TüSL96	704.5	365.74	2.74	8	460	3680	1343.07	3	1.07	35
Geo-TüSL96	705.5	366.68	3.743	32	309	9888	2641.73	8	2.08	32
Geo-TüSL96	706.5	367.62	2.88	16	407	6512	2261.11	4	1.32	33.5
Geo-TüSL96	707.5	368.55	3.04	16	435	6960	2289.47	3	0.98	32.5
Geo-TüSL96	708.5	369.49	3.06	8	481	3848	1257.52	5	1.58	30.5
Geo-TüSL96	709.5	370.43	3.16	16	309	4944	1564.56	5	1.58	30
Geo-TüSL96	710.5	371.36	3.788	8	561	4488	1184.79	4	1.09	40
Geo-TüSL96	711.5	372.30	3.67	8	448	3584	976.57	6	1.73	31
Geo-TüSL96	712.5	373.23	2.89	32	316	10112	3498.96	9	2.99	26
Geo-TüSL96	713.5	374.17	3.35	64	363	23232	6934.93	6	1.90	21.5
Geo-TüSL96	714.5	375.11	3.69	64	310	19840	5376.69	0	0.00	18
Geo-TüSL96	715.5	376.04	3.111	32	293	9376	3013.82	10	3.32	16
Geo-TüSL96	716.5	376.98	3.01	32	404	12928	4295.02	9	2.87	12
Geo-TüSL96	717.5	377.91	3.49	32	454	14528	4162.75	9	2.63	9
Geo-TüSL96	718.5	378.85	3.04	32	318	10176	3347.37	5	1.67	7
Geo-TüSL96	719.5	379.79	3	64	337	21568	7189.33	1	0.30	7.5
Geo-TüSL96	720.5	380.72	3.286	32	281	8992	2736.46	0	0.00	8
Geo-TüSL96	721.5	381.66	3.31	16	513	8208	2479.76	7	2.02	9
Geo-TüSL96	722.5	382.60	3.46	32	303	9696	2802.31	0	0.00	7.5
Geo-TüSL96	723.5	383.53	3.68	32	489	15648	4252.17	0	0.00	8
Geo-TüSL96	724.5	384.47	3.79	32	349	11168	2946.70	3	0.77	8
Geo-TüSL96	725.5	385.40	3.902	64	357	22848	5855.46	3	0.85	13
Geo-TüSL96	726.5	386.34	3.55	32	378	12096	3407.32	9	2.58	15.5
Geo-TüSL96	727.5	387.28	3.88	8	502	4016	1035.05	13	3.32	15.5
Geo-TüSL96	728.5	388.21	4.22	32	306	9792	2320.38	4	0.86	18.5
Geo-TüSL96	729.5	389.15	3.5	8	329	2632	752.00	8	2.21	16
Geo-TüSL96	730.5	390.09	4.067	8	302	19328	590.12	1	0.30	18
Geo-TüSL96	731.5	391.02	3.37	32	397	3176	3124.04	9	2.66	18.5
Geo-TüSL96	732.5	391.96	4.13	64	526	4208	4679.90	2	0.54	16.5
Geo-TüSL96	733.5	392.89	3.68	8	287	4592	863.04	6	1.67	16.5
Geo-TüSL96	734.5	393.83	3	8	321	5136	1402.67	3	1.03	15
Geo-TüSL96	735.5	394.77	2.905	16	424	6784	1580.72	6	1.98	13

GeoTü-SL96, MIS 11 planktonic foraminifera counts, benthic foraminifera counts 3/4

core	cmbsf	age	dry weight sed. (g)	split	summe split	no. planktonic forams	sum planktonic forams/g	sum benthic foraminifera	benthics in g/sediment	magnetic susceptibility
Geo-TüSL96	736.5	395.70	3.03	16	317	2536	1695.05	0	0.00	12
Geo-TüSL96	737.5	396.64	2.81	16	394	12608	2414.23	6	2.28	12
Geo-TüSL96	738.5	397.57	3.07	8	282	9024	826.06	14	4.71	9.5
Geo-TüSL96	739.5	398.51	3.4	32	402	12864	3708.24	31	9.16	10
Geo-TüSL96	740.5	399.45	3.384	32	599	19168	5664.30	39	11.40	13
Geo-TüSL96	741.5	400.38	3.51	32	392	12544	3664.96	32	9.02	14
Geo-TüSL96	742.5	401.32	3.99	32	357	11424	4804.01	31	7.79	15.5
Geo-TüSL96	743.5	402.26	3.21	32	369	11808	3907.79	44	13.83	16
Geo-TüSL96	744.5	403.19	3.47	32	504	8064	3292.22	30	8.51	15.5
Geo-TüSL96	745.5	404.13	3.878	32	409	13088	3374.94	33	8.51	15
Geo-TüSL96	746.5	405.06	3.29	16	532	17024	2451.06	50	15.09	15
Geo-TüSL96	747.5	406.00	3.71	32	567	18144	3527.76	61	16.33	15
Geo-TüSL96	748.5	406.75	3.92	32	281	8992	4342.86	55	14.13	14.5
Geo-TüSL96	749.5	407.50	3.68	32	577	18464	4930.43	90	24.57	14
Geo-TüSL96	750.5	408.25	4.07	32	327	20928	5142.01	129	31.80	15
Geo-TüSL96	751.5	409.00	3.27	32	415	26560	5646.48	99	30.19	15.5
Geo-TüSL96	752.5	410.38	4.24	64	301	38528	4935.85	251	59.09	15
Geo-TüSL96	753.5	411.77	3.52	64	399	25536	7545.45	177	50.23	15
Geo-TüSL96	754.5	413.15	4.28	128	533	34112	9001.87	149	34.88	15
Geo-TüSL96	755.5	414.54	3.928	64	457	29248	7446.03	231	58.72	15
Geo-TüSL96	756.5	415.92	4.36	64	453	28992	7823.85	274	62.75	15
Geo-TüSL96	757.5	417.31	3.57	64	675	43200	8192.72	197	55.17	15
Geo-TüSL96	758.5	418.69	3.77	64	337	21568	7690.19	453	120.12	15
Geo-TüSL96	759.5	420.08	3.33	64	418	13376	12972.97	201	60.38	14
Geo-TüSL96	760.5	421.46	3.594	64	512	16384	4558.71	296	82.32	13
Geo-TüSL96	761.5	422.85	3.11	32	349	11168	4300.96	358	115.22	13
Geo-TüSL96	762.5	424.23	3.68	32	495	15840	4452.17	300	81.59	11.5
Geo-TüSL96	763.5	425.62	3.53	32	355	22720	3163.74	289	81.80	12.5
Geo-TüSL96	764.5	427.00	4.01	32	475	15200	3950.12	263	65.64	11
Geo-TüSL96	765.5	428.38	3.885	64	498	15936	4101.93	395	101.62	11.5
Geo-TüSL96	766.5	429.77	3.7	32	426	13632	4108.11	241	65.26	13
Geo-TüSL96	767.5	431.15	3.8	32	491	15712	4193.68	239	62.97	14
Geo-TüSL96	768.5	432.54	3.43	32	473	15136	3974.34	259	75.59	13.5
Geo-TüSL96	769.5	433.92	3.81	32	397	12704	4123.88	297	77.94	13
Geo-TüSL96	770.5	435.31	3.721	0.046875	552	17664	4747.11	437	117.50	14
Geo-TüSL96	771.5	436.69	3.2	32	490	15680	3970.00	440	137.44	11
Geo-TüSL96	772.5	438.08	3.9	32	384	24576	4529.23	550	141.04	14.5
Geo-TüSL96	773.5	439.46	3.46	32	657	42048	4531.79	351	101.32	12.5
Geo-TüSL96	774.5	440.85	3.79	64	474	15168	6484.43	136	35.84	15
Geo-TüSL96	775.5	442.23	3.32	64	303	19392	5840.96	140	42.23	13.5
Geo-TüSL96	776.5	443.62	3.41	32	328	20992	4448.09	201	58.92	14
Geo-TüSL96	777.5	445.00	3.53	64	303	19392	5493.48	142	40.13	17.5
Geo-TüSL96	778.5	446.38	2.99	64	390	12480	7020.74	114	38.07	17
Geo-TüSL96	779.5	447.77	3.52	64	391	25024	5509.09	137	38.96	19

GeoTü-SL96, MIS 11 planktonic foraminifera counts, benthic foraminifera counts
4/4

core	cmbsf	age	dry weight sed. (g)	split	summe split	no. planktonic forams	sum planktonic forams/g	sum benthic foraminifera	benthics in g/sediment	magnetic susceptibility
Geo-TüSL96	780.5	449.15	3.003	32	579	18528	6169.83	200	66.67	17
Geo-TüSL96	781.5	450.54	3.57	64	319	10208	7009.52	228	63.82	17
Geo-TüSL96	782.5	451.92	3.51	32	540	17280	5278.63	168	47.83	17.5
Geo-TüSL96	783.5	453.31	3.68	32	353	11296	2773.91	258	70.09	18
Geo-TüSL96	784.5	454.69	3.31	32	314	5024	5220.54	92	27.69	18
Geo-TüSL96	785.5	456.08	3.72	32	321	5136	1380.65	82	22.06	19.5
Geo-TüSL96	786.5	457.46	2.72	16	376	3008	1847.06	34	12.57	18
Geo-TüSL96	787.5	458.85	3.34	16	312	4992	1537.72	56	16.87	21
Geo-TüSL96	788.5	460.23	3.32	8	332	2656	906.02	83	25.13	23
Geo-TüSL96	789.5	461.62	3.74	16	301	9632	1334.76	117	31.27	25
Geo-TüSL96	790.5	463.00	3.262	8	356	11392	3492.34	98	30.11	32.5
Geo-TüSL96	791.5	464.38	4.65	32	301	9632	2071.40	96	20.68	28.5
Geo-TüSL96	792.5	465.77	2.37	32	356	11392	4806.75	54	22.82	24.5

GeoTü-SL96, planktonic foraminifera counts 1/4

core	cmbsf	age	*Orbulina universa*	*Globigerinoides conglobatus*	*Globigerinoides ruber total*	*Globoturborotalita tenella*	*Globigerinoides sacc total*	*Sphaeroidinella dehiscens*	*siphonifera & calida*	*Globigerina bulloides*	*Globigerina falconensis*	*Beela digitata*	*Globoturborotalita rubescens*	*Turborotalita quinqueloba*	*Neogloboquadrina pachyderma L*	*Neogloboquadrina dutertrei*	*P/D integrade & N. pachyderma R*	*Pulleniatina obliquiloculata*	*Globorotalia inflata*	*Globorotalia truncatulinoides total*	*Globorotalia crassaformis*	*Globorotalia hirsuta*	*Globorotalia scitula*	*Globorotalia menardii & tumida*	*Globigerinita glutinata*
Geo-TüSL96	600.5	330.29	10	0	93	0	29	0	15	0	11	0	0	0	0	0	37	0	52	10	0	0	5	0	1
Geo-TüSL96	605.5	330.90	15	0	280	7	3	0	2	12	5	0	0	0	0	0	28	0	132	41	0	0	0	0	3
Geo-TüSL96	610.5	331.51	4	0	135	0	16	0	12	21	10	3	0	0	0	1	10	0	27	34	0	0	6	0	0
Geo-TüSL96	615.5	332.12	11	0	123	5	16	0	27	10	7	10	1	0	0	0	16	0	45	2	0	0	3	0	27
Geo-TüSL96	620.5	332.73	8	0	183	0	65	0	7	16	5	0	0	1	0	2	4	0	79	6	0	0	0	0	2
Geo-TüSL96	625.5	333.34	3	0	112	2	18	0	19	15	11	0	0	0	0	0	19	0	66	5	0	0	0	0	32
Geo-TüSL96	630.5	333.95	13	0	90	0	41	0	17	8	18	0	2	11	0	5	21	0	45	2	0	0	0	0	24
Geo-TüSL96	635.5	334.56	14	0	76	2	36	0	14	35	8	2	0	2	0	0	5	0	41	0	0	0	1	0	75
Geo-TüSL96	640.5	335.17	13	0	51	1	11	0	16	42	14	0	0	15	0	19	51	0	31	0	0	0	10	0	8
Geo-TüSL96	645.5	335.78	11	0	44	4	4	0	6	37	25	0	0	0	0	2	103	0	56	0	0	0	1	0	8
Geo-TüSL96	650.5	336.39	13	0	28	0	12	0	0	51	23	0	0	14	1	27	66	0	46	0	0	0	12	0	3
Geo-TüSL96	655.5	337.00	68	0	54	2	2	0	0	58	37	0	0	4	0	6	126	0	97	0	0	0	2	0	4
Geo-TüSL96	660.5	337.61	0	0	194	0	3	0	2	47	23	0	0	4	2	0	160	0	9	0	0	0	0	0	1
Geo-TüSL96	661.5	338.22	0	0	120	1	0	0	0	62	17	0	2	8	3	7	177	0	10	1	0	0	2	0	8
Geo-TüSL96	662.5	338.83	1	0	101	2	0	0	0	76	40	0	2	17	1	10	170	0	5	0	0	0	12	0	9
Geo-TüSL96	663.5	339.44	5	0	142	0	2	0	3	69	49	0	0	15	0	5	163	0	8	0	0	0	8	0	12
Geo-TüSL96	664.5	340.05	14	2	118	1	3	0	0	49	28	0	1	13	0	3	85	0	13	1	0	0	5	0	6
Geo-TüSL96	665.5	340.66	4	0	212	2	0	0	0	20	16	0	0	2	0	2	45	0	33	1	0	0	0	0	2
Geo-TüSL96	666.5	341.27	4	0	212	2	0	0	0	20	16	0	0	2	0	2	45	0	33	1	0	0	0	0	2
Geo-TüSL96	667.5	341.88	1	0	293	4	6	0	0	34	16	1	0	5	1	0	34	0	31	0	0	0	2	0	0
Geo-TüSL96	668.5	342.49	10	0	241	2	15	0	0	9	12	0	1	1	0	0	4	0	35	1	0	0	4	0	3
Geo-TüSL96	669.5	343.10	9	0	325	4	14	0	2	16	14	0	0	3	0	0	10	0	56	1	0	0	5	0	6
Geo-TüSL96	670.5	343.71	0	12	261	2	20	0	1	6	11	1	0	1	0	1	12	0	55	5	0	0	0	0	0
Geo-TüSL96	671.5	344.32	29	0	299	3	23	0	1	32	20	0	0	4	0	0	17	0	92	7	0	0	2	0	5
Geo-TüSL96	672.5	344.93	25	0	210	1	27	0	3	29	16	0	0	1	0	2	16	0	85	10	0	0	2	0	9
Geo-TüSL96	673.5	345.54	20	1	127	4	23	0	1	31	10	0	0	1	1	0	18	0	78	8	0	0	3	0	7
Geo-TüSL96	674.5	346.15	28	0	201	3	35	0	5	41	8	0	0	1	0	0	14	0	77	12	0	0	1	0	15
Geo-TüSL96	675.5	346.76	14	0	202	10	42	0	0	14	49	0	0	0	0	2	52	0	46	22	0	0	0	0	12
Geo-TüSL96	676.5	347.37	20	0	234	4	17	0	2	25	11	0	0	3	0	1	16	0	46	53	0	0	0	0	9
Geo-TüSL96	677.5	347.98	10	0	179	2	9	0	1	21	7	0	1	4	1	0	12	0	26	22	0	0	0	0	8
Geo-TüSL96	678.5	348.59	8	0	307	0	6	0	3	19	3	3	0	3	0	0	2	0	37	17	0	0	1	0	2
Geo-TüSL96	679.5	349.20	3	0	303	0	6	0	1	5	3	2	0	2	1	0	6	0	37	6	0	0	1	0	1
Geo-TüSL96	680.5	349.80	25	0	316	1	22	0	6	22	20	9	0	4	0	0	11	0	74	25	0	0	5	0	3
Geo-TüSL96	681.5	350.41	19	2	220	4	17	0	3	34	19	2	0	1	0	0	12	0	48	16	0	0	0	0	3
Geo-TüSL96	682.5	351.02	7	0	123	3	40	0	1	34	39	0	1	2	0	1	9	0	31	11	0	0	1	0	1
Geo-TüSL96	683.5	351.63	7	0	142	4	20	0	0	40	30	0	0	0	0	0	4	0	33	22	0	0	0	0	3
Geo-TüSL96	684.5	352.24	8	0	156	1	20	0	4	36	37	1	1	1	0	0	4	0	49	38	0	0	0	0	6
Geo-TüSL96	685.5	352.85	15	1	199	0	9	0	3	3	14	0	0	0	0	0	5	0	83	61	0	0	0	0	4
Geo-TüSL96	686.5	353.46	14	0	163	1	7	0	1	15	26	0	0	1	0	0	5	0	36	31	0	0	1	0	4
Geo-TüSL96	687.5	354.07	9	2	159	1	6	0	4	14	15	1	0	0	0	0	5	0	55	31	0	0	1	0	5
Geo-TüSL96	688.5	354.68	10	1	151	1	8	0	2	16	19	0	1	2	0	0	7	0	63	44	0	0	0	0	2
Geo-TüSL96	689.5	355.29	22	1	254	3	14	0	7	22	51	0	0	0	0	0	7	0	63	54	0	0	2	0	3
Geo-TüSL96	690.5	355.90	24	3	162	2	4	0	4	3	27	0	0	0	0	0	9	0	68	46	0	0	0	0	2
Geo-TüSL96	691.5	356.51	18	0	157	3	7	0	3	15	28	0	0	0	1	0	4	0	49	30	0	0	0	0	3

GeoTü-SL96, planktonic foraminifera counts 2/4

core	cmbsf	age	*Orbulina universa*	*Globigerinoides conglobatus*	*Globigerinoides ruber total*	*Globoturborotalita tenella*	*Globigerinoides sacc total*	*Sphaeroidinella dehiscens*	*siphonifera & calida*	*Globigerina bulloides*	*Globigerina falconensis*	*Beela digitata*	*Globoturborotalita rubescens*	*Turborotalita quinqueloba*	*Neogloboquadrina pachyderma L*	*Neogloboquadrina dutertrei*	*P/D integrade & N. pachyderma R*	*Pulleniatina obliquiloculata*	*Globorotalia inflata*	*Globorotalia truncatulinoides total*	*Globorotalia crassaformis*	*Globorotalia hirsuta*	*Globorotalia scitula*	*Globorotalia menardii & tumida*	*Globigerinita glutinata*
Geo-TüSL96	692.5	357.12	18	0	246	4	17	0	9	23	29	0	0	0	0	0	8	0	76	63	0	0	1	0	10
Geo-TüSL96	693.5	357.73	22	3	211	3	9	0	5	29	36	0	0	0	0	0	6	0	54	44	0	0	1	0	4
Geo-TüSL96	694.5	358.34	38	12	247	4	35	0	12	46	38	1	0	1	0	0	15	0	27	31	0	0	0	0	4
Geo-TüSL96	695.5	358.95	26	12	181	3	18	0	0	3	37	1	0	1	0	0	10	0	13	33	0	0	0	0	5
Geo-TüSL96	696.5	359.56	27	11	188	2	49	0	6	41	52	2	2	3	1	0	15	0	12	37	0	0	0	0	2
Geo-TüSL96	697.5	360.17	30	3	267	4	56	0	10	57	76	1	1	0	3	0	13	0	37	45	0	0	0	0	2
Geo-TüSL96	698.5	360.78	20	0	131	2	28	0	5	51	32	0	0	2	2	1	15	0	9	15	0	0	0	0	5
Geo-TüSL96	699.5	361.39	14	2	127	0	42	0	11	33	66	0	0	1	2	0	7	0	17	8	0	0	0	0	2
Geo-TüSL96	700.5	362.00	21	6	110	0	70	0	32	20	33	2	0	0	0	0	0	0	3	0	0	0	1	0	7
Geo-TüSL96	701.5	362.94	33	4	188	2	105	0	14	38	48	1	0	0	2	0	5	0	4	3	0	0	0	0	11
Geo-TüSL96	702.5	363.87	24	3	146	0	65	0	14	36	32	0	0	0	2	0	4	0	4	6	0	0	1	0	12
Geo-TüSL96	703.5	364.81	17	3	164	1	60	0	8	28	33	0	0	0	0	0	3	0	15	9	0	0	0	0	5
Geo-TüSL96	704.5	365.74	17	5	188	3	71	0	15	44	58	2	0	0	1	0	7	0	18	15	0	0	2	0	14
Geo-TüSL96	705.5	366.68	18	2	118	6	53	0	15	9	36	1	0	0	0	1	15	0	12	9	0	0	0	0	14
Geo-TüSL96	706.5	367.62	21	8	184	2	61	0	15	27	38	0	0	0	0	0	4	0	16	25	0	0	0	0	6
Geo-TüSL96	707.5	368.55	8	3	179	2	70	0	11	44	44	0	0	1	1	0	20	0	16	15	0	0	0	0	21
Geo-TüSL96	708.5	369.49	10	1	238	2	50	0	3	50	55	0	0	1	0	0	11	0	28	18	0	0	0	0	14
Geo-TüSL96	709.5	370.43	8	3	129	1	44	0	6	29	29	0	0	4	1	0	10	0	17	22	0	0	0	0	6
Geo-TüSL96	710.5	371.36	15	8	284	0	71	0	4	0	58	0	0	0	0	1	26	0	53	35	0	0	0	0	6
Geo-TüSL96	711.5	372.30	6	4	159	3	36	0	5	34	46	0	0	1	1	1	26	0	55	43	0	0	4	0	24
Geo-TüSL96	712.5	373.23	5	5	117	3	23	0	5	29	37	0	0	0	0	0	26	0	21	35	0	0	3	0	7
Geo-TüSL96	713.5	374.17	8	4	125	1	27	0	7	24	25	0	0	1	0	0	32	0	47	52	0	0	0	0	10
Geo-TüSL96	714.5	375.11	10	6	101	1	19	0	7	34	19	0	0	0	0	1	22	0	31	41	0	0	2	0	16
Geo-TüSL96	715.5	376.04	4	5	112	1	27	0	2	1	4	0	2	0	4	0	24	0	45	59	0	0	0	0	3
Geo-TüSL96	716.5	376.98	7	1	118	1	44	0	11	28	30	1	0	0	1	1	24	0	60	65	0	0	2	0	10
Geo-TüSL96	717.5	377.91	14	4	148	1	52	0	9	36	22	0	0	0	0	0	22	0	70	66	0	0	3	0	7
Geo-TüSL96	718.5	378.85	6	1	106	1	30	0	6	24	14	0	0	1	0	0	19	0	48	50	0	0	2	0	10
Geo-TüSL96	719.5	379.79	10	0	94	2	31	0	7	27	24	0	0	0	0	0	16	0	59	54	0	0	2	0	11
Geo-TüSL96	720.5	380.72	7	2	95	0	35	0	10	4	16	0	0	0	0	1	16	0	41	48	0	0	1	0	5
Geo-TüSL96	721.5	381.66	15	4	195	1	86	0	11	37	39	0	0	0	0	0	5	0	32	70	0	0	2	0	16
Geo-TüSL96	722.5	382.60	4	3	137	0	40	0	3	34	12	0	0	0	0	0	7	0	23	37	0	0	0	0	3
Geo-TüSL96	723.5	383.53	11	3	218	2	80	0	12	37	30	1	0	1	0	0	3	0	32	54	0	0	0	0	5
Geo-TüSL96	724.5	384.47	10	0	146	0	66	0	11	42	22	1	0	0	0	0	3	0	14	23	0	0	0	0	11
Geo-TüSL96	725.5	385.40	11	1	129	3	72	0	6	15	34	1	0	0	2	2	9	0	13	44	0	0	1	0	14
Geo-TüSL96	726.5	386.34	20	0	163	2	66	0	14	43	21	0	0	2	1	0	5	0	17	14	0	0	0	0	10
Geo-TüSL96	727.5	387.28	6	0	190	3	93	0	11	71	38	0	0	0	0	0	20	0	22	10	0	0	0	0	38
Geo-TüSL96	728.5	388.21	7	1	92	1	76	0	8	51	22	0	1	0	0	6	7	0	3	3	0	0	0	0	28
Geo-TüSL96	729.5	389.15	8	0	100	4	42	0	7	79	17	0	0	1	1	2	8	0	9	1	0	0	0	0	50
Geo-TüSL96	730.5	390.09	3	0	107	0	42	0	3	10	49	0	3	1	1	19	35	0	21	0	0	0	3	0	3
Geo-TüSL96	731.5	391.02	8	0	100	4	42	0	7	79	17	0	0	1	1	2	8	0	9	1	0	0	0	0	50
Geo-TüSL96	732.5	391.96	4	0	68	6	37	0	10	37	0	0	0	5	0	27	56	0	24	2	0	0	1	0	25
Geo-TüSL96	733.5	392.89	2	0	118	3	59	0	4	56	13	0	0	1	1	21	44	0	24	4	0	0	1	0	46
Geo-TüSL96	734.5	393.83	9	1	139	3	67	0	6	98	49	0	0	2	1	10	31	0	38	4	0	0	1	0	67
Geo-TüSL96	735.5	394.77	1	0	79	1	41	0	4	34	43	0	1	1	2	12	9	0	15	1	0	0	0	0	43

GeoTü-SL96, planktonic foraminifera counts 3/4

core	cmbsf	age	*Orbulina universa*	*Globigerinoides conglobatus*	*Globigerinoides ruber total*	*Globoturborotalita tenella*	*Globigerinoides sacc total*	*Sphaeroidinella dehiscens*	*siphonifera & calida*	*Globigerina bulloides*	*Globigerina falconensis*	*Beela digitata*	*Globoturborotalita rubescens*	*Turborotalita quinqueloba*	*Neogloboquadrina pachyderma L*	*Neogloboquadrina dutertrei*	*P/D integrade & N. pachyderma R*	*Pulleniatina obliquiloculata*	*Globorotalia inflata*	*Globorotalia truncatulinoides total*	*Globorotalia crassaformis*	*Globorotalia hirsuta*	*Globorotalia scitula*	*Globorotalia menardii & tumida*	*Globigerinita glutinata*
Geo-TüSL96	736.5	395.70	2	0	113	6	35	0	5	75	22	0	0	0	0	3	19	0	19	2	0	0	1	0	19
Geo-TüSL96	737.5	396.64	5	0	150	4	29	0	5	64	32	0	2	0	0	8	17	0	65	1	0	0	5	0	37
Geo-TüSL96	738.5	397.57	7	0	94	1	24	0	8	60	19	2	0	0	0	11	15	0	46	0	0	0	0	0	30
Geo-TüSL96	739.5	398.51	4	0	121	6	35	0	11	67	28	0	0	1	1	14	20	0	44	1	0	0	7	0	34
Geo-TüSL96	740.5	399.45	7	0	83	4	25	0	7	17	17	0	0	4	0	28	26	0	33	0	0	0	7	0	24
Geo-TüSL96	741.5	400.38	8	0	118	3	37	0	12	51	29	0	2	3	0	23	39	0	38	1	0	0	8	0	30
Geo-TüSL96	742.5	401.32	16	0	166	6	41	0	16	84	34	0	1	3	0	24	70	0	81	0	0	0	3	0	54
Geo-TüSL96	743.5	402.26	7	0	116	3	35	0	7	42	21	0	0	4	0	14	58	0	48	0	0	0	3	0	34
Geo-TüSL96	744.5	403.19	10	0	116	4	34	0	6	34	12	0	0	2	0	14	50	0	53	0	0	0	1	0	21
Geo-TüSL96	745.5	404.13	13	0	96	3	45	0	8	30	14	1	2	2	0	21	58	0	37	0	0	0	9	0	30
Geo-TüSL96	746.5	405.06	15	0	163	7	57	0	3	55	28	0	2	4	2	21	58	0	46	0	0	0	8	0	35
Geo-TüSL96	747.5	406.00	26	0	101	6	44	0	10	71	15	0	1	4	0	18	39	0	45	0	0	0	7	0	22
Geo-TüSL96	748.5	406.75	35	0	130	6	69	0	7	82	30	0	0	5	0	32	60	0	37	0	0	0	11	0	28
Geo-TüSL96	749.5	407.50	37	0	130	6	88	0	8	82	10	1	0	9	0	55	82	0	17	0	0	0	10	0	32
Geo-TüSL96	750.5	408.25	10	0	65	4	13	0	0	17	7	0	1	6	2	63	68	0	15	0	0	0	1	0	9
Geo-TüSL96	751.5	409.00	7	0	92	4	19	0	8	61	17	0	0	16	5	153	112	0	31	0	0	0	7	0	45
Geo-TüSL96	752.5	410.38	4	0	47	3	11	0	2	24	5	0	1	2	0	98	89	0	9	0	0	0	1	0	31
Geo-TüSL96	753.5	411.77	10	0	51	1	15	0	3	43	12	0	0	7	0	139	88	0	10	0	0	0	3	0	33
Geo-TüSL96	754.5	413.15	9	0	67	3	9	0	2	36	10	5	1	9	0	65	39	0	19	0	0	0	2	0	25
Geo-TüSL96	755.5	414.54	3	2	39	3	7	0	1	28	16	1	2	17	3	34	194	0	11	0	0	0	1	0	37
Geo-TüSL96	756.5	415.92	5	0	31	0	8	0	8	71	16	2	0	8	4	178	156	0	8	0	0	0	0	0	38
Geo-TüSL96	757.5	417.31	4	0	15	4	8	0	5	70	11	4	0	23	0	146	129	0	8	0	0	0	1	0	29
Geo-TüSL96	758.5	418.69	0	0	39	2	12	0	0	61	8	5	1	5	0	145	130	0	10	0	0	0	0	0	35
Geo-TüSL96	759.5	420.08	2	0	9	0	0	0	0	102	16	8	0	20	2	254	210	0	0	0	0	0	0	0	52
Geo-TüSL96	760.5	421.46	0	3	5	5	0	0	0	15	13	0	0	19	2	104	145	0	0	0	0	0	0	0	26
Geo-TüSL96	761.5	422.85	5	0	8	0	8	0	0	47	11	0	0	4	4	188	120	0	1	0	0	0	0	0	22
Geo-TüSL96	762.5	424.23	6	0	8	1	7	0	1	63	2	0	0	5	3	207	164	0	0	0	0	0	0	0	45
Geo-TüSL96	763.5	425.62	6	0	10	1	2	0	0	36	6	1	0	10	0	123	116	0	0	0	0	0	0	0	38
Geo-TüSL96	764.5	427.00	18	0	25	0	5	0	4	76	10	0	0	27	2	105	176	0	0	0	0	0	0	0	47
Geo-TüSL96	765.5	428.38	6	0	4	1	0	0	1	36	19	0	1	24	3	27	194	0	0	0	0	0	0	0	39
Geo-TüSL96	766.5	429.77	30	0	15	0	9	0	0	83	11	2	1	14	0	95	169	0	0	0	0	0	0	0	46
Geo-TüSL96	767.5	431.15	26	0	10	1	5	0	0	104	4	0	0	11	0	88	190	0	2	1	0	0	0	0	56
Geo-TüSL96	768.5	432.54	26	0	7	3	7	0	3	74	10	0	0	9	3	43	185	0	4	0	0	0	0	0	52
Geo-TüSL96	769.5	433.92	32	0	6	1	6	0	1	98	22	0	2	20	0	65	189	0	0	0	0	0	0	0	49
Geo-TüSL96	770.5	435.31	26	0	13	4	3	0	1	53	18	1	0	16	2	70	234	0	5	0	0	0	2	0	25
Geo-TüSL96	771.5	436.69	15	0	5	1	15	0	4	84	18	0	0	11	0	47	149	0	4	0	0	0	0	0	44
Geo-TüSL96	772.5	438.08	10	0	25	1	17	0	3	98	11	0	0	15	0	97	228	0	2	0	0	0	0	0	45
Geo-TüSL96	773.5	439.46	16	0	33	0	11	0	6	115	8	0	0	1	2	74	210	0	0	0	0	0	4	0	10
Geo-TüSL96	774.5	440.85	9	0	12	0	13	0	4	132	2	0	1	3	0	42	159	0	0	0	0	0	1	0	6
Geo-TüSL96	775.5	442.23	38	1	45	7	23	0	3	130	28	0	1	10	2	49	286	0	7	0	0	0	5	0	22
Geo-TüSL96	776.5	443.62	33	0	36	1	7	0	0	109	8	0	0	5	0	81	177	0	0	1	0	0	7	0	9
Geo-TüSL96	777.5	445.00	5	0	34	2	4	0	0	35	8	0	0	2	0	87	102	0	3	0	0	0	8	0	13
Geo-TüSL96	778.5	446.38	13	0	32	1	9	0	1	45	13	0	0	4	0	55	141	0	0	0	0	0	3	0	11
Geo-TüSL96	779.5	447.77	7	0	39	0	9	0	0	46	4	0	0	3	0	61	119	0	3	0	0	0	5	0	7

GeoTü-SL96, planktonic foraminifera counts 4/4

core	cmbsf	age	*Orbulina universa*	*Globigerinoides conglobatus*	*Globigerinoides ruber total*	*Globoturborotalita tenella*	*Globigerinoides sacc total*	*Sphaeroidinella dehiscens*	*siphonifera & calida*	*Globigerina bulloides*	*Globigerina falconensis*	*Beela digitata*	*Globoturborotalita rubescens*	*Turborotalita quinqueloba*	*Neogloboquadrina pachyderma L*	*Neogloboquadrina dutertrei*	*P/D integrade & N. pachyderma R*	*Pulleniatina obliquiloculata*	*Globorotalia inflata*	*Globorotalia truncatulinoides total*	*Globorotalia crassaformis*	*Globorotalia hirsuta*	*Globorotalia scitula*	*Globorotalia menardii & tumida*	*Globigerinita glutinata*
Geo-TüSL96	780.5	449.15	12	0	61	2	5	0	0	12	5	0	0	0	7	92	182	0	2	0	0	0	1	0	9
Geo-TüSL96	781.5	450.54	10	0	59	2	13	0	1	33	14	0	0	6	0	108	126	0	1	1	0	0	7	0	10
Geo-TüSL96	782.5	451.92	26	0	52	1	6	0	2	78	22	0	1	3	1	124	218	0	10	3	0	0	20	0	12
Geo-TüSL96	783.5	453.31	8	0	44	0	10	0	1	56	5	0	0	4	0	62	107	0	8	1	0	0	6	0	7
Geo-TüSL96	784.5	454.69	14	0	53	3	3	0	2	89	12	0	1	5	1	134	186	0	8	1	0	0	13	0	15
Geo-TüSL96	785.5	456.08	9	0	46	3	9	0	4	43	5	1	1	7	0	18	134	0	31	1	0	0	25	0	16
Geo-TüSL96	786.5	457.46	22	0	74	1	10	0	0	43	11	0	0	6	0	6	63	0	42	1	0	0	28	0	7
Geo-TüSL96	787.5	458.85	22	3	100	4	5	0	0	47	5	0	2	2	0	9	65	0	30	1	0	0	22	0	4
Geo-TüSL96	788.5	460.23	29	0	85	4	7	0	1	80	13	1	0	6	0	10	62	0	62	2	0	0	6	0	8
Geo-TüSL96	789.5	461.62	14	0	84	5	5	0	1	41	16	0	1	1	0	16	67	0	38	2	0	0	6	0	15
Geo-TüSL96	790.5	463.00	19	0	85	0	0	0	4	17	15	0	0	0	2	44	94	0	39	8	0	0	3	0	2
Geo-TüSL96	791.5	464.38	16	0	80	3	13	0	0	35	11	0	0	0	1	5	53	0	26	29	0	0	11	0	18
Geo-TüSL96	792.5	465.77	13	0	97	0	12	0	2	39	12	0	0	1	1	7	47	0	58	45	0	0	13	0	9

ODP Site 964, Holocene planktonic foraminifera counts, ANN results

Core	cm	age	Sample weight (g)	PF/g	Split	sum split (PF)	entire sum (PF)	ANN annual	ANN summer	ANN winter
RFHolo-964-1H1	0.5	0.00	0.019	44736.84	2	425	850	23.91	27.04	19.33
RFHolo-964-1H1	4.5	0.25	0.078	15487.18	4	302	1208	23.31	27.24	19.30
RFHolo-964-1H1	44.5	0.50	0.09	13044.44	2	587	1174	24.87	28.86	20.12
RFHolo-964-1H1	49.5	1.79	0.04	15100.00	2	302	604	23.99	27.80	19.78
RFHolo-964-1H1	54.5	3.07	0.049	28612.24	2	701	1402	24.41	27.34	19.07
RFHolo-964-1H1	59.5	4.36	0.021	83428.57	4	438	1752	22.99	23.35	17.08
RFHolo-964-1H1	64.5	5.64	0.082	16634.15	4	341	1364	23.98	27.24	19.74
RFHolo-964-1H1	69.5	6.93	0.092	16869.57	4	388	1552	23.96	26.68	19.69
RFHolo-964-1H1	72.5	7.36	0.071	17633.80	4	313	1252	22.55	26.86	17.38
RFHolo-964-1H1	73.5	7.79	0.201	6169.15	4	310	1240	23.12	27.25	18.43
RFHolo-964-1H1	74.5	8.21	0.148	12297.30	4	455	1820	23.72	27.40	18.96
RFHolo-964-1H1	77.5	8.64	0.037	35351.35	4	327	1308	22.99	26.58	18.65
RFHolo-964-1H1	78.5	9.07	0.083	22746.99	4	472	1888	24.25	27.79	19.40
RFHolo-964-1H1	79.5	9.50	0.026	31538.46	2	410	820	23.01	26.42	17.51
RFHolo-964-1H1	89.5	12.07	0.033	23151.52	2	382	764	22.10	24.59	18.10
RFHolo-964-1H1	94.5	13.36	0.129	14077.52	4	454	1816	22.24	26.42	16.45
RFHolo-964-1H1	99.5	14.82	0.055	30327.27	4	417	1668	21.67	26.17	15.62
RFHolo-964-1H1	114.5	16.11	0.077	16571.43	4	319	1276	16.10	17.98	9.97
RFHolo-964-1H1	119.5	17.39	0.078	18871.79	4	368	1472	20.45	22.91	15.13
RFHolo-964-1H1	124.5	18.68	0.199	6110.55	4	304	1216	21.06	24.34	16.41
RFHolo-964-1H1	129.5	19.97	0.094	12893.62	4	303	1212	19.38	21.85	13.67

ODP Site 964, Holocene planktonic foraminifera counts

Core	cm	age	Orbulina universa	Globigerinoides conglobatus	Globigerinoides ruber total	Globoturborotalita tenella	Globigerinoides sacc total	Sphaeroidinella dehiscens	siphonifera & calida	Globigerina bulloides	Globigerina falconensis	Beela digitata	Globoturborotalita rubescens	Turborotalita quinqueloba	Neogloboquadrina pachyderma L	Neogloboquadrina dutertrei	P/D integrade & N. pachyderma R	Pulleniatina obliquiloculata	Globorotalia inflata	Globorotalia truncatulinoides total	Globorotalia crassaformis	Globorotalia hirsuta	Globorotalia scitula	Globorotalia menardii & tumida	Globigerinita glutinata
RFHolo-964-1H1	0.5	0.00	11	0	305	1	26	0	10	45	2	4	0	0	0	1	8	0	2	7	0	0	0	0	3
RFHolo-964-1H1	4.5	0.25	25	0	202	1	16	0	8	33	5	1	0	0	0	0	7	0	2	2	0	0	0	0	0
RFHolo-964-1H1	44.5	0.50	54	0	410	0	50	0	19	33	2	6	0	2	0	0	5	0	4	1	0	0	0	0	1
RFHolo-964-1H1	49.5	1.79	15	0	225	2	23	0	11	11	2	3	0	1	0	0	2	0	0	0	0	0	0	0	7
RFHolo-964-1H1	54.5	3.07	39	0	425	4	55	0	36	79	13	12	0	0	0	0	5	0	2	3	0	0	0	0	24
RFHolo-964-1H1	59.5	4.36	24	0	170	2	36	0	34	63	13	23	0	0	0	0	13	0	36	0	0	0	0	0	23
RFHolo-964-1H1	64.5	5.64	21	0	167	4	35	0	32	45	4	4	1	0	0	0	7	0	2	0	0	0	0	0	19
RFHolo-964-1H1	69.5	6.93	16	0	173	7	34	0	50	58	3	4	2	0	0	1	12	0	0	0	0	0	0	0	28
RFHolo-964-1H1	72.5	7.36	26	0	161	6	5	0	21	52	2	6	0	0	0	3	2	0	3	0	0	0	0	0	26
RFHolo-964-1H1	73.5	7.79	29	0	159	6	14	0	15	48	2	1	1	0	0	0	4	0	3	0	0	0	0	0	28
RFHolo-964-1H1	74.5	8.21	30	0	327	7	2	0	11	45	1	0	2	1	0	0	4	0	10	0	0	0	0	0	15
RFHolo-964-1H1	77.5	8.64	18	0	215	1	8	0	16	44	4	2	0	0	0	0	0	0	5	0	0	0	0	0	14
RFHolo-964-1H1	78.5	9.07	16	0	258	2	41	0	19	37	1	1	0	0	0	0	3	0	14	3	0	0	0	0	68
RFHolo-964-1H1	79.5	9.50	2	0	245	1	7	0	1	46	2	0	0	1	0	0	2	0	41	17	0	0	0	0	45
RFHolo-964-1H1	89.5	12.07	0	0	201	2	2	0	1	26	3	1	0	5	1	16	74	0	46	0	0	0	0	0	4
RFHolo-964-1H1	94.5	13.36	1	0	208	3	0	0	1	43	3	0	0	9	0	9	48	0	56	42	0	0	0	0	31
RFHolo-964-1H1	99.5	14.82	1	0	187	0	2	0	0	69	1	0	0	5	0	3	27	0	25	84	0	0	3	0	10
RFHolo-964-1H1	114.5	16.11	0	0	107	0	0	0	1	61	4	0	0	0	0	20	81	0	1	0	0	0	9	0	35
RFHolo-964-1H1	119.5	17.39	0	0	133	1	0	0	0	59	5	0	0	0	0	31	69	0	0	0	0	0	39	0	31
RFHolo-964-1H1	124.5	18.68	0	0	124	0	1	0	0	32	3	0	0	1	0	23	72	0	0	0	0	0	30	0	18
RFHolo-964-1H1	129.5	19.97	0	0	112	1	0	0	0	46	1	0	0	0	0	29	77	0	0	0	0	0	16	0	21

leg	site	hole	core	type	section	cmbsf	age	δ13C pdb *G. rub*	δ18O pdb *G. rub*	δ13C pdb *G. bul.*	δ18O pdb *G. bul.*	ANN annual (T)	ANN season (T)	ANN summer (T)	ANN winter (T)
160	964	A	3	H	1	1714	341.55								
160	964	A	3	H	1	1715	341.80	1.17	1.93			19.49	8.25	23.90	16.30
160	964	A	3	H	1	1716	342.04	0.89	2.09			18.91	8.57	23.65	15.27
160	964	A	3	H	1	1717	342.29	0.54	1.98			19.01	8.90	23.98	15.34
160	964	A	3	H	1	1718	342.54	0.7435	1.5203			18.73	8.88	23.67	15.00
160	964	A	3	H	1	1719	342.78	0.95	1.88			19.11	8.41	23.88	15.63
160	964	A	3	H	1	1720	343.03	1.17	2.03			19.19	8.49	23.92	15.63
160	964	A	3	H	1	1721	343.28	0.76	1.88			19.26	8.86	24.33	15.67
160	964	A	3	H	1	1722	343.52	0.70	1.88			18.64	7.38	23.20	15.35
160	964	A	3	H	1	1723	343.77	1.0494	1.5976			18.08	7.29	22.25	14.65
160	964	A	3	H	1	1724	344.01	1.03	1.26			18.63	6.44	22.80	15.34
160	964	A	3	H	1	1725	344.26	0.67	1.04			19.33	8.69	24.15	15.45
160	964	A	3	H	1	1726	344.51	0.59	1.49			19.36	8.34	24.20	15.78
160	964	A	3	H	1	1727	344.75	0.35	1.78			17.71	6.27	21.85	14.50
160	964	A	3	H	1	1728	345.00	0.7291	1.2226			17.76	4.61	20.31	14.77
160	964	A	3	H	1	1729	345.25	0.30	1.55			17.43	5.50	20.87	14.08
160	964	A	3	H	1	1730	345.49	0.40	1.01			17.90	6.60	21.84	14.54
160	964	A	3	H	1	1731	345.74	0.54	0.72			18.82	9.04	23.87	15.07
160	964	A	3	H	1	1732	345.99	0.85	1.09			19.19	8.81	24.20	15.48
160	964	A	3	H	1	1733	346.23	0.6972	1.0848			19.29	9.29	24.49	15.44
160	964	A	3	H	1	1734	346.48	0.47	1.37			18.17	8.54	22.89	14.53
160	964	A	3	H	1	1735	346.72	0.43	0.90			18.84	9.60	24.05	14.61
160	964	A	3	H	1	1736	346.97	0.29	1.09			19.01	9.93	24.44	14.39
160	964	A	3	H	1	1739	347.22	0.30	1.17			19.34	9.82	24.31	15.05
160	964	A	3	H	1	1742	347.46	0.54	1.45			18.94	9.64	23.91	14.53
160	964	A	3	H	1	1744	347.71	0.33	1.40			19.29	9.84	24.69	14.56
160	964	A	3	H	1	1745	347.96	-0.46	1.49			19.44	9.77	24.40	15.04
160	964	A	3	H	1	1746	348.20	1.01	2.00			19.25	8.67	23.95	15.45
160	964	A	3	H	1	1747	348.45	1.05	1.96			19.21	8.65	23.81	15.16
160	964	A	3	H	1	1748	348.70	1.2865	1.9732			21.35	6.93	24.48	18.71
160	964	A	3	H	1	1749	348.94	1.24	2.12			19.49	8.68	24.21	15.61
160	964	A	3	H	1	1750	349.19	1.24	2.06			18.81	7.67	23.13	15.51
160	964	A	3	H	1	1755	349.43	0.27	1.65			18.52	6.85	22.58	15.15
160	964	A	3	H	1	1760	349.68	0.95	1.89			18.79	8.78	23.58	15.10
160	964	A	3	H	1	1761	349.93	0.52	1.81			19.06	9.19	24.23	15.35
160	964	A	3	H	1	1762	350.17	0.64	1.59			19.71	9.54	25.24	15.65
160	964	A	3	H	1	1763	350.42	0.5419	1.0482			19.32	8.81	24.07	15.64
160	964	A	3	H	1	1764	350.67	1.24	1.68			19.36	9.23	24.38	15.45
160	964	A	3	H	1	1765	350.91	0.59	1.44			19.30	9.11	24.17	15.43
160	964	A	3	H	1	1766	351.16	0.23	1.53			19.04	8.82	23.84	15.36
160	964	A	3	H	1	1767	351.41	0.56	1.36			19.19	8.86	23.92	15.16
160	964	A	3	H	1	1768	351.65	0.5811	1.559			18.80	8.62	23.45	15.14
160	964	A	3	H	1	1769	351.90	0.48	1.19			18.92	9.03	23.82	14.99
160	964	A	3	H	1	1770	352.14	0.26	1.27			19.10	9.52	24.16	15.07
160	964	A	3	H	1	1771	352.39	0.90	0.86			18.96	9.37	23.87	15.12
160	964	A	3	H	1	1772	352.64	0.15	0.79			18.88	8.92	23.48	15.35
160	964	A	3	H	1	1773	352.88	0.6292	0.7653			18.75	9.40	23.85	14.91
160	964	A	3	H	1	1774	353.13	0.29	0.90			19.04	9.63	23.89	14.96
160	964	A	3	H	1	1775	353.38	-0.06	1.16			19.06	9.81	24.11	14.81
160	964	A	3	H	1	1776	353.62	0.21	0.91			18.84	9.69	23.87	14.71
160	964	A	3	H	1	1777	353.87	0.44	1.30			18.91	9.65	24.00	14.86
160	964	A	3	H	1	1778	354.12	0.905	0.7625			19.18	9.31	23.84	15.28
160	964	A	3	H	1	1779	354.36	0.56	1.06			19.32	9.87	24.66	14.80
160	964	A	3	H	2	1780	354.61	0.70	1.59			18.57	9.49	24.04	14.55
160	964	A	3	H	2	1781	354.86	0.95	1.64			18.94	9.44	24.29	14.55
160	964	A	3	H	2	1782	355.10	0.74	1.56			19.39	9.82	25.21	15.31
160	964	A	3	H	2	1783	355.35	0.55	1.38			19.36	9.26	24.29	15.74
160	964	A	3	H	2	1784	355.59	0.7957	0.7454			18.73	9.67	23.86	14.47
160	964	A	3	H	2	1785	355.84	0.99	0.79			19.13	9.87	24.66	14.64
160	964	A	3	H	2	1786	356.09	0.75	0.95			18.93	9.81	24.35	14.40
160	964	A	3	H	2	1787	356.33	0.00	0.92			18.78	9.78	23.96	14.60
160	964	A	3	H	2	1788	356.58	0.01	1.03			18.66	9.99	24.02	14.11
160	964	A	3	H	2	1789	356.83	1.0244	0.3962			19.10	8.29	23.45	15.73
160	964	A	3	H	2	1790	357.07	-0.08	0.92			19.22	9.88	24.85	14.92
160	964	A	3	H	2	1791	357.32	-0.13	1.07			20.69	9.53	24.98	17.08
160	964	A	3	H	2	1792	357.57	0.16	1.20			19.79	8.80	24.28	16.19
160	964	A	3	H	2	1793	357.81	0.61	1.59			22.23	4.98	24.75	19.35
160	964	A	3	H	2	1794	358.06	0.7161	1.8102			23.04	4.74	24.65	19.98
160	964	A	3	H	2	1795	358.30	0.92	1.72			18.95	9.55	24.55	14.63
160	964	A	3	H	2	1796	358.55	1.17	1.27			19.91	9.64	24.71	15.90
160	964	A	3	H	2	1797	358.80	1.19	1.29			19.99	8.73	24.26	16.73

ODP Site 964, MIS 11, stable isotopic and ANN results 2/3

leg	site	hole	core	type	section	cmbsf	age	δ13C pdb *G. rub*	δ18O pdb *G. rub*	δ13C pdb *G. bul.*	δ18O pdb *G. bul.*	ANN annual (T)	ANN season (T)	ANN summer (T)	ANN winter (T)
160	964	A	3	H	2	1798	359.04	1.10	1.47			19.80	8.74	24.18	16.42
160	964	A	3	H	2	1799	359.29	1.1071	1.5014			19.67	7.27	23.56	16.78
160	964	A	3	H	2	1800	359.54	0.98	1.32			19.52	9.02	23.77	16.10
160	964	A	3	H	2	1802	359.78	0.65	1.22			19.61	7.34	23.41	16.22
160	964	A	3	H	2	1803	360.03	0.61	1.28			19.63	8.49	23.84	15.93
160	964	A	3	H	2	1804	360.28	1.191	1.2146			18.43	5.50	21.82	15.62
160	964	A	3	H	2	1805	360.52	0.58	1.57			19.12	8.56	23.34	15.68
160	964	A	3	H	2	1806	360.77	0.94	1.13			18.65	6.52	22.37	15.55
160	964	A	3	H	2	1807	361.01	0.45	1.18			18.65	6.51	22.08	15.50
160	964	A	3	H	2	1808	361.26	0.65	1.11			18.69	4.43	21.77	15.88
160	964	A	3	H	2	1809	361.51	0.2024	1.0031			18.29	4.54	20.21	16.02
160	964	A	3	H	2	1810	361.75	0.39	1.04			19.54	6.37	23.11	16.43
160	964	A	3	H	2	1811	362.00	0.42	0.82			20.35	6.66	24.08	17.04
160	964	A	3	H	2	1812	362.70	0.25	0.63			20.68	5.70	24.31	17.55
160	964	A	3	H	2	1813	363.40	0.54	0.73			20.03	6.98	24.13	16.42
160	964	A	3	H	2	1814	364.10	0.3318	0.8476			21.60	4.01	24.36	19.00
160	964	A	3	H	2	1815	364.81	0.49	0.64			20.55	8.57	25.10	16.84
160	964	A	3	H	2	1816	365.51	0.64	0.56			20.71	4.48	23.86	17.90
160	964	A	3	H	2	1817	366.21	0.37	0.74			19.68	7.07	23.78	16.43
160	964	A	3	H	2	1818	366.91	0.57	0.84			19.90	6.80	23.52	16.78
160	964	A	3	H	2	1819	367.61	0.8017	0.7278			20.78	4.35	22.97	18.64
160	964	A	3	H	2	1820	368.31	0.47	0.55			21.12	3.87	23.82	18.69
160	964	A	3	H	2	1821	369.01	0.43	0.69			21.68	3.85	24.06	19.06
160	964	A	3	H	2	1822	369.72	0.17	0.63			21.37	3.93	23.82	18.97
160	964	A	3	H	2	1823	370.42	0.52	0.67			21.74	3.80	23.96	19.29
160	964	A	3	H	2	1824	371.12	0.1193	0.643			20.80	5.45	23.84	18.20
160	964	A	3	H	2	1825	371.82	0.23	0.45			21.43	4.48	23.75	19.06
160	964	A	3	H	2	1826	372.52	0.37	0.47			21.88	4.29	23.85	19.36
160	964	A	3	H	2	1827	373.22	0.23	-0.01			20.58	6.52	23.85	17.79
160	964	A	3	H	2	1828	373.93	0.53	-0.22			22.13	4.71	24.17	19.50
160	964	A	3	H	2	1829	374.63	0.3192	0.1423			22.90	5.58	24.49	20.30
160	964	A	3	H	2	1830	375.33	-0.15	0.47			21.20	7.18	24.45	18.26
160	964	A	3	H	2	1831	376.03	0.02	-0.01			21.78	6.75	24.67	18.50
160	964	A	3	H	2	1832	376.73	-0.06	0.41			20.24	9.29	24.60	16.46
160	964	A	3	H	2	1833	377.43	0.06	0.37			20.06	9.12	24.28	16.39
160	964	A	3	H	2	1834	378.13	0.2464	0.5707			19.39	9.76	24.27	14.99
160	964	A	3	H	2	1835	378.84	0.00	0.48			20.23	9.10	24.29	16.48
160	964	A	3	H	2	1836	379.54	-0.02	0.47			19.49	9.52	24.09	15.39
160	964	A	3	H	2	1837	380.24	0.50	0.07			20.97	8.52	24.58	17.36
160	964	A	3	H	2	1838	380.94	0.32	0.38			20.20	9.77	24.82	15.86
160	964	A	3	H	2	1839	381.64	-0.0287	0.4109			19.32	8.59	23.61	15.64
160	964	A	3	H	2	1840	382.34	0.31	0.71			19.87	8.33	24.16	16.08
160	964	A	3	H	2	1841	383.04	0.04	0.62			19.38	8.91	23.97	15.50
160	964	A	3	H	2	1842	383.75	0.08	0.40			19.25	8.82	23.77	15.37
160	964	A	3	H	2	1843	384.45	0.36	0.59			19.23	9.41	24.00	15.22
160	964	A	3	H	2	1844	385.15	0.5289	0.5834			19.69	9.14	24.42	15.63
160	964	A	3	H	2	1845	385.85	0.18	0.56			20.25	9.63	25.08	15.87
160	964	A	3	H	2	1846	386.55	0.18	0.79			20.03	9.05	24.48	16.09
160	964	A	3	H	2	1847	387.25	0.31	0.69			20.08	9.49	24.83	15.92
160	964	A	3	H	2	1848	387.96	-0.01	0.69			19.37	8.41	23.87	15.57
160	964	A	3	H	2	1849	388.66	0.1818	0.5229			18.83	4.79	21.32	16.09
160	964	A	3	H	2	1850	389.36	0.22	0.82			19.37	5.81	23.01	15.96
160	964	A	3	H	2	1851	390.06	0.29	0.21			18.65	6.69	22.55	15.06
160	964	A	3	H	2	1852	390.76	-0.01	0.76			17.93	5.93	21.56	14.56
160	964	A	3	H	2	1858	391.46	-0.03	0.71			19.41	6.11	23.42	15.77
160	964	A	3	H	2	1864	392.16	0.3178	0.6289			20.34	5.20	24.03	17.05
160	964	A	3	H	2	1866	392.87	-0.18	0.94			17.54	5.61	21.23	14.08
160	964	A	3	H	2	1867	393.57	-0.33	0.83			18.27	5.70	22.19	14.98
160	964	A	3	H	2	1868	394.27	0.10	0.68			18.63	7.11	23.03	15.16
160	964	A	3	H	2	1869	394.97	0.1893	0.6868			19.28	6.07	23.45	16.08
160	964	A	3	H	2	1870	395.67	-0.13	0.70			18.08	6.31	22.13	14.68
160	964	A	3	H	2	1871	396.37	-0.08	0.59			18.72	6.52	23.01	15.39
160	964	A	3	H	2	1872	397.07	-0.16	0.61			18.09	5.66	22.01	15.00
160	964	A	3	H	2	1873	397.78	-0.27	0.75			19.05	8.37	23.97	15.43
160	964	A	3	H	2	1874	398.48	0.5555	0.2183			19.44	8.05	24.12	15.99
160	964	A	3	H	2	1875	399.18	-0.54	0.62			19.44	7.40	24.07	16.21
160	964	A	3	H	2	1876	399.88	-0.92	0.19			18.85	8.36	23.44	15.25
160	964	A	3	H	2	1877	400.58	-1.15	-0.46			18.77	8.61	23.57	15.15
160	964	A	3	H	2	1878	401.28	-1.01	0.02			19.02	8.52	23.82	15.54
160	964	A	3	H	2	1879	401.99	-0.5529	0.0751	-2.10	0.78	19.30	7.94	23.84	15.97
160	964	A	3	H	2	1880	402.69					19.11	8.53	23.66	15.60

ODP Site 964, MIS 11, stable isotopic and ANN results 3/3

leg	site	hole	core	type	section	cmbsf	age	δ13C pdb *G. rub*	δ18O pdb *G. rub*	δ13C pdb *G. bul.*	δ18O pdb *G. bul.*	ANN annual (T)	ANN season (T)	ANN summer (T)	ANN winter (T)
160	964	A	3	H	2	1881	403.39	-0.40	-0.22			18.57	8.68	23.52	14.94
160	964	A	3	H	2	1882	404.09	-0.81	-0.44			19.12	8.70	23.97	15.18
160	964	A	3	H	2	1883	404.79	-0.23	-1.10			17.89	8.77	23.06	14.27
160	964	A	3	H	2	1884	405.49	0.0301	-1.7222	-1.66	-0.10	17.54	9.93	22.45	13.92
160	964	A	3	H	2	1885	406.19	0.17	-0.47			18.32	8.92	23.46	14.69
160	964	A	3	H	2	1886	406.90	-0.02	-0.60			18.75	7.91	23.15	15.24
160	964	A	3	H	2	1887	407.60	0.18	-1.06	-1.78	-0.64	19.00	9.16	24.20	14.93
160	964	A	3	H	2	1888	408.30	0.23	-1.46			18.73	9.21	24.13	14.87
160	964	A	3	H	2	1889	409.00	0.4446	0.1504	-1.41	1.26	17.97	8.39	22.83	14.38
160	964	A	3	H	2	1890	410.38	0.44	0.74	-1.40	1.06	15.34	7.22	19.18	12.07
160	964	A	3	H	2	1891	411.77			-1.06	1.24	13.35	6.88	17.10	9.72
160	964	A	3	H	2	1892	413.15			-1.42	0.45	13.55	6.87	17.10	9.91
160	964	A	3	H	2	1893	414.54			-1.55	0.75	12.56	6.81	15.93	9.13
160	964	A	3	H	2	1894	415.92			-1.50	0.94	13.57	6.82	16.94	10.45
160	964	A	3	H	2	1895	417.31			-1.28	0.58	13.60	6.75	17.15	9.73
160	964	A	3	H	2	1896	418.69			-1.41	0.34	15.19	6.68	19.06	10.87
160	964	A	3	H	2	1897	420.08			-1.54	0.26	15.57	5.95	19.63	10.59
160	964	A	3	H	2	1898	421.46			-1.31	0.71	16.09	6.00	20.25	11.22
160	964	A	3	H	2	1899	422.85			-1.39	0.67	14.47	6.40	18.40	9.89
160	964	A	3	H	2	1900	424.23			-1.42	0.65	15.04	6.19	19.08	10.20
160	964	A	3	H	2	1901	425.62			-1.63	-0.27	14.89	6.65	18.90	10.39
160	964	A	3	H	2	1902	427.00			-1.08	1.05	13.46	6.38	17.02	9.12
160	964	A	3	H	2	1903	427.76			-0.81	1.42	10.74	6.16	13.49	7.68
160	964	A	3	H	2	1904	429.04			-0.67	1.48	11.23	6.91	14.73	8.40
160	964	A	3	H	2	1905	430.32			-0.81	1.48	12.95	6.87	16.80	8.81
160	964	A	3	H	2	1906	431.60			-0.65	1.68	10.69	5.95	13.34	7.65
160	964	A	3	H	2	1907	432.88			-0.78	1.64	11.51	6.42	14.59	8.45
160	964	A	3	H	2	1908	434.15			-0.44	1.83	11.24	6.46	14.28	8.20
160	964	A	3	H	2	1909	435.43			-1.03	1.71	10.05	5.54	12.67	7.59
160	964	A	3	H	2	1910	436.71					10.36	5.49	12.90	7.90
160	964	A	3	H	2	1911	437.99			-0.90	1.60	11.23	6.49	13.91	7.80
160	964	A	3	H	2	1912	439.27			-0.72	1.78	11.89	6.89	15.22	8.83
160	964	A	3	H	2	1913	440.55			-0.68	1.74	10.87	6.25	14.17	8.26
160	964	A	3	H	2	1914	441.83			-0.83	1.85	8.87	4.77	11.63	6.84
160	964	A	3	H	2	1915	443.11			-0.78	1.77	9.66	5.36	12.62	7.50
160	964	A	3	H	2	1916	444.38			-0.97	1.72	9.80	5.66	12.93	7.62
160	964	A	3	H	2	1917	445.66			-0.90	1.67	10.24	5.93	13.29	7.82
160	964	A	3	H	2	1918	446.94			-0.65	1.73	9.53	5.84	12.82	7.42
160	964	A	3	H	2	1919	448.22			-0.71	1.89	9.07	5.01	11.94	7.28
160	964	A	3	H	2	1920	449.50			-0.67	1.98	10.85	7.55	14.90	8.19
160	964	A	3	H	2	1921	450.78			-0.56	1.97	10.40	6.05	13.50	8.05
160	964	A	3	H	2	1922	452.06			-0.43	2.00	10.85	6.95	14.26	8.24
160	964	A	3	H	2	1923	453.34			-0.66	2.00	10.54	7.15	14.11	8.07
160	964	A	3	H	2	1924	454.62			-0.85	2.21	11.47	5.86	14.32	8.81
160	964	A	3	H	2	1926	455.89			-0.65	2.29	9.90	5.65	12.80	7.84
160	964	A	3	H	3	1928	457.17			-0.67	2.33	9.93	5.29	12.68	7.87
160	964	A	3	H	3	1930	458.45			-0.91	2.41	12.33	6.89	15.65	9.06
160	964	A	3	H	3	1932	459.73			-0.86	2.31	9.52	4.40	11.98	7.62
160	964	A	3	H	3	1933	461.01			-0.49	2.19	9.77	4.36	12.13	7.71
160	964	A	3	H	3	1934	462.29			-0.64	2.26	9.09	4.64	11.57	7.09
160	964	A	3	H	3	1935	463.57			-0.35	2.22	9.30	4.45	11.77	7.33
160	964	A	3	H	3	1936	464.85			-0.28	2.19	10.46	5.75	13.32	8.15
160	964	A	3	H	3	1937	466.13			-0.20	2.15	11.76	6.53	14.86	9.05
160	964	A	3	H	3	1938	467.40			-0.54	1.93	12.09	6.87	15.61	9.33
160	964	A	3	H	3	1939	468.68					10.92	6.33	14.19	8.59
160	964	A	3	H	3	1940	469.96			-1.07	2.14	10.94	6.08	13.91	8.65
160	964	A	3	H	3	1941	471.24			-1.18	2.24	10.35	5.81	13.35	8.09
160	964	A	3	H	3	1942	472.52			-1.31	2.11	11.86	6.85	15.26	9.11
160	964	A	3	H	3	1943	473.80			-0.47	2.33	11.54	6.11	14.51	8.85
160	964	A	3	H	3	1944	475.08			-0.75	1.90	11.99	6.63	15.26	9.25
160	964	A	3	H	3	1945	476.36			-0.58	1.96	12.38	6.85	15.74	9.44
160	964	A	3	H	3	1946	477.64			-0.41	1.99	14.24	7.85	18.31	10.73
160	964	A	3	H	3	1947	478.91			-0.84	1.74	12.25	7.44	16.12	9.37
160	964	A	3	H	3	1948	480.19			-0.29	1.97	12.33	7.73	16.47	9.34
160	964	A	3	H	3	1949	481.47			-0.43	2.22	13.46	5.85	16.24	10.77

ODP Site 964, MIS 11, alkenone, planktonic foraminifera counts, benthic foraminifera counts 1/3

leg	site	hole	core	type	section	cmbsf	age	T[°C] alkenones	sum alkenones (ng/g)	dry weight sed. (g)	sum planktonic forams/g	split	sum in split	sum total	No. benthische forams	benthic in g/sediment
160	964	A	3	H	1	1714	341.55	11.9	51							
160	964	A	3	H	1	1715	341.80			4.03	1302.23	16	328	5248		
160	964	A	3	H	1	1716	342.04			3.58	1271.51	8	569	4552		
160	964	A	3	H	1	1717	342.29			4.17	2079.62	16	542	8672		
160	964	A	3	H	1	1718	342.54	12.3	75	3.59	684.12	8	307	2456	1	0.28
160	964	A	3	H	1	1719	342.78			4.22	1194.31	16	315	5040		
160	964	A	3	H	1	1720	343.03			3.87	1260.98	16	305	4880		
160	964	A	3	H	1	1721	343.28			4.13	732.20	8	378	3024		
160	964	A	3	H	1	1722	343.52			3.71	1246.36	8	578	4624		
160	964	A	3	H	1	1723	343.77			3.18	1771.07	16	352	5632	0	0.00
160	964	A	3	H	1	1724	344.01	11.8	78	4.38	1095.89	16	300	4800		
160	964	A	3	H	1	1725	344.26			4.32	746.30	8	403	3224		
160	964	A	3	H	1	1726	344.51			3.45	955.36	8	412	3296		
160	964	A	3	H	1	1727	344.75			3.86	868.39	8	419	3352		
160	964	A	3	H	1	1728	345.00			3.72	1892.47	16	440	7040	1	0.27
160	964	A	3	H	1	1729	345.25	11.4	76	3.72	2873.12	32	334	10688		
160	964	A	3	H	1	1730	345.49			3.49	2622.35	16	572	9152		
160	964	A	3	H	1	1731	345.74			3.99	2053.13	16	512	8192		
160	964	A	3	H	1	1732	345.99			4.38	2107.76	16	577	9232		
160	964	A	3	H	1	1733	346.23			2.4	3640.00	16	546	8736	0	0.00
160	964	A	3	H	1	1734	346.48	15.8	65	4.29	392.85	0.1875	316	1685.33		
160	964	A	3	H	1	1735	346.72			3.63	1604.41	16	364	5824		
160	964	A	3	H	1	1736	346.97			3.69	1990.24	16	459	7344		
160	964	A	3	H	1	1739	347.22			3.38	1216.57	8	514	4112		
160	964	A	3	H	1	1742	347.46			3.62	1498.34	16	339	5424		
160	964	A	3	H	1	1744	347.71	14.4	64	3.42	1047.95	8	448	3584		
160	964	A	3	H	1	1745	347.96			3.59	1283.57	16	288	4608		
160	964	A	3	H	1	1746	348.20			3.58	858.10	8	384	3072		
160	964	A	3	H	1	1747	348.45			3.50	928.00	8	406	3248		
160	964	A	3	H	1	1748	348.70			3.48	1009.20	8	439	3512	0	0.00
160	964	A	3	H	1	1749	348.94	13.8	35	4.22	1169.67	8	617	4936		
160	964	A	3	H	1	1750	349.19			3.96	622.22	8	308	2464		
160	964	A	3	H	1	1755	349.43			4.61	1016.92	8	586	4688		
160	964	A	3	H	1	1760	349.68			3.85	1550.13	16	373	5968		
160	964	A	3	H	1	1761	349.93			3.36	1909.52	16	401	6416		
160	964	A	3	H	1	1762	350.17			3.92	1514.29	16	371	5936		
160	964	A	3	H	1	1763	350.42			3.78	2582.01	32	305	9760	2	0.53
160	964	A	3	H	1	1764	350.67	13.8	71	3.77	2571.88	32	303	9696		
160	964	A	3	H	1	1765	350.91			3.85	2152.73	16	518	8288		
160	964	A	3	H	1	1766	351.16			3.89	1530.08	16	372	5952		
160	964	A	3	H	1	1767	351.41			3.60	1515.56	8	682	5456		
160	964	A	3	H	1	1768	351.65			3.93	2768.45	32	340	10880	1	0.25
160	964	A	3	H	1	1769	351.90	15.3	46	4.25	1426.82	16	379	6064		
160	964	A	3	H	1	1770	352.14			3.34	2361.68	16	493	7888		
160	964	A	3	H	1	1771	352.39			3.89	2994.34	32	364	11648		
160	964	A	3	H	1	1772	352.64			3.65	2025.21	16	462	7392		
160	964	A	3	H	1	1773	352.88	16.1	48	3.17	2064.35	16	409	6544	1	0.32
160	964	A	3	H	1	1774	353.13			3.49	1386.82	8	605	4840		
160	964	A	3	H	1	1775	353.38			4.41	1607.26	16	443	7088		
160	964	A	3	H	1	1776	353.62			3.51	1540.74	8	676	5408		
160	964	A	3	H	1	1777	353.87	15.9	43	3.37	1675.96	16	353	5648		
160	964	A	3	H	1	1778	354.12			3.45	1720.58	16	371	5936	0	0.00
160	964	A	3	H	1	1779	354.36			3.40	2244.71	16	477	7632		
160	964	A	3	H	2	1780	354.61	15.5	19	4.35	923.22	8	502	4016		
160	964	A	3	H	2	1781	354.86			3.68	982.61	8	452	3616		
160	964	A	3	H	2	1782	355.10			4.76	510.92	8	304	2432		
160	964	A	3	H	2	1783	355.35			4.19	895.47	8	469	3752		
160	964	A	3	H	2	1784	355.59	15.6	15	3.43	1562.68	16	335	5360	1	0.29
160	964	A	3	H	2	1785	355.84			4.36	2568.81	32	350	11200		
160	964	A	3	H	2	1786	356.09			2.92	2323.29	16	424	6784		
160	964	A	3	H	2	1787	356.33			4.58	2015.72	16	577	9232		
160	964	A	3	H	2	1788	356.58			4.22	2479.62	32	327	10464		
160	964	A	3	H	2	1789	356.83	16.5	30	3.34	1944.91	16	406	6496	1	0.30
160	964	A	3	H	2	1790	357.07			4.05	1331.36	16	337	5392		
160	964	A	3	H	2	1791	357.32			3.93	1127.74	8	554	4432		
160	964	A	3	H	2	1792	357.57			4.33	779.68	8	422	3376		
160	964	A	3	H	2	1793	357.81			3.85	806.23	8	388	3104		
160	964	A	3	H	2	1794	358.06	15.8	22	3.78	1081.48	8	511	4088	0	0.00
160	964	A	3	H	2	1795	358.30			4.02	678.61	8	341	2728		
160	964	A	3	H	2	1796	358.55			4.14	2388.41	32	309	9888		
160	964	A	3	H	2	1797	358.80			4.13	3502.18	32	452	14464		

ODP Site 964, MIS 11, alkenone, planktonic foraminifera counts, benthic foraminifera counts 2/3

leg	site	hole	core	type	section	cmbsf	age	T[°C] alkenones	sum alkenones (ng/g)	dry weight sed. (g)	sum planktonic forams/g	split	sum in split	sum total	No. benthische forams	benthic in g/sediment
160	964	A	3	H	2	1798	359.04			3.82	2990.58	32	357	11424		
160	964	A	3	H	2	1799	359.29	15.9	18	4.09	1459.17	16	373	5968	5	1.22
160	964	A	3	H	2	1800	359.54			3.98	1415.08	16	352	5632		
160	964	A	3	H	2	1802	359.78			2.13	1130.52	8	301	2408		
160	964	A	3	H	2	1803	360.03			3.47	1517.00	16	329	5264		
160	964	A	3	H	2	1804	360.28	14.9	58	3.83	1526.89	8	731	5848	2	0.52
160	964	A	3	H	2	1805	360.52			4.29	1801.40	16	483	7728		
160	964	A	3	H	2	1806	360.77			4.22	1910.90	16	504	8064		
160	964	A	3	H	2	1807	361.01			4.25	1938.82	16	515	8240		
160	964	A	3	H	2	1808	361.26			4.06	1536.95	16	390	6240		
160	964	A	3	H	2	1809	361.51	16.9	18	4	1162.00	8	581	4648	0	0.00
160	964	A	3	H	2	1810	361.75			4.33	1066.05	8	577	4616		
160	964	A	3	H	2	1811	362.00			4.30	1503.26	16	404	6464		
160	964	A	3	H	2	1812	362.70			3.90	1513.85	16	369	5904		
160	964	A	3	H	2	1813	363.40			4.28	1401.87	16	375	6000		
160	964	A	3	H	2	1814	364.10	20.6	15	4.08	1103.92	8	563	4504	0	0.00
160	964	A	3	H	2	1815	364.81			4.33	1200.92	16	325	5200		
160	964	A	3	H	2	1816	365.51			4.82	1443.98	16	435	6960		
160	964	A	3	H	2	1817	366.21			3.88	1340.21	16	325	5200		
160	964	A	3	H	2	1818	366.91			4.50	1941.33	16	546	8736		
160	964	A	3	H	2	1819	367.61			4.08	1564.71	16	399	6384	0	0.00
160	964	A	3	H	2	1820	368.31			4.32	1307.41	16	353	5648		
160	964	A	3	H	2	1821	369.01			3.97	1624.18	16	402	6448		
160	964	A	3	H	2	1822	369.72			3.33	1585.59	16	330	5280		
160	964	A	3	H	2	1823	370.42			3.67	1778.75	16	408	6528		
160	964	A	3	H	2	1824	371.12	19.3	19	3.96	1709.09	16	423	6768	0	0.00
160	964	A	3	H	2	1825	371.82			4.62	2271.86	32	328	10496		
160	964	A	3	H	2	1826	372.52			3.44	4725.58	32	508	16256		
160	964	A	3	H	2	1827	373.22			4.39	3163.55	32	434	13888		
160	964	A	3	H	2	1828	373.93			4.18	3751.20	32	490	15680		
160	964	A	3	H	2	1829	374.63	20.0	16	3.13	3271.57	32	320	10240	0	0.00
160	964	A	3	H	2	1830	375.33			3.64	5292.31	64	301	19264		
160	964	A	3	H	2	1831	376.03			3.52	5709.09	64	314	20096		
160	964	A	3	H	2	1832	376.73			3.62	3730.39	32	422	13504		
160	964	A	3	H	2	1833	377.43			3.67	4202.72	32	482	15424		
160	964	A	3	H	2	1834	378.13			3.33	3449.85	32	359	11488	1	0.30
160	964	A	3	H	2	1835	378.84			4.10	3941.46	32	505	16160		
160	964	A	3	H	2	1836	379.54			3.92	2873.47	32	352	11264		
160	964	A	3	H	2	1837	380.24			4.34	2293.09	16	622	9952		
160	964	A	3	H	2	1838	380.94			3.78	2298.41	16	543	8688		
160	964	A	3	H	2	1839	381.64	21.1	14	3.84	2258.33	32	271	8672	2	0.52
160	964	A	3	H	2	1840	382.34			3.25	888.62	8	361	2888		
160	964	A	3	H	2	1841	383.04			3.81	2729.66	32	325	10400		
160	964	A	3	H	2	1842	383.75			4.13	1875.06	16	484	7744		
160	964	A	3	H	2	1843	384.45			4.24	1486.79	16	394	6304		
160	964	A	3	H	2	1844	385.15	20.5	15	3.95	2349.37	16	580	9280	0	0.00
160	964	A	3	H	2	1845	385.85			3.97	1765.24	16	438	7008		
160	964	A	3	H	2	1846	386.55			3.73	2342.09	16	546	8736		
160	964	A	3	H	2	1847	387.25			4.40	2283.64	32	314	10048		
160	964	A	3	H	2	1848	387.96			4.29	977.16	8	524	4192		
160	964	A	3	H	2	1849	388.66	19.9	15	4.08	1709.80	16	436	6976	1	0.25
160	964	A	3	H	2	1850	389.36			3.93	2206.62	16	542	8672		
160	964	A	3	H	2	1851	390.06			4.68	3494.02	32	511	16352		
160	964	A	3	H	2	1852	390.76			3.66	673.22	4	616	2464		
160	964	A	3	H	2	1858	391.46			4.16	2307.69	32	300	9600		
160	964	A	3	H	2	1864	392.16			4.69	2285.71	32	335	10720	2	0.43
160	964	A	3	H	2	1866	392.87			3.67	2886.10	32	331	10592		
160	964	A	3	H	2	1867	393.57			3.65	4585.21	32	523	16736		
160	964	A	3	H	2	1868	394.27			4.59	4364.27	32	626	20032		
160	964	A	3	H	2	1869	394.97			3.6	3955.56	32	445	14240	2	0.56
160	964	A	3	H	2	1870	395.67			4.34	2270.97	32	308	9856		
160	964	A	3	H	2	1871	396.37			3.92	3551.02	32	435	13920		
160	964	A	3	H	2	1872	397.07			4.15	4310.36	32	559	17888		
160	964	A	3	H	2	1873	397.78			4.09	4264.06	32	545	17440		
160	964	A	3	H	2	1874	398.48			4.41	3134.69	32	432	13824	0	0.00
160	964	A	3	H	2	1875	399.18			3.64	5046.15	32	574	18368		
160	964	A	3	H	2	1876	399.88			4.55	2468.57	32	351	11232		
160	964	A	3	H	2	1877	400.58			2.61	6068.97	32	495	15840		
160	964	A	3	H	2	1878	401.28			3.77	1566.05	16	369	5904		
160	964	A	3	H	2	1879	401.99			4.35	4994.94	32	679	21728	0	0.00
160	964	A	3	H	2	1880	402.69			3.66	4135.52	32	473	15136		

ODP Site 964, MIS 11, alkenone, planktonic foraminifera counts, benthic foraminifera counts 3/3

leg	site	hole	core	type	section	cmbsf	age	T[°C] alkenones	sum alkenones (ng/g)	dry weight sed. (g)	sum planktonic forams/g	split	sum in split	sum total	No. benthische forams	benthic in g/sediment
160	964	A	3	H	2	1881	403.39			3.21	5383.18	32	540	17280		
160	964	A	3	H	2	1882	404.09			3.81	6567.98	64	391	25024		
160	964	A	3	H	2	1883	404.79			3.77	4184.62	32	493	15776		
160	964	A	3	H	2	1884	405.49	20.2	374	2.59	966.80	8	313	2504	0	0.00
160	964	A	3	H	2	1885	406.19			4.15	1372.53	16	356	5696		
160	964	A	3	H	2	1886	406.90	17.6	2940	2.78	4972.66	32	432	13824		
160	964	A	3	H	2	1887	407.60			3.56	2840.45	32	316	10112		
160	964	A	3	H	2	1888	408.30			3.83	3166.58	32	379	12128		
160	964	A	3	H	2	1889	409.00	17.3	1122	4.10	3278.05	32	420	13440	246	60.00
160	964	A	3	H	2	1890	410.38			4.07	3538.08	32	450	14400		
160	964	A	3	H	2	1891	411.77			4.06	5462.07	32	693	22176		
160	964	A	3	H	2	1892	413.15			3.53	5602.27	64	309	19776		
160	964	A	3	H	2	1893	414.54			4.02	5460.70	64	343	21952		
160	964	A	3	H	2	1894	415.92	13.1	246	3.87	6234.63	64	377	24128	371	95.87
160	964	A	3	H	2	1895	417.31			4.25	5120.00	64	340	21760		
160	964	A	3	H	2	1896	418.69			4.47	4452.80	64	311	19904		
160	964	A	3	H	2	1897	420.08			3.69	3061.25	32	353	11296		
160	964	A	3	H	2	1898	421.46			3.61	4210.53	32	475	15200		
160	964	A	3	H	2	1899	422.85	12.2	167	3.93	10585.24	64	650	41600	205	52.16
160	964	A	3	H	2	1900	424.23			3.57	7206.72	64	402	25728		
160	964	A	3	H	2	1901	425.62			4.05	7237.53	64	458	29312		
160	964	A	3	H	2	1902	427.00			3.98	6625.13	64	412	26368		
160	964	A	3	H	2	1903	427.76			3.17	3977.29	32	394	12608		
160	964	A	3	H	2	1904	429.04			4.11	6804.87	64	437	27968	166	40.39
160	964	A	3	H	2	1905	430.32	11.0	115	4.54	6977.97	64	495	31680		
160	964	A	3	H	2	1906	431.60			3.63	5782.92	64	328	20992		
160	964	A	3	H	2	1907	432.88			4.21	4590.97	64	302	19328		
160	964	A	3	H	2	1908	434.15			3.71	5330.46	64	309	19776		
160	964	A	3	H	2	1909	435.43	9.6	141	4.12	2578.64	32	332	10624	102	24.76
160	964	A	3	H	2	1910	436.71			3.54	173.45	2	307	614		
160	964	A	3	H	2	1911	437.99			4.53	6498.90	64	460	29440		
160	964	A	3	H	2	1912	439.27			3.37	7007.72	64	369	23616		
160	964	A	3	H	2	1913	440.55			4.10	9490.73	128	304	38912		
160	964	A	3	H	2	1914	441.83	10.2	120	3.74	6057.75	64	354	22656	163	43.58
160	964	A	3	H	2	1915	443.11			3.72	8963.44	64	521	33344		
160	964	A	3	H	2	1916	444.38			4.30	9049.30	128	304	38912		
160	964	A	3	H	2	1917	445.66			3.90	9321.03	64	568	36352		
160	964	A	3	H	2	1918	446.94			3.31	8990.94	64	465	29760		
160	964	A	3	H	2	1919	448.22	9.4	118	4.25	9216.00	128	306	39168	71	16.71
160	964	A	3	H	2	1920	449.50			4.06	9521.18	128	302	38656		
160	964	A	3	H	2	1921	450.78			4.26	10005.63	128	333	42624		
160	964	A	3	H	2	1922	452.06			3.70	8371.89	64	483	30976		
160	964	A	3	H	2	1923	453.34			4.01	6862.84	64	430	27520		
160	964	A	3	H	2	1924	454.62	9.6	71	3.49	7096.85	64	387	24768	69	19.77
160	964	A	3	H	2	1926	455.89			3.95	5768.10	64	356	22784		
160	964	A	3	H	3	1928	457.17	7.6	116	3.31	8584.89	64	444	28416		
160	964	A	3	H	3	1930	458.45			2.70	3146.67	16	531	8496		
160	964	A	3	H	3	1932	459.73			4.81	2308.52	32	347	11104		
160	964	A	3	H	3	1933	461.01			4.23	2651.54	16	701	11216		
160	964	A	3	H	3	1934	462.29	9.4	49	4.01	8267.33	128	259	33152	89	22.19
160	964	A	3	H	3	1935	463.57			4.31	5909.98	64	398	25472		
160	964	A	3	H	3	1936	464.85			3.91	4157.54	32	508	16256		
160	964	A	3	H	3	1937	466.13			3.67	3976.02	32	456	14592		
160	964	A	3	H	3	1938	467.40			4.63	1807.34	16	523	8368		
160	964	A	3	H	3	1939	468.68	8.1	127	3.81	2040.94	16	486	7776	6	1.57
160	964	A	3	H	3	1940	469.96			4.24	2135.85	16	566	9056		
160	964	A	3	H	3	1941	471.24			4.49	4304.68	64	302	19328		
160	964	A	3	H	3	1942	472.52			4.03	4256.08	32	536	17152		
160	964	A	3	H	3	1943	473.80			4.12	3743.69	32	482	15424		
160	964	A	3	H	3	1944	475.08			3.36	2585.71	16	543	8688	37	11.01
160	964	A	3	H	3	1945	476.36			3.94	4767.51	32	587	18784		
160	964	A	3	H	3	1946	477.64			4.14	7482.13	64	484	30976		
160	964	A	3	H	3	1947	478.91			3.17	6823.97	64	338	21632		
160	964	A	3	H	3	1948	480.19			3.75	6178.13	64	362	23168		
160	964	A	3	H	3	1949	481.47			3.99	5060.65	32	631	20192	45	11.28

ODP Site 964, MIS 11, planktonic foraminifera counts 1/3

leg	site	hole	core	type	section	cmbsf	age	Orbulina universa	Globigerinoides conglobatus	Globigerinoides ruber total	Globoturborotalita tenella	Globigerinoides sacc total	Sphaeroidinella dehiscens	siphonifera & calida	Globigerina bulloides	Globigerina falconensis	Beela digitata	Globoturborotalita rubescens	Turborotalita quinqueloba	Neogloboquadrina pachyderma L	Neogloboquadrina dutertrei	P/D integrade & N. pachyderma R	Pulleniatina obliquiloculata	Globorotalia inflata	Globorotalia truncatulinoides total	Globorotalia crassaformis	Globorotalia hirsuta	Globorotalia scitula	Globorotalia menardii & tumida	Globigerinita glutinata
160	964	A	3	H	1	1714	341.55																							
160	964	A	3	H	1	1715	341.80	1	1	162	5	1	0	1	64	9	0	3	2	0	2	19	0	42	0	0	0	10	0	6
160	964	A	3	H	1	1716	342.04	15	0	267	4	8	0	0	145	11	0	1	3	0	1	7	0	77	0	0	0	7	0	23
160	964	A	3	H	1	1717	342.29	25	0	236	4	6	0	0	83	15	2	1	5	0	0	23	0	117	0	0	0	8	0	17
160	964	A	3	H	1	1718	342.54	14	0	106	3	2	0	1	54	6	1	1	4	0	0	13	0	91	0	0	0	1	0	10
160	964	A	3	H	1	1719	342.78	5	0	107	7	7	0	0	54	9	0	3	10	0	0	15	0	78	0	0	0	11	0	9
160	964	A	3	H	1	1720	343.03	2	0	143	3	4	0	0	44	7	0	0	7	0	0	14	0	66	0	0	0	9	0	6
160	964	A	3	H	1	1721	343.28	19	0	171	2	5	0	2	43	7	0	1	7	0	1	15	0	84	0	0	0	12	0	9
160	964	A	3	H	1	1722	343.52	32	0	131	5	17	0	1	153	17	0	0	4	0	1	21	0	158	0	0	0	18	0	20
160	964	A	3	H	1	1723	343.77	20	0	57	1	10	0	3	111	20	5	0	1	0	2	18	0	88	0	0	0	3	0	13
160	964	A	3	H	1	1724	344.01	15	0	61	1	12	0	2	70	11	0	0	2	0	0	17	0	90	0	0	0	7	0	12
160	964	A	3	H	1	1725	344.26	42	0	107	2	28	0	2	52	3	0	1	4	1	0	19	0	131	1	0	0	2	0	8
160	964	A	3	H	1	1726	344.51	25	0	104	8	26	0	6	86	10	0	1	6	0	0	12	0	103	0	0	0	10	0	15
160	964	A	3	H	1	1727	344.75	26	0	47	6	16	0	2	174	9	0	0	13	0	1	12	0	62	0	0	0	25	0	26
160	964	A	3	H	1	1728	345.00	39	1	24	0	20	0	3	158	24	0	0	7	0	2	19	0	108	0	0	0	9	0	26
160	964	A	3	H	1	1729	345.25	17	0	37	1	15	0	3	134	10	0	0	10	0	0	12	0	68	0	0	0	5	0	22
160	964	A	3	H	1	1730	345.49	33	0	65	7	25	0	3	198	21	1	0	9	0	0	48	0	124	1	0	0	9	0	28
160	964	A	3	H	1	1731	345.74	33	0	65	7	25	0	3	198	21	1	0	9	0	0	48	0	124	1	0	0	9	0	28
160	964	A	3	H	1	1732	345.99	37	0	113	18	20	0	6	143	8	2	2	7	0	0	43	0	150	2	0	0	5	0	21
160	964	A	3	H	1	1733	346.23	36	0	152	4	17	0	17	106	4	0	0	7	0	2	21	0	158	1	0	0	11	0	10
160	964	A	3	H	1	1734	346.48	33	0	100	1	9	0	5	28	1	0	0	1	0	4	13	0	115	2	0	0	1	0	3
160	964	A	3	H	1	1735	346.72	26	0	58	5	9	0	2	86	8	0	1	3	0	2	45	0	73	18	0	0	6	0	22
160	964	A	3	H	1	1736	346.97	37	0	113	2	11	0	8	93	4	1	1	3	0	1	24	0	97	48	0	0	3	0	13
160	964	A	3	H	1	1739	347.22	41	0	174	2	6	0	4	74	6	0	0	3	0	1	13	0	85	94	0	0	0	0	11
160	964	A	3	H	1	1742	347.46	10	0	84	2	11	0	2	59	8	0	1	5	0	0	21	0	58	61	0	0	6	0	10
160	964	A	3	H	1	1744	347.71	15	0	206	10	2	0	1	78	4	0	0	0	0	1	12	0	17	90	0	0	2	0	10
160	964	A	3	H	1	1745	347.96	9	0	99	4	14	0	5	30	12	0	1	2	0	2	12	0	39	57	0	0	0	0	2
160	964	A	3	H	1	1746	348.20	0	0	229	3	1	0	0	64	4	0	0	6	0	1	11	0	53	1	0	0	5	0	6
160	964	A	3	H	1	1747	348.45	3	0	217	1	11	0	1	59	5	0	0	6	0	1	8	0	39	47	0	0	5	0	3
160	964	A	3	H	1	1748	348.70	0	0	291	0	0	0	0	55	5	0	0	14	0	1	15	0	55	0	0	0	1	0	2
160	964	A	3	H	1	1749	348.94	4	0	413	8	0	0	0	90	5	0	0	4	0	1	6	0	81	0	0	0	0	0	5
160	964	A	3	H	1	1750	349.19	0	6	211	3	1	0	0	35	6	0	0	3	0	1	10	0	20	0	0	0	4	0	8
160	964	A	3	H	1	1755	349.43	12	1	241	1	1	0	0	133	29	0	0	4	0	0	14	0	139	0	0	0	0	0	11
160	964	A	3	H	1	1760	349.68	15	0	173	0	0	0	3	82	9	0	0	2	0	1	21	0	62	1	0	0	1	0	3
160	964	A	3	H	1	1761	349.93	21	0	170	3	4	0	1	73	7	3	1	3	1	2	11	0	84	1	0	0	9	0	7
160	964	A	3	H	1	1762	350.17	24	0	200	8	2	0	6	38	2	4	0	2	1	0	7	0	68	0	0	0	5	0	4
160	964	A	3	H	1	1763	350.42	5	0	88	2	13	0	1	78	20	0	0	8	0	6	20	0	37	6	0	0	6	0	15
160	964	A	3	H	1	1764	350.67	14	0	132	4	8	0	3	46	2	1	0	0	0	0	20	0	69	0	0	0	0	0	4
160	964	A	3	H	1	1765	350.91	14	0	221	4	18	0	2	95	4	2	0	1	0	0	23	0	118	4	0	0	3	0	9
160	964	A	3	H	1	1766	351.16	8	0	161	3	5	0	4	93	4	0	0	4	0	1	11	0	68	2	0	0	6	0	2
160	964	A	3	H	1	1767	351.41	8	0	337	11	17	0	6	155	6	5	0	15	0	1	24	0	81	2	0	0	3	0	11
160	964	A	3	H	1	1768	351.65	16	0	143	5	10	0	3	40	13	0	0	2	0	1	30	0	76	0	0	0	0	0	1
160	964	A	3	H	1	1769	351.90	3	0	102	2	2	0	4	51	3	2	0	7	0	0	15	0	146	23	0	0	11	0	8
160	964	A	3	H	1	1770	352.14	11	0	163	8	2	0	7	62	8	0	1	9	0	1	19	0	156	32	0	0	6	0	8
160	964	A	3	H	1	1771	352.39	10	0	118	6	3	0	1	49	15	2	0	4	0	2	26	0	104	19	0	0	4	0	1
160	964	A	3	H	1	1772	352.64	6	1	111	4	3	0	2	107	14	3	1	1	0	4	16	0	159	25	0	0	4	0	1
160	964	A	3	H	1	1773	352.88	18	0	124	5	0	0	2	79	14	3	0	7	0	2	8	0	115	20	0	0	7	0	5
160	964	A	3	H	1	1774	353.13	17	2	184	1	0	0	5	115	19	8	0	1	0	2	12	0	166	71	0	0	2	0	0
160	964	A	3	H	1	1775	353.38	8	0	122	7	3	0	6	61	16	3	0	3	0	0	11	0	142	55	0	0	4	0	2
160	964	A	3	H	1	1776	353.62	13	0	174	9	4	0	3	113	28	11	0	2	0	0	16	0	235	59	0	0	5	0	4
160	964	A	3	H	1	1777	353.87	11	0	108	2	1	0	1	57	9	3	0	0	0	1	8	0	111	32	0	0	5	0	4
160	964	A	3	H	1	1778	354.12	5	0	135	0	0	0	2	57	15	0	0	5	0	3	9	0	111	12	0	0	2	0	2
160	964	A	3	H	1	1779	354.36	12	0	233	2	3	0	5	45	3	6	0	4	0	1	7	0	105	38	0	0	1	0	12
160	964	A	3	H	2	1780	354.61	42	0	194	1	2	0	1	129	0	6	0	9	1	7	15	0	84	1	0	0	6	0	4
160	964	A	3	H	2	1781	354.86	27	0	178	4	5	0	13	82	6	9	0	22	0	3	13	0	88	0	0	0	1	0	1
160	964	A	3	H	2	1782	355.10	47	0	114	6	9	0	6	38	9	3	0	8	0	0	6	0	52	1	0	0	1	0	4
160	964	A	3	H	2	1783	355.35	37	2	141	8	2	0	4	64	12	2	1	7	0	4	10	0	152	14	0	0	0	0	9
160	964	A	3	H	2	1784	355.59	13	0	97	4	2	0	2	50	9	1	0	8	0	1	11	0	93	35	0	0	0	0	9
160	964	A	3	H	2	1785	355.84	19	0	118	3	6	0	2	35	2	6	0	2	0	1	9	0	105	29	0	0	1	0	12
160	964	A	3	H	2	1786	356.09	19	0	119	3	3	0	3	52	2	6	0	2	0	0	10	0	140	51	0	0	2	0	12
160	964	A	3	H	2	1787	356.33	31	0	176	3	4	0	5	93	26	8	0	2	0	3	15	0	143	52	0	0	1	0	15
160	964	A	3	H	2	1788	356.58	10	0	88	4	2	0	2	58	16	9	0	2	0	0	8	0	72	42	0	0	1	0	13
160	964	A	3	H	2	1789	356.83	0	0	159	0	2	0	3	14	23	0	0	0	0	2	6	0	126	32	0	0	0	0	4
160	964	A	3	H	2	1790	357.07	27	0	118	9	4	0	5	64	12	7	0	0	0	0	6	0	48	27	0	0	4	0	6
160	964	A	3	H	2	1791	357.32	40	9	243	9	2	0	3	100	11	15	0	0	0	1	6	0	55	52	0	0	1	0	7
160	964	A	3	H	2	1792	357.57	27	4	185	3	3	0	7	102	7	3	0	8	0	1	6	0	28	13	0	0	6	0	19
160	964	A	3	H	2	1793	357.81	46	14	126	12	4	0	8	89	6	3	1	15	0	6	10	0	37	4	0	0	3	0	4
160	964	A	3	H	2	1794	358.06	61	25	121	36	0	0	16	64	26	0	0	27	0	6	86	0	10	28	0	0	2	0	3
160	964	A	3	H	2	1795	358.30	34	1	82	11	3	0	3	83	1	1	0	19	1	28	14	0	17	39	0	0	2	0	2
160	964	A	3	H	2	1796	358.55	39	3	95	2	0	0	3	48	6	0	0	4	0	7	8	0	31	62	0	0	0	0	1
160	964	A	3	H	2	1797	358.80	21	5	164	3	0	0	6	85	5	1	1	8	0	6	6	0	108	29	0	0	3	0	1

ODP Site 964, MIS 11, planktonic foraminifera counts 2/3

leg	site	hole	core	type	section	cmbsf	age	*Orbulina universa*	*Globigerinoides conglobatus*	*Globigerinoides ruber total*	*Globoturborotalita tenella*	*Globigerinoides sacc total*	*Sphaeroidinella dehiscens*	*siphonifera & calida*	*Globigerina bulloides*	*Globigerina falconensis*	*Beela digitata*	*Globoturborotalita rubescens*	*Turborotalita quinqueloba*	*Neogloboquadrina pachyderma L*	*Neogloboquadrina dutertrei*	*PiD integrade & N. pachyderma R*	*Pulleniatina obliquiloculata*	*Globorotalia inflata*	*Globorotalia truncatulinoides total*	*Globorotalia crassaformis*	*Globorotalia hirsuta*	*Globorotalia scitula*	*Globorotalia menardii & tumida*	*Globigerinita glutinata*
160	964	A	3	H	2	1798	359.04	8	3	122	4	3	0	9	70	4	3	0	2	0	2	5	0	102	11	0	0	0	0	9
160	964	A	3	H	2	1799	359.29	15	3	112	2	11	0	7	57	38	0	4	0	0	2	7	0	83	30	0	0	0	0	2
160	964	A	3	H	2	1800	359.54	18	3	77	6	6	0	6	85	24	1	0	1	0	1	8	0	60	51	0	0	0	0	5
160	964	A	3	H	2	1802	359.78	20	4	43	3	12	0	6	98	23	2	0	1	0	1	7	0	20	49	0	0	2	0	10
160	964	A	3	H	2	1803	360.03	21	4	53	3	8	0	4	103	10	3	0	0	0	1	7	0	41	60	0	0	2	0	9
160	964	A	3	H	2	1804	360.28	31	3	144	5	11	0	22	84	235	0	0	0	0	1	47	0	62	83	0	0	2	0	1
160	964	A	3	H	2	1805	360.52	32	5	100	2	1	0	10	170	22	3	0	1	0	4	18	0	57	56	0	0	0	0	2
160	964	A	3	H	2	1806	360.77	18	4	117	2	4	0	13	196	55	5	0	0	0	7	13	0	32	31	0	0	2	0	5
160	964	A	3	H	2	1807	361.01	21	5	130	4	8	0	15	253	33	5	0	0	0	2	13	0	18	3	0	0	1	0	4
160	964	A	3	H	2	1808	361.26	19	4	96	1	11	0	6	174	37	2	0	0	0	3	10	0	24	0	0	0	0	0	3
160	964	A	3	H	2	1809	361.51	17	3	125	8	31	0	15	133	207	0	1	2	0	0	14	0	23	0	0	0	0	0	2
160	964	A	3	H	2	1810	361.75	33	4	153	9	54	0	15	232	38	3	0	1	0	1	6	0	21	0	0	0	0	0	7
160	964	A	3	H	2	1811	362.00	29	4	116	4	49	0	10	137	18	7	0	0	0	0	1	0	21	0	0	0	0	0	8
160	964	A	3	H	2	1812	362.70	39	4	111	2	49	0	10	118	18	1	1	1	0	0	1	0	9	0	0	0	0	0	5
160	964	A	3	H	2	1813	363.40	31	0	111	3	68	0	9	115	24	1	0	1	0	0	2	0	3	0	0	0	0	0	7
160	964	A	3	H	2	1814	364.10	44	10	178	5	87	0	25	139	47	1	1	0	0	2	3	0	9	1	0	0	0	0	11
160	964	A	3	H	2	1815	364.81	32	1	110	2	45	0	26	86	11	1	0	0	0	0	0	0	5	0	0	0	0	0	6
160	964	A	3	H	2	1816	365.51	39	6	131	2	53	0	16	131	37	3	0	0	0	1	3	0	6	0	0	0	0	0	7
160	964	A	3	H	2	1817	366.21	21	1	112	2	26	0	20	91	25	0	1	0	0	0	5	0	14	0	0	0	0	0	7
160	964	A	3	H	2	1818	366.91	26	5	167	8	40	0	27	172	44	9	1	0	0	1	9	0	22	1	0	0	0	0	14
160	964	A	3	H	2	1819	367.61	23	5	123	0	69	0	11	49	89	0	0	0	0	0	5	0	17	1	0	0	0	0	7
160	964	A	3	H	2	1820	368.31	20	6	99	3	47	0	10	81	34	2	0	1	0	5	7	0	28	3	0	0	0	0	7
160	964	A	3	H	2	1821	369.01	12	10	141	3	39	0	14	111	17	0	0	1	0	2	3	0	27	7	0	0	1	0	14
160	964	A	3	H	2	1822	369.72	16	8	140	0	18	0	13	72	26	0	1	1	0	7	3	0	12	2	0	0	0	0	11
160	964	A	3	H	2	1823	370.42	18	11	159	2	31	0	13	89	29	0	0	0	1	8	12	0	17	9	0	0	0	0	9
160	964	A	3	H	2	1824	371.12	9	7	166	5	24	0	9	94	25	1	1	1	0	2	27	0	28	13	0	0	2	0	9
160	964	A	3	H	2	1825	371.82	9	10	119	1	5	0	6	70	15	0	0	0	0	4	19	0	42	27	0	0	0	0	1
160	964	A	3	H	2	1826	372.52	15	18	122	8	10	0	24	111	27	0	0	0	0	17	40	0	51	50	0	0	3	0	12
160	964	A	3	H	2	1827	373.22	14	8	88	4	17	0	14	86	18	1	0	1	0	14	46	0	62	52	0	0	0	0	9
160	964	A	3	H	2	1828	373.93	8	16	88	7	32	0	13	99	11	1	0	0	0	16	45	0	70	62	0	0	14	0	8
160	964	A	3	H	2	1829	374.63	9	13	101	0	14	0	4	0	0	0	2	0	0	4	52	0	45	67	0	0	2	0	7
160	964	A	3	H	2	1830	375.33	7	6	82	1	16	0	9	47	3	1	0	0	0	9	16	0	57	43	0	0	1	0	3
160	964	A	3	H	2	1831	376.03	7	7	69	0	32	0	12	33	4	0	0	3	0	8	20	0	42	70	0	0	4	0	3
160	964	A	3	H	2	1832	376.73	19	4	104	3	17	0	12	51	9	2	0	0	0	14	29	0	76	69	0	0	7	0	6
160	964	A	3	H	2	1833	377.43	20	4	131	5	24	0	3	54	22	3	0	1	0	9	34	0	92	68	0	0	4	0	8
160	964	A	3	H	2	1834	378.13	9	0	85	1	18	0	6	44	11	0	0	0	0	7	27	0	60	78	0	0	10	0	3
160	964	A	3	H	2	1835	378.84	7	4	142	3	34	0	10	60	20	3	1	0	2	9	28	0	102	73	0	0	1	0	6
160	964	A	3	H	2	1836	379.54	3	0	82	2	28	0	10	62	19	2	0	1	0	7	10	0	73	48	0	0	4	0	1
160	964	A	3	H	2	1837	380.24	16	9	177	1	55	0	18	93	15	1	0	0	0	7	16	0	91	117	0	0	0	0	6
160	964	A	3	H	2	1838	380.94	22	2	183	4	44	0	19	79	16	2	0	0	1	2	6	0	67	89	0	0	0	0	7
160	964	A	3	H	2	1839	381.64	9	0	124	0	15	0	4	2	49	0	0	2	2	0	4	0	20	35	0	0	1	0	4
160	964	A	3	H	2	1840	382.34	6	0	168	1	35	0	8	54	22	0	0	0	0	1	7	0	22	17	0	0	0	0	20
160	964	A	3	H	2	1841	383.04	14	0	110	1	25	0	10	69	22	2	0	0	0	1	3	0	32	21	0	0	0	0	15
160	964	A	3	H	2	1842	383.75	20	0	159	0	37	0	14	115	33	2	0	0	0	3	8	0	36	37	0	0	0	0	20
160	964	A	3	H	2	1843	384.45	18	0	135	3	26	0	9	100	24	2	0	0	0	5	5	0	14	39	0	0	0	0	14
160	964	A	3	H	2	1844	385.15	35	0	242	0	58	0	8	122	24	4	0	0	1	3	11	0	19	28	0	0	1	0	24
160	964	A	3	H	2	1845	385.85	20	0	190	2	47	0	18	46	18	4	0	0	3	4	10	0	21	37	0	0	0	0	18
160	964	A	3	H	2	1846	386.55	21	1	208	4	53	0	17	92	28	1	0	1	0	0	11	0	41	43	0	0	0	0	25
160	964	A	3	H	2	1847	387.25	16	0	142	0	30	0	13	47	11	0	0	0	0	0	5	0	18	23	0	0	0	0	9
160	964	A	3	H	2	1848	387.96	25	0	212	4	40	0	13	136	24	3	0	0	0	1	9	0	19	5	0	0	0	0	33
160	964	A	3	H	2	1849	388.66	5	0	110	4	40	0	23	62	121	0	1	2	0	0	4	0	16	3	0	0	0	0	45
160	964	A	3	H	2	1850	389.36	4	1	165	4	53	0	20	160	39	4	0	0	0	2	11	0	24	4	0	0	1	0	50
160	964	A	3	H	2	1851	390.06	5	0	171	2	25	0	22	171	32	3	0	0	0	0	5	0	22	0	0	0	0	0	53
160	964	A	3	H	2	1852	390.76	2	0	212	4	4	0	26	169	51	2	0	3	0	2	6	0	19	2	0	0	0	0	114
160	964	A	3	H	2	1858	391.46	2	0	92	2	27	0	15	63	13	0	0	1	0	1	3	0	31	2	0	0	1	0	47
160	964	A	3	H	2	1864	392.16	5	0	74	1	56	0	30	39	34	0	0	0	0	0	9	0	56	0	0	0	1	0	30
160	964	A	3	H	2	1866	392.87	5	0	68	0	13	0	5	134	14	0	0	1	0	0	2	0	38	9	0	0	1	0	41
160	964	A	3	H	2	1867	393.57	7	1	124	0	5	0	17	172	25	2	0	0	0	0	3	0	99	3	0	0	4	0	61
160	964	A	3	H	2	1868	394.27	8	1	172	2	10	0	18	171	20	8	0	0	0	3	9	0	121	1	0	0	10	0	72
160	964	A	3	H	2	1869	394.97	6	0	140	0	11	0	37	38	49	0	0	0	0	0	0	0	100	0	0	0	7	0	57
160	964	A	3	H	2	1870	395.67	1	0	73	2	6	0	10	88	9	0	0	0	0	1	17	0	57	0	0	0	2	0	42
160	964	A	3	H	2	1871	396.37	6	0	77	5	17	0	17	106	14	1	0	2	0	7	21	0	106	0	0	0	9	0	47
160	964	A	3	H	2	1872	397.07	6	0	123	4	9	0	12	128	26	0	0	0	0	3	28	0	132	0	0	0	10	0	78
160	964	A	3	H	2	1873	397.78	24	0	164	7	13	0	25	131	15	2	1	1	0	0	3	0	98	0	0	0	9	0	52
160	964	A	3	H	2	1874	398.48	21	0	163	7	17	0	17	61	26	0	3	0	0	6	4	0	56	0	0	0	3	0	48
160	964	A	3	H	2	1875	399.18	21	1	188	8	24	0	7	103	13	0	2	2	1	8	27	0	94	0	0	0	22	0	53
160	964	A	3	H	2	1876	399.88	5	0	135	2	6	0	5	50	8	1	0	0	0	17	39	0	60	0	0	0	0	0	23
160	964	A	3	H	2	1877	400.58	16	0	185	5	6	0	4	66	10	1	1	1	0	26	50	0	88	0	0	0	0	0	36
160	964	A	3	H	2	1878	401.28	12	0	113	5	9	0	6	51	10	1	0	1	0	22	34	0	85	0	0	0	2	0	18
160	964	A	3	H	2	1879	401.99	15	0	100	17	40	0	34	85	11	0	0	8	0	87	135	0	89	0	0	0	12	0	46
160	964	A	3	H	2	1880	402.69	5	1	195	7	3	0	6	108	6	0	0	0	0	8	24	0	88	0	0	0	0	0	22

ODP Site 964, MIS 11, planktonic foraminifera counts 3/3

leg	site	hole	core	type	section	cmbsf	age	Orbulina universa	Globigerinoides conglobatus	Globigerinoides ruber total	Globoturborotalita tenella	Globigerinoides sacc total	Siphanoidinella dehiscens	siphonifera & calida	Globigerina bulloides	Globigerina falconensis	Beela digitata	Globoturborotalita rubescens	Turborotalita quinqueloba	Neogloboquadrina pachyderma L	Neogloboquadrina dutertrei	P/D integrade & N. pachyderma R	Pulleniatina obliquiloculata	Globorotalia inflata	Globorotalia truncatulinoides total	Globorotalia crassaformis	Globorotalia hirsuta	Globorotalia scitula	Globorotalia menardii & tumida	Globigerinita glutinata
160	964	A	3	H	2	1881	403.39	18	0	184	8	6	0	4	77	10	3	0	4	0	36	35	0	97	0	0	0	1	0	57
160	964	A	3	H	2	1882	404.09	15	0	144	9	10	0	12	48	7	0	0	12	0	12	35	0	57	0	0	0	0	0	30
160	964	A	3	H	2	1883	404.79	45	0	54	18	16	0	6	121	11	1	1	11	0	34	43	0	77	0	0	0	4	0	51
160	964	A	3	H	2	1884	405.49	112	0	27	7	6	0	3	82	37	0	8	12	0	3	11	0	5	0	0	0	0	0	0
160	964	A	3	H	2	1885	406.19	31	0	103	10	3	0	4	46	10	0	0	2	2	16	64	0	32	0	0	0	3	0	30
160	964	A	3	H	2	1886	406.90	10	0	113	7	21	0	2	80	8	0	0	8	0	50	44	0	62	0	0	0	0	0	27
160	964	A	3	H	2	1887	407.60	26	0	160	5	5	0	1	67	5	1	0	13	0	4	6	0	15	0	0	0	2	0	6
160	964	A	3	H	2	1888	408.30	31	0	163	3	2	0	3	51	1	1	0	8	0	26	25	0	31	0	0	0	4	0	30
160	964	A	3	H	2	1889	409.00	11	0	105	8	0	0	4	59	1	0	0	11	2	51	85	0	49	0	0	0	6	0	28
160	964	A	3	H	2	1890	410.38	6	0	31	1	4	0	9	50	1	0	0	9	2	90	148	0	36	0	0	0	1	0	62
160	964	A	3	H	2	1891	411.77	3	0	17	2	3	0	0	77	2	0	0	31	1	196	270	0	7	0	0	0	5	0	79
160	964	A	3	H	2	1892	413.15	0	0	9	0	3	0	1	24	0	0	0	7	3	88	133	0	2	0	0	0	1	0	38
160	964	A	3	H	2	1893	414.54	3	0	3	0	1	0	0	30	0	0	0	9	0	100	135	0	9	0	0	0	0	0	53
160	964	A	3	H	2	1894	415.92	3	0	0	0	0	0	12	10	3	0	0	11	2	97	170	0	6	0	0	0	0	0	63
160	964	A	3	H	2	1895	417.31	0	0	3	0	2	0	1	14	2	0	1	6	2	111	157	0	0	0	0	0	0	0	41
160	964	A	3	H	2	1896	418.69	2	0	1	0	3	0	1	8	2	0	0	2	0	119	145	0	5	0	0	0	0	0	23
160	964	A	3	H	2	1897	420.08	0	0	0	0	1	0	0	32	0	0	0	1	2	171	127	0	1	0	0	0	0	0	18
160	964	A	3	H	2	1898	421.46	0	0	0	1	0	0	1	30	0	0	2	2	3	230	197	0	0	0	0	0	0	0	9
160	964	A	3	H	2	1899	422.85	0	0	4	1	6	0	0	116	1	0	0	22	6	233	226	0	0	0	0	0	0	0	35
160	964	A	3	H	2	1900	424.23	0	0	1	0	2	0	0	63	0	0	0	8	4	167	141	0	1	0	0	0	0	0	15
160	964	A	3	H	2	1901	425.62	1	0	3	2	5	0	2	113	0	0	0	3	1	150	144	0	4	0	0	0	0	0	30
160	964	A	3	H	2	1902	427.00	2	0	1	0	4	0	0	70	2	0	0	11	1	145	127	0	0	0	0	0	0	0	49
160	964	A	3	H	2	1903	427.76	3	0	0	0	2	0	0	37	0	0	0	15	2	109	138	0	0	0	0	0	0	0	88
160	964	A	3	H	2	1904	429.04	19	0	0	1	0	0	0	69	0	0	0	20	4	81	188	0	0	0	0	0	0	0	55
160	964	A	3	H	2	1905	430.32	10	0	0	0	2	0	2	125	0	0	0	5	5	147	141	0	0	0	0	0	0	0	58
160	964	A	3	H	2	1906	431.60	0	0	0	0	2	0	0	40	1	0	0	13	0	90	107	0	1	0	0	0	0	0	74
160	964	A	3	H	2	1907	432.88	0	0	0	0	1	0	1	42	0	0	0	11	0	74	121	0	2	0	0	0	0	0	50
160	964	A	3	H	2	1908	434.15	0	0	0	0	0	0	0	17	0	0	0	10	2	86	137	0	0	0	0	0	0	0	57
160	964	A	3	H	2	1909	435.43	0	0	0	0	0	0	0	5	0	0	0	26	3	72	156	0	0	0	0	0	0	0	70
160	964	A	3	H	2	1910	436.71	0	0	1	0	2	0	0	6	0	0	0	25	0	63	148	0	0	0	0	0	0	0	62
160	964	A	3	H	2	1911	437.99	12	0	6	0	2	0	1	20	0	0	0	26	0	145	128	0	3	0	0	0	0	0	117
160	964	A	3	H	2	1912	439.27	29	0	26	0	0	0	0	40	2	0	0	14	0	80	95	0	1	0	0	0	0	0	82
160	964	A	3	H	2	1913	440.55	17	0	16	0	0	0	1	63	0	0	0	21	0	48	80	0	1	0	0	0	0	0	57
160	964	A	3	H	2	1914	441.83	15	0	4	0	0	0	1	105	5	0	0	41	3	47	70	0	0	0	0	0	0	0	63
160	964	A	3	H	2	1915	443.11	11	0	4	0	0	0	2	212	0	0	0	24	0	47	144	0	0	0	0	0	0	0	77
160	964	A	3	H	2	1916	444.38	11	0	0	1	1	0	2	123	0	0	0	19	0	25	79	0	0	0	0	0	0	0	43
160	964	A	3	H	2	1917	445.66	20	0	0	0	2	0	3	237	2	0	0	36	5	57	140	0	3	0	0	0	0	0	63
160	964	A	3	H	2	1918	446.94	30	0	0	0	1	0	1	215	2	0	0	27	0	35	98	0	1	0	0	0	0	0	55
160	964	A	3	H	2	1919	448.22	15	0	0	0	0	0	2	127	0	0	1	33	2	12	78	0	0	0	0	0	0	0	36
160	964	A	3	H	2	1920	449.50	21	0	0	2	0	0	0	139	1	0	0	17	2	22	78	0	0	0	0	0	0	0	20
160	964	A	3	H	2	1921	450.78	16	0	0	0	1	0	0	136	1	0	0	20	1	23	106	0	0	0	0	0	0	0	29
160	964	A	3	H	2	1922	452.06	27	0	1	0	2	0	1	244	2	0	0	31	3	32	116	0	0	0	0	0	0	0	24
160	964	A	3	H	2	1923	453.34	18	0	1	0	1	0	0	277	1	0	0	15	1	23	76	0	0	0	0	0	0	0	17
160	964	A	3	H	2	1924	454.62	0	0	0	0	0	0	0	204	12	0	0	12	0	45	90	0	0	0	0	0	0	0	24
160	964	A	3	H	2	1926	455.89	0	0	0	0	0	0	1	230	3	0	0	12	2	12	71	0	0	0	0	0	0	0	25
160	964	A	3	H	3	1928	457.17	0	0	0	0	3	0	0	270	3	0	0	10	0	18	100	0	0	0	0	0	0	0	40
160	964	A	3	H	3	1930	458.45	0	0	3	0	3	0	0	205	0	0	0	3	2	70	204	0	0	0	0	0	0	0	41
160	964	A	3	H	3	1932	459.73	0	0	1	1	0	0	0	84	2	0	0	27	2	30	143	0	0	0	0	0	0	0	57
160	964	A	3	H	3	1933	461.01	0	0	4	0	1	0	0	35	0	0	2	59	2	83	369	0	0	0	0	0	0	0	146
160	964	A	3	H	3	1934	462.29	0	0	1	0	0	0	1	52	0	0	0	37	3	33	90	0	0	0	0	0	0	0	42
160	964	A	3	H	3	1935	463.57	0	0	4	0	1	0	0	146	2	0	0	23	0	35	122	0	0	0	0	0	0	0	65
160	964	A	3	H	3	1936	464.85	0	0	1	1	1	0	2	261	5	0	0	35	3	28	134	0	1	0	0	0	0	0	36
160	964	A	3	H	3	1937	466.13	0	0	1	0	0	0	8	263	4	1	1	25	2	20	107	0	0	0	0	0	0	0	24
160	964	A	3	H	3	1938	467.40	0	0	2	0	0	0	0	43	0	0	0	13	0	58	376	0	0	0	0	0	0	0	31
160	964	A	3	H	3	1939	468.68	0	0	0	0	0	0	0	0	0	0	0	46	5	51	356	0	0	0	0	0	0	0	28
160	964	A	3	H	3	1940	469.96	1	0	1	0	1	0	0	85	0	1	0	50	4	49	333	0	0	0	0	0	0	0	41
160	964	A	3	H	3	1941	471.24	0	0	0	0	0	0	0	172	3	0	0	4	0	20	77	0	0	0	0	0	0	0	26
160	964	A	3	H	3	1942	472.52	0	0	0	1	0	0	2	291	2	0	0	5	0	29	180	0	0	0	0	0	0	0	26
160	964	A	3	H	3	1943	473.80	1	0	0	0	0	0	0	115	3	0	0	11	3	59	242	0	0	0	0	0	0	0	48
160	964	A	3	H	3	1944	475.08	3	0	5	0	0	0	3	77	2	0	0	32	0	76	298	0	0	0	0	0	0	0	47
160	964	A	3	H	3	1945	476.36	5	0	25	0	0	0	0	180	1	0	0	31	2	56	248	0	0	0	0	0	0	0	39
160	964	A	3	H	3	1946	477.64	14	0	47	1	1	0	0	248	3	0	2	5	0	29	115	0	0	0	0	0	0	0	19
160	964	A	3	H	3	1947	478.91	12	0	19	0	0	0	0	209	1	0	0	5	2	8	72	0	0	0	0	0	0	0	10
160	964	A	3	H	3	1948	480.19	11	0	8	1	0	0	0	230	2	0	0	1	1	24	79	0	0	0	0	0	0	0	5
160	964	A	3	H	3	1949	481.47	12	0	12	1	0	0	1	343	31	0	0	4	0	26	188	0	1	0	0	0	0	0	12

Stable isotopic measurements Kiel/Bremerhaven

Core	Section	cm	age	AWI *G. ruber* $\delta^{13}C$ (‰ VPDB)	AWI *G. ruber* $\delta^{18}O$ (‰ VPDB)	Kiel *G. ruber* $\delta^{13}C$ (‰ VPDB)	Kiel *G. ruber* $\delta^{18}O$ (‰ VPDB)
ODP 964	3H1	85.5	357.45				
ODP 964	3H1	90.5	359.05	0.74	1.52	0.56	1.79
ODP 964	3H1	95.5	360.64	1.05	1.60	0.41	2.11
ODP 964	3H1	100.5	360.95	0.73	1.22	0.56	1.67
ODP 964	3H1	105.5	361.27	0.70	1.08	0.70	1.20
ODP 964	3H1	110.5	361.59				
ODP 964	3H1	115.5	361.91	0.21	1.23	-0.14	1.37
ODP 964	3H1	120.5	363.82	1.29	1.97	0.94	1.91
ODP 964	3H1	125.5	364.45				
ODP 964	3H1	130.5	365.09				
ODP 964	3H1	135.5	365.41				
ODP 964	3H1	140.5	370.18	0.58	1.56	1.03	1.43
ODP 964	3H1	145.5	371.77	0.63	0.77	0.73	0.83
ODP 964	3H1	150.5	374.95	0.91	0.76	0.52	0.82
ODP 964	3H2	10.5	378.45	1.02	0.40	0.22	1.04
ODP 964	3H2	15.5	380.05	0.72	1.81	0.77	1.60
ODP 964	3H2	20.5	381.64	1.11	1.50	0.61	1.51
ODP 964	3H2	25.5	383.23	1.19	1.21	0.96	1.33
ODP 964	3H2	30.5	384.82	0.20	1.00	0.33	1.12
ODP 964	3H2	40.5	388.00	0.80	0.73	0.63	0.61
ODP 964	3H2	50.5	391.18	0.32	0.14	0.33	0.35
ODP 964	3H2	60.5	394.36	-0.03	0.41	0.00	0.62
ODP 964	3H2	70.5	397.55	0.18	0.52	0.10	0.44
ODP 964	3H2	85.5	402.32	0.32	0.63	-0.30	0.91
ODP 964	3H2	90.5	403.91	0.19	0.69	-0.48	0.59
ODP 964	3H2	95.5	405.50	0.56	0.22	0.10	0.66
ODP 964	3H2	100.5	407.09	-0.55	0.08	-0.68	-0.57
ODP 964	3H2	105.5	408.68				
ODP 964	3H2	135.5	434.30	1.25	1.62	0.99	1.88
ODP 964	3H3	15.5	457.45				

GeoTü-SL96, Holocene, stable isotopic composition of morphotypes of *G. ruber*

Core	cm	age	δ18O Type a "normal"	δ13C Type a "normal"	δ18O Type b "platys"	δ13C Type b "platys"	δ18O Type c "elongate"	δ13C Type c "elongate"	Sample weight (g)	planktonic forams/g sed.	split	sum split (PF)	entire sum (PF)
GeoTü-SL96	0.5	2300	0.461	0.663	1.107	0.516			0.44	5509.09	8	303	2424
GeoTü-SL96	1.5	2900	0.263	0.621	1.263	0.448			0.458	5519.65	8	316	2528
GeoTü-SL96	2.5	3500	0.573	0.565	1.297	0.468			0.249	24867.47	16	387	6192
GeoTü-SL96	3.5	4100	0.884	0.532	0.996	0.278			0.201	12736.32	8	320	2560
GeoTü-SL96	4.5	4700	0.724	0.358	0.819	0.600			0.216	11111.11	8	300	2400
GeoTü-SL96	5.5	5300			1.085	0.730			0.322	7950.31	8	320	2560
GeoTü-SL96	6.5	5900	0.701	0.345	1.224	0.743			0.253	11130.43	8	352	2816
GeoTü-SL96	7.5	6500	0.224	0.800	0.966	0.441			0.103	48621.36	16	313	5008
GeoTü-SL96	8.5	7100	-0.160	0.133	1.021	-0.344			0.131	56916.03	16	466	7456
GeoTü-SL96	9.5	7700	-0.652	-0.226	0.139	0.095			0.405	20187.65	16	511	8176
GeoTü-SL96	10.5	8300	-0.099	0.329	0.483	0.081	0.253	-0.503	0.308	16363.64	16	315	5040
GeoTü-SL96	11.5	8900	0.066	0.363	0.498	-0.082	0.652	-0.250	0.306	16313.73	16	312	4992
GeoTü-SL96	12.5	9500					0.857	0.161	0.474	7645.57	8	453	3624
GeoTü-SL96	13.5	9900	0.226	0.850	0.898	1.003			0.192	13625.00	8	327	2616
GeoTü-SL96	14.5	10300	0.471	1.497	1.194	1.009			0.176	30272.73	16	333	5328
GeoTü-SL96	15.5	10700	0.067	1.120	0.887	0.543			0.209	30851.67	16	403	6448
GeoTü-SL96	16.5	11100	0.450	1.365	0.861	0.912	0.796	0.523	0.249	20433.73	16	318	5088
GeoTü-SL96	17.5	11500	0.512	1.531	1.365	0.686	1.226	1.710	0.205	24351.22	16	312	4992
GeoTü-SL96	18.5	11900	0.692	1.901	1.271	0.942			0.278	19510.79	16	339	5424
GeoTü-SL96	19.5	12300	0.880	1.971	1.094	1.599			0.226	45876.11	32	324	10368
GeoTü-SL96	20.5	12700	0.637	2.150	1.057	1.979			0.616	8493.51	16	327	5232
GeoTü-SL96	21.5	13100	0.678	2.481	0.869	1.633	2.113	0.818	0.448	11857.14	16	332	5312
GeoTü-SL96	22.5	13500	0.836	2.383	1.083	1.402			0.332	15373.49	16	319	5104
GeoTü-SL96	23.5	13900	0.946	2.390	1.091	1.549			0.344	14744.19	16	317	5072
GeoTü-SL96	24.5	14300	0.903	2.480	1.074	1.605	1.362	1.641	0.368	13956.52	16	321	5136
GeoTü-SL96	25.5	14700	0.703	2.233	1.172	1.449	1.702	2.575	0.372	12989.25	16	302	4832
GeoTü-SL96	26.5	15100	0.995	2.618	0.837	1.542			0.324	8617.28	8	349	2792
GeoTü-SL96	27.5	15500	0.899	2.863	1.298	2.271			0.308	16155.84	16	311	4976
GeoTü-SL96	28.5	15900	1.027	2.572	1.367	2.324	2.175	3.549	0.297	17239.06	16	320	5120
GeoTü-SL96	29.5	16300	0.980	2.679	1.401	2.297	1.356	2.932	0.43	7795.35	8	419	3352
GeoTü-SL96	30.5	16700	1.225	2.864	1.367	2.064			0.348	10045.98	8	437	3496
GeoTü-SL96	31.5	17100	1.273	3.200	1.465	2.832			0.472	7101.69	8	419	3352

GeoTü-SL96, Holocene, counts of morphotypes of *G. ruber*

Core	cm	age	Type a "normal"	Type a "normal" (%)	Type b "platys"	Type b "platys" (%)	Type c "elongate"	Type c "elongate" (%)	G. ruber kummerform	G. ruber kummerform (%)	G. ruber pink	G. ruber pink (%)
GeoTü-SL96	0.5	2300	166	71.55	33	14.22	0	0.00	18	7.76	15	6.47
GeoTü-SL96	1.5	2900	128	69.19	31	16.76	4	2.16	15	8.11	11	5.95
GeoTü-SL96	2.5	3500	164	77.73	31	14.69	3	1.42	8	3.79	8	3.79
GeoTü-SL96	3.5	4100	198	77.04	19	7.39	4	1.56	27	10.51	13	5.06
GeoTü-SL96	4.5	4700	123	67.58	22	12.09	3	1.65	33	18.13	4	2.20
GeoTü-SL96	5.5	5300	119	68.39	37	21.26	6	3.45	14	8.05	4	2.30
GeoTü-SL96	6.5	5900	93	53.76	49	28.32	7	4.05	19	10.98	12	6.94
GeoTü-SL96	7.5	6500	128	69.95	34	18.58	8	4.37	15	8.20	6	3.28
GeoTü-SL96	8.5	7100	78	68.42	23	20.18	35	30.70	5	4.39	8	7.02
GeoTü-SL96	9.5	7700	100	58.14	17	9.88	39	22.67	14	8.14	41	23.84
GeoTü-SL96	10.5	8300	119	62.30	19	9.95	121	63.35	24	12.57	29	15.18
GeoTü-SL96	11.5	8900	130	60.19	48	22.22	39	18.06	20	9.26	18	8.33
GeoTü-SL96	12.5	9500	89	55.28	45	27.95	24	14.91	24	14.91	3	1.86
GeoTü-SL96	13.5	9900	145	59.18	67	27.35	16	6.53	19	7.76	14	5.71
GeoTü-SL96	14.5	10300	98	53.85	61	33.52	9	4.95	16	8.79	7	3.85
GeoTü-SL96	15.5	10700	100	56.18	51	28.65	8	4.49	17	9.55	10	5.62
GeoTü-SL96	16.5	11100	94	46.77	74	36.82	22	10.95	22	10.95	11	5.47
GeoTü-SL96	17.5	11500	85	50.60	59	35.12	23	13.69	15	8.93	9	5.36
GeoTü-SL96	18.5	11900	67	47.86	53	37.86	9	6.43	15	10.71	5	3.57
GeoTü-SL96	19.5	12300	67	48.20	50	35.97	14	10.07	14	10.07	8	5.76
GeoTü-SL96	20.5	12700	98	60.12	44	26.99	8	4.91	18	11.04	3	1.84
GeoTü-SL96	21.5	13100	78	45.09	66	38.15	21	12.14	25	14.45	4	2.31
GeoTü-SL96	22.5	13500	94	46.53	69	34.16	22	10.89	33	16.34	6	2.97
GeoTü-SL96	23.5	13900	57	33.53	92	54.12	18	10.59	18	10.59	3	1.76
GeoTü-SL96	24.5	14300	57	38.78	67	45.58	19	12.93	19	12.93	4	2.72
GeoTü-SL96	25.5	14700	61	38.85	75	47.77	21	13.38	18	11.46	3	1.91
GeoTü-SL96	26.5	15100	55	38.73	61	42.96	32	22.54	22	15.49	4	2.82
GeoTü-SL96	27.5	15500	68	43.87	65	41.94	42	27.10	21	13.55	1	0.65
GeoTü-SL96	28.5	15900	57	35.85	85	53.46	48	30.19	15	9.43	2	1.26
GeoTü-SL96	29.5	16300	48	34.53	79	56.83	30	21.58	12	8.63	0	0.00
GeoTü-SL96	30.5	16700	66	35.87	89	48.37	37	20.11	29	15.76	0	0.00
GeoTü-SL96	31.5	17100	56	29.17	105	54.69	11	5.73	29	15.10	2	1.04

ODP Site 964, Holocene, counts and stable isotopes of morphotypes of *G. ruber*

Core	cm	age	δ18O Type a "normal"	δ13C Type a "normal"	δ18O Type b "platys"	δ13C Type b "platys"	δ18O Type c "elongate"	δ13C Type c "elongate"	Sample weight (g)	planktonic forams/g sed.	split	sum split (PF)	entire sum (PF)
ODP Site 964 1H1	0.5	0	0.332	-0.17	0.16	0.40			0.02	44736.84	2	425	850
ODP Site 964 1H1	4.5	250	0.463	0.22	0.13	1.04			0.08	15487.18	4	302	1208
ODP Site 964 1H1	44.5	499.995	0.709	0.35	0.02	0.78			0.09	13044.44	2	587	1174
ODP Site 964 1H1	49.5	1785.71	0.764	-0.13	0.41	1.05			0.04	15100.00	2	302	604
ODP Site 964 1H1	54.5	3071.43	0.421	0.18	0.55	1.03			0.05	28612.24	2	701	1402
ODP Site 964 1H1	59.5	4357.14	0.122	-0.32	0.23	0.81			0.02	83428.57	4	438	1752
ODP Site 964 1H1	64.5	5642.86	0.565	-0.38	-0.39	0.78	-0.30	0.93	0.08	16634.15	4	341	1364
ODP Site 964 1H1	69.5	6928.57	0.126	0.15	-0.38	0.39	0.31	0.19	0.09	16869.57	4	388	1552
ODP Site 964 1H1	72.5	7357.14	0.416	-0.17					0.07	17633.80	4	313	1252
ODP Site 964 1H1	73.5	7785.71	0.387	0.07	-0.13	0.54			0.20	6169.15	4	310	1240
ODP Site 964 1H1	74.5	8214.28	0.523	-0.33	-0.17	-0.10			0.15	12297.30	4	455	1820
ODP Site 964 1H1	77.5	8642.85	0.587	0.04	-0.27	0.55	0.19	0.53	0.04	35351.35	4	327	1308
ODP Site 964 1H1	78.5	9071.42	1.293	0.24	-0.01	0.36	0.42	0.71	0.08	22746.99	4	472	1888
ODP Site 964 1H1	79.5	9500	2.217	0.10	0.21	0.47	-0.40	0.95	0.03	31538.46	2	410	820
ODP Site 964 1H1	89.5	12071.4	1.706	0.00	0.48	0.84			0.03	23151.52	2	382	764
ODP Site 964 1H1	94.5	13357.1	2.361	0.96	1.02	1.30	2.02	1.01	0.13	14077.52	4	454	1816
ODP Site 964 1H1	99.5	14822.9	2.043	0.92	1.89	0.75	1.10	1.38	0.06	30327.27	4	417	1668
ODP Site 964 1H1	114.5	16108.6	3.000	0.96	1.46	0.83	1.98	0.95	0.08	16571.43	4	319	1276
ODP Site 964 1H1	119.5	17394.3	3.422	1.21	2.52	1.26	2.22	0.96	0.08	18871.79	4	368	1472
ODP Site 964 1H1	124.5	18680	3.130	1.07	3.06	1.63	3.15	1.67	0.20	6110.55	4	304	1216
ODP Site 964 1H1	129.5	19965.7	3.146	1.25	2.89	1.47	2.68	1.36	0.09	12893.62	4	303	1212

Core	cm	age	Type a "normal"	Type a "normal" (%)	Type b "platys"	Type b "platys" (%)	Type c "elongate"	Type c "elongate" (%)	G. ruber kummerform	G. ruber kummerform (%)	G. ruber pink	G. ruber pink (%)
ODP Site 964 1H1	0.5	0	158	51.80	80	26.23	2	0.66	46	15.08	19	6.23
ODP Site 964 1H1	4.5	250	99	49.01	50	24.75	0	0.00	38	18.81	15	7.43
ODP Site 964 1H1	44.5	499.995	216	52.68	104	25.37	2	0.49	81	19.76	7	1.71
ODP Site 964 1H1	49.5	1785.71	100	44.44	81	36.00	4	1.78	34	15.11	6	2.67
ODP Site 964 1H1	54.5	3071.43	238	56.00	106	24.94	8	1.88	55	12.94	18	4.24
ODP Site 964 1H1	59.5	4357.14	78	45.88	63	37.06	7	4.12	12	7.06	10	5.88
ODP Site 964 1H1	64.5	5642.86	82	49.10	50	29.94	5	2.99	19	11.38	11	6.59
ODP Site 964 1H1	69.5	6928.57	99	57.23	23	13.29	18	10.40	5	2.89	28	16.18
ODP Site 964 1H1	72.5	7357.14	89	55.28	26	16.15	17	10.56	10	6.21	19	11.80
ODP Site 964 1H1	73.5	7785.71	119	74.84	8	5.03	9	5.66	8	5.03	15	9.43
ODP Site 964 1H1	74.5	8214.28	179	54.74	59	18.04	36	11.01	30	9.17	23	7.03
ODP Site 964 1H1	77.5	8642.85	109	50.70	46	21.40	16	7.44	17	7.91	27	12.56
ODP Site 964 1H1	78.5	9071.42	151	58.53	49	18.99	17	6.59	39	15.12	2	0.78
ODP Site 964 1H1	79.5	9500	131	53.47	54	22.04	16	6.53	33	13.47	11	4.49
ODP Site 964 1H1	89.5	12071.4	104	51.74	68	33.83	12	5.97	16	7.96	0	0.00
ODP Site 964 1H1	94.5	13357.1	109	52.40	47	22.60	25	12.02	27	12.98	0	0.00
ODP Site 964 1H1	99.5	14822.9	73	39.04	62	33.16	11	5.88	39	20.86	2	1.07
ODP Site 964 1H1	114.5	16108.6	52	48.60	18	16.82	14	13.08	23	21.50	0	0.00
ODP Site 964 1H1	119.5	17394.3	70	52.63	23	17.29	11	8.27	29	21.80	0	0.00
ODP Site 964 1H1	124.5	18680	66	53.23	21	16.94	18	14.52	18	14.52	0	0.00
ODP Site 964 1H1	129.5	19965.7	56	50.00	25	22.32	12	10.71	18	16.07	1	0.89

GeoTü-SL96, MIS 11, morphotype counts of *G. ruber*

Core	cm	age	δδ18O Type a "normal"	δ13C Type a "normal"	δ18O Type b "platys"	δ13C Type b "platys"	δ18O Type c "elongate"	δ13C Type c "elongate"	Sample weight (g)	planktonic forams/g sed.	split	sum split (PF)	entire sum (PF)
GeoTü-SL96	635.5	311.23	-0.11	-0.34	0.09	0.62	-0.41	0.52	2.71	14335.06	64	607	38848
GeoTü-SL96	640.5	319.23	0.32	0.65	0.86	0.80	0.18	1.33	3.523	4932.16	32	543	17376
GeoTü-SL96	645.5	327.06	0.5	0.20	0.79	1.02	0.76	1.12	3.993	3478.09	32	434	13888
GeoTü-SL96	650.5	334.90	0.86	0.70	0.67	0.60	1.05	1.33	4.043	4828.10	64	305	19520
GeoTü-SL96	655.5	342.73	2.26	0.79	1.02	2.08	1.98	0.96	4.098	2733.04	32	350	11200
GeoTü-SL96	660.5	343.88	2.1	0.99	1.33	1.98	2.12	1.10	4.218	1331.44	8	702	5616
GeoTü-SL96	665.5	349.64	2.64	1.47	1.66	2.63	2.45	1.68	4.649	1438.59	16	418	6688
GeoTü-SL96	670.5	355.39	1.98	1.35	1.50	1.87	1.92	1.44	3.745	1969.56	16	461	7376
GeoTü-SL96	675.5	360.67	1.35	1.28	1.38	1.47			3.554	406.30	4	361	1444
GeoTü-SL96	680.5	364.03	1.6	1.33	1.63	1.33	1.45	1.78	3.973	3721.12	32	462	14784
GeoTü-SL96	685.5	367.38	0.84	1.66	1.43	1.13	1.31	1.52	3.774	3951.25	32	466	14912
GeoTü-SL96	690.5	370.74	0.12	1.04	1.34	1.02	1.17	1.65	3.851	3830.69	32	461	14752
GeoTü-SL96	695.5	374.10	1.47	0.76	1.65	1.12	1.26	1.46	4.16	2138.46	16	556	8896
GeoTü-SL96	700.5	377.45	-0.34	0.01	0.86	0.78			3.992	1040.08	8	519	4152
GeoTü-SL96	705.5	380.81	0.67	0.99	0.97	0.72	0.24	1.55	3.743	2718.67	16	636	10176
GeoTü-SL96	710.5	384.16	0.49	0.98	1.11	0.29	0.33	1.28	3.788	1491.02	8	706	5648
GeoTü-SL96	715.5	387.52	0.06	0.65	1.04	0.46	0.37	0.77	3.111	3569.27	32	347	11104
GeoTü-SL96	720.5	390.88	0.3	0.80	0.99	0.30	0.17	1.26	3.286	4976.26	32	511	16352
GeoTü-SL96	725.5	394.23	0.21	1.05	0.88	0.35	-0.43	1.02	3.902	4346.49	32	530	16960
GeoTü-SL96	730.5	397.59	-0.04	0.65	0.73	0.78	0.03	1.32	4.067	820.26	8	417	3336
GeoTü-SL96	735.5	400.95	0.52	0.88	0.71	0.70	0.14	1.25	2.905	1608.26	8	584	4672
GeoTü-SL96	740.5	404.30	0.43	0.60	0.73	0.46	-0.42	1.04	3.384	2666.67	16	564	9024
GeoTü-SL96	745.5	407.66	0	0.50	0.75	0.18	-0.45	0.64	3.878	2723.05	32	330	10560
GeoTü-SL96	750.5	413.10	-0.33	0.13	0.88	-0.57	-1.20	0.70	4.07	4237.84	32	539	17248
GeoTü-SL96	755.5	419.93	0.31	0.57	1.01	0.84	-0.09	0.73	3.928	7250.51	64	445	28480
GeoTü-SL96	760.5	426.77					0.49	1.14	3.594	8138.01	64	457	29248
GeoTü-SL96	765.5	433.60	0.97	0.59	1.22	0.94	0.79	1.27	3.885	5263.32	32	639	20448
GeoTü-SL96	770.5	440.43	0.58	0.64	0.50	0.76	0.73	0.80	3.721	4428.92	32	515	16480
GeoTü-SL96	775.5	447.27	0.84	0.37	0.81	0.08	0.32	0.92	3.32	8240.96	32	855	27360
GeoTü-SL96	780.5	454.10	0.87	0.67	1.62	1.29	0.48	1.49	3.003	5509.16	32	517	16544
GeoTü-SL96	785.5	460.93	1.32	0.57	1.31	1.13	0.33	1.08	3.72	2847.31	32	331	10592
GeoTü-SL96	790.5	467.77	1.66	1.28	0.89	1.56	1.64	1.26	3.262	1294.91	8	528	4224

GeoTü-SL96, MIS 11, stable isotopic composition in morphotypes of *G. ruber*

Core	cm	age	Type a "normal"	Type a "normal" (%)	Type b "platys"	Type b "platys" (%)	Type c "elongate"	Type c "elongate" (%)	G. ruber kummerform	G. ruber kummerform (%)	G. ruber pink	G. ruber pink (%)
GeoTü-SL96	635.5	311.23	59	37.82	15	9.62	75	48.08	6	3.85	1	0.64
GeoTü-SL96	640.5	319.23	49	52.13	25	26.60	4	4.26	11	11.70	5	5.32
GeoTü-SL96	645.5	327.06	16	53.33	7	23.33	1	3.33	5	16.67	1	3.33
GeoTü-SL96	650.5	334.90	9	40.91	9	40.91	1	4.55	3	13.64	0	0.00
GeoTü-SL96	655.5	342.73	20	48.78	14	34.15	3	7.32	4	9.76	0	0.00
GeoTü-SL96	660.5	343.88	104	46.43	79	35.27	9	4.02	32	14.29	0	0.00
GeoTü-SL96	665.5	349.64	88	43.14	83	40.69	8	3.92	25	12.25	0	0.00
GeoTü-SL96	670.5	355.39	123	49.00	88	35.06	8	3.19	28	11.16	4	1.59
GeoTü-SL96	675.5	360.67	88	68.22	28	21.71	3	2.33	9	6.98	1	0.78
GeoTü-SL96	680.5	364.03	97	44.70	69	31.80	10	4.61	34	15.67	7	3.23
GeoTü-SL96	685.5	367.38	110	55.56	44	22.22	11	5.56	23	11.62	10	5.05
GeoTü-SL96	690.5	370.74	102	54.55	50	26.74	11	5.88	20	10.70	4	2.14
GeoTü-SL96	695.5	374.10	119	54.84	50	23.04	12	5.53	27	12.44	9	4.15
GeoTü-SL96	700.5	377.45	96	54.24	49	27.68	9	5.08	19	10.73	4	2.26
GeoTü-SL96	705.5	380.81	134	53.60	56	22.40	15	6.00	34	13.60	11	4.40
GeoTü-SL96	710.5	384.16	141	51.09	59	21.38	14	5.07	40	14.49	22	7.97
GeoTü-SL96	715.5	387.52	45	54.22	15	18.07	8	9.64	11	13.25	4	4.82
GeoTü-SL96	720.5	390.88	89	56.33	37	23.42	11	6.96	20	12.66	1	0.63
GeoTü-SL96	725.5	394.23	73	47.71	34	22.22	15	9.80	26	16.99	5	3.27
GeoTü-SL96	730.5	397.59	51	55.43	12	13.04	9	9.78	14	15.22	6	6.52
GeoTü-SL96	735.5	400.95	78	54.17	21	14.58	13	9.03	18	12.50	14	9.72
GeoTü-SL96	740.5	404.30	85	56.29	23	15.23	16	10.60	17	11.26	10	6.62
GeoTü-SL96	745.5	407.66	51	62.20	10	12.20	11	13.41	9	10.98	1	1.22
GeoTü-SL96	750.5	413.10	69	63.30	10	9.17	15	13.76	14	12.84	1	0.92
GeoTü-SL96	755.5	419.93	23	54.76	5	11.90	9	21.43	5	11.90	0	0.00
GeoTü-SL96	760.5	426.77	5	71.43	1	14.29	0	0.00	1	14.29	0	0.00
GeoTü-SL96	765.5	433.60	11	73.33	3	20.00	1	6.67	0	0.00	0	0.00
GeoTü-SL96	770.5	440.43	12	70.59	2	11.76	1	5.88	2	11.76	0	0.00
GeoTü-SL96	775.5	447.27	35	62.50	10	17.86	3	5.36	7	12.50	1	1.79
GeoTü-SL96	780.5	454.10	37	67.27	4	7.27	8	14.55	6	10.91	0	0.00
GeoTü-SL96	785.5	460.93	19	67.86	3	10.71	4	14.29	2	7.14	0	0.00
GeoTü-SL96	790.5	467.77	48	46.60	24	23.30	14	13.59	10	9.71	7	6.80

ODP Site 964, MIS 11, stable isotopic composition in morphotypes of *G. ruber*

Core	cm	age	δ18O Type a "normal"	δ13C Type a "normal"	δ18O Type b "platys"	δ13C Type b "platys"	Sample weight (g)	planktonic forams/g sed.	split	sum split (PF)	entire sum (PF)
ODP 964-3H1	85.5	357.45	1.52	0.74	1.59	1.22	4.03	1425.31	16	359	5744
ODP 964-3H1	90.5	359.05	1.60	1.05	1.55	1.17	3.87	1868.73	16	452	7232
ODP 964-3H1	95.5	360.64	1.22	0.73	0.89	0.89	4.32	783.33	8	423	3384
ODP 964-3H1	100.5	360.95	1.08	0.70	0.69	-0.19	3.49	1668.77	16	364	5824
ODP 964-3H1	105.5	361.27	1.23	0.21	0.78	1.00	3.63	2023.14	16	459	7344
ODP 964-3H1	110.5	361.59	1.05	0.54	1.03	1.34	3.62	2271.82	16	514	8224
ODP 964-3H1	115.5	361.91	1.56	0.58	1.21	1.45	3.59	1510.86	16	339	5424
ODP 964-3H1	120.5	363.82	0.77	0.63	0.54	1.33	3.96	721.21	8	357	2856
ODP 964-3H1	125.5	364.45	0.76	0.91	0.24	1.13	3.91	830.69	8	406	3248
ODP 964-3H1	130.5	365.09	0.75	0.80	0.80	1.35	3.85	1824.42	16	439	7024
ODP 964-3H1	135.5	365.41	0.40	1.02	0.55	1.10	3.85	1467.01	16	353	5648
ODP 964-3H1	140.5	370.18	1.81	0.72	1.36	1.14	3.34	1849.10	16	386	6176
ODP 964-3H1	145.5	371.77	1.50	1.11	1.08	1.13	4.41	1131.97	16	312	4992
ODP 964-3H1	150.5	374.95	1.21	1.19	1.34	1.16	3.40	1717.65	16	365	5840
ODP 964-3H2	10.5	378.45	1.00	0.20	0.78	0.84	4.05	1430.12	16	362	5792
ODP 964-3H2	15.5	380.05	0.85	0.33	0.01	0.91	4.02	1176.12	8	591	4728
ODP 964-3H2	20.5	381.64	0.73	0.80	0.41	1.18	3.98	1451.26	16	361	5776
ODP 964-3H2	25.5	383.23	0.64	0.12	0.02	1.00	4.29	2931.47	16	786	12576
ODP 964-3H2	30.5	384.82	0.14	0.32	-0.27	0.59	4.33	1271.13	8	688	5504
ODP 964-3H2	40.5	388.00	0.57	0.25	-0.09	0.55	4.32	1288.89	16	348	5568
ODP 964-3H2	50.5	391.18			0.11	0.98	3.64	5661.54	64	322	20608
ODP 964-3H2	60.5	394.36	0.41	-0.03	0.22	0.99	3.25	787.69	8	320	2560
ODP 964-3H2	70.5	397.55	0.52	0.18	0.41	1.06	3.93	1897.20	16	466	7456
ODP 964-3H2	85.5	402.32	0.63	0.32	0.54	0.75	4.69	2620.04	32	384	12288
ODP 964-3H2	90.5	403.91	0.69	0.19	0.49	0.66	4.34	4158.53	32	564	18048
ODP 964-3H2	95.5	405.50	0.22	0.56	0.10	0.55	3.64	4518.68	32	514	16448
ODP 964-3H2	100.5	407.09	0.08	-0.55	-0.03	-0.15	3.66	3488.52	32	399	12768
ODP 964-3H2	105.5	408.68	-1.72	0.03	-1.86	0.34	4.15	1592.29	16	413	6608
ODP 964-3H2	135.5	434.30					3.72	6348.39	64	369	23616
ODP 964-3H3	15.5	457.45					3.94	4702.54	32	579	18528

ODP Site 964, MIS 11, morphotype counts of *G. ruber*

Core	cm	age	Type a "normal"	Type a "normal" (%)	Type b "platys"	Type b "platys" (%)	Type c "elongate"	Type c "elongate" (%)	G. ruber kummerform	G. ruber kummerform (%)	G. ruber pink	G. ruber pink (%)
ODP 964-3H1	85.5	357.45	26	50.98	18	35.29	2	3.92	5	9.80	0	0.00
ODP 964-3H1	90.5	359.05	18	52.94	9	26.47	0	0.00	7	20.59	0	0.00
ODP 964-3H1	95.5	360.64	47	45.63	44	42.72	4	3.88	8	7.77	0	0.00
ODP 964-3H1	100.5	360.95	28	56.00	12	24.00	1	2.00	9	18.00	0	0.00
ODP 964-3H1	105.5	361.27	37	38.54	41	42.71	5	5.21	13	13.54	0	0.00
ODP 964-3H1	110.5	361.59	63	46.32	47	34.56	6	4.41	20	14.71	0	0.00
ODP 964-3H1	115.5	361.91	38	51.35	27	36.49	1	1.35	8	10.81	0	0.00
ODP 964-3H1	120.5	363.82	45	52.94	34	40.00	2	2.35	4	4.71	0	0.00
ODP 964-3H1	125.5	364.45	86	48.04	70	39.11	8	4.47	15	8.38	0	0.00
ODP 964-3H1	130.5	365.09	121	48.40	79	31.60	7	2.80	42	16.80	1	0.40
ODP 964-3H1	135.5	365.41	73	48.67	64	42.67	4	2.67	9	6.00	0	0.00
ODP 964-3H1	140.5	370.18	52	59.09	24	27.27	2	2.27	6	6.82	4	4.55
ODP 964-3H1	145.5	371.77	41	53.95	27	35.53	4	5.26	4	5.26	0	0.00
ODP 964-3H1	150.5	374.95	71	63.39	31	27.68	0	0.00	10	8.93	0	0.00
ODP 964-3H2	10.5	378.45	49	70.00	15	21.43	2	2.86	4	5.71	0	0.00
ODP 964-3H2	15.5	380.05	81	75.00	14	12.96	3	2.78	10	9.26	0	0.00
ODP 964-3H2	20.5	381.64	43	51.19	25	29.76	5	5.95	11	13.10	0	0.00
ODP 964-3H2	25.5	383.23	46	48.94	27	28.72	5	5.32	14	14.89	2	2.13
ODP 964-3H2	30.5	384.82	72	71.29	20	19.80	1	0.99	7	6.93	1	0.99
ODP 964-3H2	40.5	388.00	42	49.41	30	35.29	3	3.53	6	7.06	4	4.71
ODP 964-3H2	50.5	391.18	25	60.98	12	29.27	2	4.88	2	4.88	0	0.00
ODP 964-3H2	60.5	394.36	60	58.25	34	33.01	1	0.97	7	6.80	1	0.97
ODP 964-3H2	70.5	397.55	62	75.61	12	14.63	2	2.44	6	7.32	0	0.00
ODP 964-3H2	85.5	402.32	39	65.00	13	21.67	4	6.67	3	5.00	1	1.67
ODP 964-3H2	90.5	403.91	45	59.21	20	26.32	3	3.95	4	5.26	4	5.26
ODP 964-3H2	95.5	405.50	74	56.06	39	29.55	5	3.79	5	3.79	9	6.82
ODP 964-3H2	100.5	407.09	29	56.86	5	9.80	10	19.61	4	7.84	3	5.88
ODP 964-3H2	105.5	408.68	10	62.50	2	12.50	4	25.00	0	0.00	0	0.00
ODP 964-3H2	135.5	434.30	3	50.00	1	16.67	2	33.33	0	0.00	0	0.00
ODP 964-3H3	15.5	457.45	5	83.33	1	16.67	0	0.00	0	0.00	0	0.00

Shell size parameters in morphotypes 1/7

16-size normalized shell measurement parameters:

P9: GeoTü-SL96. 750-751 cm
P19: GeoTü-SL96. 700-701 cm
P26: GeoTü-SL96. 665-666 cm
P28: GeoTü-SL96. 655-656 cm

Description:
P= Sample; T= type; Kam=Chamber; Br=width; H=hight; T=depth; V=front; S=side

	KamBr ("e")	KamH ("c")	KamT ("m")	Kam-1Br ("j")	Kam-1H ("i")	Kam-1T ("p")	Kam-2Br ("g")	Kam-2H ("h")	Kam-2T ("o")	PerimeterV ("b")	PerimeterS ("l")	area V ("k")	area S ("n")	Tiefe ("q")	ApperturBr (3 "f")	ApperturH ("d")
P9:T b "platys"	0.91	0.54	0.92	0.77	0.57	0.85	0.63	0.51	0.58	3.6	3.69	0.94	0.89	0.9	0.29	0.21
P9:T b "platys"	0.94	0.57	0.91	0.71	0.52	0.77	0.71	0.58	0.6	3.59	3.8	0.95	0.92	0.95	0.2	0.26
P9:T b "platys"	0.83	0.56	0.89	0.75	0.53	0.86	0.69	0.55	0.46	3.75	3.75	0.91	0.92	0.92	0.23	0.21
P9:T b "platys"	0.87	0.52	0.91	0.76	0.54	0.86	0.57	0.51	0.56	3.68	3.67	0.93	0.89	0.91	0.18	0.16
P9:T b "platys"	0.79	0.49	0.74	0.71	0.45	0.83	0.71	0.68	0.47	3.82	3.58	0.95	0.87	0.88	0.16	0.15
P9:T b "platys"	0.81	0.49	0.82	0.72	0.44	0.83	0.76	0.62	0.49	3.75	3.64	0.96	0.92	0.92	0.16	0.18
P9:T b "platys"	0.68	0.46	0.71	0.75	0.47	0.82	0.68	0.58	0.49	3.51	3.46	0.91	0.88	0.93	0.28	0.26
P9:T b "platys"	0.76	0.51	0.78	0.74	0.44	0.8	0.7	0.59	0.49	3.82	3.67	0.93	0.88	0.87	0.24	0.26
P9:T b "platys"	0.74	0.45	0.75	0.72	0.43	0.83	0.69	0.6	0.52	3.5	3.44	0.89	0.85	0.89	0.28	0.29
P9:T b "platys"	0.66	0.37	0.69	0.74	0.47	0.66	0.71	0.55	0.44	3.73	3.73	0.88	0.87	0.95	0.2	0.12
P9:T b "platys"	0.86	0.55	0.91	0.75	0.48	0.8	0.62	0.51	0.54	3.77	3.69	0.92	0.88	0.91	0.18	0.15
P9:T b "platys"	0.83	0.5	0.83	0.74	0.47	0.83	0.64	0.52	0.4	3.65	3.55	0.93	0.87	0.87	0.25	0.17
P9:T c "elongate"	0.8	0.57	0.82	0.76	0.45	0.79	0.69	0.56	0.36	4.46	5.24	0.92	0.87	0.83	0.28	0.17
P9:T c "elongate"	0.59	0.4	0.58	0.79	0.76	0.65	0.7	0.52	0.46	3.94	3.77	0.96	0.89	0.93	0.22	0.21
P9:T c "elongate"	0.79	0.56	0.77	0.75	0.47	0.85	0.69	0.64	0.46	4.04	3.96	0.95	0.89	0.92	0.26	0.26
P9:T c "elongate"	0.7	0.57	0.75	0.77	0.54	0.81	0.68	0.55	0.58	3.56	3.69	0.92	0.81	0.85	0.23	0.22
P9:T c "elongate"	0.71	0.49	0.68	0.8	0.47	0.76	0.82	0.76	0.52	3.93	3.72	0.96	0.9	0.95	0.26	0.29
P9:T c "elongate"	0.77	0.48	0.74	0.73	0.45	0.74	0.71	0.57	0.43	3.73	3.82	0.92	0.88	0.89	0.24	0.23
P9:T c "elongate"	0.64	0.4	0.6	0.81	0.55	0.81	0.8	0.59	0.41	3.72	3.8	0.93	0.9	0.95	0.24	0.2
P9:T c "elongate"	0.65	0.38	0.58	0.74	0.42	0.84	0.8	0.63	0.48	3.77	3.71	0.92	0.88	0.96	0.14	0.18
P9:T c "elongate"	0.82	0.45	0.81	0.67	0.47	0.81	0.76	0.63	0.44	4.07	4.02	0.94	0.92	0.88	0.26	0.26
P9:T c "elongate"	0.7	0.46	0.74	0.7	0.47	0.73	0.69	0.65	0.34	3.91	3.82	0.92	0.85	0.86	0.28	0.22
P9:T c "elongate"	0.64	0.42	0.6	0.72	0.58	0.82	0.69	0.53	0.5	3.7	3.55	0.91	0.85	0.85	0.24	0.24
P9:T c "elongate"	0.66	0.53	0.6	0.63	0.43	0.72	0.65	0.6	0.38	3.84	3.82	0.91	0.84	0.88	0.38	0.31
P9:T c "elongate"	0.75	0.53	0.74	0.7	0.43	0.78	0.72	0.6	0.41	4.07	3.79	0.94	0.91	0.89	0.31	0.28
P9:T c "elongate"	0.67	0.4	0.84	0.69	0.44	0.74	0.59	0.53	0.35	4.15	4	1	0.94	0.94	0.17	0.16
P9:T c "elongate"	0.66	0.44	0.64	0.69	0.4	0.79	0.72	0.6	0.37	3.74	3.53	0.91	0.85	0.89	0.23	0.23
P9:T c "elongate"	0.7	0.52	0.76	0.74	0.46	0.68	0.6	0.48	0.42	3.76	3.75	0.94	0.9	0.84	0.2	0.16
P9:T c "elongate"	0.59	0.36	0.53	0.66	0.37	0.72	0.72	0.7	0.43	3.98	3.82	0.97	0.93	1.01	0.26	0.27
P9:T c "elongate"	0.64	0.42	0.59	0.69	0.37	0.76	0.8	0.76	0.59	3.9	3.81	0.96	0.95	0.97	0.26	0.25
P9:T c "elongate"	0.59	0.44	0.57	0.71	0.41	0.76	0.77	0.71	0.48	3.72	3.56	0.93	0.87	0.93	0.35	0.31
P9:T c "elongate"	0.64	0.4	0.73	0.71	0.41	0.81	0.81	0.67	0.52	3.85	3.72	0.96	0.99	1	0.22	0.22
P9:T a "normal"	0.77	0.71	0.87	0.76	0.52	0.73	0.56	0.51	0.45	4.71	4.18	0.92	0.87	0.85	0.35	0.14
P9:T a "normal"	0.76	0.57	0.81	0.75	0.49	0.81	0.65	0.56	0.46	3.54	3.73	0.92	0.88	0.86	0.23	0.23
P9:T a "normal"	0.89	0.54	0.82	0.78	0.57	0.8	0.7	0.48	0.55	3.67	3.71	0.95	0.93	0.95	0.21	0.21
P9:T a "normal"	0.91	0.66	0.93	0.75	0.62	0.73	0.51	0.4	0.39	4.06	3.87	0.98	0.93	0.91	0.14	0.12
P9:T a "normal"	0.92	0.71	0.93	0.8	0.59	0.77	0.6	0.56	0.48	4.05	4.09	1.01	0.95	0.92	0.21	0.15
P9:T a "normal"	0.8	0.54	0.74	0.79	0.55	0.73	0.67	0.55	0.43	3.77	3.5	0.94	0.87	0.85	0.23	0.24
P9:T a "normal"	0.91	0.63	0.88	0.75	0.55	0.84	0.67	0.58	0.49	4.04	4.02	0.97	0.9	0.86	0.27	0.27
P9:T a "normal"	0.86	0.59	0.84	0.69	0.5	0.79	0.72	0.61	0.48	4.15	4.17	0.95	0.93	0.88	0.26	0.21
P9:T a "normal"	0.81	0.57	0.68	0.73	0.54	0.75	0.69	0.55	0.51	3.35	3.19	0.89	0.81	0.82	0.23	0.21
P9:T a "normal"	0.94	0.72	0.91	0.67	0.58	0.73	0.54	0.47	0.52	3.99	3.92	0.97	0.93	0.92	0.26	0.16
P9:T a "normal"	0.83	0.57	0.83	0.7	0.56	0.73	0.67	0.57	0.53	3.8	3.62	0.93	0.87	0.83	0.18	0.14
P9:T a "normal"	0.92	0.57	0.82	0.76	0.55	0.81	0.65	0.51	0.55	3.73	3.62	0.96	0.87	0.84	0.31	0.24
P9:T a "normal"	0.77	0.58	0.76	0.77	0.52	0.81	0.64	0.56	0.44	4.76	3.48	0.87	0.84	0.82	0.25	0.24
P9:T a "normal"	0.85	0.62	0.83	0.65	0.53	0.85	0.68	0.54	0.55	3.62	3.45	0.94	0.88	0.85	0.3	0.26
P9:T a "normal"	0.9	0.61	0.87	0.77	0.57	0.82	0.63	0.58	0.49	4.24	4.03	0.96	0.88	0.86	0.29	0.22
P9:T a "normal"	0.76	0.54	0.79	0.81	0.55	0.83	0.71	0.58	0.51	3.84	3.42	0.93	0.85	0.8	0.23	0.29
P9:T a "normal"	0.8	0.51	0.82	0.72	0.53	0.75	0.65	0.51	0.54	3.34	3.17	0.89	0.81	0.84	0.25	0.24
P9:T a "normal"	0.91	0.61	0.91	0.77	0.58	0.81	0.62	0.51	0.5	3.7	3.68	0.95	0.93	0.91	0.24	0.21
P9:T a "normal"	0.71	0.57	0.7	0.74	0.46	0.77	0.71	0.59	0.47	3.74	3.71	0.9	0.85	0.86	0.22	0.24
P9:T a "normal"	0.82	0.57	0.75	0.74	0.48	0.82	0.71	0.58	0.45	3.59	3.66	0.93	0.89	0.87	0.26	0.22
P9:T a "normal"	0.67	0.49	0.71	0.74	0.52	0.76	0.59	0.53	0.45	3.56	3.31	0.88	0.81	0.84	0.22	0.25
P9:T a "normal"	0.74	0.52	0.78	0.74	0.43	0.76	0.67	0.62	0.41	3.94	3.72	0.92	0.86	0.86	0.22	0.22
P9:T a "normal"	0.92	0.67	0.9	0.76	0.56	0.8	0.54	0.53	0.42	3.99	3.77	0.96	0.91	0.88	0.27	0.19
P9:T a "normal"	0.85	0.54	0.83	0.77	0.53	0.81	0.67	0.6	0.48	3.91	3.86	0.97	0.91	0.87	0.25	0.22
P9:T a "normal"	0.86	0.63	0.85	0.76	0.49	0.78	0.62	0.56	0.42	3.87	3.76	0.97	0.92	0.88	0.21	0.17
P9:T a "normal"	0.77	0.5	0.73	0.74	0.57	0.83	0.64	0.53	0.58	3.36	3.23	0.89	0.84	0.9	0.17	0.15
P9:T a "normal"	0.99	0.6	0.98	0.69	0.51	0.88	0.6	0.53	0.55	3.75	3.84	0.99	0.98	1	0.16	0.15
P9:T a "normal"	0.85	0.58	0.8	0.73	0.47	0.81	0.63	0.55	0.55	3.7	3.44	0.92	0.85	0.83	0.23	0.25
P9:T a "normal"	0.93	0.62	0.95	0.7	0.58	0.83	0.61	0.49	0.45	3.83	3.79	0.96	0.94	0.93	0.26	0.25
P9:T a "normal"	0.89	0.71	0.85	0.72	0.49	0.8	0.62	0.51	0.49	3.8	3.64	0.95	0.91	0.84	0.2	0.21
P9:T a "normal"	0.79	0.55	0.85	0.74	0.53	0.77	0.61	0.56	0.43	3.64	3.49	0.91	0.86	0.83	0.31	0.29
P9:T a "normal"	0.69	0.5	0.6	0.73	0.56	0.82	0.65	0.55	0.48	3.39	3.08	0.87	0.78	0.84	0.27	0.24

Shell size parameters in morphotypes 2/7

	KamBr ("e")	KamH ("c")	KamT ("m")	Kam-1Br ("j")	Kam-1H ("i")	Kam-1T ("p")	Kam-2Br ("g")	Kam-2H ("h")	Kam-2T ("o")	PerimeterV ("b")	PerimeterS ("l")	area V ("k")	area S ("n")	Tiefe ("q")	ApperturBr (3 "f")	ApperturH ("d")
P9:T a "normal"	0.89	0.64	0.87	0.77	0.53	0.77	0.59	0.57	0.4	3.91	3.97	0.98	0.88	0.81	0.28	0.28
P9:T a "normal"	0.77	0.5	0.7	0.75	0.5	0.77	0.65	0.51	0.48	3.47	3.42	0.88	0.81	0.82	0.24	0.27
P9:T a "normal"	0.82	0.6	0.86	0.73	0.56	0.8	0.57	0.56	0.52	3.78	3.64	0.95	0.88	0.83	0.36	0.3
P9:T a "normal"	0.8	0.63	0.86	0.68	0.48	0.83	0.54	0.5	0.56	3.46	3.38	0.92	0.87	0.9	0.21	0.16
P9:T a "normal"	0.79	0.52	0.83	0.78	0.5	0.83	0.69	0.6	0.5	3.43	3.32	0.9	0.84	0.84	0.2	0.18
P9:T a "normal"	0.74	0.48	0.73	0.76	0.46	0.8	0.66	0.57	0.49	3.39	3.36	0.9	0.85	0.85	0.21	0.2
P9:T a "normal"	0.97	0.62	0.89	0.71	0.52	0.88	0.67	0.53	0.62	3.53	3.48	0.94	0.89	0.89	0.2	0.19
P9:T a "normal"	0.84	0.56	0.77	0.74	0.51	0.85	0.65	0.53	0.52	3.59	3.5	0.94	0.9	0.91	0.21	0.26
P9:T a "normal"	0.87	0.58	0.87	0.75	0.57	0.83	0.62	0.48	0.87	3.41	3.3	0.91	0.86	0.89	0.2	0.16
P9:T a "normal"	0.78	0.58	0.74	0.7	0.46	0.73	0.66	0.58	0.55	3.78	3.72	0.92	0.85	0.81	0.29	0.27
P9:T a "normal"	0.7	0.47	0.59	0.73	0.43	0.74	0.68	0.61	0.56	3.64	3.28	0.91	0.86	0.96	0.25	0.21
P9:T a "normal"	0.89	0.6	0.9	0.72	0.47	0.78	0.7	0.56	0.49	3.54	3.46	0.94	0.89	0.87	0.18	0.23
P9:T a "normal"	0.81	0.55	0.78	0.71	0.43	0.79	0.7	0.59	0.6	3.74	3.62	0.94	0.89	0.9	0.31	0.25
P9:T a "normal"	0.82	0.61	0.83	0.74	0.5	0.77	0.62	0.52	0.48	3.78	3.63	0.94	0.9	0.83	0.3	0.28
P9:T a "normal"	0.84	0.57	0.81	0.67	0.54	0.79	0.68	0.48	0.49	3.53	3.42	0.93	0.86	0.84	0.26	0.23
P9:T a "normal"	0.75	0.43	0.79	0.71	0.49	0.83	0.71	0.63	0.54	3.63	3.37	0.92	0.84	0.87	0.18	0.18
P9:T a "normal"	0.76	0.49	0.66	0.76	0.52	0.8	0.6	0.51	0.49	3.34	3.19	0.87	0.81	0.83	0.18	0.19
P9:T a "normal"	0.71	0.44	0.65	0.75	0.51	0.83	0.7	0.56	0.45	3.41	3.25	0.89	0.84	0.87	0.24	0.28
P9:T a "normal"	0.92	0.66	0.92	0.72	0.59	0.74	0.56	0.48	0.5	3.76	3.77	0.96	0.91	0.89	0.23	0.19
P9:T a "normal"	0.82	0.51	0.78	0.76	0.46	0.8	0.71	0.6	0.47	3.79	3.84	0.97	0.96	1.01	0.26	0.19
P9:T a "normal"	0.8	0.56	0.77	0.69	0.46	0.72	0.6	0.5	0.38	3.7	3.65	0.92	0.86	0.86	0.31	0.23
P9:T a "normal"	0.86	0.53	0.87	0.65	0.46	0.81	0.68	0.59	0.42	3.96	4.11	0.96	0.93	0.93	0.23	0.24
P9:T a "normal"	0.89	0.57	0.87	0.74	0.63	0.82	0.54	0.41	0.46	3.73	3.75	0.96	0.93	0.89	0.25	0.19
P9:T a "normal"	0.74	0.51	0.75	0.78	0.52	0.79	0.53	0.53	0.43	3.56	3.36	0.9	0.84	0.82	0.18	0.26
P9:T a "normal"	0.79	0.66	0.87	0.71	0.55	0.77	0.54	0.5	0.47	3.99	3.71	0.91	0.87	0.85	0.22	0.2
P9:T a "normal"	0.63	0.44	0.62	0.73	0.53	0.79	0.59	0.52	0.46	3.39	3.22	0.87	0.82	0.84	0.28	0.22
P9:T a "normal"	0.89	0.64	0.92	0.78	0.53	0.81	0.6	0.51	0.5	3.94	3.85	0.95	0.9	0.89	0.21	0.16
P9:T a "normal"	0.7	0.46	0.66	0.77	0.57	0.79	0.67	0.52	0.48	3.32	3.11	0.89	0.81	0.84	0.28	0.21
P9:T a "normal"	0.86	0.61	0.84	0.72	0.5	0.84	0.59	0.52	0.47	3.53	3.37	0.91	0.88	0.89	0.2	0.16
P9:T a "normal"	0.88	0.64	0.88	0.71	0.54	0.78	0.56	0.5	0.41	3.95	3.68	0.96	0.9	0.86	0.2	0.18
P9:T a "normal"	0.76	0.55	0.8	0.67	0.48	0.77	0.62	0.46	0.42	3.64	3.56	0.91	0.89	0.88	0.26	0.27
P9:T a "normal"	0.97	0.62	0.87	0.71	0.56	0.86	0.61	0.53	0.53	3.73	3.62	1	0.94	0.89	0.21	0.29
P9:T a "normal"	0.81	0.49	0.78	0.73	0.48	0.84	0.74	0.62	0.54	3.73	3.74	0.95	0.95	0.96	0.2	0.18
P9:T a "normal"	0.98	0.64	0.92	0.7	0.5	0.82	0.57	0.54	0.45	4.02	3.87	1	0.95	0.92	0.31	0.21
P9:T a "normal"	0.97	0.73	1.01	0.7	0.55	0.71	0.6	0.49	0.43	4.24	4	1.03	0.98	0.98	0.21	0.13
P9:T a "normal"	0.8	0.47	0.66	0.71	0.52	0.77	0.69	0.54	0.53	3.73	3.68	0.92	0.89	0.93	0.31	0.29
P9:T a "normal"	0.78	0.46	0.69	0.81	0.53	0.84	0.67	0.63	0.49	3.67	3.57	0.93	0.89	0.91	0.29	0.27
P9:T a "normal"	0.68	0.43	0.66	0.77	0.55	0.8	0.73	0.62	0.47	3.63	3.5	0.91	0.88	0.93	0.15	0.18
P9:T a "normal"	0.85	0.48	0.74	0.74	0.39	0.79	0.7	0.61	0.5	3.99	3.92	0.99	0.96	0.96	0.27	0.27
P9:T a "normal"	0.76	0.48	0.66	0.73	0.49	0.81	0.69	0.58	0.39	3.84	3.47	0.93	0.84	0.87	0.29	0.3
P9:T a "normal"	0.89	0.66	0.89	0.73	0.55	0.81	0.58	0.5	0.41	3.83	3.76	0.97	0.92	0.91	0.29	0.23
P9:T a "normal"	0.84	0.58	0.83	0.78	0.54	0.85	0.62	0.5	0.46	3.49	3.38	0.92	0.87	0.88	0.16	0.13
P19:T b "platys"	0.84	0.45	0.82	0.72	0.5	0.82	0.64	0.54	0.65	3.85	3.9	0.94	0.9	0.97	0.19	0.2
P19:T b "platys"	0.78	0.49	0.76	0.69	0.54	0.8	0.65	0.58	0.4	3.34	3.34	0.88	0.83	0.88	0.25	0.19
P19:T b "platys"	0.84	0.54	0.81	0.77	0.5	0.87	0.63	0.58	0.66	3.73	3.54	0.94	0.87	0.86	0.18	0.17
P19:T b "platys"	0.83	0.48	0.81	0.76	0.44	0.84	0.7	0.59	0.45	3.83	3.76	0.93	0.91	0.9	0.21	0.2
P19:T b "platys"	0.66	0.34	0.67	0.5	0.89	0.99	0.73	0.59	0.5	3.55	4.11	0.92	0.99	1.08	0.22	0.23
P19:T b "platys"	0.73	0.36	0.66	0.71	0.47	0.84	0.86	0.62	0.45	3.61	3.6	0.91	0.88	0.96	0.18	0.15
P19:T b "platys"	0.81	0.43	0.74	0.76	0.49	0.89	0.74	0.59	0.51	3.55	3.49	0.93	0.89	0.93	0.15	0.22
P19:T b "platys"	0.88	0.51	0.89	0.76	0.49	0.8	0.73	0.62	0.5	3.86	3.88	0.98	0.95	0.95	0.25	0.18
P19:T b "platys"	0.67	0.37	0.68	0.82	0.5	0.79	0.85	0.68	0.49	3.62	3.49	0.93	0.89	0.95	0.17	0.17
P19:T b "platys"	0.9	0.53	0.89	0.69	0.39	0.85	0.81	0.6	0.46	3.74	3.81	0.96	0.95	0.93	0.22	0.21
P19:T b "platys"	0.83	0.48	0.81	0.77	0.38	0.87	0.78	0.65	0.48	3.76	3.63	0.94	0.91	0.93	0.24	0.24
P19:T b "platys"	0.66	0.38	0.68	0.81	0.59	0.83	0.71	0.53	0.48	3.39	3.18	0.88	0.81	0.88	0.18	0.13
P19:T b "platys"	0.86	0.52	0.91	0.79	0.47	0.86	0.77	0.64	0.45	3.83	3.8	0.96	0.94	0.93	0.15	0.14
P19:T b "platys"	0.71	0.41	0.64	0.73	0.44	0.76	0.68	0.58	0.46	3.33	2.98	0.87	0.78	0.86	0.22	0.23
P19:T b "platys"	0.8	0.42	0.83	0.76	0.46	0.88	0.76	0.58	0.46	3.7	3.7	0.93	0.9	0.91	0.16	0.15
P19:T b "platys"	0.67	0.31	0.62	0.79	0.5	0.9	0.75	0.62	0.48	3.56	3.55	0.92	0.9	0.99	0.21	0.19
P19:T b "platys"	0.64	0.31	0.66	0.85	0.55	1.01	0.81	0.59	0.49	3.54	3.38	0.93	0.9	0.99	0.16	0.1
P19:T b "platys"	0.74	0.43	0.69	0.76	0.39	0.84	0.76	0.65	0.47	3.77	3.76	0.94	0.9	0.94	0.22	0.22
P19:T b "platys"	0.89	0.44	0.85	0.79	0.48	0.89	0.71	0.55	0.52	3.84	3.8	0.96	0.91	0.91	0.22	0.22
P19:T b "platys"	0.88	0.54	0.95	0.77	0.47	0.93	0.72	0.57	0.46	4.05	3.64	0.94	0.91	0.96	0.2	0.23
P19:T b "platys"	0.81	0.47	0.82	0.77	0.49	0.82	0.72	0.53	0.47	3.72	3.59	0.93	0.89	0.88	0.18	0.18
P19:T b "platys"	0.83	0.48	0.8	0.76	0.44	0.86	0.76	0.61	0.51	4.34	4.16	0.94	0.89	0.92	0.16	0.16
P19:T b "platys"	0.88	0.5	0.86	0.77	0.52	0.91	0.71	0.59	0.48	3.91	3.64	0.94	0.9	0.92	0.14	0.15
P19:T c "elongate"	0.72	0.44	0.75	0.67	0.44	0.78	0.72	0.57	0.45	3.82	3.97	0.92	0.92	0.94	0.12	0.1
P19:T c "elongate"	0.76	0.42	0.74	0.72	0.36	0.8	0.78	0.7	0.38	3.95	3.68	0.96	0.9	0.9	0.19	0.24
P19:T c "elongate"	0.63	0.45	0.61	0.81	0.44	0.84	0.75	0.65	0.47	3.82	3.56	0.93	0.88	0.95	0.24	0.27
P19:T c "elongate"	0.79	0.41	0.81	0.74	0.45	0.78	0.76	0.62	0.47	4.44	4.05	0.94	0.88	0.87	0.17	0.2
P19:T a "normal"	0.99	0.66	0.94	0.84	0.52	0.9	0.55	0.55	0.51	3.82	3.72	0.97	0.94	0.94	0.21	0.17
P19:T a "normal"	0.93	0.55	0.87	0.76	0.53	0.9	0.63	0.49	0.51	3.6	3.46	0.92	0.89	0.9	0.24	0.23
P19:T a "normal"	1.02	0.61	0.95	0.69	0.58	0.89	0.68	0.5	0.43	3.82	3.73	0.99	0.96	0.93	0.21	0.2
P19:T a "normal"	0.89	0.55	0.86	0.71	0.61	0.85	0.62	0.44	0.53	3.73	3.75	0.94	0.9	0.93	0.28	0.25
P19:T a "normal"	0.91	0.51	0.84	0.75	0.47	0.87	0.75	0.64	0.47	3.67	3.76	0.95	0.91	0.92	0.22	0.24

Shell size parameters in morphotypes 3/7

	KamBr ("e")	KamH ("c")	KamT ("m")	Kam-1Br ("j")	Kam-1H ("i")	Kam-1T ("p")	Kam-2Br ("g")	Kam-2H ("h")	Kam-2T ("o")	PerimeterV ("b")	PerimeterS ("l")	area V ("k")	area S ("n")	Tiefe ("q")	ApertурBr (3 "f")	ApertурH ("d")
P9:T a "normal"	0.89	0.64	0.87	0.77	0.53	0.77	0.59	0.57	0.4	3.91	3.97	0.98	0.88	0.81	0.28	0.28
P9:T a "normal"	0.77	0.5	0.7	0.75	0.5	0.77	0.65	0.51	0.48	3.47	3.42	0.88	0.81	0.82	0.24	0.27
P9:T a "normal"	0.82	0.6	0.86	0.73	0.56	0.8	0.57	0.56	0.52	3.78	3.64	0.95	0.88	0.83	0.36	0.3
P9:T a "normal"	0.8	0.63	0.86	0.68	0.48	0.83	0.54	0.5	0.56	3.46	3.38	0.92	0.87	0.9	0.21	0.16
P9:T a "normal"	0.79	0.52	0.83	0.78	0.5	0.83	0.69	0.6	0.5	3.43	3.32	0.9	0.84	0.84	0.2	0.18
P9:T a "normal"	0.74	0.48	0.73	0.76	0.46	0.8	0.66	0.57	0.49	3.39	3.36	0.9	0.85	0.85	0.21	0.2
P9:T a "normal"	0.97	0.62	0.89	0.71	0.52	0.88	0.67	0.53	0.62	3.53	3.48	0.94	0.89	0.89	0.2	0.19
P9:T a "normal"	0.84	0.56	0.77	0.74	0.51	0.85	0.65	0.53	0.52	3.59	3.5	0.94	0.9	0.91	0.21	0.26
P9:T a "normal"	0.87	0.58	0.87	0.75	0.57	0.83	0.62	0.48	0.87	3.41	3.3	0.91	0.86	0.89	0.2	0.16
P9:T a "normal"	0.78	0.58	0.74	0.7	0.46	0.73	0.66	0.58	0.55	3.78	3.72	0.92	0.85	0.81	0.29	0.27
P9:T a "normal"	0.7	0.47	0.59	0.73	0.43	0.74	0.68	0.61	0.56	3.64	3.28	0.91	0.86	0.96	0.25	0.21
P9:T a "normal"	0.89	0.6	0.9	0.72	0.47	0.78	0.7	0.56	0.49	3.54	3.46	0.94	0.89	0.87	0.18	0.23
P9:T a "normal"	0.81	0.55	0.78	0.71	0.43	0.79	0.7	0.59	0.6	3.74	3.62	0.94	0.89	0.9	0.31	0.25
P9:T a "normal"	0.82	0.61	0.83	0.74	0.5	0.77	0.62	0.52	0.48	3.78	3.63	0.94	0.9	0.83	0.3	0.28
P9:T a "normal"	0.84	0.57	0.81	0.67	0.54	0.79	0.68	0.48	0.49	3.53	3.42	0.93	0.86	0.84	0.26	0.23
P9:T a "normal"	0.75	0.43	0.79	0.71	0.49	0.83	0.71	0.63	0.54	3.63	3.37	0.92	0.84	0.87	0.18	0.18
P9:T a "normal"	0.76	0.49	0.66	0.76	0.52	0.8	0.6	0.51	0.49	3.34	3.19	0.87	0.81	0.83	0.18	0.19
P9:T a "normal"	0.71	0.44	0.65	0.75	0.51	0.83	0.7	0.56	0.45	3.41	3.25	0.89	0.84	0.87	0.24	0.28
P9:T a "normal"	0.92	0.66	0.92	0.72	0.59	0.74	0.56	0.48	0.5	3.76	3.77	0.96	0.91	0.89	0.23	0.19
P9:T a "normal"	0.82	0.51	0.78	0.76	0.46	0.8	0.71	0.6	0.47	3.79	3.84	0.97	0.96	1.01	0.26	0.19
P9:T a "normal"	0.8	0.56	0.77	0.69	0.46	0.72	0.6	0.5	0.38	3.7	3.65	0.92	0.86	0.86	0.31	0.23
P9:T a "normal"	0.86	0.53	0.87	0.65	0.46	0.81	0.68	0.59	0.42	3.96	4.11	0.96	0.93	0.93	0.23	0.24
P9:T a "normal"	0.89	0.57	0.87	0.74	0.63	0.82	0.54	0.41	0.46	3.73	3.75	0.96	0.93	0.89	0.25	0.19
P9:T a "normal"	0.74	0.51	0.75	0.78	0.52	0.79	0.53	0.53	0.43	3.56	3.36	0.9	0.84	0.82	0.18	0.26
P9:T a "normal"	0.79	0.66	0.87	0.71	0.55	0.77	0.54	0.5	0.47	3.99	3.71	0.91	0.87	0.85	0.22	0.2
P9:T a "normal"	0.63	0.44	0.62	0.73	0.53	0.79	0.59	0.52	0.46	3.39	3.22	0.87	0.82	0.84	0.28	0.22
P9:T a "normal"	0.89	0.64	0.92	0.78	0.53	0.81	0.6	0.51	0.5	3.94	3.85	0.95	0.9	0.89	0.21	0.16
P9:T a "normal"	0.7	0.46	0.66	0.77	0.57	0.79	0.67	0.52	0.48	3.32	3.11	0.89	0.81	0.84	0.28	0.21
P9:T a "normal"	0.86	0.61	0.84	0.72	0.5	0.84	0.59	0.52	0.47	3.53	3.37	0.91	0.88	0.89	0.2	0.16
P9:T a "normal"	0.88	0.64	0.88	0.71	0.54	0.78	0.56	0.5	0.41	3.95	3.68	0.96	0.9	0.86	0.2	0.18
P9:T a "normal"	0.76	0.55	0.8	0.67	0.48	0.77	0.62	0.46	0.42	3.64	3.56	0.91	0.89	0.88	0.26	0.27
P9:T a "normal"	0.97	0.62	0.87	0.71	0.56	0.86	0.61	0.53	0.53	3.73	3.62	1	0.94	0.89	0.21	0.29
P9:T a "normal"	0.81	0.49	0.78	0.73	0.48	0.84	0.74	0.62	0.54	3.73	3.74	0.95	0.95	0.96	0.2	0.18
P9:T a "normal"	0.98	0.64	0.92	0.7	0.5	0.82	0.57	0.54	0.45	4.02	3.87	1	0.95	0.92	0.31	0.21
P9:T a "normal"	0.97	0.73	1.01	0.7	0.55	0.71	0.6	0.49	0.43	4.24	4	1.03	0.98	0.98	0.21	0.13
P9:T a "normal"	0.8	0.47	0.66	0.71	0.52	0.77	0.69	0.54	0.53	3.73	3.68	0.92	0.89	0.93	0.31	0.29
P9:T a "normal"	0.78	0.46	0.69	0.81	0.53	0.84	0.67	0.63	0.49	3.67	3.57	0.93	0.89	0.91	0.29	0.27
P9:T a "normal"	0.68	0.43	0.66	0.77	0.55	0.8	0.73	0.62	0.47	3.63	3.5	0.91	0.88	0.93	0.15	0.18
P9:T a "normal"	0.85	0.48	0.74	0.74	0.39	0.79	0.7	0.61	0.5	3.99	3.92	0.99	0.96	0.96	0.27	0.27
P9:T a "normal"	0.76	0.48	0.66	0.73	0.49	0.81	0.69	0.58	0.39	3.84	3.47	0.93	0.84	0.87	0.29	0.3
P9:T a "normal"	0.89	0.66	0.89	0.73	0.55	0.81	0.58	0.5	0.41	3.83	3.76	0.97	0.92	0.91	0.29	0.23
P9:T a "normal"	0.84	0.58	0.83	0.78	0.54	0.85	0.62	0.5	0.46	3.49	3.38	0.92	0.87	0.88	0.16	0.13
P19:T b "platys"	0.84	0.45	0.82	0.72	0.5	0.82	0.64	0.54	0.65	3.85	3.9	0.94	0.9	0.97	0.19	0.2
P19:T b "platys"	0.78	0.49	0.76	0.69	0.54	0.8	0.65	0.58	0.4	3.34	3.34	0.88	0.83	0.88	0.25	0.19
P19:T b "platys"	0.84	0.54	0.81	0.77	0.5	0.87	0.63	0.58	0.66	3.73	3.54	0.94	0.87	0.86	0.18	0.17
P19:T b "platys"	0.83	0.48	0.81	0.76	0.44	0.84	0.7	0.59	0.45	3.83	3.76	0.93	0.91	0.9	0.21	0.2
P19:T b "platys"	0.66	0.34	0.67	0.5	0.89	0.99	0.73	0.59	0.5	3.55	4.11	0.92	0.99	1.08	0.22	0.23
P19:T b "platys"	0.73	0.36	0.66	0.71	0.47	0.84	0.86	0.62	0.45	3.61	3.6	0.91	0.88	0.96	0.18	0.15
P19:T b "platys"	0.81	0.43	0.74	0.76	0.49	0.89	0.74	0.59	0.51	3.55	3.49	0.93	0.89	0.93	0.15	0.22
P19:T b "platys"	0.88	0.51	0.89	0.76	0.49	0.8	0.73	0.62	0.5	3.86	3.88	0.98	0.95	0.95	0.25	0.18
P19:T b "platys"	0.67	0.37	0.68	0.82	0.5	0.79	0.85	0.68	0.49	3.62	3.49	0.93	0.89	0.95	0.17	0.17
P19:T b "platys"	0.9	0.53	0.89	0.69	0.39	0.85	0.81	0.6	0.46	3.74	3.81	0.96	0.95	0.93	0.22	0.21
P19:T b "platys"	0.83	0.48	0.81	0.77	0.38	0.87	0.78	0.65	0.48	3.76	3.63	0.94	0.91	0.93	0.24	0.24
P19:T b "platys"	0.66	0.38	0.68	0.81	0.59	0.83	0.71	0.53	0.48	3.39	3.18	0.88	0.81	0.88	0.18	0.13
P19:T b "platys"	0.86	0.52	0.91	0.79	0.47	0.86	0.77	0.64	0.45	3.83	3.8	0.96	0.94	0.93	0.15	0.14
P19:T b "platys"	0.71	0.41	0.64	0.73	0.44	0.76	0.68	0.58	0.46	3.33	2.98	0.87	0.78	0.86	0.22	0.23
P19:T b "platys"	0.8	0.42	0.83	0.76	0.46	0.88	0.76	0.58	0.46	3.7	3.7	0.93	0.9	0.91	0.16	0.15
P19:T b "platys"	0.67	0.31	0.62	0.79	0.5	0.9	0.75	0.62	0.48	3.56	3.55	0.92	0.9	0.99	0.21	0.19
P19:T b "platys"	0.64	0.31	0.66	0.85	0.55	1.01	0.81	0.59	0.49	3.54	3.38	0.93	0.9	0.99	0.16	0.1
P19:T b "platys"	0.74	0.43	0.69	0.76	0.39	0.84	0.76	0.65	0.47	3.77	3.76	0.94	0.9	0.94	0.22	0.22
P19:T b "platys"	0.89	0.44	0.85	0.79	0.48	0.89	0.71	0.55	0.52	3.84	3.8	0.96	0.91	0.91	0.22	0.22
P19:T b "platys"	0.88	0.54	0.95	0.77	0.47	0.93	0.72	0.57	0.46	4.05	3.64	0.94	0.91	0.96	0.2	0.23
P19:T b "platys"	0.81	0.47	0.82	0.77	0.49	0.82	0.72	0.53	0.47	3.72	3.59	0.93	0.89	0.88	0.18	0.18
P19:T b "platys"	0.83	0.48	0.8	0.76	0.44	0.86	0.76	0.61	0.51	4.34	4.16	0.94	0.89	0.92	0.16	0.16
P19:T b "platys"	0.88	0.5	0.86	0.77	0.52	0.91	0.71	0.59	0.48	3.91	3.64	0.94	0.9	0.92	0.14	0.15
P19:T c "elongate"	0.72	0.44	0.75	0.67	0.44	0.78	0.72	0.57	0.45	3.82	3.97	0.92	0.92	0.94	0.12	0.1
P19:T c "elongate"	0.76	0.42	0.74	0.72	0.36	0.8	0.78	0.7	0.38	3.95	3.68	0.96	0.9	0.9	0.19	0.24
P19:T c "elongate"	0.63	0.45	0.61	0.81	0.44	0.84	0.75	0.65	0.47	3.82	3.56	0.93	0.88	0.95	0.24	0.27
P19:T c "elongate"	0.79	0.41	0.81	0.74	0.45	0.78	0.76	0.62	0.47	4.44	4.05	0.94	0.88	0.87	0.17	0.2
P19:T a "normal"	0.99	0.66	0.94	0.84	0.52	0.9	0.55	0.55	0.51	3.82	3.72	0.97	0.94	0.94	0.21	0.17
P19:T a "normal"	0.93	0.55	0.87	0.76	0.53	0.9	0.63	0.49	0.51	3.6	3.46	0.92	0.89	0.9	0.24	0.23
P19:T a "normal"	1.02	0.61	0.95	0.69	0.58	0.89	0.68	0.5	0.43	3.82	3.73	0.99	0.96	0.93	0.21	0.2
P19:T a "normal"	0.89	0.55	0.86	0.71	0.61	0.85	0.62	0.44	0.53	3.73	3.75	0.94	0.9	0.93	0.28	0.25
P19:T a "normal"	0.91	0.51	0.84	0.75	0.47	0.87	0.75	0.64	0.47	3.67	3.76	0.95	0.91	0.92	0.22	0.24

Shell size parameters in morphotypes 4/7

	KamBr ("e")	KamH ("c")	KamT ("m")	Kam-1Br ("j")	Kam-1H ("i")	Kam-1T ("p")	Kam-2Br ("g")	Kam-2H ("h")	Kam-2T ("o")	PerimeterV ("b")	PerimeterS ("l")	area V ("k")	area S ("n")	Triefe ("q")	ApperturBr (3 "f")	AperturH ("d")
P19:T a "normal"	0.92	0.54	0.85	0.78	0.56	0.71	0.61	0.52	0.49	3.64	3.64	0.96	0.94	0.95	0.17	0.21
P19:T a "normal"	0.53	0.83	0.82	0.73	0.54	0.8	0.69	0.54	0.4	3.79	3.6	0.91	0.88	0.9	0.17	0.14
P19:T a "normal"	0.82	0.51	0.76	0.72	0.53	0.87	0.64	0.52	0.55	3.43	3.39	0.92	0.88	0.92	0.16	0.14
P19:T a "normal"	0.9	0.55	0.9	0.7	0.51	0.87	0.65	0.61	0.45	3.63	3.68	0.95	0.91	0.95	0.23	0.11
P19:T a "normal"	0.78	0.43	0.8	0.82	0.52	0.86	0.64	0.55	0.41	3.46	3.39	0.92	0.88	0.92	0.13	0.15
P19:T a "normal"	0.89	0.52	0.91	0.72	0.52	0.79	0.53	0.39	0.57	4.24	3.83	0.94	0.84	0.86	0.29	0.24
P19:T a "normal"	0.99	0.55	0.93	0.75	0.46	0.73	0.58	0.47	0.49	3.61	3.64	0.96	0.94	0.97	0.26	0.19
P19:T a "normal"	0.86	0.54	0.82	0.74	0.5	0.84	0.59	0.55	0.5	3.59	3.41	0.92	0.88	0.88	0.18	0.16
P19:T a "normal"	0.77	0.49	0.72	0.73	0.57	0.8	0.6	0.52	0.54	3.69	3.37	0.91	0.85	0.86	0.18	0.15
P19:T a "normal"	1.01	0.65	0.95	0.69	0.51	0.74	0.52	0.5	0.64	4.05	3.97	0.96	0.91	0.94	0.27	0.25
P19:T a "normal"	0.7	0.41	0.67	0.82	0.55	0.82	0.71	0.6	0.35	3.74	3.47	0.92	0.86	0.89	0.27	0.27
P19:T a "normal"	0.72	0.45	0.67	0.75	0.5	0.84	0.66	0.51	0.36	3.65	3.47	0.92	0.86	0.86	0.27	0.26
P19:T a "normal"	0.79	0.47	0.78	0.79	0.5	0.75	0.57	0.52	0.44	3.99	3.84	0.9	0.85	0.85	0.23	0.22
P26:T b "platys"	0.75	0.4	0.77	0.79	0.4	0.88	0.81	0.61	0.47	3.76	3.68	0.94	0.9	0.91	0.18	0.16
P26:T b "platys"	0.83	0.49	0.84	0.63	0.38	0.84	0.73	0.56	0.37	3.96	3.93	0.96	0.9	0.88	0.15	0.16
P26:T b "platys"	0.8	0.47	0.64	0.69	0.45	0.83	0.82	0.59	0.44	3.74	3.59	0.93	0.91	0.98	0.17	0.17
P26:T b "platys"	0.91	0.52	0.89	0.72	0.42	0.94	0.81	0.61	0.56	3.99	3.93	0.96	0.97	0.99	0.16	0.22
P26:T b "platys"	0.74	0.46	0.73	0.76	0.45	0.8	0.62	0.53	0.45	3.96	3.59	0.91	0.81	0.81	0.16	0.15
P26:T b "platys"	0.94	0.63	0.88	0.77	0.52	0.91	0.72	0.54	0.52	3.88	4.2	0.96	0.95	0.94	0.1	0.21
P26:T b "platys"	0.9	0.5	0.89	0.68	0.47	0.88	0.65	0.5	0.4	3.76	3.43	0.9	0.85	0.88	0.27	0.29
P26:T b "platys"	0.76	0.42	0.73	0.81	0.42	0.84	0.72	0.66	0.47	3.97	3.77	0.95	0.88	0.92	0.24	0.29
P26:T b "platys"	0.68	0.27	0.56	0.8	0.5	0.84	0.85	0.54	0.48	3.81	3.64	0.91	0.86	0.95	0.22	0.18
P26:T b "platys"	0.79	0.42	0.79	0.76	0.42	0.81	0.69	0.64	0.61	4.13	3.78	0.94	0.89	0.92	0.21	0.19
P26:T b "platys"	0.84	0.48	0.84	0.64	0.39	0.82	0.76	0.63	0.44	4.35	3.84	0.93	0.86	0.88	0.1	0.14
P26:T b "platys"	0.72	0.31	0.65	0.78	0.43	0.84	0.77	0.67	0.55	4.64	3.84	0.93	0.85	0.95	0.12	0.09
P26:T b "platys"	0.89	0.46	0.83	0.86	0.75	0.93	0.82	0.58	0.47	4.02	4.25	0.96	0.93	0.95	0.17	0.17
P26:T b "platys"	0.76	0.39	0.74	0.8	0.45	0.88	0.78	0.57	0.45	3.67	3.61	0.92	0.88	0.88	0.16	0.19
P26:T b "platys"	0.79	0.56	0.76	0.73	0.42	0.83	0.76	0.64	0.51	4.59	4.5	0.92	0.92	0.96	0.19	0.33
P26:T c "elongate"	0.76	0.52	0.84	0.72	0.42	0.84	0.56	0.41	0.45	3.95	4.03	0.95	0.97	0.96	0.15	0.15
P26:T c "elongate"	0.72	0.36	0.77	0.73	0.45	0.84	0.7	0.62	0.56	3.84	3.71	0.92	0.91	0.96	0.16	0.21
P26:T c "elongate"	0.79	0.49	0.74	0.71	0.47	0.83	0.59	0.45	0.31	4.15	4.48	0.94	0.94	1.01	0.22	0.21
P26:T c "elongate"	0.56	0.25	0.71	0.63	0.31	0.7	0.74	0.54	0.39	4.16	3.49	0.94	0.9	0.94	0.18	0.1
P26:T c "elongate"	0.67	0.32	0.62	0.74	0.4	0.81	0.74	0.61	0.43	4.88	4.35	0.94	0.85	0.92	0.18	0.27
P26:T c "elongate"	0.65	0.25	0.45	0.62	0.43	0.71	0.45	0.43	0.46	3.54	3.66	0.92	0.88	0.95	0.15	0.11
P26:T c "elongate"	0.63	0.35	0.66	0.7	0.35	0.74	0.7	0.55	0.39	3.72	3.52	0.94	0.88	0.96	0.19	0.21
P26:T a "normal"	0.89	0.59	0.88	0.74	0.55	0.82	0.72	0.51	0.57	3.81	3.78	0.95	0.93	0.93	0.16	0.13
P26:T a "normal"	0.92	0.49	0.93	0.73	0.56	0.95	0.66	0.5	0.54	3.86	3.74	0.95	0.93	0.97	0.26	0.17
P26:T a "normal"	0.57	0.83	0.83	0.73	0.49	0.84	0.66	0.48	0.4	4.14	4.05	0.95	0.9	0.91	0.39	0.34
P26:T a "normal"	0.92	0.58	0.86	0.76	0.56	0.83	0.62	0.46	0.46	4.34	4.02	0.98	0.91	0.9	0.16	0.22
P26:T a "normal"	0.99	0.63	1.02	0.72	0.47	0.95	0.65	0.46	0.51	3.96	3.84	0.94	0.93	1.02	0.15	0.18
P26:T a "normal"	0.74	0.4	0.7	0.77	0.38	0.84	0.67	0.62	0.5	3.8	3.74	0.91	0.88	0.93	0.11	0.1
P26:T a "normal"	1.01	0.58	1.01	0.74	0.57	0.88	0.58	0.44	0.56	3.83	3.99	0.97	0.95	1	0.17	0.17
P26:T a "normal"	0.98	0.57	0.88	0.74	0.45	0.92	0.78	0.59	0.49	4.01	4.04	0.99	0.99	0.99	0.17	0.17
P26:T a "normal"	0.95	0.56	0.92	0.68	0.42	0.87	0.63	0.61	0.5	3.96	3.91	0.95	0.94	0.96	0.17	0.17
P26:T a "normal"	0.75	0.4	0.73	0.8	0.52	0.86	0.7	0.56	0.44	3.88	3.83	0.94	0.87	0.92	0.2	0.2
P26:T a "normal"	0.92	0.56	0.88	0.71	0.49	0.88	0.65	0.55	0.51	4.24	4.18	0.95	0.91	0.91	0.23	0.22
P26:T a "normal"	0.82	0.47	0.79	0.8	0.49	0.87	0.79	0.62	0.54	3.91	3.59	0.96	0.93	0.97	0.21	0.2
P26:T a "normal"	0.77	0.47	0.85	0.7	0.5	0.75	0.61	0.55	0.37	3.94	3.8	0.93	0.89	0.89	0.1	0.17
P26:T a "normal"	0.91	0.55	0.93	0.72	0.58	0.91	0.69	0.51	0.42	4.13	4.06	0.96	0.93	0.89	0.16	0.14
P26:T a "normal"	0.78	0.52	0.75	0.73	0.44	0.76	0.65	0.52	0.51	3.96	3.92	0.9	0.85	0.91	0.18	0.18
P26:T a "normal"	0.79	0.46	0.76	0.79	0.47	0.9	0.7	0.53	0.52	3.93	3.68	0.94	0.93	0.95	0.17	0.25
P26:T a "normal"	0.78	0.48	0.75	0.78	0.49	0.89	0.69	0.61	0.51	3.62	3.45	0.94	0.89	0.93	0.13	0.18
P26:T a "normal"	0.93	0.57	0.94	0.71	0.51	0.89	0.72	0.55	0.5	3.71	3.64	0.94	0.91	0.96	0.22	0.23
P26:T a "normal"	0.95	0.59	0.91	0.74	0.54	0.89	0.71	0.5	0.54	4	3.88	0.94	0.91	0.92	0.16	0.22
P26:T a "normal"	0.83	0.47	0.84	0.7	0.41	0.86	0.75	0.56	0.53	4.14	3.97	0.95	0.92	0.93	0.19	0.23
P26:T a "normal"	0.8	0.43	0.73	0.78	0.39	0.87	0.78	0.62	0.41	4.16	4.13	0.94	0.91	0.91	0.18	0.23
P26:T a "normal"	0.89	0.53	0.89	0.67	0.39	0.85	0.75	0.58	0.39	4.34	4.14	0.96	0.97	0.97	0.17	0.15
P26:T a "normal"	0.81	0.45	0.88	0.79	0.65	0.94	0.83	0.65	0.49	4.45	4.37	0.96	0.94	0.96	0.09	0.13
P26:T a "normal"	0.93	0.59	0.92	0.68	0.58	0.86	0.5	0.43	0.62	3.62	3.63	0.93	0.89	0.91	0.18	0.16
P26:T a "normal"	0.91	0.6	0.87	0.65	0.48	0.87	0.69	0.45	0.5	3.44	3.57	0.9	0.88	0.94	0.2	0.17
P26:T a "normal"	0.9	0.51	0.87	0.74	0.51	0.88	0.66	0.54	0.59	3.51	3.56	0.93	0.9	0.9	0.12	0.15
P26:T a "normal"	0.91	0.48	0.75	0.67	0.38	0.87	0.77	0.63	0.54	4.1	3.91	0.95	0.9	0.92	0.18	0.24
P26:T a "normal"	0.81	0.41	0.72	0.71	0.49	0.91	0.77	0.58	0.47	3.94	3.92	0.96	0.95	0.96	0.14	0.16
P26:T a "normal"	0.93	0.59	1.01	0.64	0.48	0.82	0.5	0.44	0.55	4.17	4.05	0.93	0.92	0.97	0.16	0.15
P26:T a "normal"	0.91	0.49	0.91	0.76	0.58	0.88	0.66	0.53	0.56	3.92	3.78	0.92	0.91	0.94	0.16	0.19
P26:T a "normal"	0.98	0.54	0.86	0.67	0.4	0.79	0.66	0.55	0.4	3.85	3.92	0.95	0.94	0.9	0.25	0.2
P26:T a "normal"	0.88	0.48	0.89	0.77	0.48	0.91	0.75	0.59	0.46	4.13	3.94	0.97	0.96	0.99	0.1	0.14
P26:T a "normal"	0.96	0.55	0.9	0.7	0.53	0.91	0.67	0.56	0.71	3.72	3.95	0.95	0.93	0.94	0.21	0.16
P26:T a "normal"	0.84	0.54	0.84	0.75	0.51	0.8	0.58	0.55	0.41	3.91	3.39	0.92	0.83	0.8	0.15	0.18
P26:T a "normal"	0.86	0.56	0.94	0.68	0.44	0.83	0.61	0.49	0.38	3.95	3.82	0.93	0.9	0.95	0.18	0.14
P26:T a "normal"	0.71	0.46	0.69	0.72	0.43	0.8	0.72	0.57	0.44	3.83	3.68	0.92	0.86	0.91	0.17	0.2
P26:T a "normal"	0.99	0.65	0.94	0.99	0.65	0.94	0.76	0.57	0.91	3.94	3.86	0.97	0.93	0.97	0.15	0.19
P26:T a "normal"	0.78	0.37	0.73	0.68	0.5	0.77	0.68	0.53	0.44	3.63	3.67	0.9	0.84	0.91	0.15	0.14
P26:T a "normal"	0.93	0.5	0.91	0.72	0.39	0.9	0.8	0.62	0.5	4.19	3.87	0.96	0.93	0.93	0.12	0.18

Shell size parameters in morphotypes 5/7

	KamBr ("e")	KamH ("c")	KamT ("m")	Kam-1Br ("j")	Kam-1H ("i")	Kam-1T ("p")	Kam-2Br ("g")	Kam-2H ("h")	Kam-2T ("o")	PerimeterV ("b")	PerimeterS ("l")	area V ("k")	area S ("n")	Tiefe ("q")	AperturBr (3 "f")	AperturH ("d")
P26:T a "normal"	0.77	0.41	0.77	0.86	0.53	0.87	0.49	0.46	0.63	4.47	4.24	0.97	0.97	1.04	0.18	0.14
P26:T a "normal"	0.91	0.58	0.96	0.71	0.48	0.9	0.68	0.53	0.61	3.82	3.74	0.92	0.89	0.91	0.15	0.11
P26:T a "normal"	0.74	0.48	0.71	0.79	0.5	0.81	0.68	0.55	0.46	3.85	3.53	0.89	0.84	0.89	0.2	0.26
P26:T a "normal"	0.82	0.54	0.81	0.72	0.58	0.88	0.64	0.42	0.42	3.96	3.31	0.91	0.83	0.9	0.18	0.22
P26:T a "normal"	0.66	0.41	0.6	0.7	0.46	0.77	0.7	0.64	0.39	4.27	3.59	0.9	0.83	0.92	0.26	0.2
P26:T a "normal"	0.78	0.44	0.77	0.76	0.53	0.76	0.58	0.55	0.43	3.61	3.5	0.89	0.86	0.86	0.21	0.2
P26:T a "normal"	0.79	0.52	0.81	0.74	0.53	0.75	0.66	0.58	0.47	3.88	3.8	0.92	0.88	0.88	0.15	0.22
P26:T a "normal"	0.98	0.65	0.94	0.71	0.65	0.85	0.63	0.44	0.51	3.97	4.04	0.96	0.91	0.9	0.17	0.15
P26:T a "normal"	0.75	0.44	0.77	0.72	0.43	0.77	0.69	0.62	0.54	3.98	4.08	0.9	0.88	0.95	0.2	0.23
P26:T a "normal"	0.81	0.57	0.88	0.79	0.48	0.84	0.56	0.54	0.45	4.38	4.19	0.93	0.9	0.91	0.14	0.17
P26:T a "normal"	0.87	0.48	0.76	0.71	0.45	0.82	0.61	0.59	0.5	4.2	3.72	0.94	0.88	0.89	0.17	0.17
P26:T a "normal"	0.94	0.55	0.88	0.69	0.43	0.91	0.66	0.58	0.57	4.15	4.06	0.95	0.92	0.94	0.17	0.16
P26:T a "normal"	0.88	0.39	0.89	0.77	0.51	0.83	0.54	0.52	0.39	4.43	4.09	0.96	0.91	0.87	0.2	0.23
P26:T a "normal"	0.83	0.53	0.88	0.79	0.5	0.82	0.66	0.57	0.51	3.89	3.96	0.93	0.87	0.85	0.19	0.16
P26:T a "normal"	0.77	0.32	0.78	0.69	0.39	0.89	0.75	0.56	0.51	3.9	3.49	0.91	0.87	0.93	0.12	0.11
P26:T a "normal"	0.69	0.36	0.64	0.71	0.38	0.82	0.8	0.63	0.36	4.21	3.64	0.92	0.87	0.92	0.11	0.14
P26:T a "normal"	0.84	0.52	0.84	0.76	0.56	0.89	0.65	0.54	0.47	4.36	3.93	0.94	0.88	0.91	0.13	0.25
P26:T a "normal"	0.68	0.44	0.7	0.8	0.46	0.77	0.67	0.58	0.45	3.86	3.73	0.89	0.85	0.88	0.14	0.19
P26:T a "normal"	0.73	0.46	0.72	0.76	0.46	0.92	0.79	0.58	0.42	4.03	3.93	0.92	0.89	0.93	0.19	0.18
P26:T a "normal"	0.95	0.53	0.96	0.71	0.6	0.82	0.66	0.5	0.52	3.71	4.14	0.93	0.9	0.94	0.15	0.12
P26:T a "normal"	0.89	0.55	0.88	0.65	0.47	0.89	0.68	0.58	0.46	4.11	4.55	0.98	0.95	0.97	0.2	0.36
P26:T a "normal"	0.79	0.4	0.71	0.71	0.45	0.87	0.69	0.61	0.54	3.72	3.49	0.92	0.88	0.94	0.13	0.14
P26:T a "normal"	0.65	0.4	0.65	0.76	0.42	0.81	0.65	0.64	0.49	3.99	3.8	0.88	0.89	1	0.21	0.15
P26:T a "normal"	0.91	0.52	0.87	0.74	0.5	0.87	0.62	0.54	0.54	4.1	4.05	0.96	0.92	0.91	0.17	0.26
P26:T a "normal"	0.79	0.46	0.76	0.71	0.42	0.8	0.79	0.55	0.46	4.43	4.27	0.91	0.89	0.88	0.21	0.21
P26:T a "normal"	0.91	0.6	0.91	0.69	0.52	0.92	0.82	0.58	0.56	4.03	4.19	0.94	0.91	0.95	0.21	0.16
P26:T a "normal"	0.82	0.49	0.83	0.55	0.48	0.88	0.6	0.54	0.5	3.77	4.08	0.92	0.91	0.99	0.17	0.18
P26:T a "normal"	0.91	0.5	0.89	0.75	0.54	0.86	0.7	0.61	0.46	3.65	3.79	0.93	0.88	0.91	0.16	0.16
P26:T a "normal"	0.86	0.46	0.82	0.66	0.5	0.89	0.66	0.54	0.48	3.73	3.49	0.92	0.87	0.93	0.15	0.22
P26:T a "normal"	0.84	0.48	0.81	0.72	0.43	0.9	0.67	0.6	0.44	4.08	3.53	0.93	0.87	0.89	0.18	0.22
P26:T a "normal"	0.86	0.51	0.86	0.75	0.57	0.88	0.67	0.52	0.58	3.73	4.42	0.93	0.92	0.97	0.15	0.21
P26:T a "normal"	0.78	0.52	0.78	0.79	0.51	0.92	0.65	0.46	0.53	3.45	3.46	0.89	0.87	0.95	0.17	0.23
P26:T a "normal"	0.98	0.59	0.91	0.75	0.54	0.81	0.58	0.53	0.4	4.11	3.97	0.97	0.94	0.92	0.26	0.21
P26:T a "normal"	0.89	0.51	0.87	0.71	0.48	0.85	0.67	0.54	0.38	4.03	4.01	0.97	0.92	0.88	0.19	0.2
P26:T a "normal"	0.9	0.53	0.84	0.59	0.49	0.91	0.73	0.53	0.55	3.6	3.92	0.94	0.91	0.91	0.13	0.23
P26:T a "normal"	0.89	0.54	0.82	0.75	0.56	0.77	0.59	0.45	0.49	4.04	3.62	0.92	0.84	0.84	0.21	0.18
P26:T a "normal"	0.91	0.59	0.89	0.73	0.54	0.87	0.61	0.53	0.52	3.52	3.52	0.95	0.9	0.9	0.13	0.12
P26:T a "normal"	0.81	0.45	0.87	0.73	0.53	0.83	0.62	0.48	0.51	3.71	3.64	0.91	0.89	0.93	0.14	0.16
P26:T a "normal"	0.92	0.54	0.85	0.73	0.54	0.85	0.63	0.5	0.49	3.9	3.78	0.94	0.88	0.86	0.18	0.18
P26:T a "normal"	0.85	0.57	0.92	0.79	0.53	0.85	0.67	0.47	0.44	4.09	3.92	0.94	0.94	0.95	0.16	0.15
P26:T a "normal"	0.94	0.63	0.93	0.82	0.6	0.85	0.61	0.49	0.49	3.65	3.61	0.96	0.92	0.92	0.12	0.13
P26:T a "normal"	0.79	0.51	0.8	0.62	0.48	0.74	0.76	0.55	0.48	3.65	3.78	0.9	0.92	0.96	0.21	0.24
P26:T a "normal"	0.81	0.56	0.81	0.74	0.47	0.86	0.68	0.56	0.52	3.55	3.54	0.92	0.89	0.92	0.16	0.24
P26:T a "normal"	0.87	0.53	0.86	0.79	0.51	0.89	0.69	0.54	0.46	3.85	3.7	0.94	0.89	0.88	0.11	0.07
P26:T a "normal"	0.88	0.57	0.84	0.7	0.51	0.76	0.64	0.53	0.46	3.82	3.58	0.92	0.86	0.88	0.17	0.17
P26:T a "normal"	0.7	0.48	0.83	0.77	0.47	0.77	0.61	0.6	0.51	3.57	3.66	0.91	0.91	0.96	0.19	0.21
P26:T a "normal"	0.95	0.55	0.93	0.7	0.54	0.85	0.69	0.55	0.47	3.84	3.82	0.94	0.91	0.94	0.17	0.15
P26:T a "normal"	0.85	0.57	0.81	0.75	0.5	0.78	0.59	0.54	0.42	3.97	3.53	0.93	0.87	0.84	0.14	0.14
P26:T a "normal"	0.72	0.41	0.62	0.73	0.46	0.82	0.75	0.57	0.44	3.72	3.44	0.92	0.84	0.92	0.29	0.24
P26:T a "normal"	0.84	0.48	0.86	0.78	0.5	0.81	0.71	0.57	0.42	4.2	4.37	0.92	0.9	0.89	0.23	0.19
P26:T a "normal"	0.86	0.56	0.94	0.79	0.5	0.91	0.74	0.53	0.49	4.3	4.16	0.97	0.96	0.97	0.21	0.25
P26:T a "normal"	0.86	0.47	0.82	0.76	0.47	0.91	0.72	0.62	0.5	3.71	3.76	0.95	0.92	0.97	0.16	0.14
P26:T a "normal"	0.72	0.47	0.62	0.74	0.55	0.56	0.74	0.52	0.49	3.8	3.54	0.91	0.88	0.97	0.15	0.2
P26:T a "normal"	0.82	0.56	0.84	0.69	0.52	0.82	0.64	0.56	0.4	3.46	3.29	0.9	0.85	0.85	0.15	0.17
P26:T a "normal"	0.95	0.51	0.87	0.67	0.58	0.87	0.63	0.47	0.33	3.88	3.67	0.93	0.88	0.9	0.14	0.13
P26:T a "normal"	0.86	0.63	0.84	0.67	0.49	0.74	0.67	0.49	0.52	3.87	3.87	0.94	0.89	0.87	0.16	0.12
P26:T a "normal"	0.8	0.52	0.79	0.77	0.59	0.87	0.64	0.53	0.42	3.95	3.64	0.91	0.86	0.85	0.21	0.24
P26:T a "normal"	0.71	0.37	0.72	0.76	0.42	0.95	0.67	0.61	0.61	4.14	4.05	0.91	0.87	0.96	0.19	0.12
P26:T a "normal"	0.85	0.48	0.79	0.66	0.6	0.79	0.8	0.49	0.54	3.6	3.5	0.93	0.86	0.87	0.12	0.12
P26:T a "normal"	0.65	0.43	0.62	0.7	0.49	0.88	0.81	0.53	0.59	4.16	3.88	0.89	0.86	0.95	0.11	0.11
P26:T a "normal"	0.93	0.7	0.94	0.77	0.49	0.88	0.64	0.52	0.45	4.4	4.15	0.98	0.94	0.92	0.2	0.27
P26:T a "normal"	0.93	0.55	0.88	0.69	0.58	0.86	0.66	0.52	0.62	4.05	3.79	0.95	0.9	0.89	0.12	0.07
P26:T a "normal"	0.78	0.58	0.75	0.75	0.49	0.74	0.7	0.57	0.45	3.6	3.59	0.92	0.88	0.91	0.22	0.24
P26:T a "normal"	0.89	0.59	0.89	0.73	0.54	0.83	0.63	0.55	0.47	3.99	3.78	0.94	0.87	0.86	0.18	0.2
P26:T a "normal"	0.86	0.5	0.75	0.78	0.54	0.8	0.61	0.52	0.46	3.76	3.6	0.92	0.83	0.81	0.2	0.23
P28:T b "platys"	0.9	0.53	0.88	0.7	0.53	0.87	0.66	0.54	0.52	3.49	3.43	0.91	0.87	0.91	0.14	0.19
P28:T b "platys"	0.93	0.51	0.89	0.74	0.46	0.96	0.73	0.61	0.54	4.06	4.03	0.95	0.95	0.96	0.19	0.25
P28:T b "platys"	0.91	0.5	0.93	0.63	0.5	0.97	0.7	0.59	0.49	3.66	3.71	0.93	0.92	1	0.16	0.16
P28:T b "platys"	0.91	0.54	0.88	0.72	0.51	0.89	0.78	0.57	0.45	4.1	4.06	0.95	0.92	0.9	0.15	0.18
P28:T b "platys"	0.79	0.42	0.77	0.86	0.54	0.91	0.75	0.55	0.52	3.65	3.57	0.93	0.91	0.96	0.13	0.17
P28:T b "platys"	0.7	0.43	0.63	0.79	0.47	0.75	0.63	0.51	0.53	3.64	3.16	0.88	0.81	0.87	0.15	0.22
P28:T b "platys"	0.78	0.48	0.8	0.78	0.46	0.81	0.68	0.55	0.37	4.22	3.88	0.95	0.88	0.88	0.18	0.25
P28:T b "platys"	0.72	0.35	0.68	0.84	0.51	0.83	0.73	0.56	0.52	3.63	3.66	0.9	0.85	0.93	0.17	0.2
P28:T b "platys"	0.87	0.53	0.84	0.75	0.58	0.87	0.73	0.49	0.44	4.36	4.22	0.95	0.9	0.89	0.2	0.28

Shell size parameters in morphotypes 6/7

	KamBr ("e")	KamH ("c")	KamT ("m")	Kam-1Br ("j")	Kam-1H ("i")	Kam-1T ("p")	Kam-2Br ("g")	Kam-2H ("h")	Kam-2T ("o")	PerimeterV ("b")	PerimeterS ("l")	area V ("k")	area S ("n")	Tiefe ("q")	AperturBr (3 "f")	AperturH ("d")
P28:T b "platys"	0.97	0.55	1	0.83	0.54	0.93	0.73	0.61	0.53	4.29	4.17	0.98	0.97	0.96	0.21	0.23
P28:T b "platys"	0.85	0.55	0.82	0.62	0.44	0.76	0.68	0.56	0.43	4.18	4.11	0.89	0.85	0.85	0.3	0.3
P28:T b "platys"	0.93	0.56	0.9	0.79	0.49	0.89	0.65	0.61	0.5	4.15	4.14	1	0.95	0.92	0.19	0.25
P28:T b "platys"	0.82	0.43	0.73	0.72	0.56	0.84	0.73	0.49	0.43	3.39	3.35	0.89	0.85	0.87	0.1	0.11
P28:T b "platys"	0.79	0.48	0.8	0.76	0.43	0.88	0.76	0.58	0.42	3.82	3.89	0.94	0.91	0.92	0.16	0.14
P28:T b "platys"	0.66	0.48	0.69	0.77	0.46	0.82	0.78	0.57	0.44	3.72	3.59	0.89	0.84	0.88	0.23	0.25
P28:T b "platys"	0.67	0.37	0.72	0.93	0.44	0.85	0.73	0.55	0.33	3.74	3.61	0.93	0.88	0.9	0.16	0.16
P28:T b "platys"	0.92	0.54	0.87	0.76	0.47	0.84	0.7	0.6	0.5	4.29	3.96	0.95	0.94	0.93	0.17	0.29
P28:T b "platys"	0.82	0.48	0.85	0.86	0.52	0.9	0.66	0.55	0.45	3.82	3.75	0.93	0.91	0.88	0.18	0.2
P28:T b "platys"	0.8	0.54	0.92	0.76	0.54	0.76	0.62	0.52	0.45	3.52	3.32	0.91	0.87	0.91	0.14	0.14
P28:T b "platys"	0.71	0.37	0.67	0.79	0.51	0.82	0.72	0.55	0.43	4.11	3.83	0.92	0.83	0.83	0.26	0.27
P28:T c "elongate"	0.64	0.35	0.66	0.72	0.49	0.79	0.85	0.57	0.47	4.12	3.74	0.92	0.88	0.95	0.17	0.14
P28:T c "elongate"	0.45	0.26	0.47	0.72	0.47	0.47	0.71	0.31	0.66	4.39	4.09	0.9	0.9	1.01	0.29	0.14
P28:T c "elongate"	0.69	0.49	0.63	0.65	0.43	0.78	0.67	0.59	0.37	4.08	3.67	0.91	0.85	0.91	0.24	0.31
P28:T c "elongate"	0.86	0.49	0.8	0.66	0.4	0.75	0.77	0.59	0.38	4.76	4.34	1	0.98	0.94	0.23	0.24
P28:T c "elongate"	0.74	0.41	0.64	0.72	0.49	0.77	0.69	0.52	0.04	4.03	3.75	0.93	0.88	0.94	0.18	0.22
P28:T c "elongate"	0.89	0.66	0.81	0.72	0.53	0.77	0.67	0.54	0.43	3.98	3.89	0.95	0.91	0.88	0.19	0.24
P28:T c "elongate"	0.68	0.4	0.63	0.8	0.45	0.81	0.67	0.62	0.36	3.49	3.42	0.87	0.87	0.95	0.23	0.19
P28:T a "normal"	0.76	0.5	0.8	0.75	0.54	0.78	0.62	0.62	0.43	3.61	3.65	0.9	0.88	0.9	0.16	0.15
P28:T a "normal"	0.87	0.58	0.97	0.76	0.54	0.9	0.6	0.5	0.45	3.6	3.67	0.92	0.91	0.96	0.14	0.16
P28:T a "normal"	0.76	0.59	0.78	0.66	0.53	0.67	0.58	0.49	0.46	3.68	3.31	0.9	0.84	0.8	0.18	0.11
P28:T a "normal"	0.98	0.72	0.91	0.69	0.51	0.8	0.48	0.47	0.5	4.05	3.69	0.96	0.89	0.85	0.26	0.25
P28:T a "normal"	0.84	0.52	0.77	0.73	0.52	0.69	0.68	0.5	0.46	3.9	3.73	0.94	0.86	0.84	0.2	0.23
P28:T a "normal"	0.85	0.61	0.84	0.7	0.49	0.76	0.67	0.55	0.45	4.11	3.97	0.93	0.87	0.9	0.24	0.21
P28:T a "normal"	0.9	0.59	0.85	0.7	0.55	0.77	0.66	0.5	0.49	3.57	3.49	0.92	0.89	0.92	0.17	0.18
P28:T a "normal"	0.9	0.55	0.85	0.71	0.48	0.85	0.73	0.58	0.51	3.92	3.7	0.94	0.9	0.9	0.22	0.29
P28:T a "normal"	0.8	0.53	0.78	0.72	0.51	0.76	0.47	0.47	0.52	3.55	3.48	0.91	0.85	0.81	0.09	0.12
P28:T a "normal"	0.8	0.57	0.79	0.72	0.52	0.73	0.55	0.52	0.42	3.88	3.62	0.89	0.84	0.84	0.17	0.24
P28:T a "normal"	0.87	0.56	0.91	0.78	0.56	0.77	0.68	0.52	0.51	3.74	4	0.95	0.93	0.91	0.23	0.23
P28:T a "normal"	0.67	0.39	0.67	0.77	0.47	0.76	0.63	0.58	0.52	3.76	3.48	0.86	0.79	0.88	0.09	0.1
P28:T a "normal"	0.85	0.49	0.87	0.74	0.51	0.79	0.67	0.56	0.5	3.43	3.49	0.93	0.9	0.94	0.15	0.12
P28:T a "normal"	0.76	0.37	0.71	0.72	0.49	0.83	0.66	0.66	0.45	3.69	3.64	0.9	0.89	0.94	0.16	0.16
P28:T a "normal"	0.8	0.43	0.79	0.83	0.34	0.88	0.77	0.65	0.43	4.02	3.98	0.95	0.9	0.93	0.18	0.26
P28:T a "normal"	0.82	0.55	0.79	0.78	0.55	0.79	0.65	0.5	0.53	3.97	3.5	0.9	0.83	0.86	0.1	0.14
P28:T a "normal"	0.93	0.6	0.87	0.73	0.57	0.79	0.64	0.53	0.5	3.95	3.56	0.95	0.89	0.88	0.17	0.21
P28:T a "normal"	0.82	0.54	0.82	0.76	0.52	0.76	0.61	0.5	0.59	3.56	3.45	0.92	0.88	0.88	0.16	0.16
P28:T a "normal"	0.8	0.58	0.73	0.75	0.48	0.77	0.65	0.59	0.44	4.08	4.09	0.92	0.91	0.95	0.2	0.21
P28:T a "normal"	0.65	0.39	0.62	0.78	0.56	0.76	0.6	0.49	0.43	3.51	3.25	0.86	0.8	0.85	0.15	0.12
P28:T a "normal"	0.72	0.52	0.76	0.77	0.46	0.88	0.73	0.6	0.46	3.5	3.42	0.9	0.88	0.93	0.2	0.28
P28:T a "normal"	0.93	0.65	0.93	0.76	0.51	0.78	0.63	0.51	0.55	4.12	4.01	0.96	0.92	0.88	0.21	0.18
P28:T a "normal"	0.87	0.62	0.85	0.69	0.42	0.78	0.72	0.59	0.48	3.78	3.89	0.95	0.93	0.91	0.21	0.23
P28:T a "normal"	0.85	0.53	0.93	0.79	0.47	0.84	0.67	0.54	0.4	4.38	4.14	0.94	0.92	0.91	0.26	0.19
P28:T a "normal"	0.79	0.44	0.85	0.8	0.39	0.85	0.68	0.58	0.39	3.52	3.37	0.93	0.88	0.86	0.21	0.19
P28:T a "normal"	0.68	0.21	0.57	0.79	0.44	0.86	0.71	0.6	0.39	3.53	3.52	0.89	0.87	0.96	0.08	0.08
P28:T a "normal"	0.76	0.46	0.77	0.71	0.43	0.89	0.72	0.59	0.47	3.58	3.51	0.92	0.91	0.95	0.15	0.17
P28:T a "normal"	0.86	0.47	0.77	0.68	0.51	0.75	0.62	0.52	0.42	3.4	3.37	0.88	0.86	0.93	0.14	0.23
P28:T a "normal"	0.9	0.55	0.87	0.75	0.59	0.83	0.57	0.48	0.6	3.76	3.61	0.92	0.88	0.92	0.13	0.24
P28:T a "normal"	0.85	0.51	0.86	0.73	0.53	0.87	0.76	0.61	0.62	3.55	3.51	0.9	0.89	0.96	0.11	0.14
P28:T a "normal"	0.83	0.48	0.77	0.76	0.53	0.86	0.73	0.56	0.42	3.58	3.65	0.92	0.9	0.93	0.14	0.21
P28:T a "normal"	0.83	0.51	0.84	0.77	0.53	0.89	0.77	0.57	0.44	4.17	3.63	0.92	0.88	0.91	0.14	0.18
P28:T a "normal"	0.74	0.41	0.65	0.72	0.44	0.77	0.65	0.58	0.45	4	3.76	0.9	0.86	0.89	0.21	0.25
P28:T a "normal"	0.85	0.49	0.91	0.77	0.58	0.85	0.63	0.5	0.5	3.53	3.46	0.9	0.9	0.93	0.11	0.14
P28:T a "normal"	0.76	0.49	0.74	0.79	0.48	0.85	0.72	0.59	0.53	3.73	3.62	0.92	0.9	0.95	0.18	0.24
P28:T a "normal"	0.79	0.57	0.72	0.7	0.5	0.78	0.61	0.55	0.44	4.07	4.05	0.95	0.89	0.86	0.2	0.28
P28:T a "normal"	0.89	0.56	0.83	0.75	0.55	0.83	0.62	0.56	0.59	3.63	3.63	0.93	0.89	0.92	0.12	0.09
P28:T a "normal"	0.87	0.61	0.85	0.72	0.49	0.81	0.63	0.5	0.4	3.68	3.64	0.93	0.89	0.89	0.18	0.2
P28:T a "normal"	0.73	0.43	0.65	0.75	0.53	0.77	0.68	0.58	0.48	3.47	3.4	0.88	0.81	0.83	0.17	0.18
P28:T a "normal"	0.67	0.33	0.72	0.73	0.55	0.76	0.62	0.4	0.52	3.47	3.45	0.86	0.81	0.87	0.16	0.1
P28:T a "normal"	0.83	0.55	0.8	0.71	0.47	0.84	0.77	0.62	0.52	4.08	4.02	0.93	0.95	0.97	0.13	0.22
P28:T a "normal"	0.9	0.56	0.82	0.75	0.58	0.82	0.63	0.55	0.56	3.58	3.63	0.94	0.9	0.91	0.14	0.18
P28:T a "normal"	0.82	0.51	0.81	0.74	0.48	0.74	0.68	0.62	0.53	4.3	4.21	0.94	0.91	0.92	0.19	0.21
P28:T a "normal"	0.75	0.47	0.85	0.77	0.49	0.84	0.62	0.46	0.43	3.4	3.36	0.88	0.85	0.9	0.17	0.2
P28:T a "normal"	0.71	0.39	0.73	0.67	0.42	0.87	0.76	0.58	0.47	3.82	3.34	0.91	0.83	0.85	0.14	0.13
P28:T a "normal"	0.8	0.51	0.92	0.83	0.49	0.91	0.7	0.51	0.49	4.29	4.17	0.95	0.92	0.92	0.21	0.17
P28:T a "normal"	0.89	0.48	0.86	0.73	0.45	0.83	0.71	0.61	0.38	4.29	4.13	0.97	0.93	1	0.19	0.22
P28:T a "normal"	0.85	0.51	0.79	0.69	0.64	0.84	0.71	0.49	0.63	3.66	3.66	0.9	0.86	0.87	0.17	0.14
P28:T a "normal"	0.84	0.44	0.79	0.78	0.56	0.89	0.63	0.54	0.5	3.33	3.23	0.89	0.84	0.88	0.15	0.19
P28:T a "normal"	0.72	0.46	0.69	0.81	0.54	0.84	0.67	0.59	0.48	3.81	3.49	0.9	0.85	0.88	0.11	0.18
P28:T a "normal"	0.91	0.54	0.84	0.64	0.49	0.73	0.72	0.59	0.39	4.89	4.48	0.97	0.91	0.92	0.22	0.2
P28:T a "normal"	0.73	0.42	0.68	0.78	0.49	0.8	0.74	0.64	0.45	3.52	3.57	0.91	0.89	0.96	0.17	0.13
P28:T a "normal"	0.74	0.42	0.75	0.74	0.48	0.79	0.72	0.63	0.42	4.04	3.79	0.91	0.86	0.87	0.17	0.22
P28:T a "normal"	0.95	0.61	0.91	0.78	0.57	0.87	0.68	0.52	0.47	4.3	3.77	0.94	0.91	0.91	0.18	0.15
P28:T a "normal"	0.76	0.5	0.77	0.76	0.55	0.78	0.61	0.49	0.49	3.55	3.41	0.89	0.86	0.87	0.14	0.22
P28:T a "normal"	0.77	0.46	0.84	0.71	0.48	0.86	0.67	0.59	0.53	3.61	3.61	0.91	0.9	0.93	0.21	0.19

Shell size parameters in morphotypes 7/7

	KamBr ("e")	KamH ("c")	KamT ("m")	Kam-1Br ("j")	Kam-1H ("i")	Kam-1T ("p")	Kam-2Br ("g")	Kam-2H ("h")	Kam-2T ("o")	PerimeterV ("b")	PerimeterS ("l")	area V ("k")	area S ("n")	Tiefe ("q")	ApertурBr (3 "f")	ApertурH ("d")
P28:T a "normal"	0.79	0.49	0.81	0.81	0.56	0.6	0.73	0.45	0.61	4.05	4.04	0.95	0.92	0.93	0.18	0.26
P28:T a "normal"	0.78	0.47	0.69	0.76	0.53	0.81	0.65	0.52	0.54	3.54	3.55	0.89	0.83	0.87	0.2	0.22
P28:T a "normal"	0.81	0.57	0.8	0.75	0.63	0.84	0.71	0.45	0.58	3.55	3.54	0.92	0.88	0.9	0.13	0.12
P28:T a "normal"	0.87	0.54	0.92	0.79	0.53	0.86	0.68	0.57	0.4	4.08	3.98	0.95	0.95	0.96	0.19	0.18
P28:T a "normal"	0.87	0.56	0.86	0.76	0.46	0.82	0.65	0.62	0.54	3.98	4.04	0.95	0.95	0.98	0.16	0.24
P28:T a "normal"	0.94	0.56	0.9	0.6	0.46	0.8	0.71	0.59	0.43	3.7	3.77	0.95	0.91	0.91	0.14	0.23
P28:T a "normal"	0.75	0.46	0.69	0.75	0.4	0.82	0.73	0.58	0.53	3.62	3.34	0.9	0.85	0.91	0.18	0.22
P28:T a "normal"	0.74	0.49	0.79	0.78	0.44	0.81	0.67	0.56	0.42	4.01	3.74	0.93	0.87	0.85	0.21	0.23
P28:T a "normal"	0.78	0.5	0.81	0.79	0.47	0.81	0.72	0.54	0.45	3.82	3.69	0.93	0.86	0.83	0.22	0.18
P28:T a "normal"	0.83	0.5	0.83	0.74	0.47	0.83	0.67	0.54	0.46	4	3.77	0.93	0.86	0.85	0.17	0.24
P28:T a "normal"	0.87	0.55	0.85	0.74	0.46	0.46	0.63	0.54	0.81	4.14	3.81	0.94	0.91	0.92	0.16	0.14
P28:T a "normal"	0.85	0.62	0.89	0.75	0.45	0.78	0.64	0.58	0.52	3.64	3.73	0.93	0.89	0.9	0.13	0.14
P28:T a "normal"	0.75	0.4	0.75	0.76	0.43	0.81	0.74	0.62	0.48	4.04	3.97	0.93	0.89	0.95	0.27	0.24
P28:T a "normal"	0.88	0.51	0.85	0.74	0.52	0.85	0.72	0.59	0.5	4.1	3.94	0.95	0.9	0.95	0.26	0.2
P28:T a "normal"	0.87	0.51	0.75	0.78	0.48	0.74	0.63	0.56	0.46	3.55	3.37	0.93	0.86	0.87	0.13	0.18
P28:T a "normal"	0.83	0.49	0.78	0.77	0.52	0.84	0.62	0.55	0.57	3.72	3.68	0.92	0.9	0.94	0.11	0.22
P28:T a "normal"	0.99	0.58	0.92	0.7	0.53	0.86	0.59	0.51	0.51	3.98	3.83	0.95	0.94	0.94	0.23	0.16
P28:T a "normal"	0.88	0.62	0.86	0.73	0.5	0.8	0.6	0.48	0.4	3.71	3.67	0.93	0.9	0.87	0.24	0.24
P28:T a "normal"	0.91	0.63	0.87	0.73	0.55	0.86	0.61	0.47	0.49	3.62	3.43	0.94	0.9	0.89	0.14	0.14
P28:T a "normal"	0.75	0.42	0.66	0.73	0.39	0.76	0.79	0.69	0.43	4.02	3.52	0.94	0.87	0.93	0.22	0.25
P28:T a "normal"	0.78	0.48	0.74	0.77	0.38	0.82	0.66	0.57	0.38	4.01	3.8	0.95	0.88	0.89	0.22	0.23
P28:T a "normal"	0.9	0.58	0.88	0.78	0.51	0.87	0.72	0.58	0.45	3.84	3.73	0.96	0.91	0.91	0.12	0.12
P28:T a "normal"	0.91	0.54	0.86	0.73	0.54	0.81	0.59	0.55	0.36	3.54	3.38	0.93	0.86	0.84	0.17	0.15
P28:T a "normal"	0.89	0.54	0.89	0.81	0.52	0.85	0.62	0.54	0.42	3.64	3.66	0.93	0.89	0.9	0.16	0.12
P28:T a "normal"	0.85	0.59	0.95	0.78	0.5	0.86	0.69	0.52	0.46	4.06	3.83	0.94	0.91	0.93	0.18	0.21
P28:T a "normal"	0.99	0.69	0.9	0.75	0.52	0.75	0.53	0.47	0.4	3.91	3.69	0.98	0.93	0.9	0.12	0.12
P28:T a "normal"	0.84	0.45	0.84	0.7	0.53	0.83	0.66	0.51	0.52	3.66	3.47	0.9	0.88	0.91	0.22	0.21
P28:T a "normal"	0.83	0.54	0.81	0.76	0.48	0.81	0.64	0.54	0.47	3.41	3.24	0.91	0.86	0.88	0.26	0.16
P28:T a "normal"	0.74	0.42	0.76	0.76	0.52	0.79	0.64	0.52	0.43	3.35	3.22	0.87	0.82	0.87	0.1	0.12
P28:T a "normal"	0.83	0.53	0.81	0.69	0.54	0.81	0.56	0.49	0.46	3.96	3.7	0.92	0.88	0.87	0.21	0.21
P28:T a "normal"	0.98	0.65	0.94	0.72	0.54	0.77	0.64	0.54	0.45	4.22	4.2	1	0.96	0.95	0.25	0.29
P28:T a "normal"	0.63	0.43	0.65	0.8	0.43	0.74	0.75	0.54	0.56	3.69	3.49	0.91	0.88	0.94	0.17	0.15
P28:T a "normal"	0.97	0.56	0.94	0.79	0.56	0.86	0.64	0.59	0.57	4.01	3.88	0.99	0.94	0.93	0.16	0.2
P28:T a "normal"	0.81	0.46	0.79	0.75	0.52	0.81	0.65	0.61	0.51	3.61	3.58	0.91	0.87	0.91	0.17	0.18
P28:T a "normal"	0.73	0.55	0.75	0.78	0.46	0.77	0.65	0.52	0.51	3.87	3.73	0.9	0.85	0.86	0.23	0.32
P28:T a "normal"	0.83	0.49	0.83	0.75	0.51	0.84	0.69	0.54	0.45	3.89	3.67	0.94	0.89	0.88	0.18	0.15
P28:T a "normal"	0.81	0.54	0.83	0.7	0.5	0.82	0.66	0.53	0.46	4.02	3.7	0.93	0.87	0.85	0.28	0.28
P28:T a "normal"	0.94	0.61	0.9	0.79	0.53	0.88	0.58	0.56	0.65	3.59	3.47	0.95	0.91	0.94	0.17	0.13
P28:T a "normal"	0.91	0.56	0.9	0.7	0.49	0.85	0.6	0.56	0.46	3.72	3.68	0.93	0.9	0.93	0.15	0.2
P28:T a "normal"	0.85	0.56	0.81	0.71	0.46	0.82	0.7	0.58	0.54	4.11	4.13	0.95	0.93	0.94	0.18	0.21
P28:T a "normal"	0.79	0.46	0.74	0.79	0.47	0.83	0.67	0.57	0.45	4.15	4.07	0.96	0.89	0.89	0.18	0.14
P28:T a "normal"	0.77	0.56	0.81	0.72	0.49	0.79	0.65	0.54	0.54	3.87	3.62	0.9	0.86	0.84	0.15	0.19
P28:T a "normal"	0.97	0.7	0.98	0.75	0.55	0.85	0.52	0.48	0.48	4.47	4.43	0.98	0.95	1	0.25	0.21
P28:T a "normal"	0.8	0.55	0.75	0.74	0.52	0.74	0.56	0.54	0.53	3.56	3.52	0.9	0.86	0.87	0.14	0.23
P28:T a "normal"	0.89	0.59	0.92	0.74	0.52	0.83	0.65	0.58	0.48	4.06	3.92	0.94	0.89	0.88	0.16	0.13
P28:T a "normal"	0.91	0.55	0.82	0.69	0.55	0.75	0.64	0.49	0.44	3.52	3.55	0.93	0.89	0.91	0.2	0.19
P28:T a "normal"	0.83	0.52	0.83	0.71	0.52	0.84	0.64	0.52	0.49	3.8	3.61	0.94	0.9	0.9	0.17	0.24
P28:T a "normal"	0.92	0.6	0.93	0.73	0.54	0.8	0.62	0.51	0.48	3.63	3.7	0.95	0.91	0.94	0.15	0.13
P28:T a "normal"	0.46	0.23	0.49	0.72	0.33	0.79	0.72	0.61	0.44	3.91	3.71	0.88	0.83	0.86	0.17	0.13
P28:T a "normal"	0.82	0.49	0.85	0.79	0.5	0.86	0.67	0.57	0.52	3.56	3.64	0.91	0.9	0.96	0.14	0.17
P28:T a "normal"	0.88	0.61	0.81	0.77	0.53	0.79	0.64	0.57	0.51	3.73	3.64	0.94	0.87	0.85	0.22	0.14
P28:T a "normal"	0.96	0.5	0.95	0.74	0.51	0.84	0.56	0.56	0.48	3.66	3.76	0.94	0.93	0.96	0.16	0.19
P28:T a "normal"	0.88	0.64	0.94	0.88	0.51	0.88	0.6	0.56	0.51	3.83	4.07	0.95	0.94	0.96	0.2	0.18
P28:T a "normal"	0.81	0.44	0.8	0.6	0.43	0.82	0.69	0.66	0.49	3.86	4	0.92	0.92	0.97	0.21	0.18
P28:T a "normal"	0.91	0.58	0.89	0.71	0.43	0.81	0.74	0.64	0.39	4.27	3.97	0.97	0.9	0.86	0.24	0.22
P28:T a "normal"	0.59	0.36	0.63	0.82	0.48	0.78	0.65	0.5	0.39	3.37	3.28	0.86	0.8	0.82	0.15	0.18
P28:T a "normal"	0.87	0.5	0.82	0.77	0.5	0.8	0.65	0.57	0.48	3.65	3.67	0.93	0.87	0.88	0.17	0.18
P28:T a "normal"	0.82	0.5	0.81	0.75	0.57	0.81	0.67	0.54	0.48	3.73	3.73	0.92	0.87	0.85	0.16	0.14
P28:T a "normal"	0.88	0.51	0.89	0.82	0.52	0.91	0.71	0.58	0.52	3.67	3.63	0.93	0.9	0.9	0.22	0.17
P28:T a "normal"	0.87	0.46	0.83	0.77	0.53	0.82	0.6	0.56	0.44	3.57	3.63	0.93	0.86	0.83	0.13	0.08
P28:T a "normal"	0.81	0.49	0.79	0.77	0.56	0.77	0.59	0.53	0.37	4.12	3.91	0.94	0.88	0.87	0.21	0.23
P28:T a "normal"	0.98	0.62	0.91	0.62	0.44	0.84	0.62	0.47	0.41	3.81	3.7	0.95	0.9	0.94	0.11	0.07
P28:T a "normal"	0.85	0.45	0.85	0.79	0.51	0.81	0.66	0.56	0.48	3.73	3.73	0.92	0.87	0.85	0.16	0.12
P28:T a "normal"	0.91	0.6	0.89	0.72	0.4	0.78	0.59	0.58	0.5	4.22	4.1	0.93	0.86	0.85	0.2	0.2
P28:T a "normal"	0.89	0.58	0.93	0.68	0.45	0.74	0.56	0.54	0.57	4.06	4.01	0.97	0.92	0.92	0.2	0.19
P28:T a "normal"	0.99	0.64	0.95	0.72	0.53	0.8	0.58	0.57	0.47	4.22	4.1	0.99	0.94	0.93	0.23	0.31
P28:T a "normal"	0.64	0.42	0.65	0.81	0.54	0.81	0.8	0.62	0.35	4.03	3.72	0.89	0.84	0.91	0.13	0.13
P28:T a "normal"	0.77	0.44	0.77	0.75	0.48	0.84	0.64	0.55	0.48	3.78	3.55	0.93	0.89	0.93	0.14	0.18
P28:T a "normal"	0.64	0.42	0.61	0.71	0.48	0.79	0.62	0.57	0.52	3.59	3.38	0.88	0.85	0.93	0.18	0.19
P28:T a "normal"	0.85	0.61	0.84	0.68	0.57	0.75	0.62	0.47	0.49	3.62	3.43	0.92	0.88	0.89	0.14	0.12